Central Washington University
ScholarWorks@CWU

All Master's Theses | Master's Theses

Winter 2018

The Origin of Dark Mats at the Sunrise Ridge Borrow Pit Site (45PI408) Mount Rainier National Park, Washington

Sean Stcherbinine
sean.stcherb@gmail.com

Follow this and additional works at: https://digitalcommons.cwu.edu/etd

Part of the Archaeological Anthropology Commons, Geochemistry Commons, Geology Commons, Geomorphology Commons, and the Physical and Environmental Geography Commons

Recommended Citation

Stcherbinine, Sean, "The Origin of Dark Mats at the Sunrise Ridge Borrow Pit Site (45PI408) Mount Rainier National Park, Washington" (2018). *All Master's Theses*. 894.
https://digitalcommons.cwu.edu/etd/894

This Thesis is brought to you for free and open access by the Master's Theses at ScholarWorks@CWU. It has been accepted for inclusion in All Master's Theses by an authorized administrator of ScholarWorks@CWU. For more information, please contact pingfu@cwu.edu.

THE ORIGIN OF DARK MATS AT THE SUNRISE RIDGE BORROW PIT SITE

(45PI408) MOUNT RAINIER NATIONAL PARK, WASHINGTON

A Thesis

Presented to

The Graduate Faculty

Central Washington University

In Partial Fulfillment

of the Requirements for the Degree

Master of Science

Cultural and Environmental Resource Management

---

by

Sean Michael Stcherbinine

March 2018

CENTRAL WASHINGTON UNIVERSITY

Graduate Studies

We hereby approve the thesis of

Sean Michael Stcherbinine

Candidate for the degree of Master of Science

APPROVED FOR THE GRADUATE FACULTY

______________ ________________________________

Dr. Patrick T. McCutcheon, Committee Chair

______________ ________________________________

Dr. Karl D. Lillquist

______________ ________________________________

Dr. Patrick M. Lubinski

______________ ________________________________

Dean of Graduate Studies

ABSTRACT

THE ORIGIN OF DARK MATS AT THE SUNRISE RIDGE BORROW PIT SITE

(45PI408) MOUNT RAINIER NATIONAL PARK, WASHINGTON

by

Sean Michael Stcherbinine

March 2017

The Sunrise Ridge Borrow Pit Site is a precontact archaeological site located in the upland forest soils of Mount Rainier National Park. Site stratigraphy is complicated, consisting of tephra deposits from mostly known origins that are intercalated with dark sediments of unknown origin, referred to here as dark mats. Precontact occupation has been split previously into two components based on the ambiguous depositional history of the dark mats, notably their unknown parent material, depositional environment, and relationship with adjacent tephra strata. Stratigraphic samples from excavation units, features, and one off-site excavation unit was used to investigate these data gaps. Grain size, chemistry, organic content, pH, and calcium carbonate content are characterized to document parent material and depositional environment of adjacent strata. Dark mats typically had higher organic content and similar chemistry and grain-size properties compared to underlying tephra strata, and interpreted as buried A horizons that formed in tephra of known regional origin. However, a few dark mats were reworked, and at times the product of multiple or unknown parent material. These determinations are used to revise a depositional history model of the Sunrise Ridge Borrow Pit Site that places the main occupation at 471 years BP to 2,200 cal years BP yet supports previous site assemblage organization into two precontact components.

ACKNOWLEDGMENTS

First and foremost, I would like to thank my mother, Sue, my father, Mike, and my brother, Scott for their consistent support and encouragement throughout my graduate studies. Without them I may not have stayed motivated and completed this project. Secondly, I would like to thank my field school instructor, graduate school advisor and committee chair, Dr. Patrick T. McCutcheon. I am grateful he helped generate a research topic that bridged both of our academic goals. His, focused on better understanding the depositional history of an archaeological site he has invested a good portion of his career in. Myself, taking gearchaeological methods and techniques I learned during coursework and applying them towards a project that would aid me in a future career in archaeology. For this, I thank you.

I would also like to thank my other two committee members, Dr. Karl Lillquist and Dr. Patrick Lubinski. Dr. Karl Lillquist was my instructor for two courses: Geomorphology, and Soils. Without his high standards in those courses, the foundational knowledge needed to begin and carry out this project would not have been possible. Dr. Lubinski was my instructor in Geoarcheology. His course was critical in teaching me how important the relationship between the sediment matrix and cultural materials is at archeological sites. I use knowledge gained in both of their courses every day at work. Both were also instrumental in the proposal and editing phases of this project.

There are many other people and institutions that played pivotal roles assisting with this project’s completion: Dr. Ian Buvit helped guide me during the proposal and grain-size analysis phase; my friends and graduate school cohort were always encouraging; and Anne B. Parfitt helped excavate and document the off-site excavation unit, she was also a great asset with questions due to her years of experience with site data. Central Washington University's Graduate School provided $1000 grant that mitigated the financial burden of geochemistry measurements. Washington State University's Peter Hooper Geoanalytical Lab provided a discounted price for students who come to the lab to personally prepare samples. I would also like to thank the dozens of people who have worked on Sunrise Ridge Borrow Pit Site-related research. Former graduate students, field school students, and employees of Mount Rainier National Park, all require recognition. Your hard work and devotion to good data collection, all with the goal of historic preservation in mind, needs to be acknowledged.

Lastly, I would like to thank the staff, present and former, of Archaeological and Historical Services at Eastern Washington University. Specifically, Jennifer Wilson, Stan Gough, Fred Crisson, Becky Stevens, and Ryan Ives, who all provided consistent encouragement, as well as communicating the need for me to finish. Without them trusting me to lead projects, and their mentorship over the last decade, I may not have become interested in geoarchaeology, or even pursued a career in cultural resources management. For this, I am truly indebted.

TABLE OF CONTENTS

TABLE OF CONTENTS (CONTINUED)

LIST OF TABLES

LIST OF TABLES (CONTINUED)

LIST OF FIGURES

LIST OF FIGURES (CONTINUED)

LIST OF FIGURES (CONTINUED)

CHAPTER 1

INTRODUCTION

Documenting the nature and origin of the sediment matrix containing artifacts at archaeological sites is necessary to grasp a complete understanding of the archaeological record (Waters, 1992:15). Determining if adjacent strata is deposited simultaneously, and if stratification is the result of soil formation, is necessary for accurate organization of subsurface archaeological components (Goldberg & McPhail, 2006:30-31). Documenting soil parent material (unconsolidated mineral and/or organic matter that develop into soil) assists in understanding how a specific sediment develops into soils (Brady & Weil, 2010:33). Once parent material is classified, depositional environments (e.g. volcanic ash fall, aeolian, alluvial, etc.) can be more easily interpreted (Prognon, Cojan, Kindler, Thiry, & Demange, 2011), and depositional histories created (Fedje, White, Wilson, Nelson, Vogel, & Southon, 1995).

Creating a depositional history model is a prerequisite to identifying artifact locations and archaeological components, increasing the likelihood that subsurface artifact frequencies are interpreted accurately (Goldberg & McPhail, 2006:221). Without a model explaining sediment parent material and depositional environment at an archaeological site, the temporal resolution represented by artifact densities can be ambiguous (Kowalewski, 1996). Defining whether artifact assemblages accumulated over brief or long periods of time is critical to understanding occupational intensity and periodicity (Binford, 1980), which is necessary when incorporating a site into discussions of regional subsistence and settlement patterns (Ferring & Peter, 1987). If the depositional history of an archaeological site is not established, data generated from the site has limited use when incorporating artifact assemblages into regional models of changing land use practices.

Problem

The archaeological record on the slopes of Mount Rainier occurs overlying or within sediments deposited by glacial and/or pyroclastic processes (Franklin, Moir, Hemstrom, Greene, & Smith, 1988). Glacial drift and pyroclastic sediments have been investigated most thoroughly by Crandell and Miller (1974) and Mullineaux (1974). Mullineaux (1974) analyzed stratigraphic sections at five locations within Mount Rainier National Park (MORA), describing tephra depths, thicknesses, and physical and chemical properties. However, this same level of description and analysis has not been granted towards darker sediments occurring between tephra strata (Mullineaux, 1974). Mullineaux (1974:12) describes that "the tephra layers studied are separated by beds of mostly darker sand- and silt-size, predominantly lithic particles. Some of these dark beds probably are also tephra, and, if so, they represent additional eruptions of the volcano. They were not studied in detail, however, because they could not be readily distinguished from sand and dust that actually was picked up from the volcano's slopes and redeposited by wind." Sisson and Vallance (2009:600) describe the same dark sediments in vague terms as "thin, dark, poorly vesicular tephras from Mount Rainier, and non-eruptive accumulations of ash-sized sediments reworked from earlier tephra deposits or carried by water and wind from nearby till." Understanding the parent material and depositional environment of these dark sediments observed between tephra deposits at MORA is essential when drawing conclusions about the archaeological record occurring within them**.**

After eight years of sub-surface investigations at the Sunrise Ridge Borrow Pit (SRBP) archaeological site, located inside MORA, the site's tephra strata have been documented and discussed (Dampf, 2002; Nickels, 2002; Evans, 2011; Lewis, 2015). Site stratigraphy has previously been recorded as either tephra, paleosol, or a combination of both. In this document, the term dark mats refers to the darker-colored sediments that are intercalated between tephra strata (Figures 1 and 2). These dark mats have previously been interpreted as paleosols but will be referred to as dark mats due to their ambiguous nature and distinguishability to adjacent tephra strata (cf. "black mats" (Haynes, 2008:6520)).

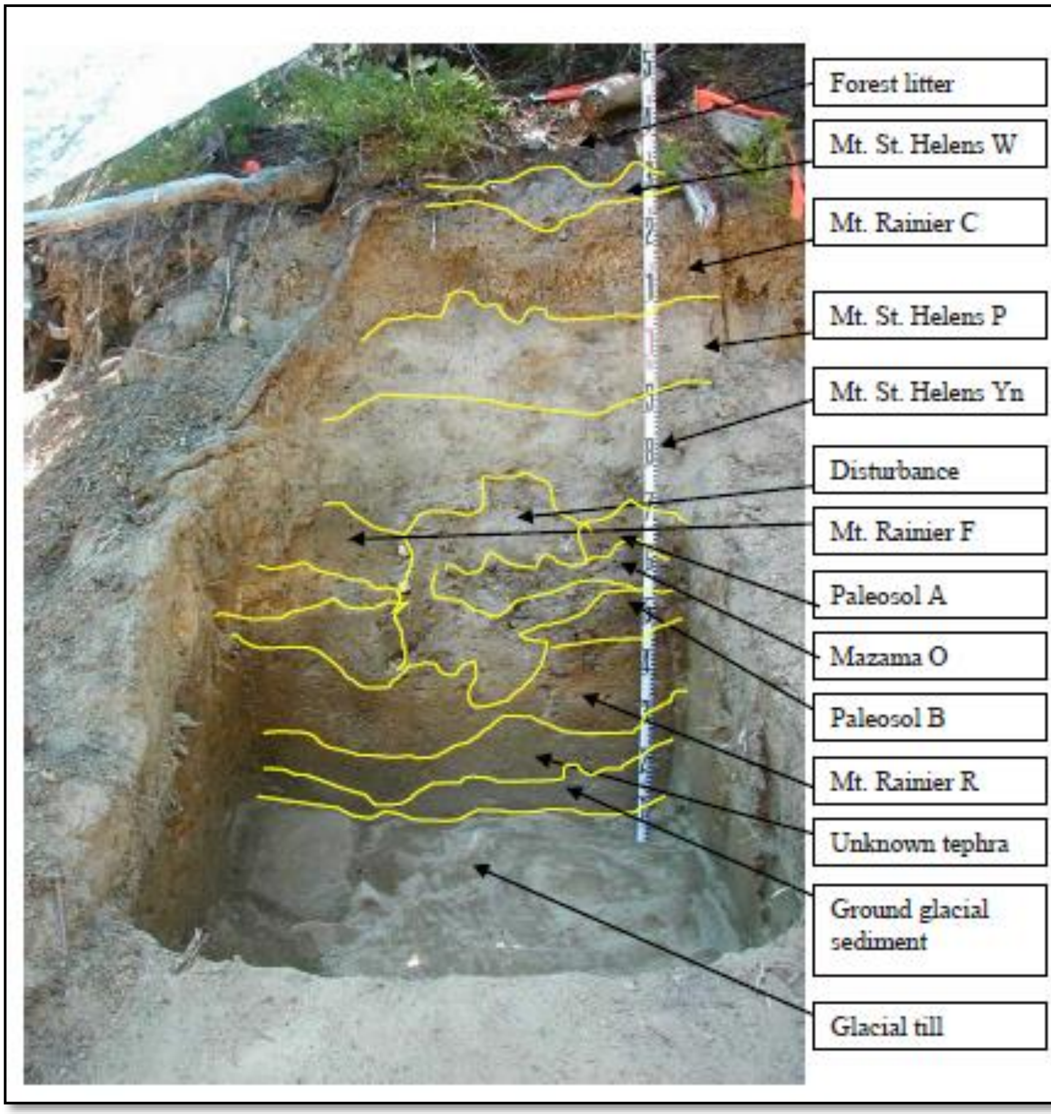

Figure 1: Typical profile from the SRBP Site. This study seeks to characterize the origin of dark mats located between tephra strata. Dark mats were only observed in two locations in this photo, and referred to as Paleosol A and Paleosol B. Figure from Evans (2011:31), interpretations from James Vallance and Adam Nickels, photo from Nickels (2001:2).

Figure 2: Dark mats (question marks) in excavation unit 30N/24E at the SRBP site. From top to bottom, question marks are superimposed on the dark mats overlying Mount Rainier-C, Mount St. Helens-Yn, and an unidentified tephra, respectively. Photo taken by Anne B. Parfitt in 2013.

Stratigraphy at the SRBP site has been investigated by Evans (2011), Nickels (2002), and Dampf (2002). Dampf (2002) analyzed lithics and > 2 phi grain-size distributions within three 50-x-50 centimeter (cm) shovel test pits, concluding stratigraphy in proximity to the test pits was intact. However, Dampf's investigation lacked any examination or discussion of dark mats occurring between tephra strata.

To investigate precontact fire occurrence at MORA, Nickels (2002) utilized a profile at the SBRP site to describe the site's tephra strata and document charcoal frequencies stratigraphically. Working with James Vallance, an authority on MORA tephras (e.g. Sisson & Vallance, 2009), Nickels (2002) identified seven of the major MORA tephras at the SRBP site. However, Nickels (2002) only observed dark mats directly above and below Mazama ash (see Figure 1), and did not discuss dark mat parent material, depositional environment, or relationship with adjacent strata.

Evans (2011) compared microartifact distributions and sediment grain-size distributions of > 2 phi to see if vertical mixing of small artifacts had occurred, concluding that sampled artifact-bearing strata lacked evidence of mixing. Evans (2011) documented the occurrence of dark mats at the SRBP site, finding dark mats had larger percentages of smaller grains compared to tephra strata, with several dark mats containing polymodal grain-size distributions. Evans (2011) noted that dark mats showed characteristics of underlying tephra strata and suggested they were formed by weathering on top of the parent tephra. It remains unclear if polymodal grain-size distributions are the result of weathering, humification, illuviation, eluviation, or the signature of a composite matrix containing parent material from multiple depositional environments or events.

Evans' (2011) noted her investigation did not measure enough of each sample to produce meaningful statistical statements about the grain-size analysis. Evans (2011) used GRADISTAT (Blott & Pye, 2001), a computer program that calculates grain-size statistics, to generate statistical grain-size information from sampled units. To generate reliable grain-size statistics of a sample, the program requires 95% of a sample's grain size distribution be determined and fall into interval size classes (Blott & Pye, 2001:1242). Only two of 28 samples from Evans' (2011) grain-size analysis consisted of distributions where 95% was assigned interval size classes because Evans' grain-size distributions lacked measurements of grains smaller than 2 phi. This created grain-size distributions with one large size class representing fine sand to clay-size grains, which at maximum made up to 60% of the total distribution. Evans' technique was not flawed for answering her investigation's research questions. While Evan's (2011) study produced the most resolved understanding of the depositional history to date, the investigation did not produce the data necessary to identify and interpret qualitative or quantitative relationships between dark mats and adjacent tephra strata. Thus, precisely what the depositional relationship is between dark mats and adjacent tephra strata remains a data gap prohibiting reconstruction of accurate depositional histories at the SRBP site.

The Holocene depositional history of MORA has been recorded by investigating its unconsolidated sediments, namely tephra, lahar, and glacial deposits (Vallance & Pringle, 2008). Currently, there exists a void in the published literature concerning the parent material and depositional environment of dark mats intercalated between tephra deposits at MORA. It remains unclear if dark mats are (1) buried A horizons: the upper elevations of weathered tephra, whose main constituents were deposited simultaneously with underlying, less altered tephra; or (2) if dark mats represent parent material and depositional environments contrasting with adjacent tephra strata; or (3) if dark mats are composite strata with additions from multiple, more prolonged depositional processes; or (4) combinations of tephra and organics. At the SRBP site, a significant amount of artifacts have been recovered from within these poorly understood dark mats (Lewis, 2015). Without creating a depositional history that explains the depositional relationship between dark mats and adjacent, underlying tephra strata at the SRBP site, the temporal resolution of site use based on artifact densities will remain unclear.

Purpose

The purpose of this SRBP site investigation is to document the dark mat parent material and describe and interpret the depositional environment between dark mats and adjacent tephra strata by measuring their physical and chemical properties. Knowledge of sediment parent material and depositional environment permits the creation of a SRBP site depositional history, allowing for a more accurate interpretation of artifact locations and components at this site.

To create a depositional history of the SRBP site that takes into account all possible inputs, the following are sampled: 1) stratigraphy from each of the four main SRBP site excavation areas, 2) concentrated site-use areas (archaeological features), and 3) stratigraphy from an off-site location, in a non-archeological context. Measuring properties like these will permit the documentation of any differences between dark mats and tephra strata within an archaeological context (feature and non-feature), and between a non-archaeological and archaeological context.

I achieved this purpose by:

1. Reviewing the nature of tephra-derived soils and existing depositional models of upland settings in and around Mount Rainier National Park to build on the SRBP site's current depositional context. Existing depositional models provided analogs for data generated during this investigation. Comprehending the current understanding of source, sequence, and properties of soils near the SRBP site ensures that previous descriptions and current interpretations at the site are built on the most recent and relevant literature.

2. Establishing complete grain-size distributions from each sampled dark mat and tephra strata of four column samples from each of the four excavation areas (n = 35 sediment samples), archaeological feature samples from the site's artifact-bearing dark mats (n = 3 sediment samples), and an off-site column sample (n = 9 sediment samples), for a total of 47 distributions. A list of samples and associated location data can be found in Appendix B. Column samples from four excavation areas were chosen to account for potential intra-column and intra-site variability. Of the 35 samples from four columns, 16 were recorded as dark mats and 19 were recorded as tephra. Feature samples were chosen to account for any measurable anthropogenic inputs existing site-wide, which might be strongest in feature samples. An off-site column sample was chosen to serve as a control sample when describing and interpreting the origin of strata between a non-archaeological and archaeological context. Grain-size distributions were created as a way to describe, compare and interpret depositional environment, post-depositional processes, and defining the most commonly occurring grain size(s) within each dark mat and tephra strata.
3. Measuring the chemistry of the most commonly occurring grain sizes from each grain-size distribution. Since polymodal distributions often suggest complex depositional histories (Lirer, Sheridan, & Vinci, 1996), modes of unimodal and bimodal distributions were sampled and measured for chemistry to document the elemental constituents and parent material of modal grain-size groups. Chemical

measurements result in a weight percentage or parts per million (ppm) of twenty-nine major and trace elements of each sample.

4. Analyzing the chemistry and grain-size data to quantitatively define whether or not there are relationships between dark mats and adjacent, underlying or overlying tephra strata. Relationships between quantities of elements and combinations of elements are used to describe the chemical signature of each strata to determine its likely parent material. Once parent material is described, it and depositional environment interpretations generated from grain size data can be used to discuss relationships between adjacent strata and whether they share similar depositional histories.
5. Creating a new depositional history model that organizes depositional environment and parent material determinations from this investigation with archaeological data from past site investigations into a more revised depositional model. This model shows relationships between artifact location/concentrations and the artifact-bearing strata to determine if artifacts from adjacent strata should be grouped or separated into different or similar archaeological components. The overarching objective of this SRBP site depositional history model is to determine the source, transport agent, depositional environment, and post-depositional alterations of site strata, potentially allowing for future finer-grained analyses.

Significance

This investigation is significant because it will be the first to document the parent material and depositional environment of poorly understood, dark mats observed often at

MORA. The nature of these dark mats in archaeological contexts has long been of interest (Burtchard, 1998; Nickels, 2002; Vaughn, 2010; Evans, 2011; Lewis, 2015; Ferry, 2015; Chatters, Brown, Hackenberger, McCutcheon, & Adler, J., 2017; Brown, Feathers, Chatters, McCutcheon, & Hackenberger, 2017). The results of this investigation will be useful to understanding past investigations and subsequent archaeological investigations at MORA concerned with the depositional history of dark mats. It will also be the first specific investigation focused on the SRBP site's dark mats. Finally, establishing the depositional history of the SRBP site is significant because it is a necessary prerequisite for examining past human occupational intensity and periodicity, which better permits the SRBP site's entry into discussions of precontact human land use in the upland contexts of the southern Washington Cascade Range (e.g., Vaughn, 2010; Ferry 2015).

Theoretical frameworks applying the forager to collector transition model in the Cascade Range (Dampf, 2002; Burtchard, 2007; Ferry, 2015; Lewis, 2015) require knowledge of depositional history and the nature of artifact characteristics both within and between components so that similarities and/or differences can be properly weighted and made comparable (Stein & Deo, 2003). These frameworks rely on changes in artifact frequencies and types as evidence of shifting land use practices (Burtchard, 2007). In previous studies at SRBP that investigated technological change through time, artifact frequencies were grouped into two coarse components because the depositional history of all strata had yet to be documented (Dampf, 2002; Evans, 2011). If adjacent strata share the same depositional history, artifacts within them can be grouped into the same component, creating a more resolved view and better understanding of changing site use. Without a more complete understanding of strata parent material and depositional environment at the SRBP site, conclusions about where the site fits into regional forager/collector models may be inaccurate.

Thesis Organization

The organization of this thesis is split between five thesis chapters and an imbedded article manuscript to be submitted for publication. Chapter II gives an overview of the study area, split between location, and the biophysical and cultural context of the MORA area. The biophysical context focuses on tephra deposits and stratigraphy typical of MORA generally and the SRPB site specifically. The cultural context focuses on archaeology at MORA, as well as excavations and material culture at the SRBP site. Chapter III is a literature review of the following topics: MORA forest soils, properties of Andisols and Spodosols, properties and development of A horizons, soil survey results, tephra-derived soils, regional depositional models, grains-size analysis, geochemical analysis, and depositional history models. Chapter IV describes methods used to achieve the purpose, which include sample selection and collection of column samples and archaeological feature samples, grain-size analysis, and geochemical analyses. Grain size analysis is further split into subsections describing dry sieving, wet sieving, sample pretreatment, and fine-grain fraction measurements. The geochemical analysis is discussed by focusing on X-ray fluorescence (XRF) analysis of major and trace elements. Chapter V presents the results and interpretations of this study. Results are organized by test unit and split between grain-size analysis and geochemical analysis. Interpretations follow by identifying individual strata relationships to adjacent strata, along with classifying of parent material, depositional environment, and soil formation, which are presented in a site depositional history model. Chapter VI contains the embedded manuscript, which consists of a condensed version of the previously mentioned chapters, along with a discussion of how study results relate to the SRBP site archaeological record, notably the organization of the artifact locations into components. Following the article are comprehensive references and appendices.

CHAPTER II

STUDY AREA

Location

The SRBP site is located in the northeast quadrant of Mount Rainier National Park (MORA), approximately 20 kilometers northeast of the mountain's summit, and 100 kilometers southeast of Tacoma, WA (Figure 3). Interpreted as a remnant of a glacial kame-like terrace (McCutcheon & Dampf, 2002:19), the site is situated on a mid-slope bench, on the west valley wall of the White River drainage basin, at around 1,500 meters (m) above mean sea level.

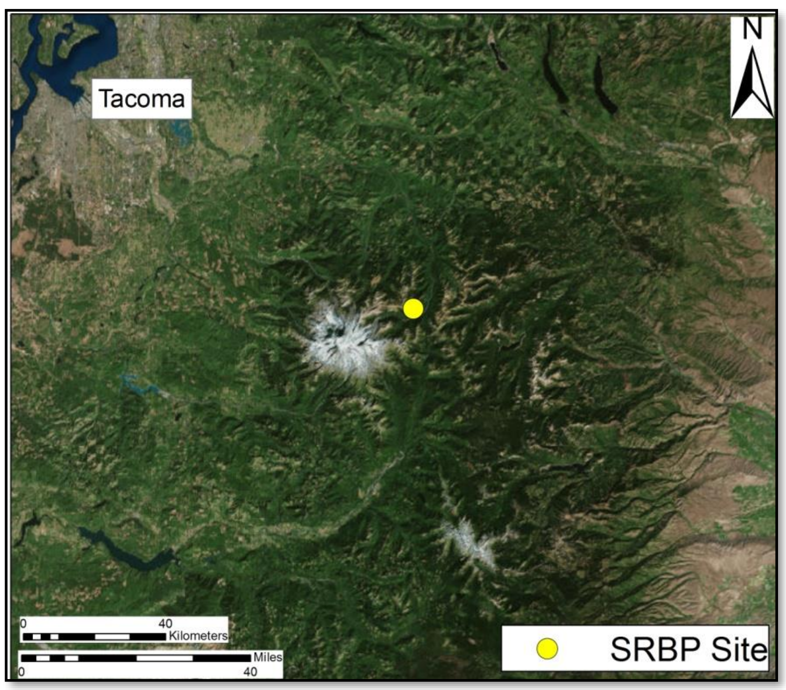

Figure 3: The SRBP site located northeast of Mount Rainer. Created in ArcGIS 10.4.1 by Sean Stcherbinine.

Biophysical Context

The region surrounding Mount Rainier has been altered by natural processes for millennia (Vallance & Pringle, 2008). These processes are primarily associated with volcanism and glaciation, which molded landforms into their current forms (Crandell & Miller, 1974). Mount Rainier is a stratovolcano situated directly above faults in the earth's crust that radiate from the Cascadia subduction zone, the product of the Juan de Fuca Plate sinking beneath the North American Plate (Vallance & Pringle, 2008). The subduction zone recycling of bedrock has resulted in numerous mountain-building eruptions over Mount Rainier's existence. Mount Rainier is composed primarily of Pleistocene-Pliocene-aged dacite and andesite lava flows and breccias (DNR, 2018), which is situated on an eroded surface of volcanic and plutonic rocks up to 66 million years old (Crandell & Miller, 1974). The SRBP site lies directly atop a granodiorite pluton formed during the Miocene epoch (23 to 5.3 million years ago) (DNR, 2018). Granodiorite is typical at similar elevations in the White River drainage (DNR, 2018).

During the Pleistocene the Cascade Range experienced multiple episodes of alpine glaciation responsible for eroding bedrock and depositing sediment (Vallance & Pringle, 2008). The Hayden Creek alpine glaciation (130 to 170 thousand years before present (BP)) caused a significant amount of erosion in the MORA area. Upland icecaps fed into large valleys, carving the characteristic U-shape as glaciers advanced and receded. The White River drainage is a great example of a U-shaped valley (Vallance & Pringle, 2008). The Evans Creek alpine glaciation (22 to 15 thousand years BP) is the most recent regional Pleistocene glaciation that would have affected the SRBP site vicinity (Crandell & Miller, 1974). Evans Creek till overlies the granodioritic and more recent andesitic bedrock in areas surrounding the SRBP site. During Evans Creek time the White River Basin was influenced by valley glaciers that deposited unconsolidated, poorly sorted sediments atop areas previously eroded to bedrock (Crandell & Miller, 1974). Evans Creek Drift in the White River drainage consists of varying sized rock fragments in a matrix of purplish-gray sand and silt (Crandell & Miller, 1974). At the SRBP site, Evans Creek Drift can be observed around one meter below the ground surface (Nickels, 2002). The mid-slope bench the SRBP site is situated on has been interpreted as a glacial kame terrace, a landform created by glacial outwash deposited between the receding valley glacier and adjacent slope (McCutcheon & Dampf, 2002).

Holocene tephra deposits surrounding Mount Rainier have been studied most thoroughly by Mullineaux (1974), which serves as the foundation for all subsequent studies of tephra-derived soils in the MORA area (e.g. Sisson & Vallance, 2009). The Mullineaux (1974) report notes that a complete tephra sequence is best observed along stream banks in alpine meadows between 5,000 and 7,000 feet (1,525 to 2,135 meters) above mean sea level. Beneath this elevation range, good profile exposures are lacking, with tephra sequences often incomplete, mixed, eroded, or obscured by more recent deposition (Mullineaux, 1974:8). Mullineaux's (1974) work presents a sequence of dated tephra strata and intercalated deposits. The report describes properties of 22 postglacial tephra deposits, including source volcano, color, thickness, distribution, distinctive features, and age.

Depositional Models

Mullineaux (1974) described the properties of 22 tephras layers in his comparative study (Figure 4 and Tables 1 and 2). Properties most useful when comparing to SRBP strata are grain-size maximum, thickness, and distribution around the park (plume).

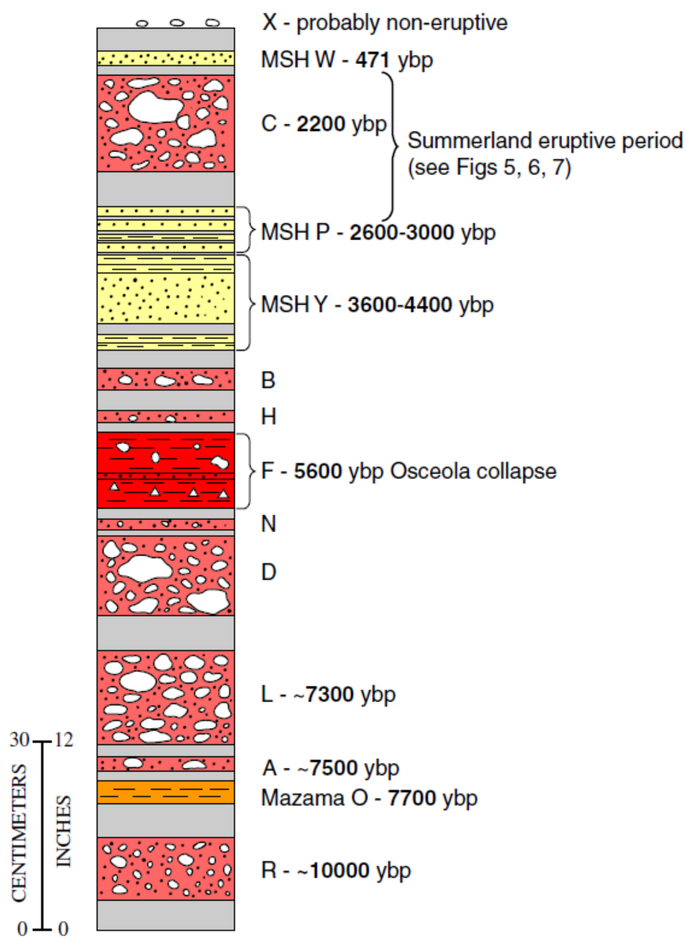

Figure 4. Mullineaux's adapted tephra sequence model for MORA. Gray layers correlate to this study's dark mats. Dates are in calibrated years BP (Sisson & Vallance, 2009:600 adapted from Mullineaux, 1974:14).

Table 1. Properties of Mount Rainier National Park Tephra Units (Adapted from Mullineaux, 1974:16).

Tephra Unit	Source Volcano	Color	Thickness Range (cm)	Grain Size Maximum (cm)	Principal Distribution	Common Field Characteristics	[1]Age
X	Mt. Rainier (MR)	Grayish brown	Does not form a stratum	3	Northeast-east-southeast from summit	Scattered lapilli on young surfaces	150
W	Mt. St. Helens (MSH)	White	0 -8	< 1	Most of park	White sand-sized ash at or near surface	471
C	MR	Brown	0-30	15	Eastern two-thirds of park	Lapilli deposit at or near surface	2200
P-bed 1	MSH	White to light gray	0-2	< 1	Most of park	Occurs with P-bed 2 as a distinct pair, coarser and more commonly preserved than others in set P	2600-2900
P-bed 2	MSH	White to light gray	0-2	< 0.4	Most of park	Occurs with P-bed 1 as a distinct pair, coarser and more commonly preserved than others in set P	2600-2900
P-bed 3	MSH	White to light gray	0-< 1	< 0.4	Eastern part of park	Not distinguishable from thin beds of set Y	2600-2900
P-bed 4	MSH	Brown	0-1	< 1	Southeastern part of park	Relatively coarse, brown	2600-2900
Y-beds 1&2	MSH	White	[1]0- < 1	< 0.4	Southeastern part of park	Indistinctive	2900-3700
Yn	MSH	Yellow or brown	2-30	1	Entire park	Coarse, yellow ash, very thick west of volcano	3700
Y-beds 3&4	MSH	White	[1]0- < 1	< 0.4	East and southern parts of park	Distinguishable in field only by stratigraphic position	3700-4000

[1]Age of eruption and subsequent deposition expressed in calibrated years before present. Dates are from Sisson and Vallance (2009) and Mullineaux (1974).

Table 1 (Continued). Properties of Mount Rainier National Park Tephra Units (Adapted from Mullineaux, 1974:16).

Tephra Unit	Source Volcano	Color	Thickness Range (cm)	Grain Size Maximum (cm)	Principal Distribution	Common Field Characteristics	[1]Age
B	MR	Reddish brown	0-7	5	East and southeast of summit	Scattered bombs and lapilli in dark ash	4000
H	MR	Grayish brown	0-5	1	East of summit	Obscure-scattered lapilli in brown to gray ash	5000
F	MR	Reddish yellow to pale yellow	0-15	1	Eastern two-thirds of park	Light-colored clayey ash above MAZ-O	5600
S	MR	Pinkish to brownish gray	0-150	100	Northeast of summit	Angular blocks in ash	5600-6000
N	MR	Reddish brown	0-4	1	East of summit	Sparse lapilli in coarse ash	5600-6000
D	MR	Reddish brown	0-15	10	Northeast to southeast of summit	Scoria bombs and lapilli	6000
L	MR	Yellowish brown	0-20	5	East to southeast of summit	Brown pumice of relatively uniform size between dark-gray ash beds	7300
A	MR	Brownish gray	0-3	2	East to south of summit	White pumice lapilli in brown ash	7500
O	Mt. Mazama	Reddish yellow to pale yellow	2-7	< 0.4	Entire park	Oldest light-colored ash, very widespread and well preserved	7700
R	MR	Reddish brown	0-15	4	NE to SE of summit	Reddish-brown lapilli below MAZ-O	10000

[1]Age of eruption and subsequent deposition expressed in calibrated years before present. Dates are from Sisson and Vallance (2009) and Mullineaux (1974).

Sisson and Vallance (2009) provide the most recent model of MORA tephra strata, emphasizing Mount Rainier eruptions from the last 2,600 years (Figure 5). Exposures on the eastern and northeastern flanks of Mount Rainier show evidence of 10 to 12 eruptions over the last 2,600 years, contrasted with previous work documenting 11 to 12 eruptions for all of the Holocene in this part of the Park. One exposure contains four previously unrecorded fine-grained tephra deposits in a portion (zone) of a profile between MR-C tephra and MSH-P tephras (see Figure 5). Mullineaux (1974) characterized this zone as lacking a tephra deposit associated with an eruptive event, documenting it as simply containing lithic sand and silts. Sisson and Vallance (2009) used field observations and geochemical proportions to achieve a more accurate description of Holocene-age Mount Rainier eruptions, improving our understanding of depositional histories at MORA. Mullineaux (1974) and Sisson and Vallance (2009) both focused on documenting the parent material and timing of tephra deposits, giving less attention to sediments occurring between them, here referred to as dark mats (see Figures 4 and 5). To date, no study has focused on the parent material or depositional processes responsible for the intercalated dark mats. Since these dark mats may represent stable surfaces, their source and agent of deposition is of interest to archaeologists working in the southern Cascade Range.

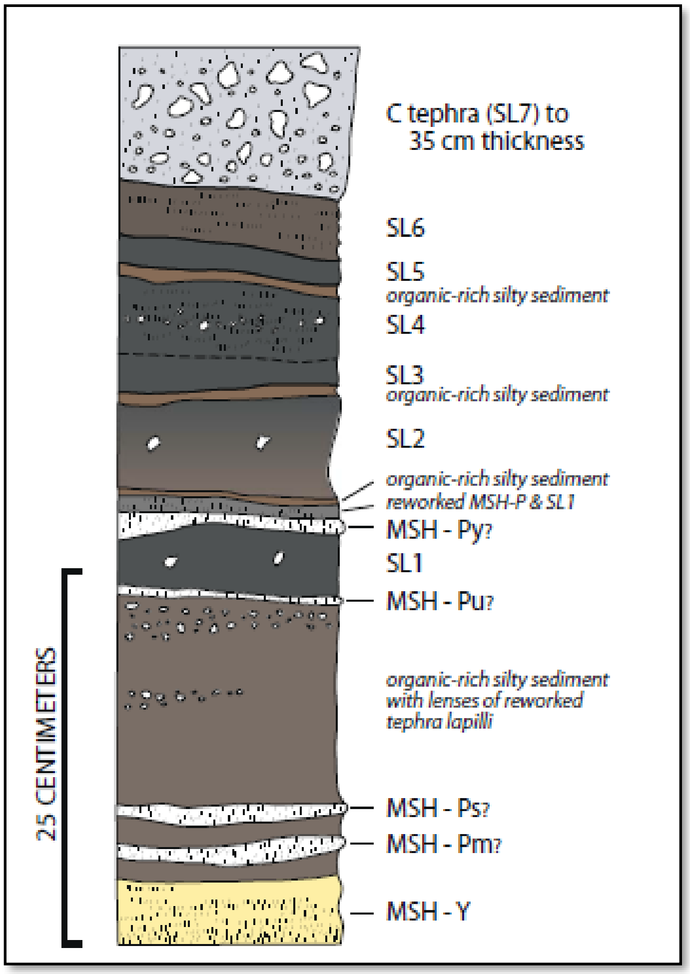

Figure 5. Exposure at the Summerland campsite (on the northeast flank of Mount Rainier at approximately 5,900 feet AMSL) used to model eruptions over the last 2600 years. Notice tephra strata and intercalated, fine-grained dark mats. Previously unidentified Summerland Period (2,600-2,200 cal. year BP) stratigraphic units are abbreviated as SL (e.g. SL6) (Sisson & Vallance, 2009:602).

SRBP Site Sediments

Sediments overlying drift at the SRBP site can be grouped into two categories: ambiguous, dark mats that are the subject of this investigation, and tephra strata. A typical stratigraphic profile contains tephra strata and intercalated dark mats previously interpreted as paleosols (Table 3, also see Figures 1 and 2). Tephra strata are abbreviated as follows: Mount St. Helens W Tephra (MSH-W), Mount Rainier C tephra (MR-C), Mount St. Helens P tephra (MSH-P), Mount St. Helens Yn tephra (MSH-Yn), Mount Rainer F, S, N, D, A, and R tephras are all abbreviated with the "MR" prefix (e.g. MR-F), and Mazama tephra is abbreviated MAZ-O. Dark mats are abbreviated with "DM" followed with another abbreviation of the tephra strata recorded in the field as overlying/underlying the dark mat (e.g. DM W/C represents the dark mat between MSH-W and MR-C tephra strata). Tephra strata thickness ranges from approximately 5 to 20 centimeters, with significant variation occurring across the site (Evans, 2011). Tephra texture ranges from lapilli and bomb-sized (pebble and cobble-sized) grains typical of nearby Mount Rainier volcanic ejecta, to ash (sand-sized and smaller) characteristic of more distant Mount St. Helen's and Mazama eruptions (Evans, 2011).

Dark mat and tephra strata distribution, thickness, color, and other characteristics are inconsistent across the site, but show some similarities and trends (Evans, 2011). In undisturbed locations where all strata are observable and discrete, there is a surface organic horizon, seven tephra strata, eight intercalated dark mats, and a basal glacial drift deposit. Table 3 describes dark mats and tephra strata observed at the site.

Dark mats are approximately 1 to 12 centimeters thick, relatively fine grained compared to tephra strata, with 30% to 60% of dark mats weight consisting of medium sand-sized grains or smaller (Evans, 2011). Color ranges from medium brown to dark grayish brown, always darker and less reddish/yellowish than the tephra strata (Evans, 2011). Previous SRBP site investigations (e.g. Burtchard, 1998; Dampf, 2002; Evans, 2011) focused little on dark mats beyond physical descriptions of texture and color.

Table 2. SRBP Site Stratigraphy and Properties (Evans, 2011:34; McCutcheon et al., 2017).

Stratum Name	Distribution range (cm)	Thickness range (cm)	Color	Texture	Depth to top	[2]Age
Duff/Organic	Site wide	0-5	Dark brown		surface	Recent to < 471
[1]DM Duff/MSH-W	Some units	0-5	brown		5	< 471
MSH-W	Site wide	0.5-22	Light gray	Pumice ash to lapilli	8	471
DM MSH-W/MR-C	Some units	1-4.5	Dark yellowish brown	Silty clay	22	471-2200
MR-C	Site wide	2.5-44.5	Yellowish brown	Pumice and lithic lapilli to bombs	35	2200
DM– MR-C/MSH-P	Some units	1-19	Medium brown	Fine clay	45	2200-2900
MSH-P	Some units	2-25.5	Dark grayish brown	Clay to loose fine pumice ash and lapilli	48	2600-2900
DM– MSH-P/MSH-Yn	Some units	1	Dark brown	Fine clay	50	2600-3700
MSH-Yn	Site wide	3-44	Brownish yellow	Pumice ash to loose pumice lapilli	55	3700
DM MSH-Yn/MR-F	Some units	1-21	Dark brown	clay	75	3700-5600
MR-F	Some units	6-15.5	Reddish yellow	Clay and weathered pumice and lapilli to bombs	82	5600
DM MR-F/MAZ-O	Few units	1-15			100	5600-7700

[1] DM denotes the dark mats observed between tephra, which is abbreviated after DM.
[2] Years BP maximum age range as surface deposit from initial deposition of main constituents to burial by subsequent volcanic eject**.** Ages from Mullineaux (1974) and Sisson and Vallance (2009).

Table 2 (Continued). SRBP Site Stratigraphy and Properties (Evans, 2011:34; McCutcheon et al., 2017).

Stratum Name	Distribution range (cm)	Thickness range (cm)	Color	Texture	Depth to top	[2]Age
MAZ-O	Few units	5-15	Light yellowish orange to pale brown	clay	105	7700
DM MAZ-O/MR-R	Few units	1-10			110	7700-10000
MR-R	Few units	1-15	Reddish brown	lapilli	112	10000
DM MR-R/Drift	Few units		unknown		115	> 10000
Glacial Drift	Few units	Purple-gray	Purple gray	Clay to gravel	> 115	> 10000

[1] DM denotes the dark mats observed between tephra, which is abbreviated after DM.
[2] Years BP maximum age range as surface deposit from initial deposition of main constituents to burial by subsequent volcanic eject**.** Ages from Mullineaux (1974) and Sisson and Vallance (2009).

Climate at the SRBP site is typical of the upland Western Cascades and characterized as a cool and moist, temperate, maritime climatic regime, with precipitation waning in the summer months (Dunwiddie, 1986). During fall and winter a high pressure region over the northern Pacific Ocean shifts south, moving warm, sometimes cool and moist air southwesterly towards the Cascade Range. This air condenses, precipitating as it rises along mountain slopes during the rainy season that lasts until spring (Figure 6) (Franklin et al., 1988).

Climate in the MORA area changed throughout the Holocene, exhibiting a warming and cooling periods that affected plant species type and location (Burtchard, 2003) (Figure 7). Recent investigations into the fire history of the Sunrise Ridge area at MORA found evidence of major climatic shifts and climate-induced changes in vegetation throughout the Holocene (Walsh, Lukins, McCutcheon, & Burtchard, 2017). Walsh et al. (2017) developed a climate and vegetation history of the early Holocene (12,000 to 8,000 cal years BP), middle Holocene (8,000 to 4,000 cal years BP), and late Holocene (4,000 cal years BP to present) for the Sunrise Ridge area. Early Holocene climate at the Sunrise Ridge area transitioned from a cold and dry glacial environment to a warmer and dryer regime, which changed tundra and parkland areas into forests of pines and firs, as well as an expansion of shrubs and herbs. During the middle Holocene the modern Sunrise Ridge landscape stabilized as climate became cooler and wetter, creating environments for adapted species of fir, western hemlock and mountain hemlock. Late Holocene climate became cooler and wetter still. It was during the Holocene when dark mats at the SRBP site would have been exposed on the ground surface, being influenced by temporally associated climate and plant regimes.

Plant life at the SRBP site is characteristic of upper elevations of the Northwest Maritime Forest environmental zone situated between 2,000 and 5,800 feet (Burtchard 2003). Upper elevations of this zone correspond to the Mount Hemlock Zone described by Franklin (1966) situated between 4,000 and 6,000 feet. Tree species at the site's elevation include mountain hemlock, subalpine fir, pacific silver fir and western white pine (Burtchard 2003). These species were observed at the site (Lewis, 2015). Understory vegetation contains shrubs (blueberry and huckleberry), low herbs (dogwood and varieties in the lily family), and ground cover mosses.

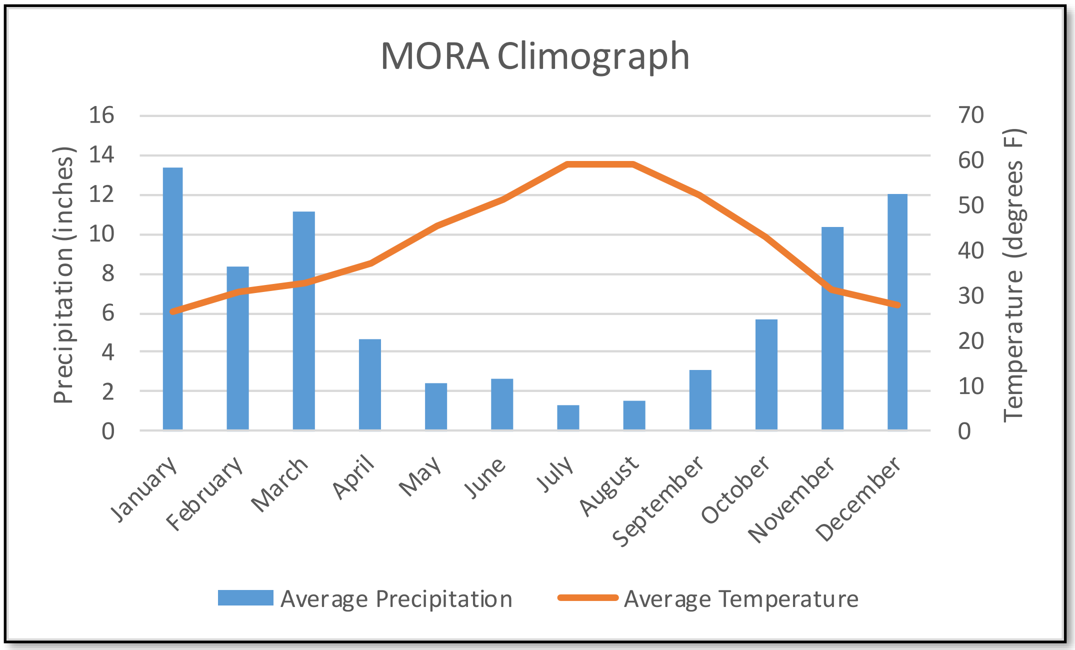

Figure 6. Climograph based on 1971 to 2000 climate normal precipitation and temperature averages from the White River Ranger Station. Data from Western Regional Climate Center (2018). Created in Microsoft Excel by Sean Stcherbinine.

Animals observed at the SRBP site include ants, worms and spiders (Evans, 2011). Animals known to be in the area that could potentially influence sediments include mice, voles, chipmunks, shrews, mountain beaver and marmots (Evans, 2011). Other animals known to be in the area include raccoon, coyote, deer, elk, cougar, and black bear (Evans, 2011). Evidence of burrowing animals, manifested as krotovinas, was observed during SRBP site excavations (McCutcheon et al., 2017).

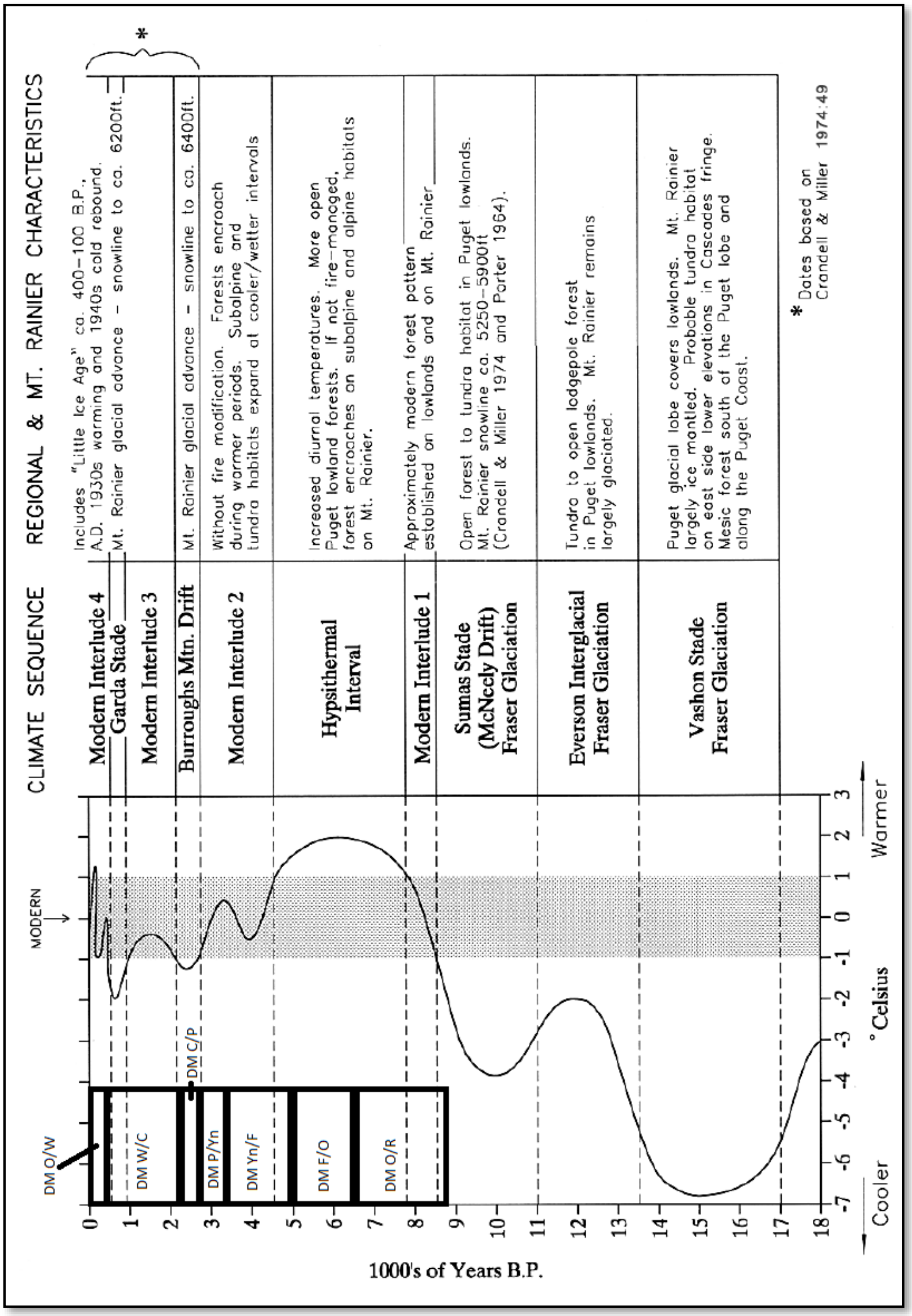

Figure 7. Climate and forest regime fluctuations of the Holocene. Dark mats (DM) with thicknesses based on years exposed have been amended to Burtchard's Climate Sequence Model (Burtchard 2003: 37).

Cultural Context

The SRBP site is located near the boundary of the Northwest Coast and Plateau culture areas (Walker, Jr., 1998). The Plateau culture area is geographically defined as lands drained by the Columbia and Frasier rivers, and as such, regions east of the Cascade Mountain Range (Walker Jr., 1998). The Northwest Coast culture area includes lands west of the Cascade Crest (Suttles, 1990). Culture area separation is based not only on geography, but distinctions among a variety of characteristics like settlement patterns, subsistence reliance, fishing technology, kinship systems (Walker, Jr., 1998:3). Mount Rainier and the surrounding Cascade Range is thought to represent lands used during the trans-Cascadian trade of regional resources like berries, mountain goat wool (Burtchard, 2003), marine shells (Dampf & McCutcheon, 2002), and obsidian (Parfitt & McCutcheon, 2017).

Archaeological data suggests lands now encompassing MORA have been used by humans for the past 8,500 to 9,500 years (Burtchard, 2007). However, the oldest dated site on Mount Rainier is the Buck Lake site (45PI438), dating to 7,925 to 8,001 calibrate years before present (cal BP) (Burtchard, 2007). It is unlikely Mount Rainier contains archaeological sites older than early Holocene times due to glacial ice (Burtchard, 2007). From the early Holocene until European contact, land use at MORA is sparse, but hypothesized to have evolved from low population, mobile foraging strategies that relied on lowland environments, to more population-dense, intensive collectors that utilized upland as well as lowland environments (Burtchard, 2007). As of 2008, almost 100 sites and isolates have been recorded at MORA (Burtchard 2007:4), nearly all of which occur in upper elevation forests, in subalpine and alpine environmental zones (Burtchard, 2007:4). Most of these sites are surface sites, with sub-surface sites either discovered during sub-surface surveys or contained surface artifacts easily observable during pedestrian surveys (personal communication Burtchard, 2014).

The SRBP site is a sub-surface precontact archaeological site that was initially documented by Rick McClure in 1990, where he noted a cut-bank exposure containing lithic debitage (McClure, 1990). The bank exposure was the scarp or edge of a borrow pit where sediments were gathered for the construction of Sunrise Road (Dampf, 2002). In 1998, Burtchard and Hamilton (1998) reevaluated the site, recording the presence of fire-cracked rock and a ground stone hammer head among the lithic tools observed. They proposed that the wide dispersion and dense concentration of surface artifacts suggested the site was the result of multiple occupations (Burtchard & Hamilton, 1998), and used as a precontact, residential base camp (Burtchard, 2007).

Beginning in 1997 Central Washington University conducted eight summer field school sessions as part of a National Park Service cooperative agreement, one task of which was to assess the site for eligibility to the national register of historic places (Dampf, 2002). During these summers, 30-centimeter diameter shovel test pits, 50-x-50 centimeter test pits, and 1-x-1 meter excavation units were excavated. Recovered artifacts consisted of chipped stone, ground stone, formed tools, and associated thermal features (Sheldon et al., 2013). Between 2011 and 2013, 8,621 of the 13,036 chipped stone artifacts recovered were from dark mats or strata recorded as a mixture of dark mats and tephra strata (McCutcheon et al, 2017). The fact that artifact concentrations have been recovered in association with dark mats suggested that they may represent stable surfaces. Thus, a significant amount of cultural materials were located in a potentially stable matrix with an unknown parent material and depositional environment.

CHAPTER III

GEOARCHAEOLOGICAL REVIEW

The following literature review provides the context of previous research and is organized to correspond to the objectives listed in Chapter I. Properties of forest soils, Spodosols, tephra-derived soils (Andisols), A horizon formation, and soil survey results relevant to the SRBP site and southern Washington Cascade Range are discussed. Previous research that used similar methods and techniques of grain-size analysis and geochemical analysis are described and discussed. Lastly, previous depositional history models used in archaeological contexts are reviewed.

Soils Review

Forest Soils

Franklin et al. (1988) summarizes soils of MORA by describing major diagnostic soil features, soil parent material and depositional environments, as well as typical stratigraphic profiles. Soils of MORA have a podzolic nature (spodosol diagnostic horizons) and contain buried soil horizons due to numerous pyroclastic depositional events. Soils typically develop in Holocene-aged glacial, colluvial, alluvial, or tephra parent materials. Among these parent materials, tephra resulting from Mount Rainier, Mount St. Helens, and Mount Mazama eruptions is the most common.

Individual soil layers in tephra-derived soils at MORA are distinguished by layers of ash, contrasting colors, and presence or absence of lapilli-sized grains (Franklin et al., 1988). Once deposited, tephra blankets the old surface, which may or may not contain developed A horizons that formed on the forest floor. Once buried and beyond the reach of soil forming processes, the former A horizon becomes a buried A horizon, existing under a layer of new tephra parent material (Franklin et al., 1988). Franklin et al. (1988) note numerous buried soil horizons resulting from volcanic eruptions, with one profile containing a buried A horizon intercalated between MSH-W and MR-C tephra (Figure 8).

Figure 5. Many of the soils in Mount Rainier National Park are formed in pyroclastic materials such as the conspicuous tephra W, the whitish deposit, underlain by coarse-textured lapilli of the tephra C.

Figure 8. Figure from Franklin et al. (1988:11) depicting a profile at MORA. The profile is described (Franklin et al., 1988:13) as follows: surface (organic duff); 0-2 centimeters below surface (cmbs): A21 (post W tephra); 2-8 cmbs: IIA22 (MSH-W tephra); 8-12 cmbs: IIIA21b (pre-MSH-W tephra); 12-20 cmbs: IVBirb (MR-C tephra); 20-35 cmbs: IVC1b (MR-C tephra); 35-47 cmbs: VC2b (MR-C tephra + unknown); 47-57 cmbs: VIC3b (MSH-P + unknown); and 57-77 cmbs: VIIC4b (unknown + MSH-Yn tephra).

As mentioned by Franklin et al. (1988), soils in the forests of MORA can be broadly characterized as having a podzolic nature and typically forming in tephra parent material. These two characteristics are similar to Spodosol and Andisol soil orders, respectively, which are two of the twelve soil orders described in soil taxonomy (Soil Survey Staff, 2014). Spodosol and Andisol soils are two of the most common soil orders mapped in the central Cascade Range and at MORA (Soil Survey Staff, 2014; Soil Survey Staff, 2018). Spodosol and Andisol soils are each defined by specific criteria involving the existence of diagnostic epipedons (surface layers) and general measurable properties, which are described below.

Spodosols

Spodosols typically occur in humid regions, under coniferous forests, where soil texture is relatively coarse, pH is acidic, with low clay content, and little agricultural potential. Spodosol profiles have a dark surface A horizon, underlain by pale-colored E horizon, underlain by a reddish B horizon. The diagnostic property of a Spodosol is evidence of eluviation of organic matter (OM), iron, and aluminum from the E horizon and illuviation of the same materials into the B horizon. In soil surveys, significant illuviation in the B horizon is symbolized as “Bs”, with “s” referencing an accumulation of amorphous sesquioxides and OM complexes. The Bs horizon is known as a spodic horizon. This phenomena results from the interaction between high precipitation, acidic surface litter in a coniferous forest, and coarse-textured soils, which creates high levels of amorphous materials. Presence of a spodic horizon and albic horizon (E horizon) are diagnostic features of a spodosol. When assigning a specific soil to one of the twelve soil orders, the diagnostic spodic and albic horizons that typify a Spodosol take precedent over andic soil properties that typify an Andisol. For example, if a soil shows both spodic and andic soil properties, the soil is a Spodosol (Soil Survey Staff, 2014).

Tephra-Derived Soils

Volcanic eruptions have significantly influenced the properties and development of forest soils in the Cascade Range (Kimsey, Gardner, & Busacca, 2007). Soils formed fully or partially from volcanic ejecta have different physical and chemical properties compared to other types of soils (McDaniel & Wilson, 2007). Unique properties of tephra-derived soils include low bulk density resulting from the porous nature of accumulated deposits, and presence of glass (McDaniel & Wilson, 2007). Grain sizes of pyroclastic deposits decrease with distance from the source volcano. For example, regions of central Oregon contain Mount Mazama-derived strata dominated by pebble-sized grains (McDaniel & Wilson, 2007). Contrast this with Mazama-derived strata near Mount Rainier that contain mostly silt and sand-sized grains (Mullineaux, 1974). Within coarse tephra deposits like MR-C observed inside MORA, normal grading has been observed, which takes the form of coarser, lapilli-sized grains occurring at the bottom of a deposit (Mullineaux, 1974). After deposition, tephra-derived soils can be influenced by reworking, additions of loess, and soil forming processes of physical and chemical weathering, bioturbation, humification, eluviation, and illuviation (McDaniel & Wilson, 2007; Lowe, 2010).

Tephra deposits are influenced by the following six soil forming factors: parent material, climate, topography, organisms, time, and humans (Brady & Weil, 2010:32).

These factors cause recently deposited tephra, in much the same way as other types of sediments, to develop into soil. Tephra-derived soils are known for rapid accumulation of dark, organic-rich surface horizons that can be diagnostic (Brady & Weil, 2010:71). Quickly forming, dark surface horizons that are known to weather into A horizons, as explained above, are a potential explanation of the formation of dark mats at the SRBP site.

Tephra-derived soils are known for a lack of translocation of colloids (clay-sized particles) downward through the soil profile, and little profile development generally (Brady & Weil, 2010:71). After tephra is deposited by a volcanic eruption, soil formation begins immediately at the surface of the deposit (Brady & Weil, 2010:12-13; 49-51). If given enough time, inputs of organics, other weathering processes, and stability, an A horizon will form at the surface of the tephra deposit. In montane environments of volcanically active regions, A horizons that form in tephra are often buried by subsequent eruptions. If conditions are right, this results in a stratigraphic sequence of alternating buried A horizons that formed in tephra parent materials (Scarciglia, Zumpano, Sulpizio, Terribile, Pulice, & La Russa, 2014).

Andisols

Andisols form in volcanically-derived parent materials that include tephra, lava flows, pyroclastic flows, lahars, and other pyroclastic materials. As a result, Andisols are located in regions with active or recently active (Holocene) volcanoes, typically in mountainous areas with moderate to high rainfall, and cool temperature regimes. The diagnostic property of Andisols is a presence of numerous short-range-order compounds that include ferrihydrite, aluminosilicates, and organometallic complexes, collectively known as andic soil properties. The presence of such compounds is due to volcanic ash being mineralogically unique compared to other parent materials. After ejection, volcanic materials cool so rapidly it prevents the crystallization of long-range atomic order minerals, instead creating vitric material (glass). This results in a highly weatherable soil parent material compared to crystalline types, such as quartz. In addition to andic properties, Andisols typically contain buried A horizons (Ab horizons) that become covered under sequential eruptions. Andisols also typically contain weakly weathered, occasionally buried B horizons (Bw horizons), where the "w" references development of structure and color in a horizon with little or no illuviation, contrasting to a Bs horizon (Buol, Southard, Graham, & McDaniel, 2011).

Soil Horizons and Properties of A Horizons

A soil pedon (or profile) is made up of master horizons, which are a series of visible layers. From the ground surface to the bottom of a pedon, horizons are typically ordered as O, A, E, B, C, and R. Additionally, there are horizon designations used less often, that for limnic materials (L), human-manufactured materials (M), and water layers (W). Specific to this study, soil A horizon requires review. Soil A horizons are a mineral soil horizon that forms at the earth's surface or under an O horizon. A mineral soil horizon is one defined as being composed of mineral soil material, which is defined as containing less than 20% organic carbon content (by weight) (Soil Survey Staff, 2014). Conversely, organic soil material is defined as containing greater than 20% organic carbon content (by weight), also referred to as OM content. Soil O horizons are defined as horizons containing organic soil material, therefore, a soil horizon having greater than 20% OM content would be classified as an O horizon (Soil Survey Staff, 2014).

Soil A horizons are further defined as mineral soil horizons that have an accumulation of humified organic material intermixed with the mineral matrix and not dominated by properties diagnostic to underlying E, B or C horizons. Properties diagnostic to E, B, and C horizons can be generalized as exhibiting eluviation, illuviation, and showing no alteration by soil forming processes, respectively. Soil A horizons overlying B horizons can have lower percentages of clay size particles because of eluviation from the A to the B horizon. Recent aeolian or alluvial deposits that contain much of the original rock structure cannot be classified as A horizons, the exception being if they are cultivated (Soil Survey Staff, 2014).

A horizons are typically dark in color as a result of the accumulation of humified organic matter, and darker than underlying E, B, and C horizons (Soil Survey Staff, 2014). When color is described using a Munsell soil color chart, dark color is reflected by a low value and low chroma. For example, a 10YR 3/2 corresponds to very dark grayish brown color and a 10YR 7/6 corresponds to a yellow color. The set of numbers after the "10YR" represents the value and chroma, respectively. Dark grayish brown is darker than yellow, which is why it has a lower corresponding value and chroma.

Soil Survey Review

Only one mapped soil unit encompasses the SRBP site (Soil Survey Staff, 2018). The mapped unit symbol is 9220, representing the Tipsoo-Owyhigh-Mysticlake Complex, 20 to 65 percent slopes. A soil complex is a mapped unit that is characterized by two or more types of soils, known as a series. In this case, the SRBP site area has been mapped as the Tipsoo-Owyhigh-Mysticlake Complex, which means, an area likely to have soil properties of each named soil series.

The Tipsoo Series' taxonomic class is medial, glassy Andic Haplocryods (Spodosol). The soil forms in volcanic ash over colluvium, and is found on mountain slopes, cirques, glacial valley walls, and ridges. A typical pedon consists primarily of sandy loam, and is found on forested, north-facing ridges with 40% slopes at an elevation of 1,745 m. The pedon contains E, Bhs, Bs1, and Bs2 horizons identified as MSH-W, MR-C, MSH-P, and MSH-Yn tephras, respectively. However, the pedon lacks A horizons, buried or surficial. Refer to Appendix A for more details on the soil series' discussed in this section.

The Owyhigh Series' taxonomic class is medial, glassy Andic Haplocryods (Spodosol). The soil forms in volcanic ash over colluvium over andesite, and is found on bedrock benches, ridges, glacial valley walls, and cirques. A typical pedon consists primarily of sandy loam, and is found on a forested, north-facing glacial valley wall with 35% slopes at an elevation of 1,597 m. The pedon contains E, Bs1, and Bs2 horizons identified as MSH-W, MR-C, and MSH-Yn tephras, respectively. However, the pedon lacks A horizons, buried or surficial (see Appendix A).

The Mysticlake Series' taxonomic class is medial, glassy Typic Cryaquands (Andisol). The soil forms in volcanic ash over colluvium, and is found on debris aprons, glacial valley walls, and cirques. A typical pedon consists primarily of sandy loam, and is found on a west-facing forested debris apron with 20% slopes at an elevation of 1,625

m. The pedon contains A2, Bw, Bg1, Bg2, and Bg3 horizons identified as MSH-W, MR-C, MSH-P, MSH-Yn, and MR-F tephras, respectively. However, the pedon lacks buried A horizons, only containing two surficial A horizons overlying MSH-W and underlying organic horizons (see Appendix A for more details).

The Mountwow Series is part of two complexes mapped one kilometer north of the SRBP site, near Sunrise Lake at an elevation of about 1,750 m. The series is not on a similar landform or at the same elevation as the SRBP site. However, it has a similar stratigraphic profile (pedon). The Mountwow Series' taxonomic class is medial, glassy, acid Thaptic Cryaquands (Andisol). The soil forms in volcanic ash over colluvium, and is found on swales cirques, and parklands. A typical pedon consists primarily of sandy loam, and is found on a meadow or north-facing cirque with 2% slopes at an elevation of 1,805 m. The pedon contains A, Bw1, Bw2, Bw3, Agb, Bgb1, Bgb2, and Bgb3 horizons identified as MSH-W, MR-C, MSH-P, MSH-Yn, unknown, MR-F, MR-D, and MAZ-O, respectively. The pedon contains a buried A horizon with no known parent material between MSH-Yn and MR-F, and a buried A horizon underlying MAZ-O tephra, described as forming in colluvium.

Grain-Size Analysis

Grain size is the most fundamental characteristic of a sediment because the composition of grains, their size and sorting can provide basic information on sediment source, transport agent, environment of deposition, and post-depositional alternations (Stein & Deo, 2003).   Grain-size analysis (GSA) is a method commonly used when classifying sedimentary environments (Blott & Pye, 2001). Individual grains fall under a size range spectrum classified from clay size (< 2µm) to boulder size (< 25.6 cm). The grain-size scale used commonly by American archaeologists, in soil science and by the United States Department of Agriculture is used in this study. GSA results in a frequency of size classes from a population of many grains. For example, a sample dominated by grains measuring between 0.062 millimeters (mm) and 2 mm is considered a sand. A single grain measuring between 0.25 mm and 0.5 mm is considered a grain of medium-sized sand, or medium sand.

There are several techniques commonly used when conducting a GSA, each suited to the size of grains measured (Goldberg & Macphail, 2006:336-337). All grains are grouped into two size categories: fine fraction (< 2 mm in length) and coarse fraction (> 2 mm in length). The coarse fraction corresponds to pebbles, cobbles, and boulders. The fine fraction corresponds to sand silt, and clay. Simple length measurements using a caliper or hand sieving with nested screens are typical techniques used to measure a sample consisting of coarse fraction-sized grains. Wet screening is a typical technique for sand-sized grains. Hand sieving is used for sand-sized grains as well, but wet screening is preferred because it is more accurate. A laser particle analyzer is a commonly used and accurate way to measure silt and clay-sized grains (Goldberg & MacPhail, 2006).

Grain size analysis has long been used when investigating a sediment's parent material and depositional environment (Folk & Ward, 1957; Blott & Pye, 2001; Bertrand & Fagel, 2008). Lirer et al. (1996) explain GSA as an essential first step in documenting the provenance of clastic deposits, and vital to understanding how grain size is often a function of transport mechanisms and depositional processes. Friedman, Sanders, & Kopaska-Merkel (1992:32) stress that the distribution of sizes in sediments relate to (1) availability of parent material grain size; (2) processes operating during transport and deposition; and (3) post-depositional processes operating after deposition. Because GSA is relatively simple and economical method that yields data useful for understanding sediment origin and deposition, it is a common earth science method borrowed by geoarchaeologists (Goldberg & McPhail, 2006:336).

A grain-size distribution is the product of a GSA, which indicates the proportion of grains expressed in weight percent or volume percentage of a particular size interval (Mycielska-Dowgiallo & Ludwikowska-Kedzia, 2011). Grain-size distributions are typically visualized through diagrams in the form of bar graphs, frequency curves, cumulative frequency curves, and probability curves (Burrman et al., 2004; Evans, 2011; Gallello et al., 2013) (see Figure 9 for example of a frequency curve).

Tanner's (1995) research points out that displaying grain-size distributions as frequency curves reveals sub-populations that may be the result of multiple depositional events or post-depositional processes like stratigraphic mixing. Probability curves are viewed as the most robust analytical tool among the grain-size curve types because normal distributions (bell curves) are plotted as straight lines. Deviations from a straight line are viewed by Tanner (1995) as potential additional depositional events, the result of stratigraphic mixing, or influences from multiple depositional environments. Using a comparative approach, multiple curves can be placed on the same diagram to see if multiple distributions share similar depositional environments or histories (Tanner, 1995).

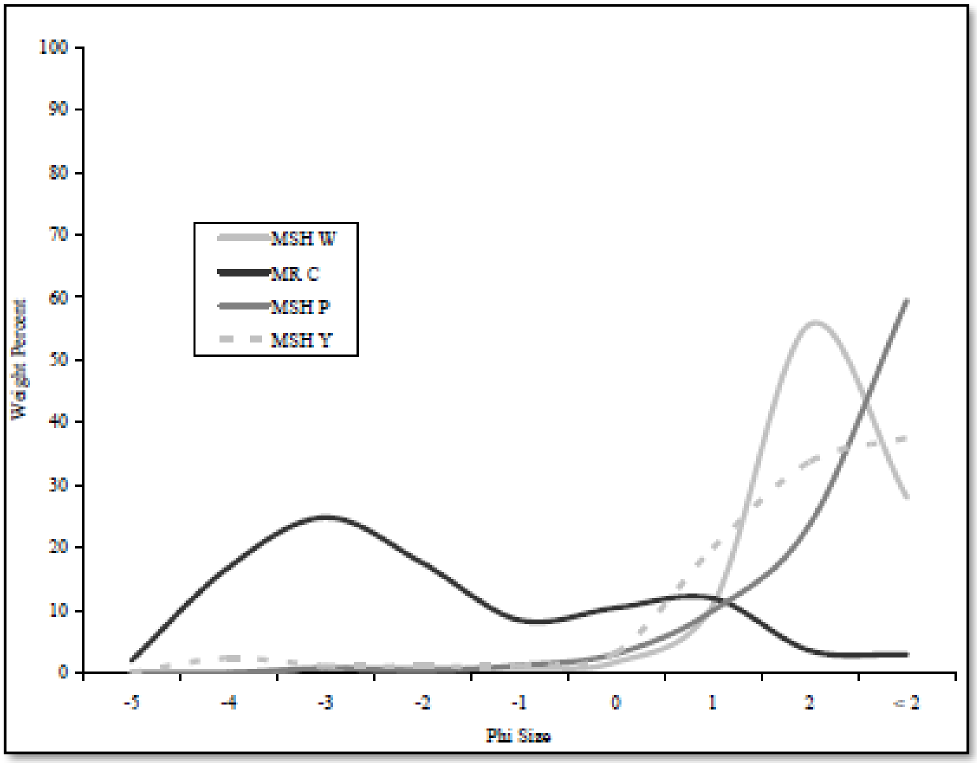

Figure 9. Grain-size distribution frequency curves from the SRBP site (Evans, 2011:81).

Measures of central tendency are used when quantitatively comparing grain-size distributions (Tanner, 1995; Blott & Pye, 2001). Parameters used are those measuring: (1) the average size; (2) the spread (standard deviation affected by sorting) around the average; (3) the symmetry or preferential spread (skewness); and (4) the degree of concentration of grains relative to the average (kurtosis) (Blott & Pye, 2001:1238-1240). GRADISTAT, a computer program, is often used to plot grain-size distributions and calculate measures of central tendency (Bertrand, Castiaux, Juvigne, 2008:349; Gatti, Saidin, Talib, Rashidi, Gibbard, & Oppenheimer, 2013:232). GRADISTAT runs in Microsoft Excel and is offered free online (http://www.kpal.co.uk/gradistat.html). Once GRADISTAT has calculated statistics the data can be more easily analyzed, presented, and compared.

Grain-size statistical data has been used to discuss the depositional environments of sediment samples from unknown settings (Pettijohn, 1975:51; Lewis & McConchie, 1994:118-121; Lirer & Vinci, 1991), and used to determine quantitative relationships between sediments from the same soil profile/pedon (Gatti et al., 2013). Pettijohn (1975:51) demonstrates how standard deviation and skewness of grain sizes can show observable distinctions between two types of depositional environments. Lewis and McConchie (1994:121) demonstrate that the relationship between skewness and standard deviation can be used to distinguish sands from different depositional environments. Lirer and Vinci (1991) use statistical parameters of tephra grain-size distributions to distinguish different types of pyroclastic deposits, clearly differentiating pyroclastic fall, flow, and surge deposits from the relationship between median grain size and standard deviation.

It is critical to understand whether a grain-size distribution is homogenous and unimodal, or represents collections of subpopulations, each possibly the result of different types of grain transport (Lirer & Vinci 1991:1075). This understanding has led researchers to more accurately characterize samples as containing either homogenous grain sizes or mixed grain sizes. If a sediment sample’s grain-size distribution is polymodal (consisting of subpopulations), any accurate characterization of the sediment will require exploration of the processes responsible for multiple modes (Lirer et al., 1996:914), whether due to multiple deposition events, or soil forming processes such as bioturbation or illuviation. Polymodal grain-size distributions have been associated with complex depositional environments associated with reworked tephra (Gatti et al., 2013), as well as sheetwash and rill erosion (Jones, 2010).

Geochemical Analysis

Geochemical or multi-element analysis is a method commonly used when attempting to identify the origin of rock, sediment, or soil (Huff et al., 1992; Douglas et al., 2003; Miller et al., 2015). The method is based on the concept that rocks and their weathered products (sediment and soil) contain a unique chemical signature. This signature, termed tracer or geochemical fingerprint, is used to classify rocks to a source outcrop, eruption, consolidation event, etc. Once a sample is measured for chemistry, its chemical fingerprint can be compared to geologic sources with known fingerprints to discuss the sample's parent material candidates.

There are several types of geochemical analyses, each suited for specific research goals (Miller et al., 2015). The principal analyses measure: (1) major elements (e.g. silica and aluminum); (2) rare earth elements (e.g. lanthanum and ytterbium); (3) trace metals and metalloids (e.g. copper and zinc); and 4) isotopic ratios (e.g. $^{204}Pb/^{206}Pb$). Some geochemical analysis techniques measure multiple types of the above groupings. For example, most x-ray florescence techniques measure major and trace elements.

The geochemical fingerprint most often used when determining the origin of sediments in volcanic, montane environments is the relationship between alkali (potassium and sodium) and silica, referred to as total alkali silica or TAS (Fujioka, Nishimura, Matsuo, & Rodolfo, 1992; Donoghue, Vallance, Smith, & Stewart, 2007; Bertrand et al., 2008). TAS is also the elemental relationship used to classify extrusive igneous rocks, because those extrusive rocks are a parent material source other than direct ash fall in volcanic regions. TAS diagrams are used to articulate this relationship between alkali (expressed as weight percent Na_2O+K_2O) on the y-axis and silica (expressed as weight percent SiO_2) on the x-axis (Figure 10).

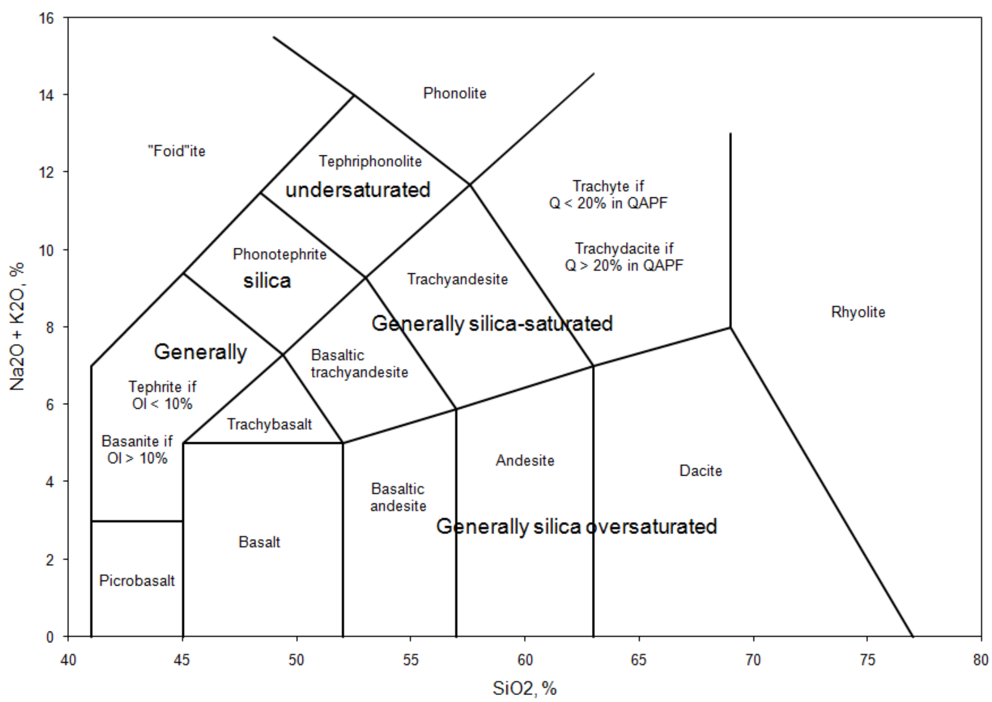

Figure 10. TAS diagram example (Le Bas, Le Maitre, Streckeisen, Zanettin, & IUGS, 1986:747).

Because soils in volcanically active, montane settings often form from pyroclastic ejecta (Brady & Weil, 2010:70), elemental proportions, like TAS, can be an indicator of parent material and depositional environment (Fujioka et al., 1992; Bertrand et al., 2008). Bertrand and Fagel (2007) used TAS proportions to suggest that a poorly understood soil's parent material was consistent with regional volcanism, and not the result of loess. Scarciglia et al. (2014) used ratios of Si:Zr and Ti:Zr to characterize a buried soil intercalated between tephras as having either single or multiple parent materials, affecting its depositional history. Donoghue, Vallance, Smith, & Stewart (2007) used TAS proportions to identify, discriminate, and correlate andesitic tephras within the Mount Rainier area. Those authors used the X-ray fluorescence technique to distinguish types of lapilli tephra, and along with stratigraphic position, facilitate correlations between profiles that shared similar depositional histories.

Sisson and Vallance (2009) used a multi-method approach to investigate previously un-recorded late-Holocene eruptions of Mount Rainier. Using the relationship between SiO_2 and Al_2O_3, the authors were able to discuss how the chemical signatures of unknown tephras related to known tephras (Figure 11). This allowed complex depositional histories in the study area to be unwound, permitting ambiguous tephra deposits a place in the depositional history model.

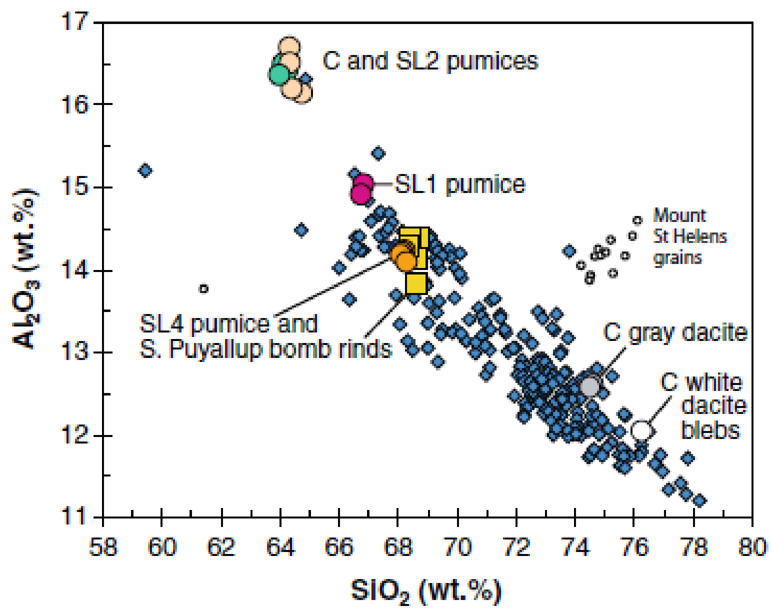

Figure 11. Diagram showing the relationship between weight percent SiO_2 and Al_2O_3 from individual glass-rich grains and tephra fragments collected near Mount Rainier (Sisson & Vallance, 2009:609).

Whole rock chemical composition from the ejecta of major Cascade Range eruptions found in MORA shows several trends. Tephra from Mount Rainier eruptions is andesitic in nature, characterized by approximately 55% to 60% silica (Mullineaux, 1974:73). However, silica content of the glass found within tephra fragments ranges considerably and can exceed 70% (Mullineaux, 1974:73; Sisson & Vallance, 2009). Mullineaux (1974) also notes that several MR-C tephra deposits suggest ejecta from magma of different chemical compositions, indicating magma sources of pyroclastic material were not homogeneous. This could explain slight differences in silica content of MR-C, for example, from different studies (Mullineaux, 1974; Sisson & Vallance, 2009).

Silica content of whole rock tephra from Mount St. Helens and Mount Mazama eruptions found in MORA is higher than that of Mount Rainier Eruptions, usually exceeding 60% (Mullineaux, 1974). This exotic tephra inside MORA is expected to have higher silica even if the source volcanoes are not known to be silica rich. This phenomena is due to eruptions of silica-rich magma being more explosive compared to mafic magma, which would spread farther in a plume from the source volcano (Mullineaux, 1974).

Depositional History Models

The depositional history of a stratigraphic sequence explains: 1) the process depositing sediments of each strata; 2) where the source sediment originated; 3) the age; and 4) post-depositional processes, if present, that occurred after original deposition (Schiffer, 1987; Goldberg & McPhail, 2007). Documenting the depositional history at an archaeological site, especially a subsurface site, is necessary to accurately contextualize subsurface artifacts and features (Goldberg & McPhail, 2007). Once documented, it can be used to model relationships between strata properties and associated cultural materials. For example, a stratum with a parent material and depositional environment associated with rapid sedimentation influences the interpretation of the archaeological record occurring within that stratum (Holdaway & Wandsnider, 2009). The following describes three examples of how depositional history models have been used to better understand the archaeological record.

Fedje et al. (1995) created a depositional history model that combined stratigraphic location, depositional environment, radiocarbon dates, faunal remains, and artifacts to show that locations of discrete cultural deposits represent intact stable surfaces (Figure 12). The model confirmed at least six cultural components at the site, significantly contributing to the knowledge of Paleo-Indian land use in a region of Alberta. Neall, Wallace, and Torrence (2008) created a depositional history model that demonstrated site use corresponded with soil formation during intervals between volcanic events (Figure 13). Site-use intensity and character were interpreted as being dependent on the scale of the associated volcanic event. After significant events, humans abandoned the region entirely. After short duration events and during prolonged ash fall, site-use intensity suggests humans were able to tolerate or adapt to this type of environment (Neall et al., 2008). Fitzsimmons, Stern, and Murray-Wallace (2014) created a depositional history model integrating the paleoenvironmental and archaeological record (Figure 14). The model shows that the archaeological record is present in every depositional environment, demonstrating humans occupied the study area in every environment type after 50,000 years BP.

The three models discussed show the usefulness of creating site depositional history models that organize natural environmental processes influencing the site to contextualize recovered data. Drawing from stratigraphic paleoenvironmental, artifact, feature, and radiometric dating information, the models consolidate site data and explain the depositional context of artifact concentrations. These models act as a framework that guides the creation of the SRBP site depositional model, the main objective of this study.

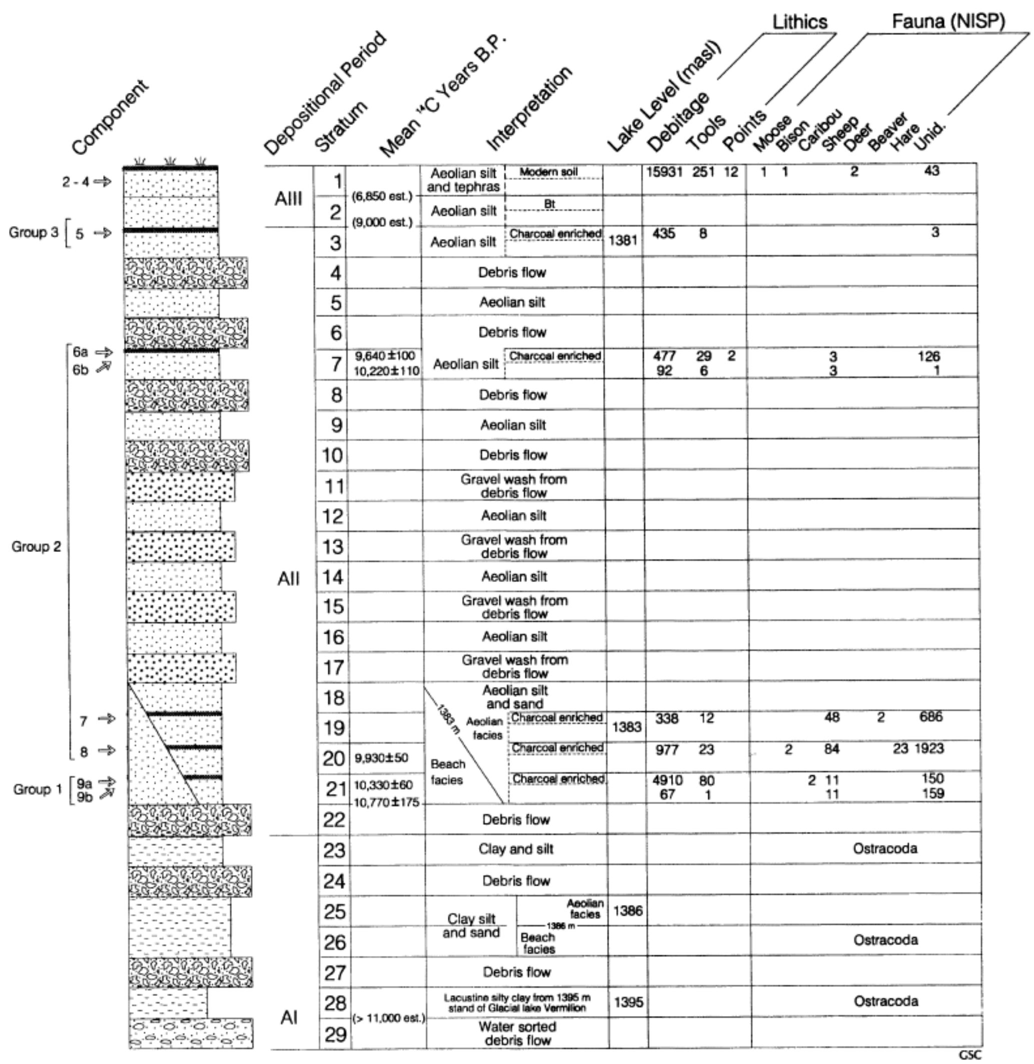

Figure 12. Depositional history model of the Vermillion Lakes Site in Banff National Park, Alberta, Canada (Fedje et al., 1995:86).

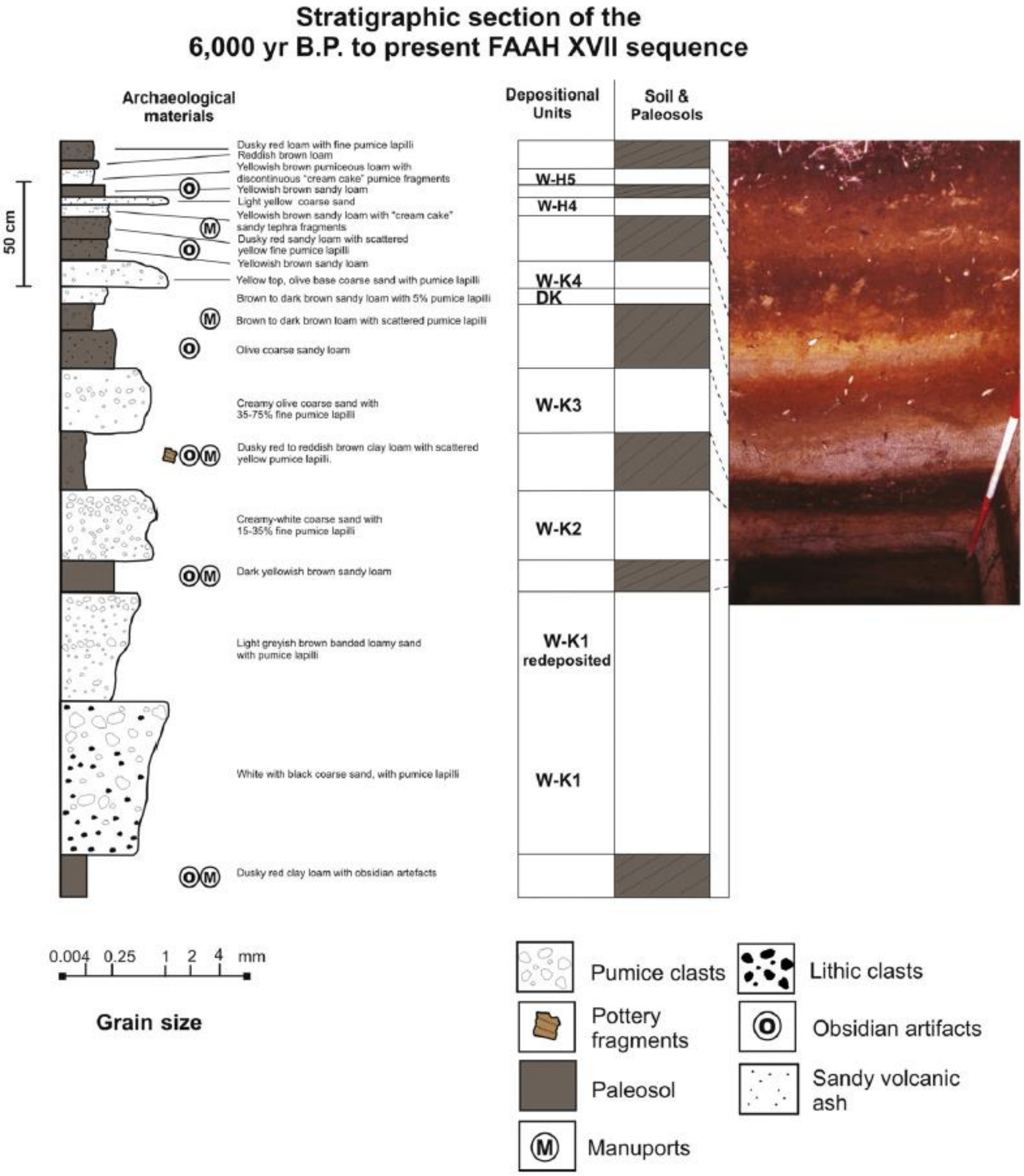

Figure 13. Depositional history model of the FAAH XVII site on the Willaumez Isthmus, West New Britain, Papua New Guinea (Neall et al., 2008:334).

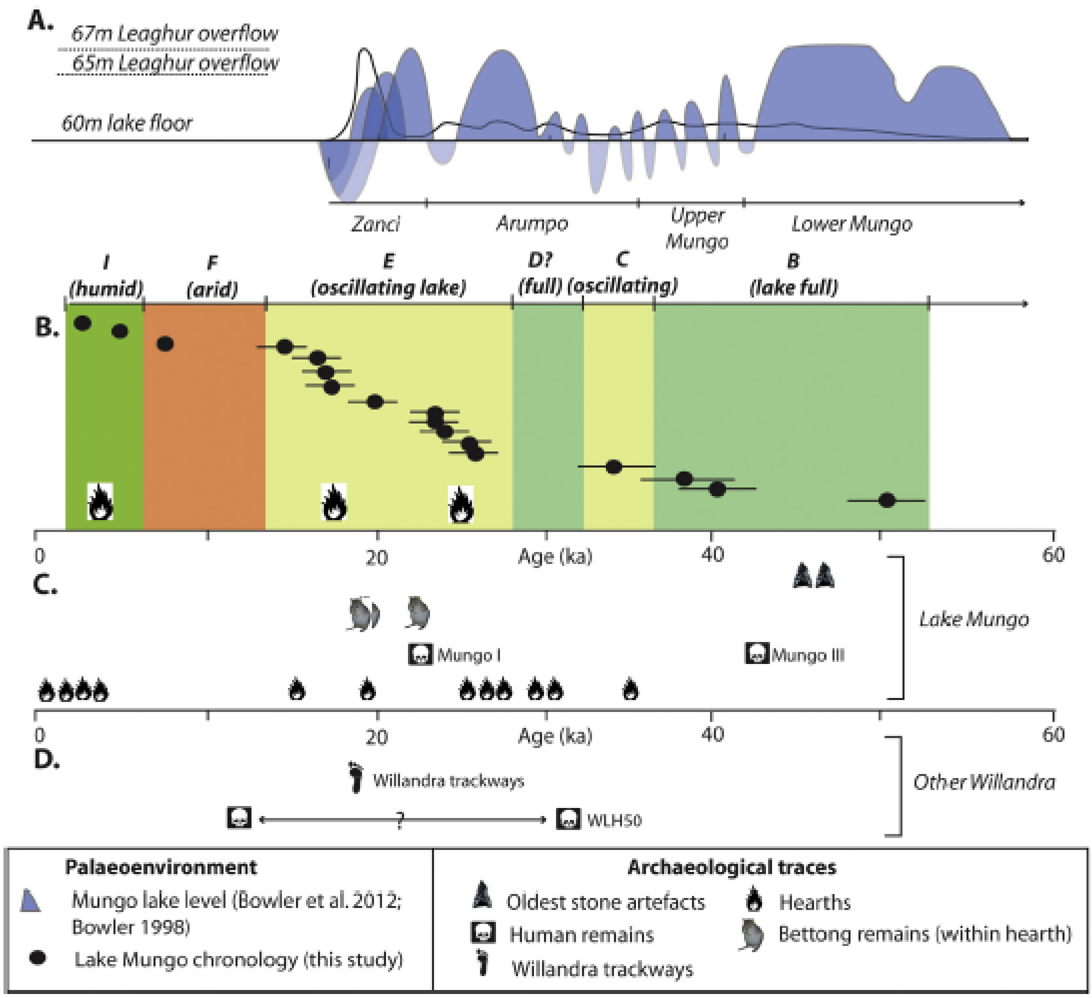

Figure 14. Depositional history model at central Lake Mungo Iunette, Willandra Lakes, Australia (Fitzsimmons et al., 2014).

CHAPTER IV

METHODS

This chapter details the materials, methods, and techniques used to carry out the purpose of establishing whether or not there are depositional relationships between dark mats and tephra strata at the SRBP site. This chapter is split into two main sections that separate the grain-size analysis (GSA) from the geochemical analysis. Sections are split further to organize details of sample selection, collection, and measurement. The GSA will be described first as it was the initial laboratory component that dictated sample collection for the geochemical analysis. Following these two main sections, construction of the depositional history model will be briefly explained.

Grain-Size Analysis

Sample Selection and Collection - Excavation Areas

The SRBP site contains four primary excavation areas: 30N, 61.5N, 64N, and 71.5N areas (Figure 15). Excavations and column sample extraction occurred during 2011 through 2013 summer field schools. Each excavation area was composed of contiguous 1-x-1 m excavation units that were excavated stratigraphically (i.e. by natural strata) using trowels. Column sample locations were selected from each excavation area in the least disturbed location containing the largest number of dark mats and tephra strata observed in that excavation area. A total of 13 column samples were collected at the SRBP site excavation areas by prior researchers; four were chosen for this study. A column sample is analogous to a narrow slice of layer cake. It consists of a series of individual bulk samples of each strata observed in that excavation unit. Column samples were approximately one m tall (depending on excavation unit depth) by 20 cm wide by 10 cm deep (Figure 16).

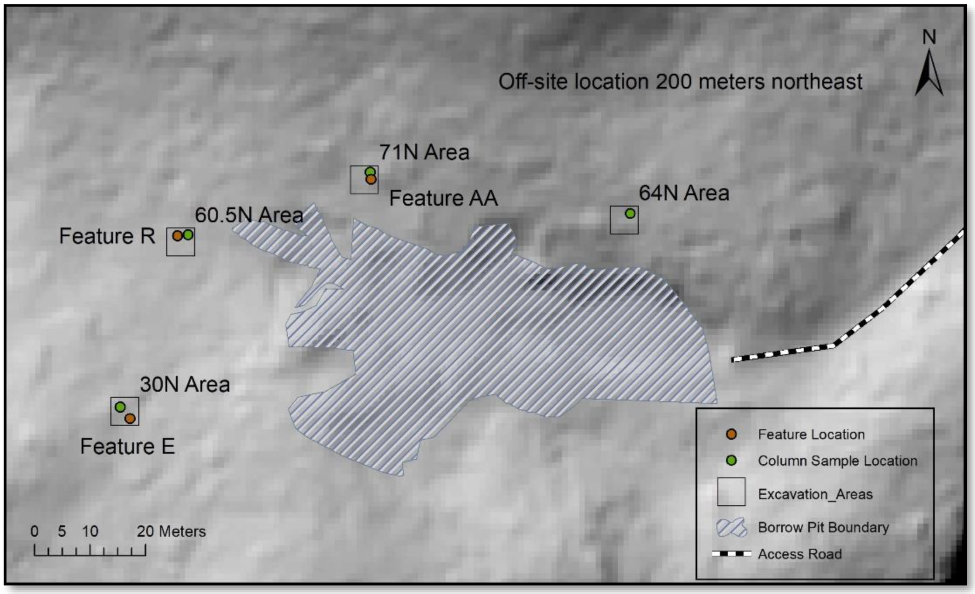

Figure 15. Map showing the SRBP site's main excavation areas, approximate column sample and feature locations, and access road. Created in ArcGIS 10.4.1 by Sean Stcherbinine.

Figure 16. Column sample at excavation unit 30N/24E (north wall). Scale is one meter long. Photo taken by Anne B. Parfitt in 2013.

During 2011 through 2013, individual bulk samples from each observable dark mat and tephra strata were extracted from each column in a sequence beginning at the ground surface and ending at the excavation unit floor (see Figure 16). This technique is the same as horizon sampling, which is a common soil science sampling technique (Schoeneberger, Wysocki, Benham, & Soil Survey Staff, 2012). Horizon sampling involves taking a bulk sample of the entire horizon (or stratum), top to bottom, as opposed to incremental sampling (e.g. every 10 cm) or fixed depth sampling (e.g. 10 cm, 50 cm, 100 cm, etc.) (Schoeneberger et al., 2012). Each bulk sample was placed in a plastic bag and labeled with the strata as recorded in the field, elevation, date, and excavator. Column samples (series of bulk samples) were then brought back to CWU and air-dried indoors. In 2014 all 13 column samples stored at CWU were assessed, with one column sample that best represented overall site stratigraphy chosen from each of the four excavation areas for this project, for a total of four column samples. It is the bulk samples from these four column samples that are used in this study (n = 35). The four column samples chosen were from excavations units 30N/24E, 61.5N/36E, 64N/115E, and 71.5N/66.5E (see Figure 15). Refer to Appendix B for a list of samples, unit association, stratigraphic location, and the depositional unit they were recorded as.

Sample Selection and Collection - Features

Twenty-nine cultural features were recorded by field school students at the SRBP site during 2011 through 2013 excavations. Most features consisted of unstructured fire cracked rock (FCR) and discolored sediment (Figure 17). During fieldwork, features were bisected with half excavated and screened in the field and half collected as a bulk sample and brought back to CWU. Only features recorded in dark mats and associated with other evidence of occupation (e.g., lithics, burned bone, and fire-cracked rock) were considered for this study. Feature R (associated with dark mat W/C), Feature AA (associated with dark mat C/P), and Feature E (associated with dark mat P/Yn) were selected for this study (n = 3).

Figure 17. Feature AA in excavation unit 71.5N/66.5E. The feature was classified as an unstructured surface feature associated with the dark mat between MR-C and MSH-P tephras. Photo taken by by Anne B. Parfitt in 2013.

Sample Selection and Collection – Off-site Sample

A comparable landform approximately 250 m northeast of the SRBP site's northeastern boundary was selected for the off-site sample. The location was chosen because of its proximity to the SRBP site and shared characteristics, which include elevation, biology (Northwest Maritime Forest), landform location (mid-slope), landform type (remnant of a glacial kame terrace), and landform shape (relatively flat). During the fall of 2014, a 1-x-1 m excavation unit was excavated by Anne B. Parfitt and the author on the landform in the only flat area lacking deadfall or living trees. The off-site sample was excavated from ground surface to 140 cm below ground surface, by natural level, with all sediments sifted through 1/8 inch mesh. No cultural materials were observed.

Ten strata were observed in the off-site unit, which consisted of six tephra strata, three dark mats, and one surface organic stratum (forest litter or duff). With the same technique previously discussed, a column sample measuring 140 cm tall by 20 cm wide by 10 cm deep was extracted from the wall with the least observable disturbances (Figure 18). The column sample consisted of bulk samples from six tephra strata and three dark mats, placed in one-liter bags, and labeled with the observed depositional unit, and elevation (n = 9) (see Appendix B for sample data). The upper most organic horizon was omitted due to being composed almost entirely of poorly decomposed organic matter (an Oi horizon), and therefore not suitable for this study. Anne B. Parfitt, who holds a geology degree and worked on the SRBP site for two field seasons excavating and documenting stratigraphy, assisted with sampling.

Figure 18. Column sample at off-site excavation unit. Photo taken by Sean Stcherbinine in 2014.

Measurement

In total, column samples from four excavation units (n = 35), features (n = 3), and an offsite column sample (n = 9), for a total of 47 samples were used in this study. Refer to Appendix B for a list of all 47 samples, which excavation units they were sampled from, and sample elevations. Three techniques were used to measure the grain size of 47 sediment samples: dry sieving, wet sieving, and laser particle analyzer. The GSA was conducted on the second floor of Dean Hall, second floor of Hebeler Hall, and second floor of Farrell Hall at CWU by the author and Dr. Ian Buvit in the spring of 2015. Dr.

Buvit holds a PhD in Anthropology and focused on geoarchaeology in his graduate research.

Grains larger than 1/8 inch were measured by pouring bulk samples into a column of nested sieves measuring 1 inch (-4.7 phi), ½ inch (-3.7 phi), ¼ inch (-2.7 phi), and 1/8 inch (-1.7 phi). Organic debris, mostly roots, observed in samples were removed by hand, placed in separate bags, weighed, and total sample weights were adjusted to reflect removal as this study was not concerned with the various sizes and weights of roots. The column was gently shaken for 15 minutes by hand. Sediments caught in each sieve were weighed and recorded. Grains smaller than 1/8 inch (3.175 mm) were caught in the pan, weighed, recorded, then poured into a Humboldt riffle-type sample splitter to produce representative samples weighing at least 100 g for further analysis.

The 100 g sample size was based on recommendations of Lewis and McConchie (1994:95), who note that the sample weight used in a sieving analysis be proportional to the largest grain size found in substantial proportion within a sample. This ensures measurements accurately reflect the grain sizes of the larger population. Since all samples should be substantially in the sand-sized range or smaller (Evans, 2011:81-82), Lewis and McConchie (1994) recommend a sample weight of no less than 100 grams.

Wet sieving was used to measure the grain sizes smaller than 3.175 mm (granule-sized) and larger than 0.062 millimeters (coarse silt). This size range represents all sand-sized and granule-sized grains (also called very fine pebbles). Wet sieving is preferred to the Ro-tap technique due to the friable nature of tephra, which if crushed can introduce error into quantitative analyses (Fisher & Schmincke, 1984). Samples weighing 100 g were poured into a stacked column of five United States standard mesh sizes with a collection pan at the bottom. The sieve mesh measured -1, 0, 1, 2, 3, 4, phi representing the lower size limits of very small pebbles (granules), very coarse sand, coarse sand, medium sand, fine sand, and very fine sand, respectively.

Before wet sieving, a lid was placed on the top sieve and the column was gently shaken for 15 minutes as recommended by Lewis and McConchie (1994) and followed by Evans (2011). This dry sieving component was undertaken to create fine fraction (silt and clay – smaller than the 4 phi screen) sub-samples for future laser diffraction measurements. Fine fraction sub-samples were bagged, labeled, and set aside.

Next, the bottom pan was removed and water was run through the sieves until no more grains (silt and clay size) passed through the smallest mesh. The sieve column was then disassembled while keeping the newly sorted samples in their respective sieve, then air dried for at least 48 hours. Sorted samples were weighed and sample properties were recorded on a sieve analysis data sheet. The difference between the total weight retained in the various sieves and original weight represented the weight of silt and clay-sized grains lost during flushing, for which there was already a sub-sample. Organics caught in sieves were minimal if present, and consisted of very fine, almost hair-sized roots. As described above, they were removed with all totals adjusted to normalize the weights. Sample properties included date, sample number, depositional unit, screen size, gross weight, weighing paper weight (weight inside screen), net sample weight retained, individual weight percent, and cumulative weight percent. All newly sorted samples representing each size class measured were placed in individual bags and labeled for future geochemistry measurements.

Fine Fraction Sample Collection and Pretreatment

Laser light diffraction was used to measure the silt and clay-sized grains of 47 samples. Laser light diffraction is based on the concept that grains of a known size diffract light at known angle (Loizeau et al., 1994:353). Inside the laser diffraction apparatus being used, a laser beam is scattered by grains suspended in a solution being continuously circulated. The scattered laser produces a diffraction pattern that is a detected as the solution flows through a flow cell. The pattern is then compared against a diffraction pattern from a known sample. Using an algorithm the machine computes a distribution of volume percentage for a possible 64 size classes from 0.01 microns to 60 microns (16.6 phi to 4.05 phi).

Similar to the GSA, pretreatment was conducted by Dr. Ian Buvit and the author. Accurate laser diffraction measurement requires the input sample be disaggregated and lacking carbonates and organics or the diffraction pattern would not reflect the size distribution of individual mineral grains (Malvern Instruments, 2007). Therefore, samples must be tested for calcium carbonates and adequately disaggregated by removing organic matter that cause particles to aggregate. Calcium carbonate presence was ascertained by placing one large drop of 10% hydrochloric acid (HCl) on each sample. No sample reacted with HCl so further steps to rid samples of carbonates were omitted.

Organic content was removed by placing 5 g of each fine fraction subsample into a beaker and adding 30 ml of 30% hydrogen peroxide solution. This technique for removing organics is common in soil science and geology (Jensen, Schjonning, Watts, Christensen & Munkholm, 2017)   Beakers were placed in an electric skillet filled with deionized (DI) water and heated to approximately 170º F for one hour, with additional DI water added periodically to the bath to keep samples from burning. Samples were then cooled for 24 hours. Next, the 5 gram samples were transferred from beakers to 100 ml centrifuge tubes, and DI water was added up to the fill line. In order to remove the supernatant creating during organic content removal, we had to separate the soil minerals. We could have let samples sit overnight, and except for some clays that could have taken weeks. In order to save time, we centrifuged the samples. Samples were centrifuged at 2000 revolutions per minute for 10 minutes using the centrifuge stored in CWU's Farrell Hall, now in Dean Hall. Being centrifuged caused particles to concentrate at bottom of the tube, requiring excess water be gently poured out as to not lose any particles. This technique of using a centrifuge in a pedology lab is typical in soil science and geology (Pansu & Gautheyrou, 2007).

Fine Fraction Measurement

A Malvern Mastersizer 2000, located in Hebeler Hall, was used to measure the silt and clay size grains from 47 samples. The technique used was guided by Dr. Buvit, as informed by the machine instruction manual (Malvern, 2007) and Sperazza, Moore, and Hendrix (2002). This technique began by using a clean spatula to extract an approximately one gram sample from each centrifuge tube, making an attempt to bisect the sample to acquire representative silt and clay-sized grains, followed by placing it in a beaker with DI water. The beaker was then sonicated in a Bransonic Ultrasonic Cleaner

8510 for approximately 60 seconds at 80% strength. This was to ensure all grains were disaggregated without fracturing primary mineral grains. Next, samples were poured into the Mastersizer's dispersion unit until an obscuration range was between 0.15 and 0.2 (when the obscuration bar read green). Obscuration refers to the percentage of light lost, of which 15% to 20% is ideal. If the machine reads outside of this range, more water or sediment sample is needed to achieve an accurate measurement (Malvern Instruments 2007: 4-3). Each sample was measured three times by the Mastersizer, followed by a computed average, for a total of four measurements. The Mastersizer is connected to a computer that converts measurements into spreadsheets. The result was a Microsoft Excel-compatible spreadsheet with a percentage distribution (by volume) of grains for a possible 64 size classes for each sample.

Grain-Size Analysis – Creating Grain-Size Distributions

Grain-size measurements from dry sieving, wet sieving, and laser diffraction were entered into an Excel spreadsheet. A grain-size distribution with 20 size classes was created for each of the 47 samples. Size classes ranged from 13 phi (fine clay) to -5 phi (coarse pebble). These fine and coarse categories were chosen because it was immediately clear no grain sizes occurred outside of this range, which aligns with one of the purposes of this study of measuring the entire grain-size distribution of every sample. Inputting a percentage for each size class was simple for coarse classes, as the percentage of the total bulk sample was used. Measurements for grains smaller -1.7 phi had to be multiplied by a coefficient as these measurements represented a subset of the larger bulk sample grain-size distribution.

After 47 grain-size distributions were created in Excel, GRADISTAT software (Blott & Pye, 2001) was used to create grain-size distribution curves and calculate grain-size statistics. After inputting percentages and size classes into the input table and clicking *Calculate Statistics*, the program populated grain-size distribution curves, cumulative distribution curves, and a soil texture triangle. Grain-size frequencies with multiple modes resulted in an error message warning that grain-size statistics could be incorrect. Therefore, all grain-size statistics were checked by hand, explained below, resulting in no changes compared to GRADISTAT results.

The primary GRADISTAT result output consists of a grain-size distribution bar graph, a breakdown of the percentage of grains in each size class, and descriptive graphical statistics. Descriptive graphical statistics used in this study include graphical mean, median, mode, inclusive graphical standard deviation, inclusive graphical skewness, and inclusive graphical kurtosis. These statistics were calculated from equations described as "logarithmic (original) Folk and Ward graphical measures" in Blott and Pye (2001:1241). Attention was directed towards bimodal distributions as candidates for the geochemical analysis phase of this study.

Probability curves were created using the GRANPLOTS program created for plotting curves of grain-size data (Balsillie, Donoghue, Butler, & Koch, 2002). Additionally, probability curves were hand-drawn on probability line paper for each of the 47 samples to ensure accuracy. Drawings were compared to the program with no changes needing to be made. Using the hand-drawn probability graphs, the above mentioned statistical measurements of mean, standard deviation, skewness, and kurtosis were checked with no changes made. Refer to Appendix C for hand drawn curves.

Geochemical Analysis

Sample Selection and Collection

The most commonly occurring grain sizes from 47 grain-size distributions were selected and measured for chemistry. Essentially, at least one size class from each distribution was sampled. The exception being the distribution from sample 36 (DM Organic/MSH-W) from the off-site column sample, which was omitted by the lab technician conducting the geochemical analysis because of its low weight. All other grain-size distributions were sampled once (unimodal) or twice (if bimodal) to understand the parent material of major and minor grain-size populations.

After analyzing 47 grain-size distributions, some unimodal and some bimodal, it was agreed upon by Dr. McCutcheon and I that 67 major modes (commonly occurring size classes) from 47 grain-size distributions be measured for chemistry. Chemistry samples are listed in Chapter V, and organized by excavation unit and feature. There are more chemical measurements than grain size distributions because some distributions were bimodal, in which case more than one size class was subsampled and measured for chemistry. GRADISTAT computes modes to the thousandth of a phi measurement, which would be an unrealistic level of precision to attempt to sample and beyond the scope of this research. Therefore, samples were gathered at the whole-phi size. For example, if a grain-size distribution mode is 2.432, a sample from between the 2 and 3 phi size (medium sand) was collected for chemical measurement. Since all grains had been separated by size and individually bagged during dry and wet sieving, sample retrieval was simple. Sample modes were created that weighed between 20 and 50 grams as recommended by the chemical analysis technique's standard operating procedure (WSU, 2015).

Pretreatment

Chemistry of selected modes was measured using the X-ray fluorescence (XRF) technique. Due to CWU lacking XRF capabilities in the spring of 2015, chemical measurements were conducted at Washington State University's (WSU) Geoanalytical Lab using a ThermoARL Advant'XP+ sequential X-ray fluorescence spectrometer. This XRF spectrometer measures the amount of 29 major, minor, and trace elements. Major and minor elements include silica (S), aluminum (Al), titanium (Ti), iron (Fe), manganese (Mn), calcium (Ca), magnesium (Mg), potassium (K), sodium (Na), and phosphorus (P). Trace elements measured by XRF consist of scandium (Sc), vanadium (V), nickel (Ni), chromium (Cr), barium (Ba), strontium (Sr), zirconium (Zr), yttrium (Y), rubidium (Rb), niobium (Nb), gallium (Ga), copper (Cu), zinc (Zn), lead (Pb), lanthanum (La), cerium (Ce), thorium (Th), neodymium (Nd), and uranium (U).

Mode samples were brought to WSU and prepared by the author with the assistance of lab technicians in June 2015 using the lab's standard operating procedure (Johnson et al., 1999). Each 20 to 50 gram sample was ground to a fine powder in a swing mill with tungsten carbide surfaces for two minutes. This type of powder mill is used because it will not contaminate the sample with elements of interest by the spectrometer (Johnson et al., 1999). Ground samples were placed in labeled plastic cups. Between grinding sessions, mills were cleaned with high-pressured air under a ventilated laboratory hood.

Next, four grams of each powdered sample was mixed in a plastic cup with 8 grams of powdered dilithium tetraborate ($Li_2B_4O_7$). The mixtures were emptied into graphite crucibles and heated in a muffle furnace at 1000°C for five minutes, creating a sample glass bead. Crucibles were cooled, beads removed, weighed (for normalizing calculations) and reground in the swing mill for 35 seconds. The bead powder was returned to the graphite crucibles and re-fused at 1000°C for five minutes.

All subsequent procedures described in Johnson et al. (1999:844-846) were completed by lab technicians. After the second fusion, beads were cooled, labeled with an engraver, ground on 600 silicon carbide grit, and finished on a glass plate (600 grit with alcohol) to remove possible residual metal from the grinding wheel. Beads were then washed in an ultrasonic cleaner, rinsed in alcohol, and wiped dry.

Elemental Measurement

Concentrations of 29 elements were measured by a ThermoARL Advant'XP+ automated sequential wavelength spectrometer. The spectrometer compares a sample bead's X-ray intensity to the intensity of nine United States Geologic Survey standard sample beads (PCC-1, BCR-1, BIR-1, DNC-1, w-2, AGV-1, GSP-1, G-2, and STM-1, using values recommended by Govindaraju, 1994) and two beads of pure vein quartz. To ensure precision, a randomly chosen duplicate bead out of each 20 bead set is made; in this case sample 2, 15a, and 31 had duplicate beads made. This ensures laboratory precision and provides a quick measure of whether small variations in the elemental concentrations of samples are analytically significant. This resulted in the measurement of 70 beads from 67 samples.

Elemental concentrations were converted into an Excel spreadsheet containing major and minor elements expressed in weight percentage oxides and trace elements expressed in ppm. All elements were presented in un-normalized concentrations and also normalized to 100% based on the matter loss during fusion. Normalized elemental concentrations were used for this study as the mineral constituents were of primary concern. These were the concentrations used to analyze TAS relationships and create TAS diagrams.

This chapter detailed available samples, sample selection, sample collection in the field and laboratory, sample pretreatment, grain-size and elemental measurements, followed by measurement and data organization. Such a method-heavy study with numerous steps was necessary to generate accurate data described in the following chapter. Data described in the following chapter (Chapter V Results) moves between descriptive and interpretative before a depositional history model is presented at the end of the chapter.

CHAPTER V

RESULTS AND INTERPRETATION

Results and interpretations are combined into subsections by SRBP site excavation unit, the off-site unit, and SRBP site features. Within each subsection, results are structured by first describing ranges and trends of grain sizes, chemistry, and followed by organic matter (OM), calcium carbonate content ($CaCO_3$), sediment hydrogen ion activity (pH), and sediment Munsell color. When a specific measurement is stated, the sample number is listed in parenthesis after the measurement. For example, “Gravel ranges within the unit column samples from 3% (S7) to 28.9% (S4)”, where S7 and S4 refer to sample 7 and sample 4, which are listed at the beginning of each results subsection (see Table 3).

The GSA resulted in the measurement of the entire grain-size distribution for all 47 samples. Figures 19, 24, 27, 30, 33, and 36 show percentages of gravel, sand, silt, and clay. Percentages are displayed beside the stratum number in stratigraphic order within the profile. Stratum numbers correspond to this study’s sample numbers, which are listed in tables 3, 7, 11, 15, 19, and 23 throughout Chapter V. In the following figures that have stratigraphic profiles, dark shaded squares indicate strata recorded in the field as dark mats. No-fill squares indicate strata recorded as tephra. Tables 4, 8, 12, 16, 20, and 24 summarize grain-size results by listing texture, mode and modes (if polymodal), and grain-size distribution statistics: mean, standard deviation (sorting), skewness, and kurtosis. Grain-size distribution modes and statistics are expressed in phi (ϕ) units. Figure 20, 25, 28, 31, 34, and 37 show grain-size probability curves for all 47 samples.

Probability curves are grouped by proximity of stratigraphic position. Because the goal of the grain size analysis is resolving unclear depositional environment, strata groupings are intended to show similarities and differences in the distributions of under and overlying strata, as well as presence and absence of clear deviations from normal grain-size distributions (abrupt changes in an otherwise smooth line).

The geochemical analysis resulted in the measurement of 29 major and trace elements of 67 samples. Figures 21, 26, 29, 32, 35, and 38 show the amount of four selected trace elements: Strontium (Sr), Barium (Ba), Chromium (Cr), and Nickel (Ni), which are placed beside each associated sample in stratigraphic position, showing trends. In trace element figures, when grain-size distributions had multiple modes and chemistry was measured twice, the coarser of the two modes is represented with circles and is the lower of the two in stratigraphic position. Organic matter content, $CaCO_3$ content, and pH content is listed for each excavation unit and features in tables 5, 9, 13, 17, 21, and 25.

Immediately following results for each excavation unit and feature is an interpretation subsection that compares results of this study to that of published literature and established definitions for soil horizons, parent material, and depositional environment, allowing for classification of each. Interpretations are summarized at the end of each subsection in tables 6, 10, 14, 18, 22, and 26. Interpretation summary tables list depositional environment and parent material interpretations for samples of this study by stating source volcano, environment type, and soil horizon. The section and chapter conclude with the introduction of a new site depositional history model that incorporates results and interpretations of this study and combines them with site data generated by previous studies. A complete breakdown of the depositional history model, specifically, how it increases our understanding of land use at the SRBP site, is discussed in the article that follows (Chapter VI).

Results and Interpretation

Excavation Unit 30N/24E Results

Excavation unit 30N/24E contains thirteen strata, seven of which were recorded as dark mats, and six recorded as tephra (Table 3). Gravel ranges from 3% (S7) to 28.9% (S4), sand ranges from 48.3% (S13) to 84.1% (S7), silt ranges from 4% (S3) to 31% (S11), and clay ranges from 0.3% (S3) to 1.7% (S8) (Figure 19). There are higher percentages of coarser, gravel-sized grains in S1 through S5, decreasing sharply to mostly sand-sized grains by S7 (Figure 19). Below S7, grain sizes becomes gradually coarse again, with notable spikes in silt content in S8 and S11.

Table 3. Excavation Unit 30N/24E Samples.

[1]Sample Number	[2]Depositional Unit	Location	Grain size in phi & Wentworth units
1	MSH-W	30N/24E	2 (medium sand)
2	[3]DM MSH-W/MR-C	30N/24E	1 (coarse sand)
3	MR-C	30N/24E	1 (coarse sand)
4a	DM MR-C/MSH-P	30N/24E	1 (coarse sand)
4b	DM MR-C/MSH-P	30N/24E	-2.7 (fine to medium pebbles)
5a	MSH-P	30N/24E	2 (medium sand)

[1] Sample number refers to the stratum sampled and either the associated fine-grained or coarse-grained sub sample. [2]Depositional unit refers to the tephra or tephra-associated dark mat the sample was recorded as in the field, during field collection in 2011-2013. [3] Dark Mats are abbreviated as "DM".

Table 3 (Continued). Excavation Unit 30N/24E Samples.

[1]Sample Number	[2]Depositional Unit	Location	Grain size in phi & Wentworth units
5b	MSH-P	30N/24E	-1.7 (very fine to fine pebbles)
6a	DM MSH-P/MSH-Yn	30N/24E	3 (fine sand)
6b	DM MSH-P/MSH-Yn	30N/24E	-1.7 (very fine to fine pebbles)
7	MSH-Yn	30N/24E	2 (medium sand)
8a	DM MSH-Yn/MR-F	30N/24E	-1 (very fine pebbles)
8b	DM MSH-Yn/MR-F	30N/24E	4 (very fine sand)
9a	MR-F	30N/24E	2 (medium sand)
9b	MR-F	30N/24E	-1 (very fine pebbles)
10a	DM MR-F/MAZ-O	30N/24E	3 (fine sand)
10b	DM MR-F/MAZ-O	30N/24E	-1 (very fine pebbles)
11a	MAZ-O	30N/24E	3 (fine sand)
11b	MAZ-O	30N/24E	-1 (very fine pebbles)
12a	DM MAZ-O/MR-R	30N/24E	3 (fine sand)
12b	DM MAZ-O/MR-R	30N/24E	-1 (very fine pebbles)
13a	MR-R	30N/24E	4 (very fine sand)
13b	MR-R	30N/24E	-1 (very fine pebbles)

[1] Sample number refers to the stratum sampled and either the associated fine-grained or coarse-grained sub sample. [2]Depositional unit refers to the tephra or tephra-associated dark mat the sample was recorded as in the field, during field collection in 2011-2013. [3] Dark Mats are abbreviated as "DM".

Mean grain size ranges from 2.85 phi (S8) to -0.01 phi (S3), standard deviation ranges from 1.71 phi (S7) to 2.93 phi (S5), skewness ranges from -0.17 phi (S5) to 0.32 phi (S7), and kurtosis ranges from 0.81 phi (S13) to 1.71 phi (S3) (Table 4). Probability curves exhibit pronounced deviations from normal distributions in S3, S6, and S7 (Figure 20). Deviations take the form of multiple line segments as opposed to a relatively smooth line.

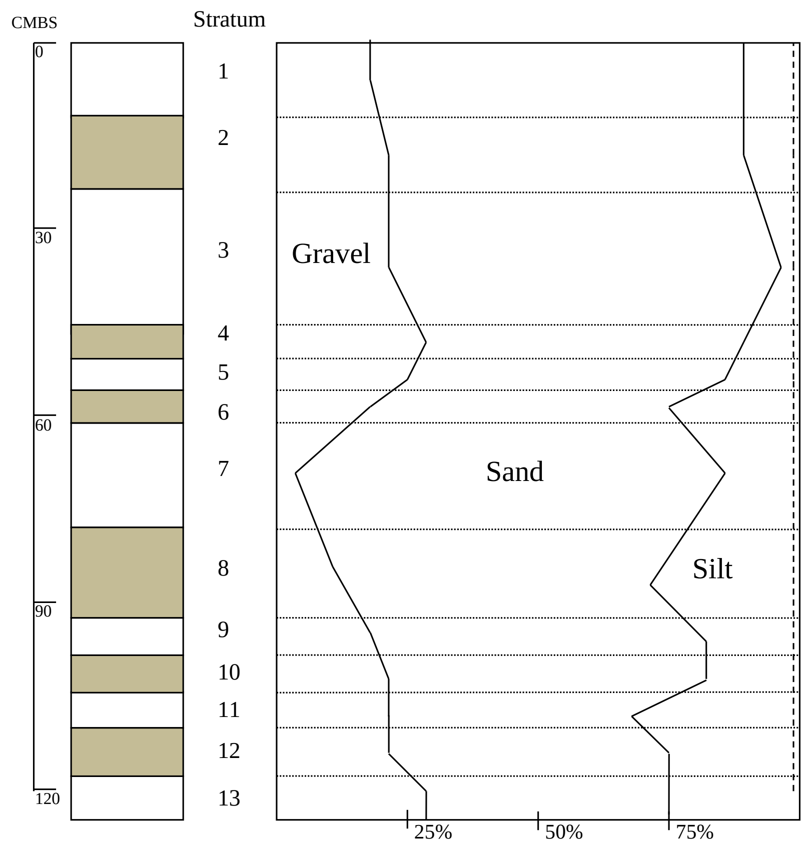

Figure 19. Profile of unit 30N/24E (left) and associated texture by strata (right), organized by cumulative percent. Clay content (dashed line) is 0.3% to 1.7%, peaking in stratum 8. Dark mats (strata 2, 4, 6, 8, 10, & 12) are shaded dark.

Table 4. Excavation Unit 30N/24E Grain-Size Data.

#	[1]Texture	Mode 1	Mode 2	$\overline{x}$	σ	*Sk*	*K*
1	Gravelly Sand	1.5	-	0.945	2.495	-0.082	1.575
2	Gravelly Loamy Sand	0.5	-4.167	0.865	2.678	0.065	1.369
3	Gravelly Sand	0.5	-	-0.006	1.790	-0.112	1.705
4	Gravelly Sand	0.5	-3.167	0.550	2.797	-0.070	0.893
5	Gravelly Sand	1.5	-2.167	1.171	2.934	-0.167	0.947
6	Gravelly Loamy Sand	2.5	-1.334	2.171	2.856	-0.147	1.092
7	Sand	1.5	-	1.881	1.706	0.319	1.171
8	Sandy Loam	3.5	-1.334	2.853	2.553	0.020	1.114
9	Gravelly Loamy Sand	1.5	-1.334	1.785	2.643	-0.121	1.126
10	Gravelly Loamy Sand	2.5	-1.334	1.618	2.714	-0.088	1.062
11	Gravelly Sandy Loam	-1.34	2.5	2.293	3.079	-0.137	0.869
12	Gravelly Sandy Loam	2.5	-1.334	2.050	2.945	-0.066	0.955
13	Gravelly Sandy Loam	-1.34	3.5	1.702	3.227	0.065	0.809

[1]Texture based on USDA classification.

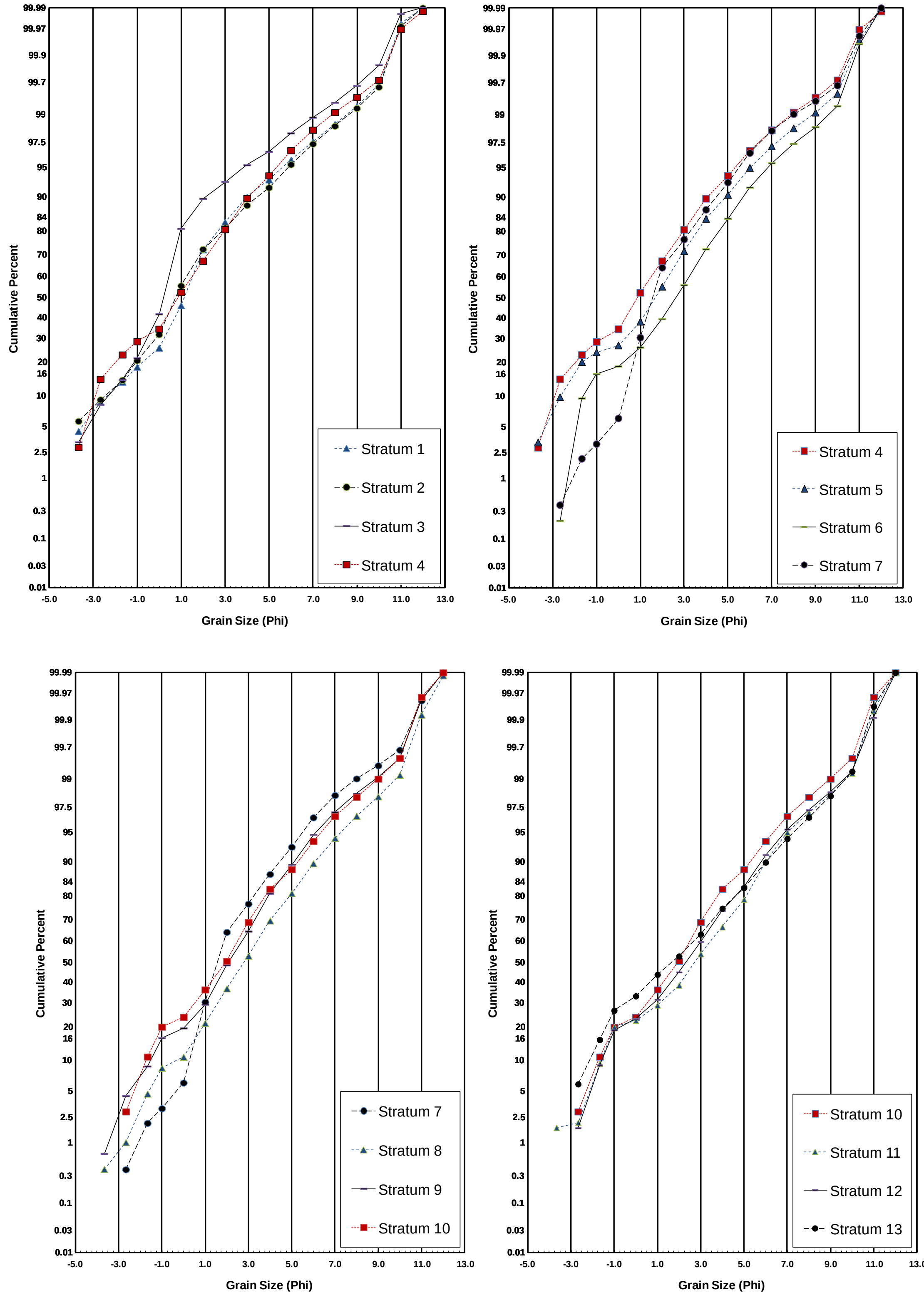

Figure 20. Probability curves of grain size within each stratum from unit 30N/24E.

Silica content ranges from 58.1% (S3) to 61.4% (S11), and total alkali content ranges from 4.52% (S13b) to 5.8% (S1) (Appendix D). Silica content is lowest among samples adjacent to S3, S8, and S13 in stratigraphic position. Silica content is highest in S1, S7, and S11. Trace element trends are summarized here (Figure 21) and show abrupt decreases in Cr and Ni from S4 to S5 to below 75 ppm and 50 ppm, respectively, and abrupt changes in Sr and Ba proportions from S6 to S7.

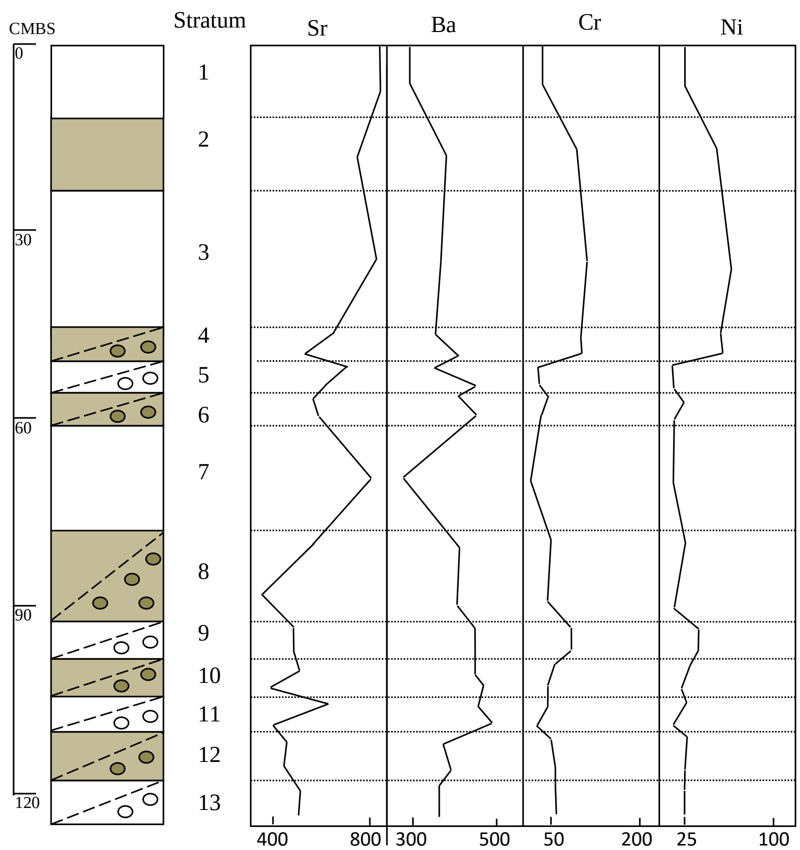

Figure 21. Profile of unit 30N/24E (left) with strata associated trace element proportions (right) expressed in parts per million (ppm). Dark mats (strata 2, 4, 6, 8, 10, & 12) are shaded dark. Circles denote the coarser grain-size class sampled within that stratum, which is expressed as the lower measurement.

Organic matter content ranges from 1.93% (S3) to 8.87% (S4), $CaCO_3$ content ranges from 0.05% (S1) to 1.68% (S11), and pH ranges from 4.91 (S1) to 5.84 (S9) (Table 5). This pH range places all strata on the acidic side of neutral. Organic matter content is higher in four of six dark mats compared to underlying, adjacent tephra strata (see Table 5). Color ranges from 10YR 3/2-very dark grayish brown (S1 and S2) to 10YR 6/8-brownish yellow (Appendix F). These color ranges have a low hue and chroma (dark) to a moderate hue and chroma (less dark), respectively, with dark mats typically darker than adjacent/underlying tephras

Table 5. Excavation Unit 30N/24E OM, $CaCO_3$, and pH Data.

Sample Number	[1]Depositional Unit	Excavation Unit	OM (%)	$CaCO_3$ (%)	pH
1	MSH-W	30N/24E	3.83	0.05	4.91
2	DM MSH-W/MR-C	30N/24E	3.02	0.12	5.12
3	MR-C	30N/24E	1.93	0.10	5.51
4	DM MR-C/MSH-P	30N/24E	8.87	0.27	5.23
5	MSH-P	30N/24E	3.91	0.17	5.29
6	DM MSH-P/MSH-Yn	30N/24E	3.24	0.24	5.52
7	MSH-Yn	30N/24E	5.16	0.57	5.47
8	DM MSH-Yn/MR-F	30N/24E	6.44	0.17	5.19
9	MR-F	30N/24E	4.28	0.77	5.84
10	DM MR-F/MAZ-O	30N/24E	7.23	1.29	5.75
11	MAZ-O	30N/24E	7.52	1.68	5.82
12	DM MAZ-O/MR-R	30N/24E	7.62	1.46	5.66
13	MR-R	30N/24E	6.73	1.49	5.58

[1] Denotes depositional unit as recorded in the field by field school students.

Excavation Unit 30N/24E Interpretation

Coarse, lapilli-sized (gravel-sized) grains that occur in significant proportions (≥ 8.7% gravel) in all 13 samples except S7 are consistent with grain sizes from Mount Rainier eruptions (Mullineaux 1974; Sisson and Vallance, 2009). Sample 7 grain sizes are consistent with MSH-Yn ash that should be primarily sand sized (ash sized) (Mullineaux, 1974; Sisson and Vallance, 2009). Depositional environments unrelated to volcanism require well-sorted grain sizes, and grain-size distributions with standard deviations of approximately 1.5 phi or lower (Pettijohn, 1974; Lewis & McConchie, 1994). Standard deviation (1.71 phi to 2.93 phi) and skewness (-0.17 phi to 0.32 phi) of 30N/24E grain-size distributions are consistent with tephra and ash air fall in volcanic-related depositional environments (Lirer et al., 1996). Figure 22 shows the relationship between the standard deviation (sorting) and skewness of all 47-sample grain-size distributions, which are overlain atop established sorting and skewness relationships for specific depositional environments and volcanic deposits. Mount St. Helens-Yn ash consistently had the most well sorted grain sizes (lowest standard deviation) and was always positively skewed, which is reflected by the upper left four samples' placement in figure 22.

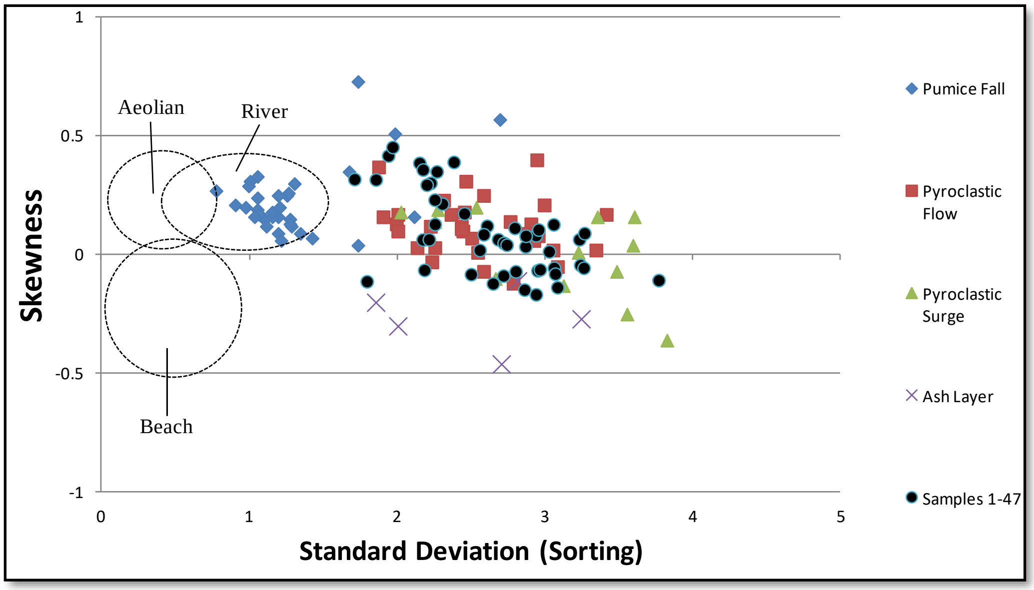

Figure 22. Relationship between standard deviation and skewness of grain-size distributions from different depositional environments, tephra deposits, and samples of this study. Pumice fall, pyroclastic flow, pyroclastic surge, and ash data from Lirer et al. (1996). Aeolian, river, and beach data from Lewis and McConchie (1994) and Pettijohn (1975). Created in Microsoft Excel by Sean Stcherbinine.

Figure 23 shows the relationship between total alkali (combined weight percentage of aluminum and potassium) and silica for all 67 chemistry samples, which are overlain atop a grid of established volcanic rock-type parent materials. Chemistry measurements from S1 through S13 resulted in silica content (58.1% to 61.4%) and total alkali content (4.52% to 5.8%) consistent with andesitic parent materials (Figure 23). An andesitic parent material determination requires silica content be approximately 57% to 63%, and total alkali content be approximately 4% to 6% (La Bas et al., 1986). Low silica content in S3, S8, and S13, which were either recorded as Mount Rainier tephras (S3 and S13) or a Mount Rainier tephra-associated dark mat (S8), is consistent with low silica content for tephra from Mount Rainier eruptions (Mullineaux 1974; Sisson and

Vallance, 2009). Tephra from Mount Rainer eruptions should have a silica content not exceeding approximately 60% (Mullineaux, 1974). Low silica content in S4 (58.1%) is a good example of a sample that was recorded as Mount St. Helens tephra, in this case DM C/P, but contains silica content typical of Mount Rainier tephra. Additionally, lapilli-sized grains in S4 through S6 are larger than the typical sand-sized grains deposited by Mount St. Helens eruptions (Mullineaux, 1974). The occurrence of MR-C slightly below the main deposit is understandable because of the nature of how a thick deposit of lapilli-sized grains would blanket a thin layer of Mount St. Helens-derived sand-sized grains. It is also consistent with field observations of bioturbation and mild sediment mixing (Dampf, 2002; Evans, 2011). Trace element trends of abrupt decreases in Cr and Ni from S4 to S5 mirror the previously stated contribution of Mount Rainier lapilli in S4 as they both drop below normal parts per million proportions for MR-C tephra, which are approximately 75 ppm (Cr) and 50 ppm (Ni) (Sisson and Vallance, 2009). Abrupt changes in Sr and Ba proportions from S6 to S7 underline a stratigraphic change to a poorly weathered MSH-Yn ash (see Figure 23).

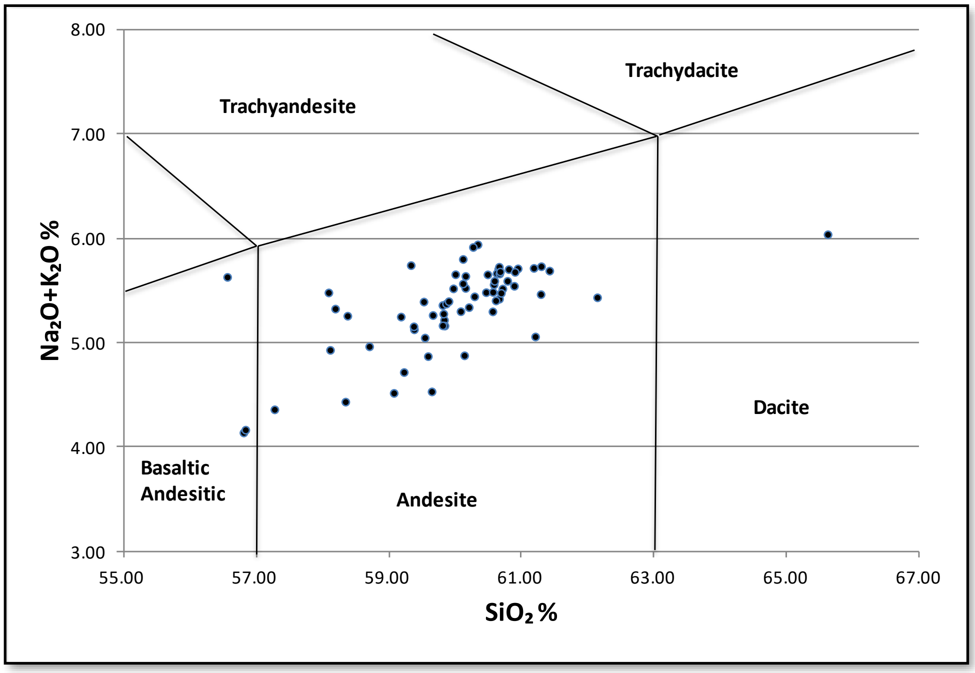

Figure 23. Total alkali silica (TAS) diagram for all 67 geochemistry samples superimposed on interpretative grid with rock type definitions from La Bas et al. (1986). Created in Microsoft Excel by Sean Stcherbinine.

All samples have less than 20% OM and meet the definition of a mineral soil (Soil Survey Staff, 2014). The definition of an A horizon is a mineral soil horizon that is typically a darker Munsell color than underlying horizons, and has a higher OM content due to the humification of organic materials. Four dark mats (S2, S4, S8, and S12) have higher OM content compared to adjacent, underlying tephra strata. Two dark mats (S6 and S10) have less OM content, with S10 containing 7.23% OM content compared to the underlying S11 with 7.62% OM content, a negligible difference. All six dark mats are as dark, or darker than underlying tephra strata (see Appendix F). Based on organic content being typically higher than underlying strata, and color darker than underlying strata, dark mats in 30N/24E are interpreted as buried A horizons–the result of soil formation.

In other words, dark mats formed due to tephra weathering in place on the ground surface with additions of humified organic materials, before being covered by subsequent volcanic ejecta that removed the A horizon from major soil forming processes, thereby arresting soil formation.

Calcium carbonate ($CaCO_3$) content (0.05% to 1.68%) is far lower than the necessary 50% needed for the soil taxonomy suffix symbol “k” to be used (Soil Survey Staff, 2014). Tipsoo, Owyhigh, Mysticlake, and Mountwow soil series’ that are mapped at or near the SRBP site all lack $CaCO_3$ content necessary to include soil horizons with “k” suffixes (see Chapter II and Appendix A) (Soil Survey Staff, 2018). Acidity (pH of 4.91 to 5.84) is similar to pH content described in Tipsoo, Owyhigh, Mysticlake, and Mountwow soil series’, which have mineral soil horizon pH ranges of 5.2 to 5.4 (Soil Survey Staff, 2018). Collectively, soil properties of volcanic parent material, presence of diagnostic tephra layers, the occurrence of buried A horizons, low acidity and $CaCO_3$ content are all consistent with soil series’ discussed previously, but compare best to the Mountwow series, which is an Andisol.

Results of grain-size measurements exhibit one clear discrepancy compared to the expected results of grain sizes for each regional tephra recorded at the SRBP site. Sample 8 and 9 were recorded as a MR-F-related dark mat and tephra, respectively (see Figure 19). Data generated from this study suggest these strata may be the result of additional Mount Rainier eruptions occurring before MSH-Yn and after MAZ-O. MR-F deposits have one uniquely distinguishable characteristic– they contain between 5% to 25% clay (Mullineaux, 1974). Sample 8 and 9 contain 1.7% and 0.9% clay, respectively, and the highest clay content of any sample of this study is 2.1%. The plume of MR-F is well documented in this part of MORA, but so are plumes of MR-S, MR-N, MR-D, and MR-A, which contain similar grain sizes as MR-F (Mullineaux, 1974; Soil Survey Staff, 2018).

Excavation unit 30N/24E contains an Andisol soil profile of tephra and intercalated A horizons whose primary constituents (parent material) are andesitic–the result of regional volcanism (see Figure 23). The profile appears to have been recorded accurately, the only exception being a zone below S7 (MSH-Yn) and above S10 (DM F/O), which cannot be directly attributable to MR-F, but may contain tephra from temporally close Mount Rainier eruptions. Differentiating between Mount Rainier eruptions is difficult because they have similar grain sizes and chemistry profiles. Depositional environment is direct ash and tephra fall based on grain-size statistics (see Figure 22). After deposition, soil forming processes weathered tephra surfaces into A horizons, creating the dark mat-over-weakly weathered tephra sequence observed during excavations. Whether as a surface horizon or horizon buried by subsequent eruptions, post-depositional alterations took place as evidenced by probability curve deviations and the displaced occurrence of Mount Rainier lapilli-sized grains. Post-depositional alterations, interpreted as reworked surfaces, occurred in S1, S4, S5, S6, S10, S11, all samples recorded as non-Mount Rainier ash. See Table 6 for a complete list of S1 through S13 interpretations.

Table 6. Excavation Unit 30N/24E Sample Interpretations.

Sample	Originally Recorded As	Interpretation
1	MSH-W	Reworked MSH-W ash with MR-C lapilli
2	DM MSH-W/MR-C	Buried A horizon: MR-C tephra
3	MR-C	Poorly weathered parent material: MR-C tephra
4	DM MR-C/MSH-P	Reworked MSH-P or Yn buried A horizon with MR-C lapilli
5	MSH-P	Reworked MSH-P or Yn buried A horizon with MR-C lapilli
6	DM MSH-P/MSH-Yn	Reworked MSH-Yn buried A horizon with MR-C lapilli
7	MSH-Yn	Poorly weathered parent material: MSH-Yn ash
8	DM MSH-Yn/MR-F	MR-F/S/N/D/A buried A horizon
9	MR-F	MR-F/S/N/D/A parent material
10	DM F/MAZ-O	Reworked MAZ-O buried A horizon and MR-F/S/N/D/A/R ash and lapilli
11	MAZ-O	Reworked MAZ-O ash and MR-F/S/N/D/A/R ash and lapilli
12	DM MAZ-O/MR-R	Buried A horizon: MR-R tephra
13	MR-R	Poorly weathered parent material: MR-R

Excavation Unit 61.5N/36E Results

Excavation unit 61.5N/36E contains nine strata, four of which were recorded as dark mats, and five recorded as tephra (Table 7). Gravel ranges from 3% (S19) to 69.5% (S16), sand ranges from 26.8% (S16) to 80% (S19), silt ranges from 3.4% (S16) to 25.9% (S17), and clay ranges from 0.3% (S16) to 1.9% (S17) (see Figure 24). There are higher percentages of coarser, lapilli-sized grains in S15 through S17, decreasing sharply to mostly sand-sized grains by S19 (see Figure 24). Below S19 the sand content decreases, with an increase in lapilli and silt-sized grains. Silt content abruptly increases in S17 and S18, both dark mats, compared to adjacent tephra strata.

Table 7. Excavation Unit 61.5N/36E Samples.

[1]Sample Number	[2]Depositional Unit	Location	Grain size in phi & Wentworth units
14a	MSH-W	61.5N/36E	2 (medium sand)
14b	MSH-W	61.5N/36E	1 (coarse sand)
15a	[3]DM MSH-W/MR-C	61.5N/36E	1 (coarse sand)
15b	DM MSH-W/MR-C	61.5N/36E	-1.7 (very fine to fine pebbles)
16a	MR-C	61.5N/36E	1 (coarse sand)
16b	MR-C	61.5N/36E	-2.7 (fine to medium pebbles)
17a	DM MR-C/MSH-P	61.5N/36E	2 (medium sand)
17b	DM MR-C/MSH-P	61.5N/36E	-1.7 (very fine to fine pebbles)
18	DM MSH-P/MSH-Yn	61.5N/36E	2 (medium sand)
19	MSH-Yn	61.5N/36E	2 (medium sand)
20	DM MSH-Yn/MR-F	61.5N/36E	2 (medium sand)
21a	MR-F	61.5N/36E	2 (medium sand)
21b	MR-F	61.5N/36E	-1 (fine pebbles)
22a	MR-R	61.5N/36E	3 (fine sand)
22b	MR-R	61.5N/36E	-1(fine pebbles)

[1] Sample number refers to the stratum sampled and either the associated fine-grained or coarse-grained sub sample. [2]Depositional unit refers to the tephra or tephra-associated dark mat the sample was recorded as in the field, during field collection in 2011-2013. [3] Dark Mats are abbreviated as "DM".

Mean grain size ranges from 2.56 phi (S18) to -1.75 phi (S16), standard deviation ranges from 1.94 phi (S19) to 3.23 phi (S17), skewness ranges from -0.06 phi (S22) to 0.42 phi (S19), and kurtosis ranges from 0.83 phi (S22) to 2.33 phi (S14) (Table 8). Probability curves exhibit pronounced deviations from normal distributions in S14 and S17 (Figure 25). Deviations take the form of multiple straight line segments that intersect in the sand-sized intervals near 1 phi in both S14 and S17.

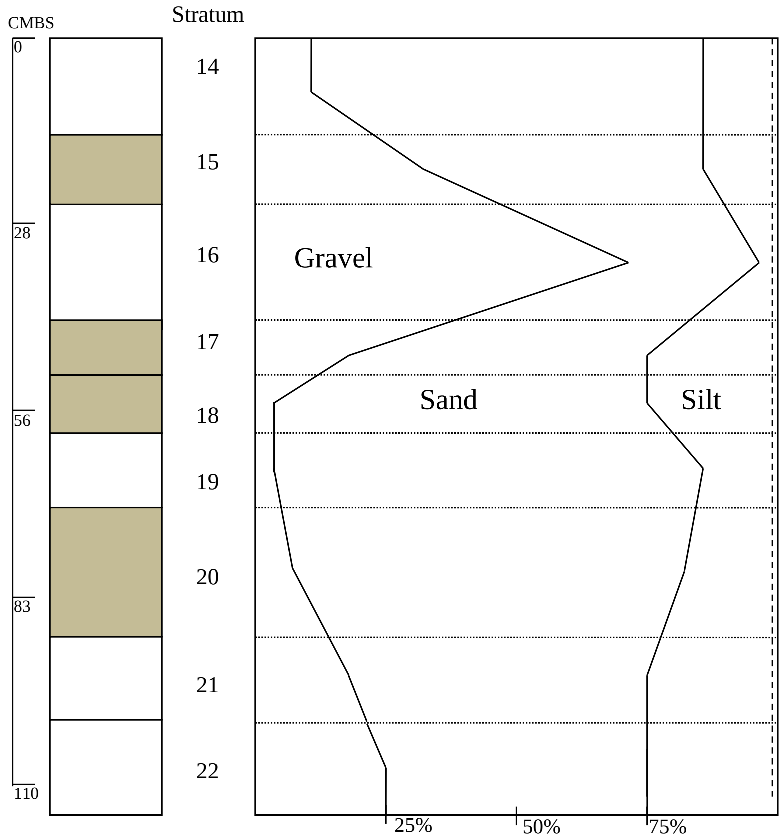

Figure 24. Profile of unit 61.5N/36E (left) and associated texture by strata (right), organized by cumulative percent. Clay content (dashed line) ranges from 0.3% to 1.9 %, peaking in stratum 17.
Dark mats (strata 15, 17, 18, & 20) are dark shaded.

Table 8. Excavation Unit 61.5N/36E Grain-Size Data.

#	[1]Texture	Mode 1	Mode 2	$\bar{x}$	σ	*Sk*	*K*
14	Loamy Sand	1.5	-	1.748	2.168	0.064	2.331
15	Gravelly Loamy Sand	0.5	-2.167	0.708	3.053	0.128	0.918
16	Extremely Gravelly Sand	-3.167	0.5	-1.747	2.221	0.303	1.075
17	Gravelly Sandy Loam	1.5	-2.167	2.149	3.234	-0.043	1.090
18	Loamy Sand	1.5	-	2.555	2.263	0.351	1.013
19	Loamy Sand	1.5	-	2.040	1.935	0.418	1.163
20	Loamy Sand	1.5	-	2.187	2.195	0.295	1.253
21	Gravelly Sandy Loam	1.5	-1.334	2.040	3.023	0.014	0.945
22	Gravelly Sandy Loam	-1.334	2.5	1.876	3.056	-0.055	0.828

[1]Texture based on USDA classification.

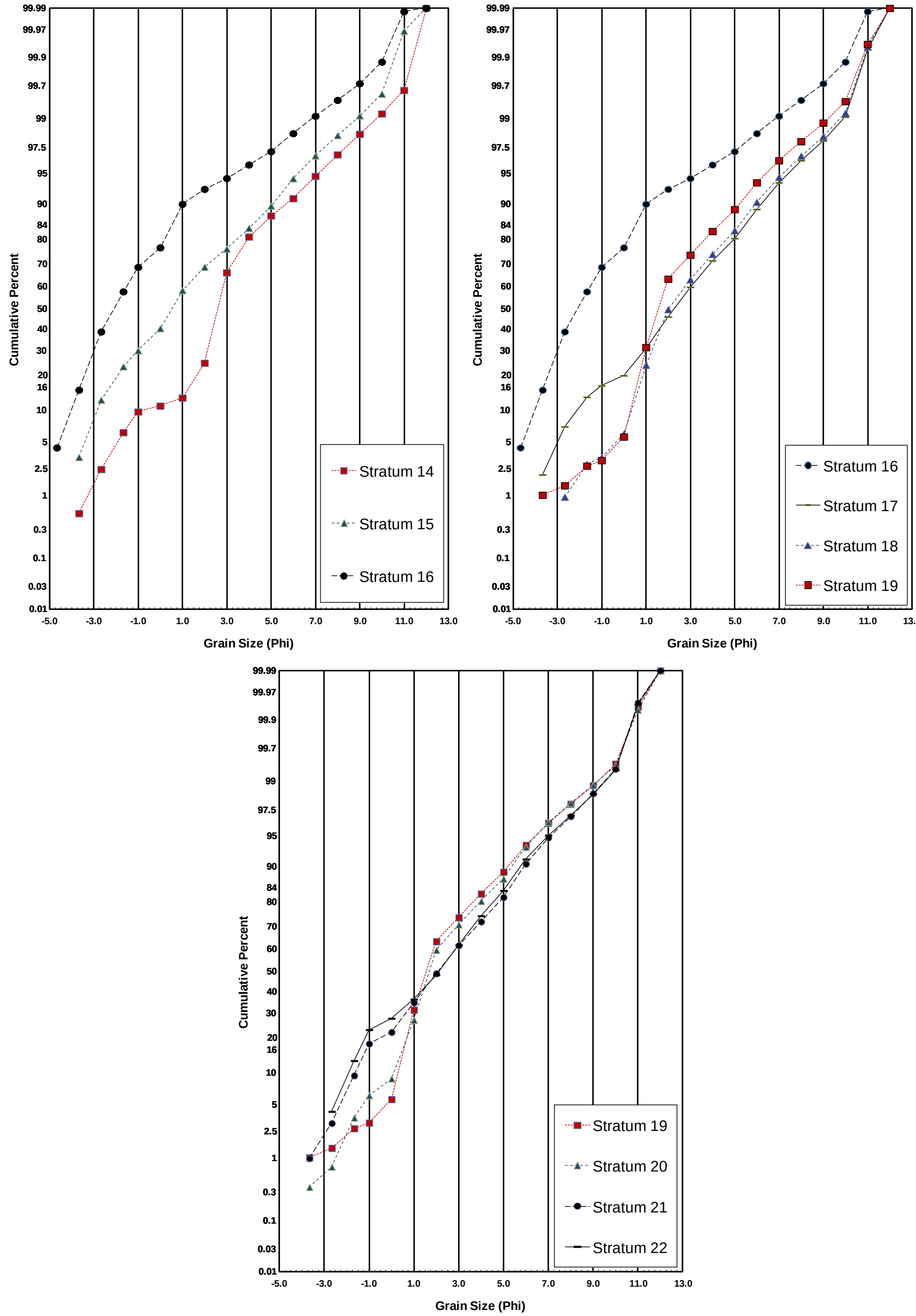

Figure 25. Probability curves of grain size within each stratum from unit 61.5N/36E.

Silica content ranges from 57.3% (S16) to 65.6% (S14), and total alkali content ranges from 4.36% (S16a) to 6.04% (S14b) (see Appendix D). Silica content is lowest in S15, S16, and S22, and highest in S14, S18, and S19. Trace element trends show abrupt decreases in Cr and Ni from S16 to S17 to below 75 ppm and 50 ppm, respectively, and abrupt changes in Sr and Ba proportions associated with S19 (Figure 26).

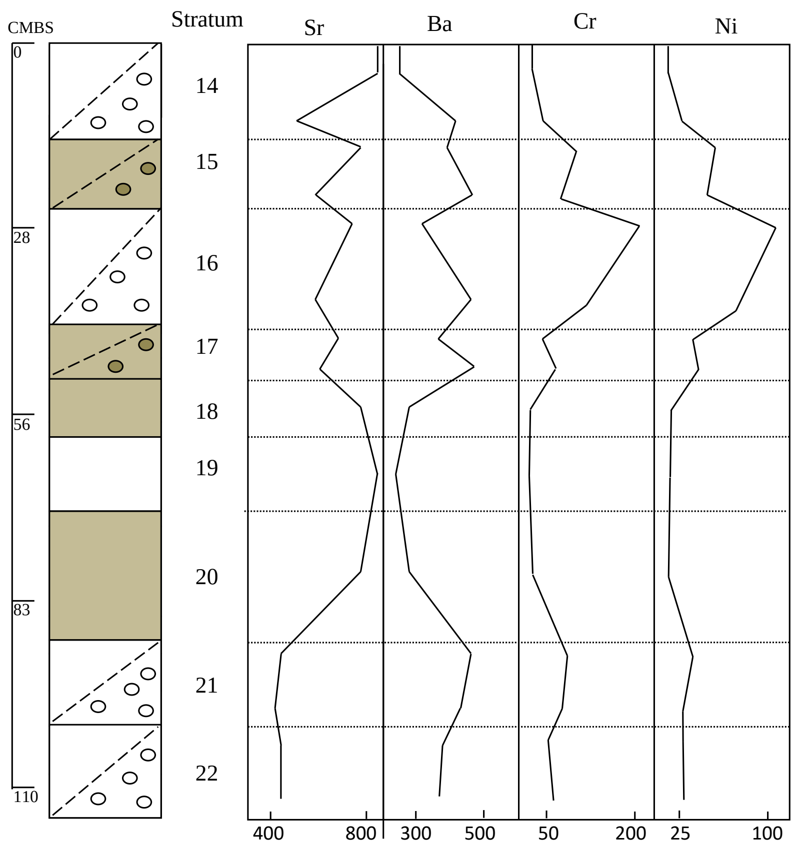

Figure 26. Profile of unit 61.5N/36E (left) and strata associated trace element proportions (right) expressed in parts per million (ppm). Dark mats (strata 15, 17, 18, & 20) are shaded dark. Circles denote the coarser grain-size class sampled within that stratum, which is expressed as the lower measurement.

Organic matter content ranges from 2.01% (S16) to 8.5% (S22), $CaCO_3$ content ranges from 0.05% (S14) to 1.87% (S22), and pH ranges from 4.91 (S14) to 6.2 (S17) (Table 9). This pH range places all strata on the acidic side of neutral. Organic matter content is higher in two of four dark mats compared to underlying, adjacent tephra strata in excavation unit 61.5N/36E (see Table 9). Color ranges from 10YR 3/2-very dark grayish brown to 10YR 5/4-yellowish brown. This corresponds to a low (dark) hue and chroma to a moderate hue and chroma (less dark), with dark mats typically darker than adjacent/underlying tephra strata (see Appendix F).

Table 9. Excavation Unit 61.5N/36E OM, $CaCO_3$, and pH Data.

Sample Number	[1]Depositional Unit	Excavation Unit	OM (%)	$CaCO_3$ (%)	pH
14	MSH-W	61.5N/36E	3.83	0.05	4.91
15	DM MSH-W/MR-C	61.5N/36E	5.35	0.34	5.83
16	MR-C	61.5N/36E	2.01	0.18	5.87
17	DM MR-C/MSH-P	61.5N/36E	2.88	0.29	6.20
18	DM MHS-P/MSH-Yn	61.5N/36E	2.35	0.28	5.99
19	MSH-Yn	61.5N/36E	2.61	0.40	6.06
20	DM MSH-Yn/MR-F	61.5N/36E	3.07	0.51	6.00
21	MR-F	61.5N/36E	6.94	1.65	6.17
22	MR-R	61.5N/36E	8.50	1.87	6.08

[1] Denotes depositional unit as recorded in the field by field school students.

Excavation Unit 61.5N/36E Interpretation

Excavation unit 61N/36E contains coarse, lapilli-sized grains in S15 through S17 that are the product of Mount Rainier eruptions. Sample 14, S18, and S19 grain sizes are consistent with Mount St. Helens ash that should be primarily sand sized (Mullineaux, 1974; Sisson & Vallance, 2009). Standard deviation (1.94 phi to 3.23 phi) and skewness

(-0.06 phi to 0.42 phi) of grain-size distributions are consistent with volcanic-related depositional environments, specifically tephra and ash fall and do not appear to be the result of other depositional environments (see Figure 22).

Chemistry measurements from S14 through S22 resulted in alkali content of 4.46% to 6.04% and silica content ranging from 57.3% to 65.6%. Sample 14 contained by far the highest silica content of any sample in this study and represents the only major outlier in Figure 23. High silica content in S14 may be influenced by dacitic lithic material (volcanic not cultural) observed at the SRBP site (McCutcheon et al., 2017). All other alkali and silica content is consistent with andesitic parent material (see Figure 23). Low silica content in S15, S16, and S22 is consistent with Mount Rainier tephra. High silica content in S14, S18, and S19 is consistent with Mount St. Helens tephra. Trace element trends of abrupt decreases in Cr and Ni from S16 to S17 are the result of a transition from a Mount Rainier to a Mount St. Helens parent material as both samples drop below normal parts per million proportions for MR-C tephra, which are approximately 75 ppm (Cr) and 50 ppm (Ni) (Sisson & Vallance, 2009). Abrupt changes in Sr and Ba proportions from S17 to S19 underline a stratigraphic change to a poorly weathered MSH-Yn ash (see Figure 26). This same trend was observed associated with S7 in 30N/24E, which was also interpreted as poorly weathered MSH-Yn ash.

Organic matter content of S14 through S22 (2.01% to 8.52%) meet criteria for mineral soil horizons, and therefore a candidate for an A horizon. Two dark mats (S15 and S17) have higher OM content compared to underlying tephras, while the other two dark mats (S18 and S20) have less OM content compared to underlying tephra. Organic matter content in S18 (2.35%) is only slightly less than S19 (2.61%), while the low OM content in S20 (3.07%) compared to S21 (6.94) is likely do to the reworked nature of S19 and S20. All four dark mats are as dark, or darker than underlying tephra strata (Appendix F). Based on more intact dark mats (S15 and S18) having higher OM content compared to underlying tephra strata, and having color as dark or darker than underlying tephra, they are interpreted as A horizons. Calcium carbonate ($CaCO_3$) content (0.05% to 1.87%) and acidity (pH of 4.91 to 5.84) is similar to ranges described in Tipsoo, Owyhigh, Mysticlake, and Mountwow soil series' (Soil Survey Staff, 2018). Collectively, and similar to 30N/24E, soil properties in unit 61.5N/36E compare best to the Mountwow series, which is an Andisol.

Excavation unit 61.5N/36E contains an Andisol soil profile of tephra and intercalated A horizons that formed in andesitic parent material (see Figure 23). The profile was recorded accurately, the exception being the zone, described previously, below S19 (MSH-Yn) and above S22 (MR-R), which cannot be directly attributable to MR-F tephra. Parent material options of this zone of the profile are MR-F, MR-S, MR-N, MR-D, and MR-A tephras. Depositional environment is direct ash and pumice fall based on grain-size statistics (see Figure 22). Post-depositional alterations took place as evidenced by probability curve deviations and the improper occurrence of coarse sand and lapilli-sized grains, most notably in S14 and S17. See Table 10 for a complete list of S14 through S22 interpretations.

Table 10. Excavation Unit 61.5N/36E Sample Interpretations.

Sample	Originally Recorded As	Interpretation
14	MSH-W	Reworked MSH-W ash and MR-C lapilli
15	DM MSH-W/MR-C	Buried A horizon: MR-C tephra
16	MR-C	Poorly weathered parent material: MR-C tephra
17	DM MR-C/MSH-P	Reworked MSH-P or Yn buried A horizon with MR-C lapilli
18	DM MSH-P/MSH-Yn	Buried A horizon: MSH-Yn ash
19	MSH-Yn	Poorly weathered parent material: MSH-Yn ash
20	DM MSH-Yn/MR-F	Reworked Buried A horizon: pre MSH-Yn (MR-F/S/N/D/A/R)
21	MR-F	Reworked parent material: pre MSH-Yn (MR-F/S/N/D/A/R)
22	MR-R	Poorly weathered parent material: pre MSH-Yn (MR-F/SN/D/A/R)

Excavation Unit 64N/115E Results

Excavation unit 64N/115E contains six strata, four of which were recorded as dark mats or a combination of dark mat and tephra, and two recorded as tephra (Table 11). Gravel ranges from 2.8% (S27) to 32.2% (S23), sand ranges from 54.3% (S23) to 79.8% (S27), silt ranges from 12.6% (S23) to 25.4% (S25), and clay ranges from 0.9% (S23 and S27) to 1.8% (S28) (see Figure 27). There are higher percentages of coarser, lapilli-sized grains in S23 through S25, decreasing sharply to mostly sand-sized grains in S26 and S27 (see Figure 27). Below S27 the sand content decreases, with an increase in lapilli and silt-sized grains. Silt content abruptly increases in S25, S26, and S28, all dark mats, compared to adjacent tephra strata.

Table 11. Excavation Unit 64N/115E Samples.

[1]Sample Number	[2]Depositional Unit	Location	Grain size in phi & Wentworth units
23a	DM MSH-W/MR-C	64N/115E	2 (medium sand)
23b	DM MSH-W/MR-C	64N/115E	-1.7 (very fine to fine pebbles)
24a	MR-C	64N/115E	1(coarse sand)
24b	MR-C	64N/115E	-2.7 (fine to medium pebbles)
25	DM MR-C/MSH-P & MSH-P	64N/115E	2 (medium sand)
26	DM MSH-P/MSH-Yn	64N/115E	2 (medium sand)
27	MSH-Yn	64N/115E	2 (medium sand)
28	DM MSH-Yn/F	64N/115E	2 (medium sand)

[1] Sample number refers to the stratum sampled and either the associated fine-grained or coarse-grained sub sample. [2]Depositional unit refers to the tephra or tephra-associated dark mat the sample was recorded as in the field, during field collection in 2011-2013. [3] Dark Mats are abbreviated as "DM".

Mean grain size ranges from 2.64 phi (S28) to 0.55 phi (S23), standard deviation ranges from 1.96 phi (S27) to 3.26 phi (S24), skewness ranges from 0.04 phi (S28) to 0.45 phi (S27), and kurtosis ranges from 0.83 phi (S23) to 1.29 phi (S27) (Table 12). Probability curves exhibit pronounced deviations from normal distributions in S25, S26 and S27 (Figure 28). Deviations are due to multiple straight line segments that intersect at 0 phi, which is the demarcation between coarse and very coarse sand. Compare this to S23 and S24, which are great examples of normal Gaussian distributions lacking multiple straight line segments.

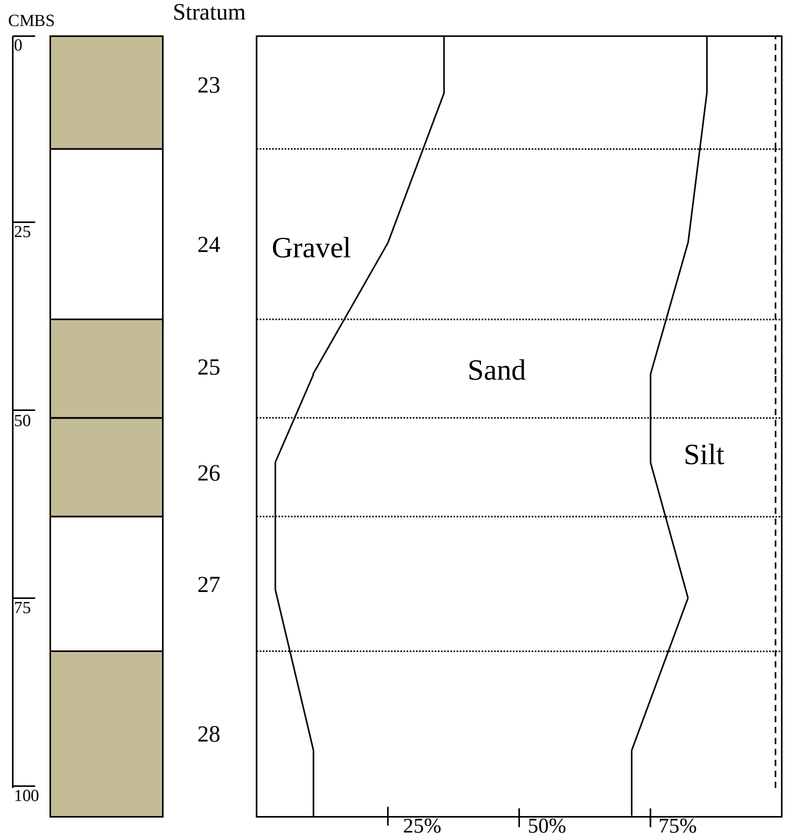

Figure 27. Profile of unit 64N/115E (left) and associated texture by strata (right), organized by cumulative percent. Clay content (dashed line) ranges from 0.9% to 1.8 %, peaking in stratum 28. Dark mats (strata 23, 25, 26, & 28) are shaded dark.

Table 12. Excavation Unit 64N/115E Grain-Size Data.

#	[1]Texture	Mode 1	Mode 2	$\bar{x}$	σ	*Sk*	*K*
23	Gravelly Loamy Sand	1.5	-2.167	0.551	2.933	0.082	0.831
24	Gravelly Loamy Sand	0.5	-3.167	0.928	3.262	0.091	1.0
25	Sandy Loam	1.5	-1.334	2.562	2.603	0.122	1.151
26	Loamy Sand	1.5	-	2.408	2.146	0.387	1.003
27	Loamy Sand	1.5	-	2.050	1.964	0.454	1.290
28	Sandy Loam	1.5	-1.334	2.635	2.863	0.035	1.159

[1]Texture based on USDA classification.

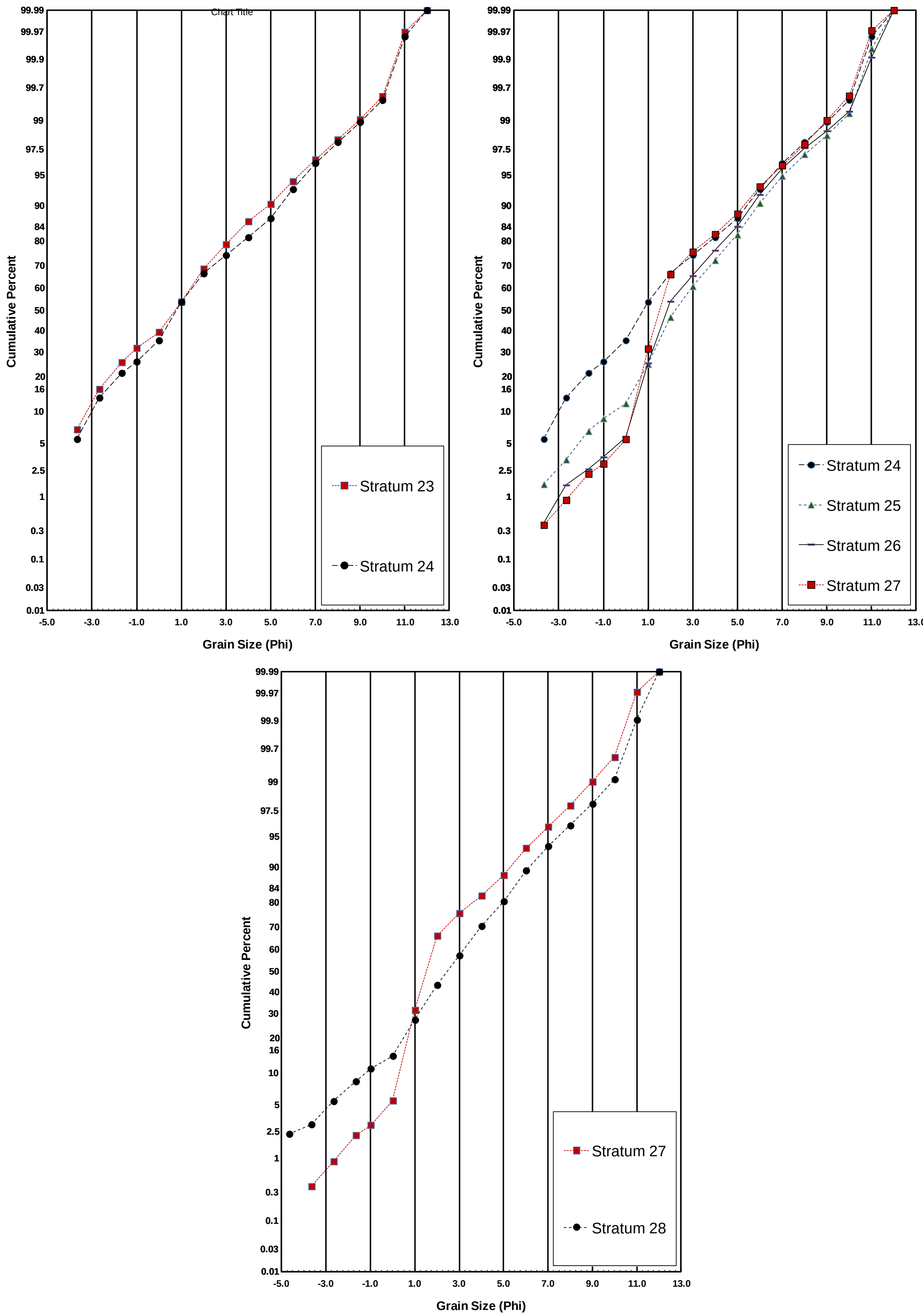

Figure 28. Probability curves of grain size within each stratum from unit 64N/115E

Silica content ranges from 59.5% (S24) to 60.7% (S26), and total alkali content ranges from 5.05% (S24a) to 5.66% (S26 and S27) (see Appendix D). Silica content is lowest in S23 and S24, and highest in S25 and S26. Trace element trends show abrupt decreases in Cr and Ni from S24 to S25 to below 75 ppm and 50 ppm, respectively, and abrupt changes in Sr and Ba proportions associated with S27 (Figure 29).

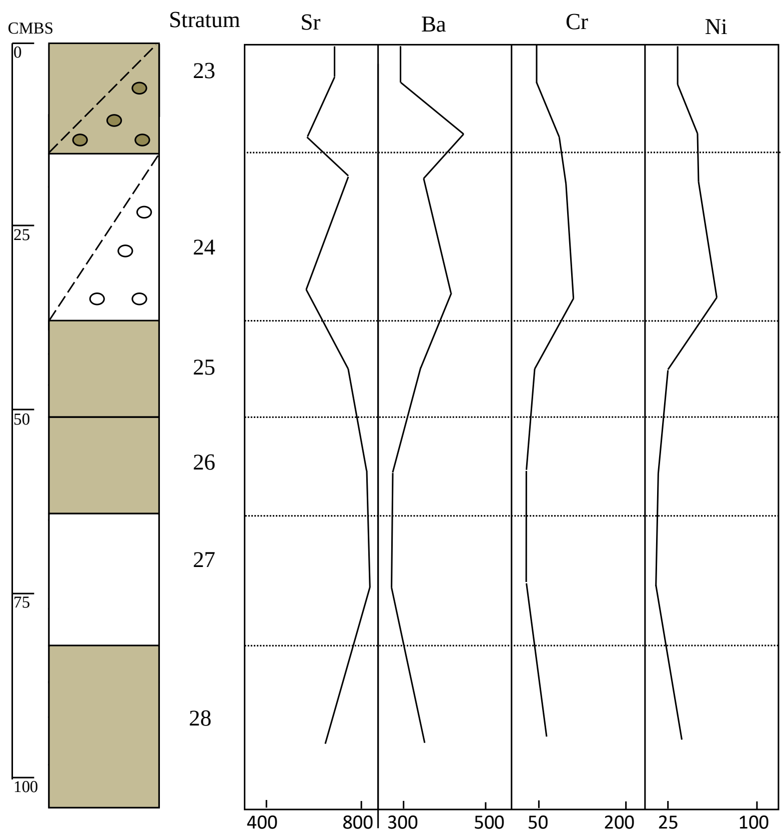

Figure 29. Profile of unit 64N/115E (left) and strata associated trace element proportions (right) expressed in parts per million (ppm). Dark mats (strata 23, 25, 26, & 28) are shaded dark. Circles denote the coarser grain-size class sampled within that stratum, which is expressed as the lower measurement.

Organic matter content ranges from 2.88% (S27) to 6.56% (S23), $CaCO_3$ content ranges from 0.12% (S25) to 0.56% (S24), and pH ranges from 5.33 (S23) to 6.63 (S27) (Table 13). Similar to previous excavation units, pH is acidic in all strata. Organic matter content is higher in all three dark mats compared to underlying, adjacent tephras in excavation unit 64N/115E (see Table13). Color ranges from 10YR 4/1-dark gray (S14) to 10YR 6/6-brownish yellow, with dark mats typically darker than adjacent/underlying tephra strata (see Appendix F).

Table 13. Excavation Unit 64N/115E OM, $CaCO_3$, and pH Data.

Sample Number	[1]Depositional Unit	Excavation Unit	OM (%)	$CaCO_3$ (%)	pH
23	DM MSH-W/MR-C	64N/115E	6.56	0.46	5.33
24	MR-C	64N/115E	3.91	0.56	6.21
25	DM MR-C/MSH-P & MSH-P	64N/115E	3.08	0.12	5.73
26	DM MSH-P/MSH-Yn	64N/115E	3.22	0.15	5.77
27	MSH-Yn	64N/115E	2.88	0.13	6.63
28	DM MHS-Yn/F	64N/115E	5.35	0.27	6.12

[1] Denotes depositional unit as recorded in the field by field school students.

Excavation Unit 64N/115E Interpretations

Excavation unit 64N/115E contains coarse, lapilli-sized grains in S23 through S25 that are the product of Mount Rainier eruptions. Sample 26, S27, and to a lesser degree S28 have sand-sized grains more consistent with Mount St. Helens ash (Mullineaux, 1974; Sisson and Vallance, 2009). Standard deviation (1.96 phi to 3.26 phi) and skewness (0.04 phi to 0.45 phi) of grain-size distributions is consistent with tephra and ash fall as opposed to other depositional environments (see Figure 22).

Chemistry measurements from S23 through S28 resulted in silica content (59.5% to 60.7%) and total alkali content (5.05% to 5.66%) is consistent with andesitic parent materials (see Figure 23). Low silica content in S23 and S24 is consistent with the chemistry of Mount Rainier tephra, while high silica content in S25 and S26 is consistent with Mount St. Helens tephra. Trace element trends of abrupt decreases in Cr and Ni from S24 to S25 are the result of a transition from Mount Rainier to Mount St. Helens parent material, as both samples drop below normal parts per million proportions for MR-C tephra, which are approximately 75 ppm (Cr) and 50 ppm (Ni) (Sisson and Vallance, 2009). Abrupt changes in Sr and Ba proportions from S25 to S27 underline a stratigraphic change to a poorly weathered MSH-Yn ash (see Figure 29). This trend is similar to trends observed in S7 in 30N/24E and S19 in 61.5N/115E.

Organic matter content of S23 through S28 (2.88% to 6.56%) meet criteria for mineral soil horizons. All three dark mats (S23, S25, and S26) have higher OM content compared to underlying tephra strata, while the fourth dark mat (S28) is the basal stratum where no comparison can be made. The three shallow dark mats are as dark, or darker than underlying tephra strata (Appendix F). Based on all dark mats having more OM content compared to underlying tephra, and having color as dark, or darker than underlying tephra, they are interpreted as A horizons. Sample 28 is also interpreted as an A horizon based on its relatively high OM content (5.35%) compared to poorly weathered tephra strata site wide. Calcium carbonate ($CaCO_3$) content (0.12% to 0.56%) and acidity (pH of 5.33 to 6.63), even though pH is verging on neutral, all compare well to ranges described in Tipsoo, Owyhigh, Mysticlake, and Mountwow soil series' (Soil

Survey Staff, 2018). Collectively, and similar to previous excavation units, unit 64N/115E soil properties compare well to the Mountwow series, which is an Andisol.

Excavation unit 64N/115E contains an Andisol soil profile of tephra and intercalated A horizons that formed in andesitic parent material (see Figure 23). The profile was recorded accurately, the exception being the zone, described previously, below S27 (MSH-Yn), which cannot be directly attributable to MR-F. Depositional environment is direct ash and pumice fall based on grain-size statistics (see Figure 22). Post-depositional alterations took place as evidenced by probability curve deviations and occurrence of coarse, lapilli-sized grains, most notably in S25, which is interpreted as being reworked. See Table 14 for a complete list of S23 through S28 interpretations.

Table 14. Excavation Unit 64N/115E Sample Interpretations

Sample	Originally Recorded As	Interpretation
23	DM MSH-W/MR-C	Buried A horizon: MR-C tephra
24	MR-C	Poorly weathered parent material: MR-C
25	DM MR-C/MSH-P & MSH-P	Reworked MSH-P or Yn buried A horizon with MR-C lapilli
26	DM MSH-P/MSH-Yn	Buried A horizon: MSH-Yn ash
27	MSH-Yn	Poorly weathered parent material: MSH-Yn ash
28	DM MSH-Yn/MR-F	Buried A horizon: pre MSH-Yn (MR-F/S/N/D/A/R)

Excavation Unit 71.5N/66.5E Results

Excavation unit 71.5N/66.5E contains seven strata, four of which were recorded as dark mats or a combination of dark mat and tephra, and three recorded as tephra (Table 15). Gravel ranges from 4.1% (S32) to 35.4% (S31), sand ranges from 48.9% (S31) to

77.5% (S33), silt ranges from 14.7% (S29 and S31) to 32.4% (S34), and clay ranges from 1% (S31) to 2.1% (S35) (see Figure 30). There are higher percentages of coarser, lapilli-sized grains in S30 and S31, decreasing sharply to mostly sand-sized grains in S32 through S35 (see Figure 30). Silt content abruptly increases in S30, S32, and S34, two of which are dark mats (S30 and S34), compared to adjacent tephra strata.

Table 15. Excavation Unit 71.5N/66.5E Samples.

[1]Sample Number	[2]Depositional Unit	Location	Grain size in phi & Wentworth units
29	DM Duff/MSH-W	71.5N/66.5E	2 (medium sand)
30	MSH-W & DM MSH-W/MR-C	71.5N/66.5E	2 (medium sand)
31	DM MSH-W/MR-C & MR-C	71.5N/66.5E	2(medium sand)
32	MSH-P	71.5N/66.5E	2 (medium sand)
33	MSH-Yn	71.5N/66.5E	2 (medium sand)
34	DM MSH-Yn/MR-F	71.5N/66.5E	2 (medium sand)
35	MR-F	71.5N/66.5E	2 (medium sand)

[1] Sample number refers to the stratum sampled and either the associated fine-grained or coarse-grained sub sample. [2]Depositional unit refers to the tephra or tephra-associated dark mat the sample was recorded as in the field, during field collection in 2011-2013. [3] Dark Mats are abbreviated as "DM".

Mean grain size ranges from 2.87 phi (S34) to 0.22 phi (S31), standard deviation ranges from 2.17 phi (S33) to 3.76 phi (S31), skewness ranges from -0.11 phi (S31) to 0.39 phi (S32), and kurtosis ranges from 0.85 phi (S31) to 2.13 phi (S29) (Table 16). Probability curves exhibit pronounced deviations from normal distributions in S30 and S31 (Figure 29). Deviations take the form of multiple straight segments intersecting at 0 phi, which is the transition from coarse to very coarse sand.

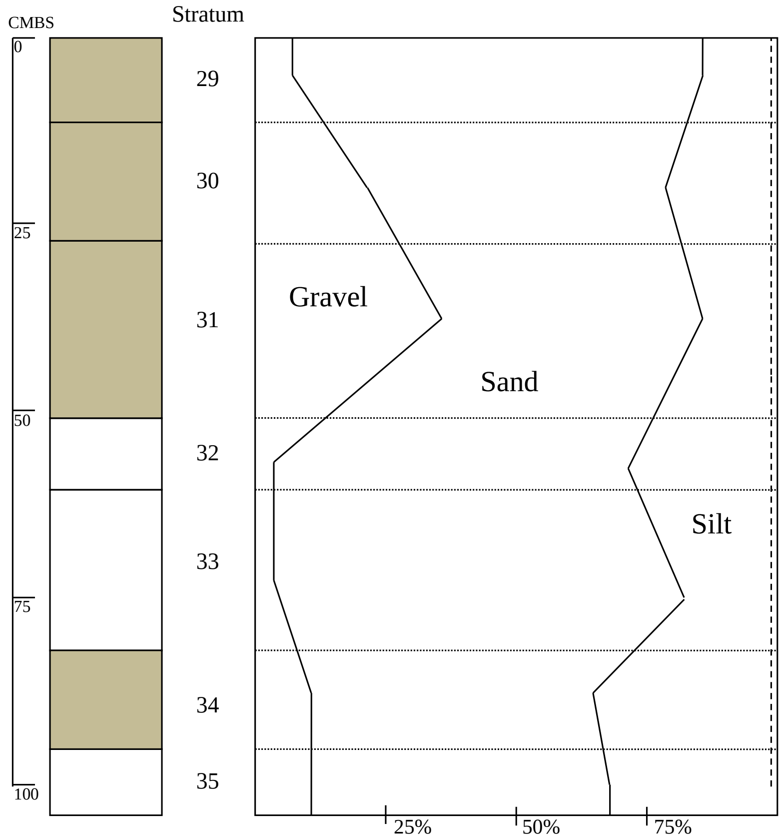

Figure 30. Profile of unit 71.5N/66.5E (left) and associated texture by strata (right), organized by cumulative percent. Clay content (dashed line) ranges from 1.0% to 2.1%, peaking in stratum 35. Dark mats (strata 29, 30, 31, & 34) are dark shaded.

Table 16. Unit 71.5N/66.5E Grain-Size Data.

#	[1]**Texture**	**Mode 1**	**Mode 2**	$\bar{x}$	σ	***Sk***	***K***
29	Loamy Sand	1.5	-	2.051	2.300	0.215	2.129
30	Gravelly Sandy Loam	1.5	-2.167	1.488	3.257	-0.055	1.285
31	Very Gravelly Loamy Sand	0.5	-5.167	0.218	3.764	-0.107	0.847
32	Sandy Loam	1.5	5.5	2.721	2.378	0.391	1.030
33	Loamy Sand	1.5	-	2.051	2.169	0.359	1.370
34	Sandy Loam	1.5	3.5	2.871	2.961	-0.062	1.187
35	Sandy Loam	1.5	5.5	2.795	2.951	0.106	1.015

[1]Texture based on USDA classification.

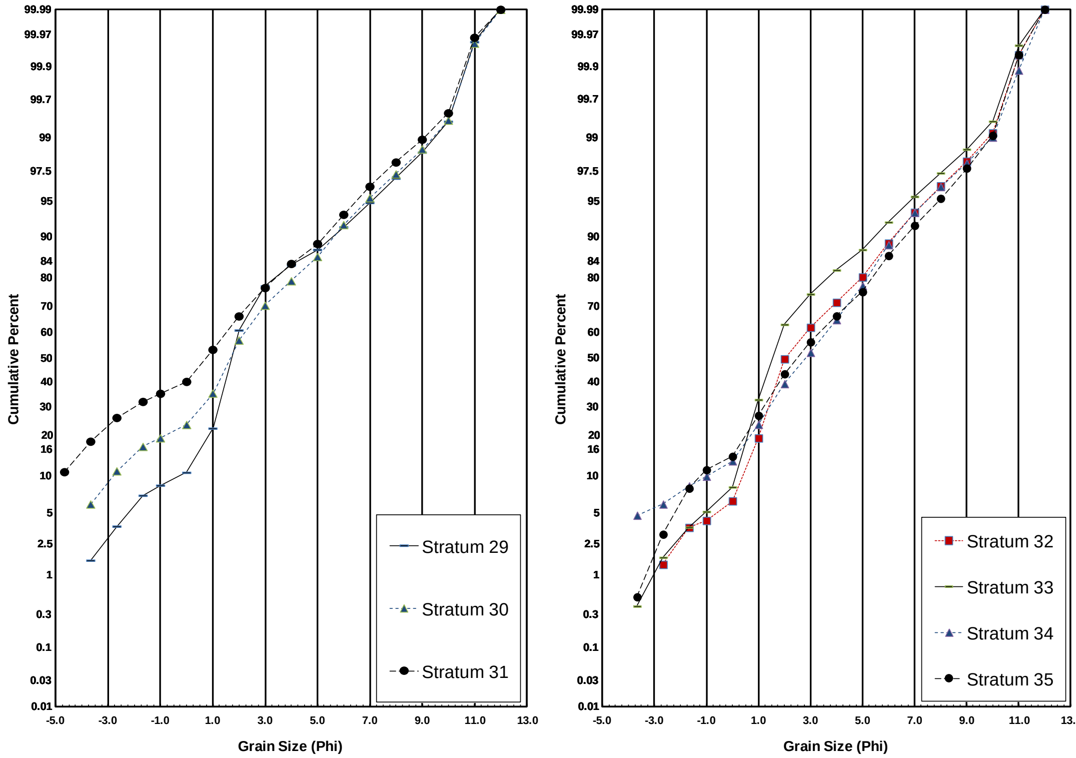

Figure 31. Probability curves of grain size within each stratum from unit 71.5N/66.5E

Silica content ranges from 60.3% (S29) to 61.2% (S32), and total alkali content ranges from 5.48% (S31) to 5.92% (S29) (see Appendix D). Silica content is lowest in S29 and S35, but not less than 60.3%, which is relatively high compared to other excavation units in this study. Silica content is highest in S32. Trace element trends show slight decreases in Cr and Ni from S31 to S32, but not the rate of decreases observed in previous excavation units. Abrupt changes in Sr and Ba proportions are associated with S33 (Figure 32).

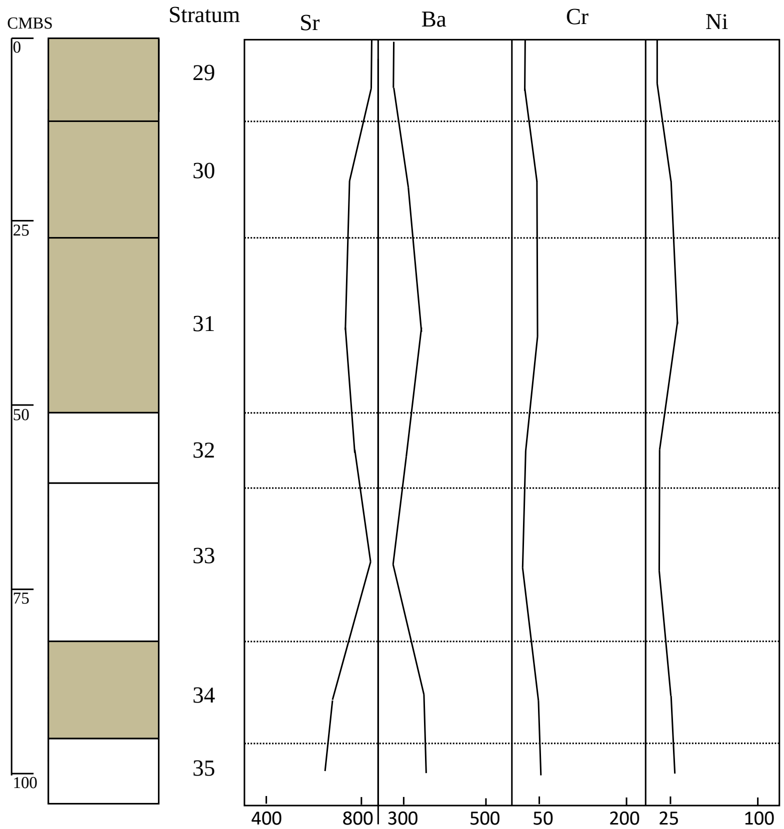

Figure 32. Profile of unit 71.5N 36E (left) and strata associated trace element proportions (right) expressed in parts per million (ppm). Dark mats (strata 29, 30, 31, & 34) are shaded dark.

Organic matter content ranges from 2.9% (S32) to 6.22% (S30), $CaCO_3$ content ranges from 0.04% (S29) to 0.35% (S35), and pH ranges from 5.11 (S29) to 6.21 (S35) (Table 17). Organic matter content is higher in three of four dark mats compared to underlying, adjacent tephra strata in excavation unit 71.5N/66.5E (Table 17). It should be noted that the difference in OM content between S34 (5.51%) and S35 is (5.55%) is rather negligible. Color ranges from 10YR 5/1-gray to 10YR 4/6- dark yellowish brown, with dark mats typically darker than adjacent/underlying tephra strata (see Appendix F).

Table 17. Excavation Unit 71.5N/66.5E OM, $CaCO_3$, and pH Data.

Sample Number	[1]Depositional Unit	Excavation Unit	OM (%)	$CaCO_3$ (%)	pH
29	DM Duff/MSH-W	71.5N/66.5E	5.08	0.04	5.11
30	MSH-W & DM MSH-W/MR-C	71.5N/66.5E	6.22	0.12	5.25
31	DM MSH-W/MR-C & MR-C	71.5N/66.5E	4.41	0.18	5.47
32	MSH-P	71.5N/66.5E	2.90	0.10	5.64
33	MSH-Yn	71.5N/66.5E	3.10	0.14	5.57
34	DM MSH-Yn/MR-F	71.5N/66.5E	5.51	0.26	5.59
35	MR-F	71.5N/66.5E	5.55	0.35	6.21

[1] Denotes depositional unit as recorded in the field by field school students.

Excavation Unit 71.5N/66.5E Interpretations

Excavation unit 71.5N/66.5E contains coarse, lapilli-sized grains in S30 and S31 that are the product of Mount Rainier eruptions. Sample 29, S32 and S33 have primarily sand-sized grains more consistent with Mount St. Helens ash (Mullineaux, 1974; Sisson and Vallance, 2009). Standard deviation (2.17 phi to 3.76 phi) and skewness (-0.11 phi to 0.39 phi) of grain-size distributions is consistent with tephra and ash fall as opposed to other depositional environments (see Figure 22).

Chemistry measurements from S29 through S35 resulted in silica content (60.3% to 61.2%) and total alkali content (5.48% to 5.92%) consistent with andesitic parent materials (see Figure 23). There is no low silica content (less than 60%) characteristic of Mount Rainier tephra. Samples recorded as Mount St. Helens ash (S32 and S33) have typical silica content associated Mount St. Helens eruptions. This could be potentially due to the disturbed nature of the profile, which is discussed at the end of this subsection. Trace element trends that exhibit slight decreases in Cr and Ni from S31 to S32 suggest a transition from a Mount Rainier to a Mount St Helens parent material. Relatively abrupt changes in Sr and Ba proportions from S31 to S33 underline a stratigraphic change to a poorly weathered MSH-Yn ash observed in MSH-Yn previously (see Figure 32).

Organic matter content of S29 through S35 (2.9% to 6.22%) meet criteria for mineral soil horizons. Three dark mats (S29, S30, and S31) have higher OM content compared to underlying tephras (S32 and S33). The fourth dark mat (S34) has only slightly less OM content (5.51%) compared to the underlying tephra strata (5.55%). All four dark mats are as dark, or darker than underlying horizons (see Appendix F). Based on dark mats predominantly having more OM content compared to underlying tephra, and having color as dark, or darker than underlying tephra, they are interpreted as A horizons. Calcium carbonate ($CaCO_3$) content (0.04% to 0.35%) and acidity (pH of 5.11 to 6.21) is slightly more towards a neutral pH, but still compares well to ranges described in Tipsoo, Owyhigh, Mysticlake, and Mountwow soil series' (Soil Survey Staff, 2018). Collectively, and similar to previous excavation units, soil properties compare well to the Mountwow series, which is an Andisol.

Excavation unit 71.5N/66.5E contains an Andisol soil profile of tephra and A horizons that formed in andesitic parent material (see Figure 23). The profile was recorded accurately, the exception being the zone, described previously, below S33 (MSH-Yn), which cannot be directly attributable to MR-F. Depositional environment is direct ash and pumice fall based on grain-size statistics (see Figure 22). Post-depositional alterations took place as evidenced by probability curve deviations in S30 and S31 (see Figure 31), and the fact S30 and S31 were recorded as mixed strata with characteristics of dark mat and tephra. Because of this, S30 and 31 are interpreted as reworked surfaces in but not necessarily indicative of overall excavation unit integrity. See Table 18 for a complete list of S29 through S35 interpretations.

Table 18. Excavation Unit 71.5N/66.5E Sample Interpretations.

Sample	Originally Recorded As	Interpretation
29	DM Duff/MSH-W	A horizon: MSH-W ash
30	MSH-W & DM MSH-W/MR-C	Reworked MSH-W ash and buried A horizon of MR-C ash & lapilli
31	DM MSH-W/MR-C & MR-C	Reworked buried A horizon and parent tephra: MR-C tephra
32	MSH-P	Reworked MSH-Yn with possibly MSH-P
33	MSH-Yn	Poorly weathered parent material: MSH-Yn ash
34	DM MSH-Yn/MR-F	Buried A horizon: pre MSH-Yn (MR-F/S/N/D/A/R)
35	MR-F	Poorly weathered parent material: pre MSH-Yn (MR-F/S/N/D/A/R)

Off-site Unit

The off-site unit contains nine strata, three of which were recorded as dark mats, and six recorded as tephra (Table 19). Gravel ranges from 4.5% (S41) to 29.7% (S43), sand ranges from 51.4% (S43) to 79.3% (S36), silt ranges from 5.2% (S37) to 27.1% (S42), and clay ranges from 0.3% (S36 and S37) to 1.9% (S32) (see Figure 33). There are higher percentages of coarser, lapilli-sized grains in S37 and S38, decreasing steadily to mostly sand-sized grains by S42, then increasing sharply in S43 (see Figure 33). Silt content abruptly increases in S42, a tephra stratum, but otherwise exhibits relatively smooth transition between strata in the excavation unit.

Table 19. Off-site Excavation Unit Samples.

[1]Sample Number	[2]Depositional Unit	Location	Grain size in phi & Wentworth units
36	DM MSH-W/Organic	Off-site	No chemistry data
37	MSH-W	Off-site	2 (medium sand)
38a	MR-C	Off-site	1(coarse sand)
38b	MR-C	Off-site	-1.7 (very fine to fine pebbles)
39	MSH-Yn	Off-site	2 (medium sand)
40	DM MSH-Yn/MR-F	Off-site	2 (medium sand)
41	MR-F	Off-site	3 (fine sand)
42	MAZ-O	Off-site	3 (fine sand)
43	DM MAZ-O/MR-R	Off-site	3 (fine sand)
44	MR-R	Off-site	1 (coarse sand)

[1] Sample number refers to the stratum sampled and either the associated fine-grained or coarse-grained sub sample. [2]Depositional unit refers to the tephra or tephra-associated dark mat the sample was recorded as in the field, during field collection in 2011-2013. [3] Dark Mats are abbreviated as "DM".

Mean grain size ranges from 2.67 phi (S42) to 0.63 phi (S37), standard deviation ranges from 1.85 phi (S36) to 3.06 phi (S43), skewness ranges from -0.08 phi (S43) to 0.32 phi (S36), and kurtosis ranges from 0.79 phi (S43) to 1.2 phi (S39) (Table 20). Probability curves exhibit relatively few deviations from normal distributions, the exception being in S39 (Figure 34).

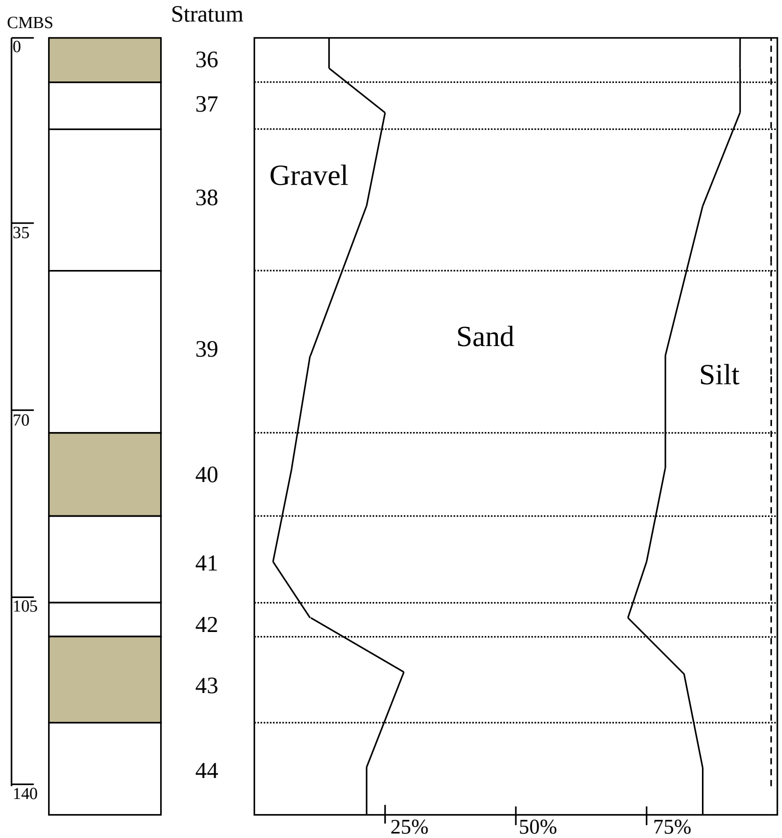

Figure 33. Profile of off-site unit (left) and associated texture by strata (right), organized by cumulative percent. Clay content (dashed line) ranges from 0.3% to 1.9%, peaking in stratum 42. Dark mats are strata (36, 40, & 43).

Table 20. Off-site Excavation Unit Grain-Size Data.

#	[1]Texture	Mode 1	Mode 2	$\bar{x}$	σ	*Sk*	*K*
36	Gravelly Sand	0.5	-	0.783	1.851	0.317	1.109
37	Gravelly Sand	1.5	-1.334	0.627	2.179	-0.064	1.025
38	Gravelly Loamy Sand	0.5	-2.167	1.020	2.716	0.050	1.036
39	Loamy Sand	1.5	-2.167	2.124	2.449	0.174	1.195
40	Loamy Sand	1.5	-	2.383	2.210	0.065	1.078
41	Sandy Loam	2.5	-	2.656	2.250	0.129	1.042
42	Sandy Loam	2.5	5.5	2.674	2.865	0.080	1.107
43	Gravelly Sandy Loam	2.5	-2.167	1.290	3.064	-0.080	0.793
44	Gravelly Loamy Sand	-1.334	0.5	1.342	2.580	0.086	0.913

[1]Texture based on USDA classification.

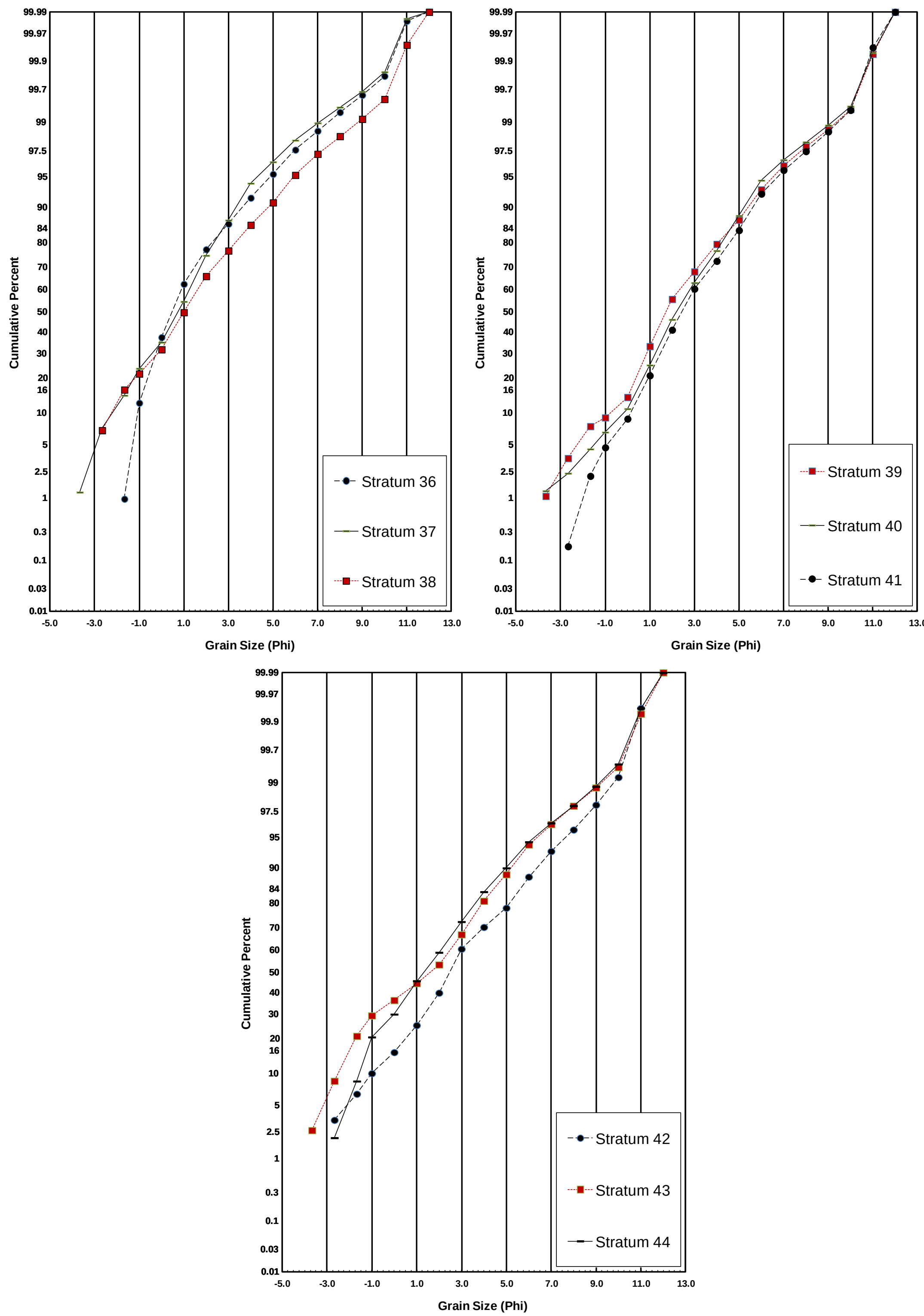

Figure 34. Probability curves of strata from off-site unit

Silica content ranges from 56.8% (S43 and S44) to 60.9% (S37), and total alkali content ranges from 5.16% (S38a) to 5.71% (S37) (see Appendix D). Silica content is lowest in S38, S43, and S44, and highest in S37 and S39. Trace element trends show decreases in Cr and Ni from S38 to S39 to below 75 ppm and 50 ppm, respectively, in addition to abrupt changes in Sr and Ba proportions associated with S39 (Figure 35).

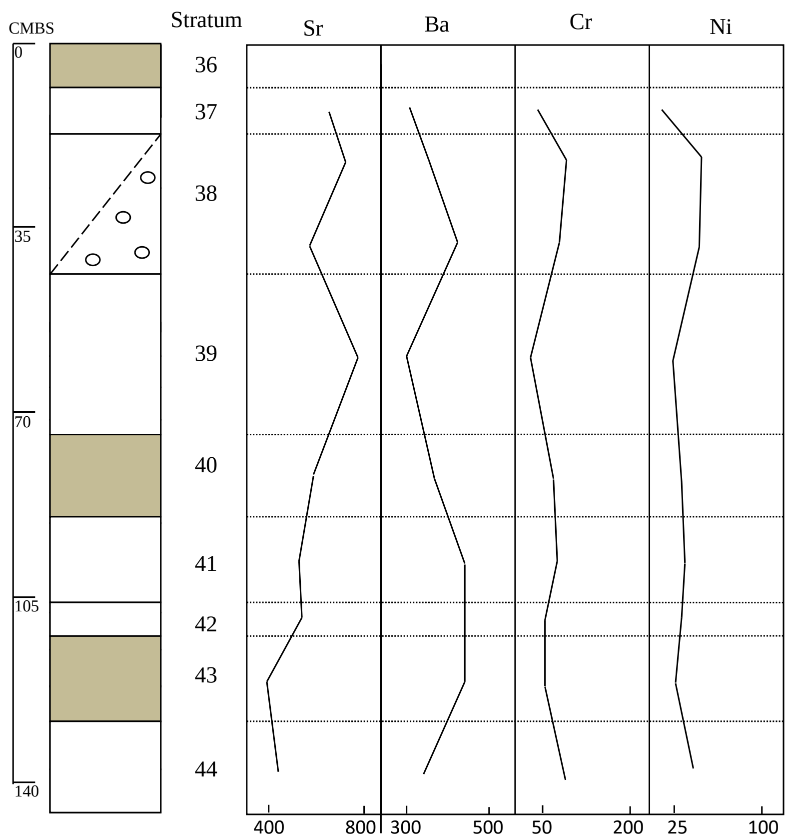

Figure 35. Profile of off-site unit (left) and strata associated trace element proportions (right) expressed in parts per million (ppm). Dark mats (strata 36, 40, & 43) are shaded dark. Circles denote the coarser grain-size class sampled within that stratum, which is expressed as the lower measurement.

Organic matter content ranges from 2.67% (S39) to 67.48% (S36), $CaCO_3$ content ranges from 0.08% (S37) to 0.59% (S44), and pH ranges from 3.71 (S36) to 7.64 (S43) (Table 21). Disregarding S36 (an extreme outlier discussed later), OM content is higher in one of two dark mats compared to underlying, adjacent tephra strata in the off-site excavation unit (see Table 21).

Table 21. Off-site Excavation Unit OM, $CaCO_3$, and pH Data.

Sample Number	[1]Depositional Unit	Excavation Unit	OM (%)	$CaCO_3$ (%)	pH
36	DM O/W	Off-site	67.48	0.14	3.71
37	MSH-W	Off-site	14.77	0.08	3.66
38	MR-C	Off-site	5.49	0.26	5.91
39	MSH-Yn	Off-site	2.67	0.14	6.96
40	DM MSH-Yn/MR-F	Off-site	4.11	0.27	7.36
41	MR-F	Off-site	5.90	0.50	7.42
42	MAZ-O	Off-site	7.67	0.58	7.33
43	DM MAZ-O/MR-R	Off-site	8.34	0.57	7.64
44	MR-R	Off-site	7.11	0.59	7.46

[1] Denotes depositional unit as recorded in the field by field school students.

Off-site Unit Interpretation

The off-site excavation unit contains coarse, lapilli-sized grains in S37, S38, S43, and S44 that are the product of Mount Rainier eruptions. Sample 39, S40, S41, and S42 have primarily sand and silt-sized grains more consistent with either Mount St. Helens or Mount Mazama tephra (Mullineaux, 1974; Sisson & Vallance, 2009). Standard deviation (1.85 phi to 3.06 phi) and skewness (-0.08 phi to 0.32 phi) of grain-size distributions are consistent with tephra and ash fall as opposed to other depositional environments (Figure 37).

Chemistry measurements from S36 through S44 resulted in silica content (56.8% to 60.9%) and total alkali content (5.16% to 5.71%) consistent with andesitic parent materials (see Figure 23). Low silica content in S38, S43, and S44 is consistent with the chemistry of Mount Rainier tephra, while high silica content in S37 and S39 is consistent with Mount St. Helens tephra. Trace element trends that exhibit slight decreases in Cr and Ni from S38 to S39 suggest a similar transition from a Mount Rainier to a Mount St Helens parent material discussed in excavation units at the SRBP site. Relatively abrupt changes in Sr and Ba proportions associated with S39 underline a stratigraphic change to a poorly weathered MSH-Yn ash (see Figure 35).

Organic matter content of S37 through S43 (2.67% to 14.77%) meet criteria for mineral soil horizons, and potential A horizons. However, S36 has an OM content of 67.48%, well exceeding the 20% OM content threshold for mineral soil horizons. Organic matter content of this degree places S36 well into the O horizon category, and with its highly decomposed nature, is classified as an Oa horizon. Of the other samples recorded as dark mats, S43 has a higher OM content compared to adjacent/underlying tephra, and S40 has a lower OM content compared to adjacent/underlying tephra. Both dark mats (S40 and S43) are darker in color compared to underlying tephra, and both share similar grain-size distributions compared to underlying tephra (see Figures 33 and 34). Therefore, it seems more likely than not that S40 is a buried A horizon that formed in S41 tephra, and S43 is a buried A horizon that formed in S43 tephra. Calcium carbonate ($CaCO_3$) content (0.08% to 0.59%) and acidity (pH of 3.71 to 7.64) is significantly more alkaline compared to SRBP site excavation units, but is still similar to ranges described in Tipsoo, Owyhigh, Mysticlake, and Mountwow soil series' (Soil Survey Staff, 2018). Collectively, and similar to SRBP site excavation units, soil properties compare well to the Mountwow series, which is an Andisol.

The off-site excavation unit contains an Andisol soil profile of tephra and A horizons that formed in andesitic parent material (see Figure 23). The profile was recorded accurately, the exception being the initial dark mat being mostly organic, as well as a zone, described previously, between S39 (MSH-Yn) and S42 (MAZ-O) that cannot be directly attributable to MR-F. Depositional environment is direct ash and pumice fall based on grain-size statistics (see Figure 22). Post-depositional alterations took place as evidenced by probability curve deviations in S39 due to about 10% lapilli-sized grains (see Figures 33 and 34). See Table 22 for a complete list of S29 through S35 interpretations.

Table 22. Off-site Excavation Unit Sample Interpretations.

Sample	**Originally Recorded As**	**Interpretation**
36	DM Duff/MSH-W	Highly-weathered organic horizon (Oa Horizon)
37	MSH-W	Reworked MSH-W ash and MR-C lapilli
38	MR-C	Poorly weathered parent material: MR-C
39	MSH-Yn	Reworked MSH-Yn ash with MR-C lapilli
40	DM Yn/F	Buried A horizon: pre MSH-Yn (MR-F/S/N/D/A)
41	MR-F	Poorly weathered parent material: (MR-F/S/N/D/A)
42	MAZ-O	Reworked MAZ-O ash and MR-F/S/N/D/A/R ash and lapilli
43	DM MAZ-O/MR-R	Buried A horizon: MR-R tephra
44	MR-R	Poorly weathered parent material: MR-R tephra

The off-site unit and 30N/24E are the only two units in this study containing MAZ-O tephra (S10, S11, and S42). Sample 11 and S42 were recorded as parent tephra (non-dark mat), and have two of the three highest silt contents of any samples of this study at 31% and 27.1%, respectively. Such high silt content suggests they were recorded correctly since MAZ-O ash is known to be the finest-grained ash in the park (Mullineaux, 1974). Presence of clear horizons of MAZ-O ash can act as temporal boundaries when interpreting artifact locations occurring below and beneath them. The occurrence of MAZ-O ash (S42) allows for easy identification of MR-R, which is the only tephra underlying MAZ-O in this area of MORA (Mullineaux, 1974).

The lack of buried A horizons associated with MAZ-O, MSH-Yn, and MR-C parent tephras is peculiar. This could be attributed to erosional events that took place at the off-site location that were lacking at the SRBP site, or vegetation destroyed by eruptions. Another potential explanation is a lack of inputs from people as the off-site landform and unit had no evidence of precontact land use. Other soil forming factors should be similar as the off-site unit was on a similar landform as the SRBP site, with the same precipitation, vegetation, etc. The dearth of A horizons at the off-site location is interpreted as likely being due to natural processes since, at this time, there is no direct evidence A horizons that formed in tephra strata at the SRBP site were the direct result or assisted by human land use.

Archaeological Feature Results

Three features were analyzed in this study, all of which were recorded in association with dark mats (Table 23). Gravel ranges from 5.4% (S47) to 20.4% (S45), sand ranges from 63.9% (S45) to 73.3% (S47), silt ranges from 14.7% (S45) to 19.9% (S47), and clay ranges from 1% (S45) to 1.4% (S47) (Figure 36). Among the feature samples, S45 has the highest percentage of coarse, lapilli-sized grains, followed by S46, then S47 (see Figure 34). Conversely, S47 has the highest sand and silt-sized grains, followed by S46, then S45.

Table 23. Archaeological Feature Samples.

[1]Sample Number	[2]Depositional Unit	Location	Grain size in phi & Wentworth units
45a	Feature R (DM MSH-W/MR-C)	61.5N/36E	1 (coarse sand)
45b	Feature R (DM MSH-W/MR-C)	61.5N/36E	-1.7 (very fine to fine pebbles)
46a	Feature AA (DM MR-C/MSH-P)	71.5N/66.5E	1 (coarse sand)
46b	Feature AA (DM MR-C/MSH-P)	71.5N/66.5E	-1.7 (very fine to fine pebbles)
47a	Feature E (DM MSH-P/MSH-Yn)	28N 25E	2 (medium sand)
47b	Feature E (DM MSH-P/MSH-Yn)	28N 25E	-1.7 (very fine to fine pebbles)

[1] Sample number refers to the stratum sampled and either the associated fine-grained or coarse-grained sub sample. [2]Depositional unit refers to the tephra or tephra-associated dark mat the sample was recorded as in the field, during field collection in 2011-2013. [3] Dark Mats are abbreviated as "DM".

Mean grain size ranges from 2.47 phi (S47) to 1.11 phi (S45), standard deviation ranges from 2.25 phi (S47) to 2.79 phi (S45), skewness ranges from 0.04 phi (S46) to 0.23 phi (S47), and kurtosis ranges from 1.05 phi (S45) to 1.27 phi (S47) (Table 24).

Probability curves show sharpest deviations from normal distributions in S46 and 47 (Figure 37).

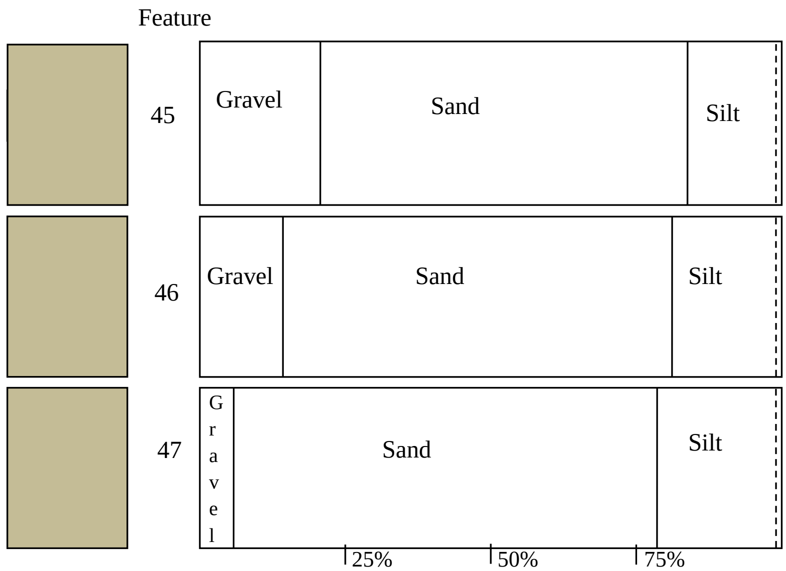

Figure 36. Archaeological feature texture, organized by cumulative percent. Clay content (dashed line) ranges from 1.0% to 1.4%, peaking in sample 47. Sample 45 is from Feature R in 6.5N/36E, and was recorded in association with DM W/C. Sample 46 is from Feature AA in 71.5N/66.5E, and was recorded in association with DM C/P. Sample 47 is from Feature E located in 28N/25E and was recorded in association with DM P/Yn.

Table 24. Archaeological Feature Grain-Size Data.

#	[1]Texture	Mode 1	Mode 2	$\bar{x}$	σ	*Sk*	*K*
45	Gravelly Loamy Sand	0.5	-2.167	1.113	2.790	0.113	1.045
46	Loamy Sand	0.5	-2.167	1.798	2.736	0.042	1.169
47	Loamy Sand	1.5	-	2.474	2.249	0.232	1.270

[1]Texture based on USDA classification.

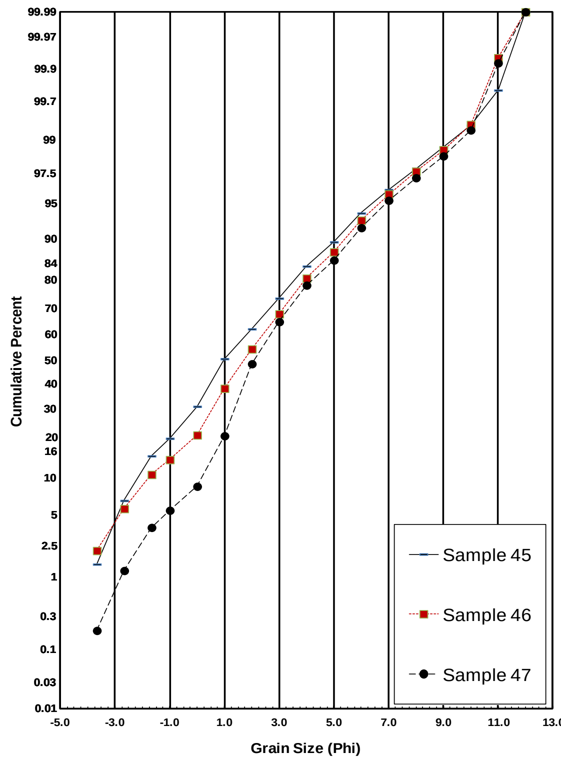

Figure 37. Probability curves for archaeological features.

Silica content ranges from 58.2% (S47) to 62.1% (S46), and total alkali content ranges from 5.25% (S45a) to 5.68% (S47a) (see Appendix D). Trace element data is similar to those in the previous excavation units (Figure 38). Organic matter content ranges from 4.34% (S46) to 5.42% (S45), $CaCO_3$ content ranges from 0.11% (S45) to 0.59% (S46), and pH ranges from 5.98 (S47) to 6.91 (S45) (Table 25).

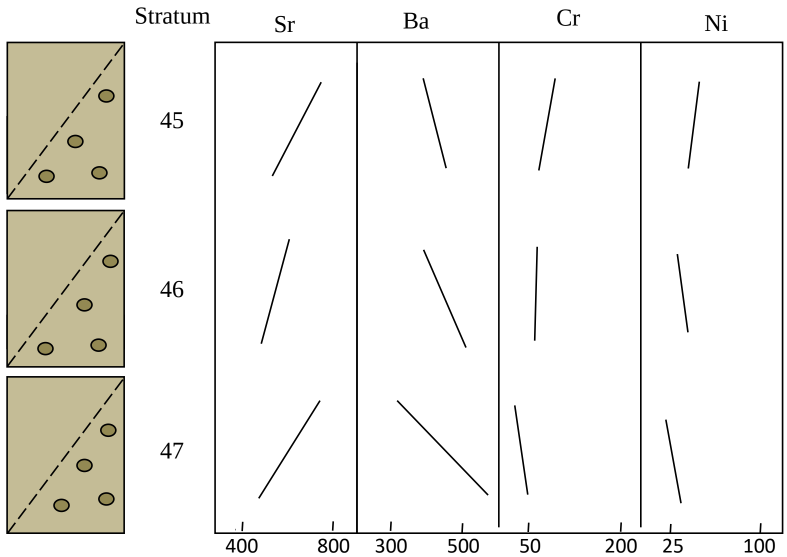

Figure 38. Archaeological feature trace element proportions expressed in parts per million (ppm). Circles denote the coarser grain-size class sampled within that feature sample, which is expressed as the lower measurement.

Table 25. Archaeological Feature OM, $CaCO_3$, and pH Data.

Sample Number	[1]Depositional Unit	Excavation Unit	OM (%)	$CaCO_3$ (%)	pH
45	Feature R (DM MSH-W/MR-C)	61.5N/36E	5.42	0.11	6.91
46	Feature AA (DM MR-C/MSH-P)	71.5N/66.5E	4.34	0.20	6.56
47	Feature E (DM MHS-P/MSH-Yn)	28N 25E	5.18	0.16	5.98

[1] Denotes depositional unit as recorded in the field by field school students.

Features Interpretation

Features in this study contained coarse, lapilli-sized grains in S45, S46, and in a small percentage of S47 (5.4%), which are the product of Mount Rainier eruptions. Sample 47 has 73.3% sand-sized grains that is consistent with Mount St. Helens Yn ash (Mullineaux, 1974; Sisson & Vallance, 2009). Standard deviation (2.25 phi to 2.79 phi) and skewness (0.04 phi to 0.23 phi) of grain-size distributions are similar to ranges discussed previously, and suggest tephra and ash fall depositional environments (Figure 22).

Sample 45, S46, and S47 have silica content (58.2% to 62.1%) and total alkali content (5.25% to 5.68%) consistent with andesitic parent materials (Figure 23). The lowest silica content occurs in S47 but was measured from the -1.7 phi-size mode (lapilli size) and is almost certainly Mount Rainier related, being a product of MR-C or a Mount Rainier eruption predating MSH-Yn. Disregarding that, silica content is consistent with a spectrum of S45 being the product of Mount Rainier tephra to, in order, S46 and S47 likely the product of MSH-Yn tephra. Trace element trends in S45, S46, and S47 compare well to trends exhibited in MR-C, a mix of MR-C and MSH-Yn, and MSH-Yn tephras, respectively (see Figure 38). Organic matter content (4.34% to 5.42%), and $CaCO^3$ content (0.11% to 0.59%) is similar to samples previously determined to be A horizons. However, acidity (pH of 5.98 to 6.91) is slightly higher than samples determined to be A horizons, and more similar to deeper strata of poorly weathered tephra.

Feature R (sample 45) was recorded within the dark mat directly overlying poorly weathered MR-C tephra. Grain size, chemistry, and OM content suggest that sample 45 feature fill is the reworked A horizon that formed in MR-C parent material (Table 26). This determination is primarily due to lapilli-sized grains, and relatively low silica content (59.2% to 60%). Feature AA (sample 46) was recorded within the dark mat directly overlying MSH-P tephra. Grain size, chemistry, and OM content suggest sample 46 feature fill is likely mixture of MR-C and MSH-Yn tephras and not a purely reworked

A horizon that formed in MSH-P tephra (see Table 26). This determination is primarily due to lapilli-sized grains and relatively high silica content (61.3% to 62.1%) consistent with MSH-Yn tephra (Mullineaux, 1974). Feature E (sample 47) was recorded within the dark mat directly above MSH-Yn poorly weathered tephra. Grain size, chemistry, and OM content suggest that sample 47 feature fill is the reworked A horizon of MSH-Yn parent material with a few lapilli-sized grains from a Mount Rainier eruption (see Figure 26).

Table 26. Archaeological Feature Interpretations.

Sample	Originally Recorded As	Interpretation
45	Feature R (DM MSH-W/MR-C)	Reworked buried A horizon: MR-C tephra
46	Feature AA (DM MR-C/MSH-P)	Reworked buried A horizon: MSH-Yn ash with MR-C lapilli
47	Feature E (DM MSH-P/MSH-Yn)	Reworked buried A horizon: MSH-Yn ash with MR lapilli

New Site Depositional History Model

The new site depositional history model builds on previous site stratigraphic data, sediment data, and depositional histories (Dampf, 2002; Nickels, 2002; Evans, 2011). The new depositional history model is organized similar to models discussed previously (Fedje et al., 1995; Neall et al., 2008; Fitzsimmons et al., 2014), and summarizes this study's results and interpretations into one comprehensive model that will aid in interpreting artifact frequencies (Figure 39). The model consists of a representative stratigraphic profile with accompanying parent material, depositional environment, soil horizon and strata-associated site data. Site data consists of feature locations, radiocarbon dates, chipped stone artifact totals, bone totals, and estimated surface exposure ranges.

Site data comes from excavations conducted during the 1997 to 2001 and 2011 to 2013 summer field schools. Only data recorded with associations to a specific tephra unit or dark-mat related tephra unit are used. Only features incorporated into this study are placed in the model. For information on additional features see McCutcheon et al. (2017). Only chipped stone and bone totals recovered from depositional units incorporated into the model are listed. For example, three chipped stone artifacts were recovered from a stratum recorded as being a combination of multiple depositional units: MR-C tephra and the dark mat overlying MR-C tephra. Because no such horizon was incorporated into the model, said counts are left out. Counts not included represent 2% (n = 261 of 13,036) of the total chipped stone artifacts recovered from 2011 to 2013.

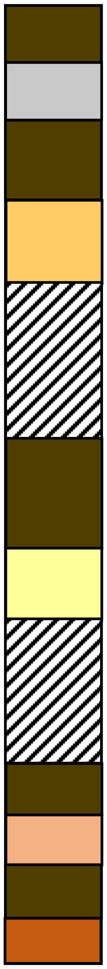

PM[1]	DE[2]	SH[3]	O[4]	Feature	Dates in cal BP[10]	Chipped Stone[11]	Bone	Exposure [12]
MSH-W	[5]DA	A	[7]MS			86 (694/m^3)	0	0-471
MSH-W	DA	C	[8]SW			742 (586/m^3)	1	0-471
MR-C	DA	Ab2	SW	45(R) 46(AA)	1350-1521; 1417-1688 1445-1707; 1636-1821	6201 (2338/m^3)	249 (94/m^3)	471-2200
MR-C	DA	C2	SW	45(R) 46(AA)		883 (338/m^3)	9 (3/m^3)	471-2200
MR-C, MSH-P, MSH-Yn	[6]RDA	Ab/C3	SW	46(AA) 47(E)	2158-2338 2350-2677 2351-2682 2354-2684	2099 (1127/m^3)	334 (179/m^3)	2200-3700
MSH-Yn	DA	Ab4	SW	47(E)	2520-2758 2991-3176	841 (455/m^3)	101 (55/m^3)	2200-3700
MSH-Yn	DA	C4	SW		2543-2758 3899-4086	869 (360/m^3)	144 (60/m^3)	2200-3700
MR-F,S,N,D, A	RDA	Ab/C5	MS	46(AA)		970 210/m^3	23 (5/m^3)	3700-7700
MAZ-O	RDA	Ab6	[9]FL			41 (43/m^3)	35 (37/m^3)	3700-7700
MAZ-O	DA	C6	FL			27 (34/m^3)	60 (74/m^3)	5600-7700
MR-R	DA	Ab7	FL			16 (59/m^3)	59 (219/m^3)	7700-10000
MR-R	DA	C7	FL			0	0	7700-10000

110 CMBS

Figure 39. New Site Depositional History Model. Dark-shaded boxes represent A horizons. Colored strata represent poorly weathered tephra C horizons. Hatched strata represent reworked deposits of multiple parent materials. "b" denotes a buried horizon. Ab/C represents a buried horizon with characteristics of an A and C horizon. Abbreviations: [1]PM (parent material), [2]DE (depositional environment), [3]SH (soil horizon), [4]O (Occurrence), [5]DA (direct ash fall), [6]RDA (reworked direct ash fall), [7]MS (most of site), [8]SW (site wide), [9]FL (few locations). [10]Dates are in c14 years before present calibrated at 2σ from McCutcheon et al. (2017). [11] Chipped stone artifacts expressed in counts and (counts per m^3). [12] Exposure is in calibrated years BP with ranges of the maximum amount of time exposed as potential ground surface inferred from Mullineaux (1974) and Sisson and Vallance (2009). Feature locations, chipped stone and bone counts, and carbon dating information is from McCutcheon et al. (2017).

The new site depositional history model organizes site stratigraphy into three types of strata: (1) A horizons that formed in tephra parent material from a single eruption; (2) C horizons of poorly weathered tephra parent material from the same eruption as the overlying A horizon; and (3) deposits of reworked sediment containing parent materials from multiple eruptions or undetermined eruptions (e.g. combination of A horizons and C horizons of MSH-Yn, MSH-P, and MR-C parent materials). For a comprehensive discussion of the model that includes a breakdown of each horizon, associated cultural materials, and implications on site use, see the article in Chapter VI.

CHAPTER VI

THE ORIGIN OF DARK MATS AT THE SUNRISE RIDGE BORROW PIT SITE (45PI408) MOUNT RAINIER NATIONAL PARK, WASHINGTON

The student coauthors this manuscript with the committee chair and it will be submitted to *Geoarchaeology: An International Journal*. The manuscript begins on the next page; the final manuscript (if accepted) may result in differences based on the results of editorial and blind peer review.

The Origin of Dark Mats at the Sunrise Ridge Borrow Pit Site (45PI408) Mount Rainier, Washington

Sean M. Stcherbinine, [1]M.S., and Patrick T. McCutcheon, Ph.D.[1,2]

[1]Cultural and Environmental Resource Management Program, Central Washington University, Ellensburg, Washington, USA

[2]Department of Anthropology and Museum Studies, Central Washington University, Ellensburg, Washington, USA

Contact information:

Sean Stcherbinine, M.S.

Central Washington University

400 E. University Way

Ellensburg, WA 98926-7544 USA

E-mail: sean.stcherb@gmail.com

- Sean M. Stcherbinine has worked in archaeology for 10 years in 9 culture areas and recently received a M.S. Cultural and Environmental Resource Management degree. He is interested in Northwest archaeology and geoarchaeology.
- Dr. Patrick T. McCutcheon has worked on stone tool analysis in the Pacific Northwest Region for over 20 years and has been working as a professional archaeologist in North American for the last 30 years. He has

conducted over 25 field schools recording and excavating the archaeological record in the Plateau and Cascade Mountains.

Abstract

The Sunrise Ridge Borrow Pit Site is a precontact archaeological site located in the upland forest soils of Mount Rainier National Park. Site stratigraphy is complicated, consisting of tephra deposits from mostly known origins that are intercalated with dark sediments of unknown origin, referred to here as dark mats. Precontact occupation has been split previously into two components based on the ambiguous depositional history of the dark mats, notably their unknown parent material, depositional environment, and relationship with adjacent tephra strata. Stratigraphic samples from excavation units, features, and one off-site excavation unit was used to investigate these data gaps. Grain size, chemistry, organic content, pH, and calcium carbonate content are characterized to document parent material and depositional environment of adjacent strata. Dark mats typically had higher organic content and similar chemistry and grain-size properties compared to underlying tephra strata, and interpreted as buried A horizons that formed in tephra of known regional origin. However, a few dark mats were reworked, and at times the product of multiple or unknown parent material. These determinations are used to revise a depositional history model of the Sunrise Ridge Borrow Pit Site that places the main occupation at 471 years BP to 2,200 cal years BP yet supports previous site assemblage organization into two precontact components.

INTRODUCTION

The archaeological record from the upland forests surrounding Mount Rainier, Washington, is often found associated with well stratified tephra deposits (Burtchard 1998) that are intercalated with dark deposits referred to here as dark mats (Lewis, 2015; McCutcheon et al., 2017). The advantage for archaeologists working in the region is that most of the tephra layers have been identified and dated (e.g., Mullineaux 1974). The stratigraphy in the region has been documented by several investigations that have focused on glacial drift and tephra-derived soils (Mullineaux, 1974; Crandell & Miller, 1974; Franklin et al., 1988; Sisson & Vallance, 2009). These investigations have generated robust data sets documenting the age and properties of major glacial drift and tephra deposits in the southern Cascade Range. However, the same focus has not been given towards dark mats observed between well-known tephra strata in the southern Cascade Range.

The parent material and depositional environment of these dark mats is of great interest to archaeologists working in the uplands surrounding Mount Rainier (Burtchard, 1998; Burtchard 2007). Understanding if these dark mats are the product of weathered tephra that represent relict stable surfaces, or the result of unknown depositional circumstances influences how the nature, timing, and duration of use for these archaeological sites in the region are interpreted. Creating a depositional history model that incorporates the relationship between tephra strata and dark mats at archaeological sites in the region would assist in discussing cultural chronologies and understanding how precontact land use changes over time in the southern Cascade Range.

Study Location

The Sunrise Ridge Borrow Pit Site (SRBP Site) is a precontact archaeological site located in the Southern Cascade Range and contains stratigraphy characterized as regional tephra strata and intercalated dark mats. The SRBP site is located at around 1,500 meters above sea level, in the Northwest Maritime Forest environmental zone of Mount Rainier National Park (Figure 1). Soils in Mount Rainier National Park at the similar elevations as the SRBP site are typically Spodosols or Andisols that form in tephra parent materials and can contain buried A horizons (Franklin et al., 1988; Soil Survey Staff, 2014; Soil Survey Staff, 2018).

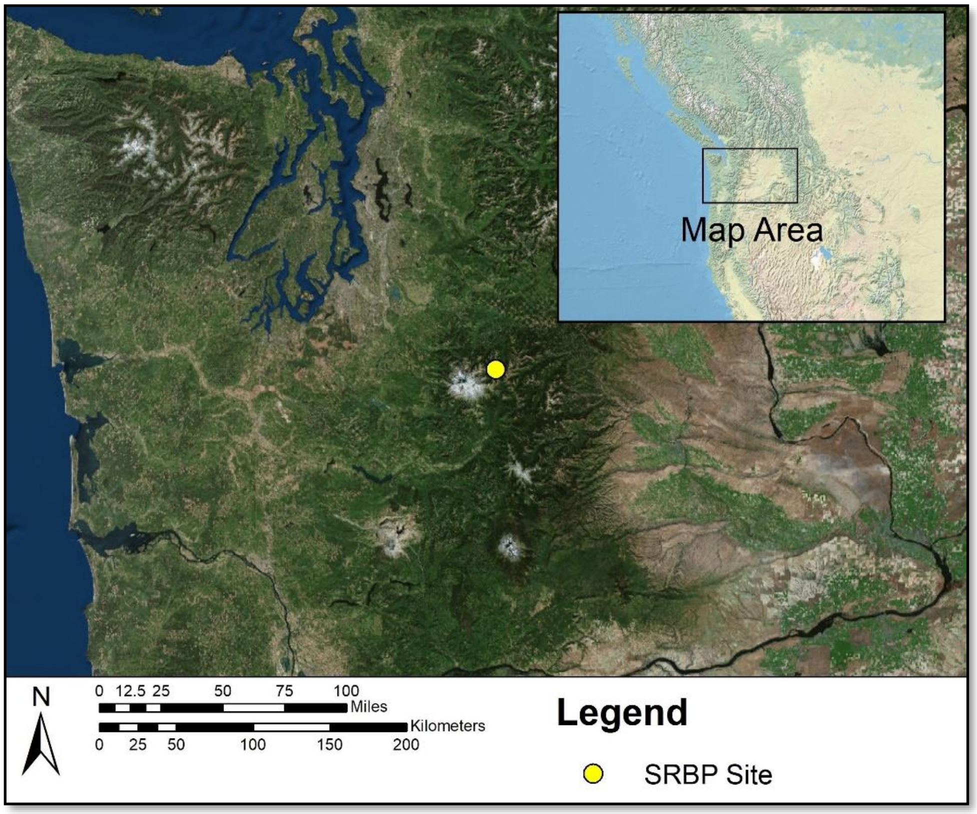

Figure 1. The Sunrise Ridge Borrow Pit Site located northeast of the summit of Mount Rainier. Created in ArcGIS 10.4.1 by Sean Stcherbinine.

The SRBP site has evidence of precontact occupation from 471 cal. BP to at least 4,000 cal. yr B.P (Chatters et al., 2017; McCutcheon et al., 2017). This chronological range is based on variety of radiometric dates on charcoal, burned bone and fire-altered rock and a subsurface artifact assemblage associated with tephra strata. Recovered artifacts from the site have been split into two precontact components (above and below Mount Rainier-C tephra). Central Washington University has excavated the SRBP site over eight summer field schools, and site data has been the source of multiple theses (Dampf, 2002; Nickels, 2002; Evans, 2011; Lewis, 2015). Site strata has been recorded as tephra, paleosol, or a combination of both (Dampf, 2002; Nickels, 2002; Evans, 2011). In this document “dark mats” refer to relatively dark-colored strata previously interpreted as paleosols intercalated between tephra (Figure 2). The majority of the artifact assemblage at the SRBP site has been recovered from dark mats (McCutcheon et al., 2017).

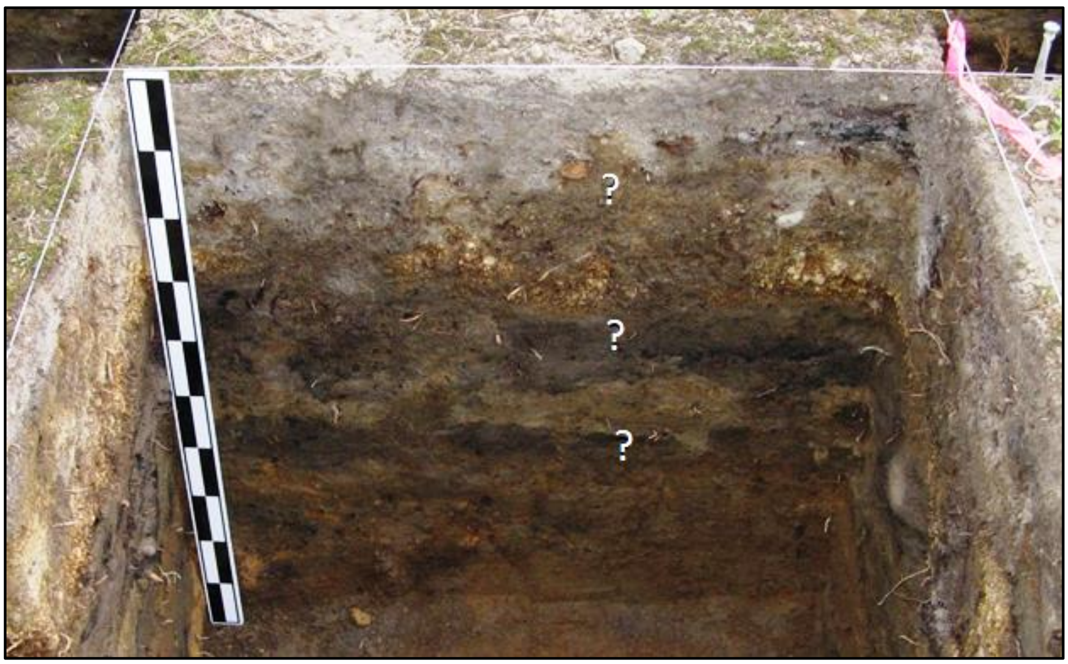

Figure 2. SRBP site excavation unit 30N/24E (east wall) with buried strata (question marks). Photo taken by Anne B. Parfitt in 2013.

Previous Investigations

Dampf (2002) analyzed lithics and > 2 phi grain-size distributions within three 50-x-50 centimeter shovel test pits, concluding stratigraphy in proximity to the test pits was largely intact. However, Dampf (2002) lacked any examination or discussion of dark mats. Nickels (2002) described multiple tephra strata from a profile the site, but only observed dark mats directly overlying and underlying MAZ-O tephra, and did not discuss dark mat parent material or depositional environment. Evans (2011) noted the occurrence of dark mats at the SRBP site, documenting that many sediment grain-size distributions were polymodal, and interpreting the dark mats as having similar properties of underlying tephra strata and likely formed by weathering on top of the parent tephra. It remains unclear if dark mats have depositional relationships to underlying tephras at the site. Without this information a complete depositional history for the site cannot be created, and current organization of site components cannot be justified.

Study Purpose

The purpose of this study is to establish the depositional relationships between dark mats and under/overlying tephra strata at the SRBP site. To establish possible depositional relationships, the physical and chemical properties are measured. By doing so, we will document the parent material and identify and explain the depositional environment. Knowledge of sediment parent material and depositional environment allows for the creation of a SRBP site depositional history model, which permits a more accurate interpretation of changes in the evidence of past land use at the SRBP site.

The data for this study comes from measuring the entire grain-size distributions from all observable strata of four 1-x-1 meter excavation units, strata from a control unit located on a similar landform in proximity to the SRBP site, and three features located at the site recorded in association with dark mats. This work is the first attempt to measure the entire grain-size distribution from sediment samples at the SRBP site. Grain-size distributions were sampled to see the chemical signatures of the most commonly occurring grain sizes in order to discuss the source of the dark mat deposits intercalated among tephra deposits in order to identify the parent material relationships among adjacent strata.

Results from grain-size and chemical measurements are used to create a depositional history model that organizes determinations of soil horizon, depositional environment, and parent material from this investigation with archaeological data from past site investigations into a new depositional model. The model will also reinterpret tephra identifications made in previous studies. This new model shows relationships between artifact location/concentrations and the artifact-bearing-strata to determine if stable surfaces occur at the site and whether artifacts from adjacent strata should be grouped or separated into different or similar archaeological components.

METHODS

The SRBP site contains four primary excavation areas: 30N, 61.5N, 64N, and 71.5N area (Figure 3). Between 2011 and 2013, these areas were excavated stratigraphically (by natural strata) using trowels. After excavations, column samples were extracted from the unit wall in each excavation area that contained the most site strata with intact stratigraphy (Figure 4). Column samples were approximately one meter tall (depending on excavation unit depth) by 20 centimeters wide by 10 centimeters deep (see Figure 4). Column sample consisted a series of individual bulk samples, one of each strata observed, in this case, tephra strata and intercalated dark mats. Each bulk sample was placed in a plastic bag and labeled with the dark mat or tephra as recorded in the field, elevation, date, and excavator. One column sample that best represented overall site stratigraphy was chosen from each of the four excavation areas for this study. The four column samples chosen were from excavations units 30N/24E, 61.5N/36E, 64N/115E, and 71.5N/66.5E (see Figure 3). Refer to Table 1 for a list of samples and sample data.

Twenty-nine features were recorded at the SRBP site. Most features consisted of unstructured fire cracked rock (FCR) and dark sediment. Only features recorded in dark mats and associated with other evidence of occupation (e.g., lithics, burned bone, and fire-cracked rock) were considered for this study. Feature R (associated with dark mat W/C), Feature AA (associated with dark mat C/P), and Feature E (associated with dark mat P/Yn) were selected for this study.

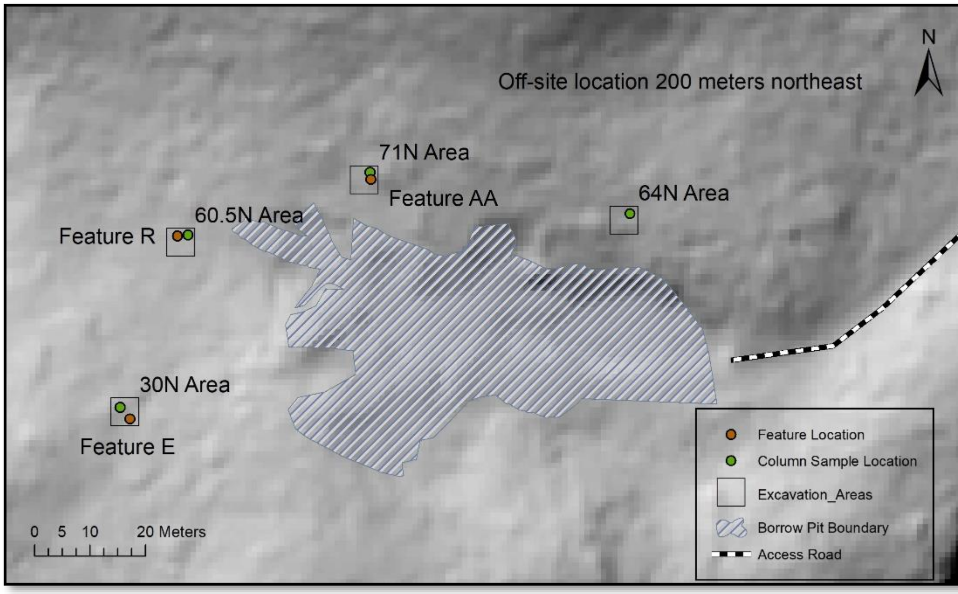

Figure 3. Map showing the SRBP site's main excavation areas, approximate column sample and feature locations. Created in ArcGIS 10.4.1 by Sean Stcherbinine.

Figure 4. Column sample at excavation unit 30N/24E (north wall). Scale is one-meter long. Photo taken by Anne B. Parfitt in 2013.

Table 1. Column Sample Data.

Sample Number	[1]Depositional Layer	Location	Elevation (cmbs)
1	MSH-W	30N/24E	0-13
2	DM MSH-W/MR-C	30N/24E	13-26
3	MR-C	30N/24E	26-45
4	DM MR-C/MSH-P	30N/24E	45-51
5	MSH-P	30N/24E	51-57
6	DM MSH-P/MSH-Yn	30N/24E	57-63
7	MSH-Yn	30N/24E	63-76
8	DM MSH-Yn/MR-F	30N/24E	76-93
9	MR-F	30N/24E	93-98
10	DM MR-F/MAZ-O	30N/24E	98-104
11	MAZ-O	30N/24E	104-108
12	DM MAZ-O/MR-R	30N/24E	108-115
13	MR-R	30N/24E	115-123
14	MSH-W	61.5N/36E	0-13
15	DM MSH-W/MR-C	61.5N/36E	13-26
16	MR-C	61.5N/36E	26-40
17	DM MR-C/MSH-P	61.5N/36E	40-51
18	DM MSH-P/MSH-Yn	61.5N/36E	51-59
19	MSH-Yn	61.5N/36E	59-69
20	DM MSH-Yn/MR-F	61.5N/36E	69-88
21	MR-F	61.5N/36E	88-100
22	MR-R	61.5N/36E	100-112
23	DM MSH-W/MR-C	64N/115E	0-14
24	MR-C	64N/115E	14-32
25	[2] DM MR-C/MSH-P & MSH-P	64N/115E	32-51
26	DM MSH-P/MSH-Yn	64N/115E	51-61
27	MSH-Yn	64N/115E	61-83
28	DM MSH-Yn/F	64N/115E	83-105
29	DM Duff/MSH-W	71.5N/66.5E	0-13
30	MSH-W & DM MSH-W/MR-C	71.5N/66.5E	13-27
31	[2]DM MSH-W/MR-C & MR-C	71.5N/66.5E	27-51
32	MSH-P	71.5N/66.5E	51-59
33	MSH-Yn	71.5N/66.5E	59-80
34	DM MSH-Yn/MR-F	71.5N/66.5E	80-94
35	MR-F	71.5N/66.5E	94-103
36	Duff/MSH-W	Off site	0-9
37	MSH-W	Off site	9-18
38	MR-C	Off site	18-40

[1]Depositional layer listed as recorded in the field during collection. [2]Depositional layer containing multiple depositional units.

Table 1 (Continued). Column Sample Data.

Sample Number	[1]Depositional Layer	Location	Elevation (cmbs)
39	MSH-Yn	Off site	40-73
40	DM MSH-Yn/MR-F	Off site	73-87
41	MR-F	Off site	87-106
42	MAZ-O	Off site	106-113
43	DM -MAZ-O/MR-R	Off site	113-130
44	MR-R	Off site	130-147
45	Feature R (DM MSH-W/MR-C)	61.5N/36E	19-35
46	Feature AA (DM MR-C/MSH-P)	71.5N/66.5E	20-35
47	Feature E (DM MSH-P/MSH-Yn)	28N 25E	45-55

[1]Depositional layer listed as recorded in the field during collection. [2]Depositional layer containing multiple depositional units.

A comparable landform was selected for the off-site sample approximately 250 meters northeast of the SRBP site's northeastern boundary. The location was chosen because of its proximity to the SRBP site and shared characteristics. In 2014, a 1-x-1 meter excavation unit was excavated on the landform in the only flat area lacking deadfall or living trees. The unit was excavated from ground surface to 140 centimeters below ground surface, by natural level, with all sediments sifted through 1/8-inch (3.175cm) mesh. No cultural materials were observed.

Measurement

Dry sieving, wet sieving, and laser particle analyzer were used to measure the grain size distribution of 47 samples. Grains larger than 1/8 inch were measured by pouring bulk samples into a column of nested sieves measuring 1 inch, ½ inch, ¼ inch, and 1/8 inch, and later converted to phi units. The column was gently shaken for 15 minutes similar to Evans (2011) and recommend by Lewis and McConchie (1994).

Sediments trapped in each sieve were weighed and recorded. Grains smaller than 1/8 inch were caught in the pan, weighed, recorded, then poured into a Humboldt riffle-type sample splitter to produce representative 100-gram samples.

Wet sieving was used to measure the grain sizes smaller than 3.175mm and larger than 0.062 millimeters. Samples were poured into a stacked column of five United States standard mesh sizes measuring -1, 0, 1, 2, 3, 4 phi and gently shaken for 15 minutes again. This dry sieving component was undertaken to create fine fraction (silt and clay) subsamples for future laser diffraction measurements. Next, the bottom pan was removed and water was run through the sieves until no more grains (silt and clay size) passed through the smallest mesh. The sieve column was then disassembled while keeping the newly sorted samples in their respective sieve, then dried for 48 hours, then weighed and recorded. All newly sorted samples representing each size class measured were placed in individual bags and labeled for potential future chemistry tests.

Laser light diffraction was used to measure the silt and clay-sized grains of 47 samples. Samples were tested for calcium carbonates by placing one drop of hydrochloric acid (HCl diluted to10 percent). No sample reacted with HCl so further steps to rid samples of carbonates were omitted. Organic content was removed by the technique of using a 30% hydrogen peroxide solution (Jensen, Schjonning, Watts, Christensen & Munkholm, 2017).

A Malvern Mastersizer 2000 was used to measure the silt and clay-sized grains from 47 samples. Sample were first sonicated in a Bransonic Ultrasonic Cleaner 8510 for approximately 60 seconds at 80% strength to ensure all grains were disaggregated without fracturing primary mineral grains. After 47 grain-size distributions were created in Excel, GRADISTAT software (Blott & Pye, 2001) was used to create grain-size distribution curves and calculate grain-size statistics. Probability curves were created using the GRANPLOTS program created for plotting probability curves of grain-size distributions (Balsillie et al., 2002).

Geochemical Analysis

The most commonly occurring grain sizes from 47 distributions were selected and measured for chemistry. Every grain-size distribution was sampled except the distribution from sample 36, which was omitted by the lab technician conducting the geochemical analysis because of its low weight, which created too small of a XRF bead after firing in a furnace. All other distributions were sampled once or twice to characterize the parent material of major and minor grain-size populations.

After analyzing grain-size curves, 67 distribution modes were measured for chemistry (Table 2). Mode samples were created that weighed between 20 and 50 grams as recommended by the chemical analysis technique's standard operating procedure (WSU, 2015).

Table 2. Chemical Analysis Data.

[1]Sample Number	[2]Depositional Layer	Location	Grain size in phi & Wentworth units
1	MSH-W	30N/24E	2 (medium sand)
2	DM MSH-W/MR-C	30N/24E	1 (coarse sand)
3	MR-C	30N/24E	1 (coarse sand)
4a	DM MR-C/MSH-P	30N/24E	1 (coarse sand)
4b	DM MR-C/MSH-P	30N/24E	-2.7 (fine to medium pebbles)
5a	MSH-P	30N/24E	2 (medium sand)
5b	MSH-P	30N/24E	-1.7 (very fine to fine pebbles)
6a	DM MSH-P/MSH-Yn	30N/24E	3 (fine sand)
6b	DM MSH-P/MSH-Yn	30N/24E	-1.7 (very fine to fine pebbles)
7	MSH-Yn	30N/24E	2 (medium sand)
8a	DM MSH-Yn/MR-F	30N/24E	-1 (very fine pebbles)
8b	DM MSH-Yn/MR-F	30N/24E	4 (very fine sand)
9a	MR-F	30N/24E	2 (medium sand)
9b	MR-F	30N/24E	-1 (very fine pebbles)
10a	DM MR-F/MAZ-O	30N/24E	3 (fine sand)
10b	DM MR-F/MAZ-O	30N/24E	-1 (very fine pebbles)
11a	MAZ-O	30N/24E	3 (fine sand)
11b	MAZ-O	30N/24E	-1 (very fine pebbles)
12a	DM MAZ-O/MR-R	30N/24E	3 (fine sand)
12b	DM MAZ-O/MR-R	30N/24E	-1 (very fine pebbles)
13a	MR-R	30N/24E	4 (very fine sand)
13b	MR-R	30N/24E	-1 (very fine pebbles)
14a	MSH-W	61.5N/36E	2 (medium sand)
14b	MSH-W	61.5N/36E	1 (coarse sand)
15a	DM MSH-W/MR-C	61.5N/36E	1 (coarse sand)
15b	DM MSH-W/MR-C	61.5N/36E	-1.7 (very fine to fine pebbles)
16a	MR-C	61.5N/36E	1 (coarse sand)
16b	MR-C	61.5N/36E	-2.7 (fine to medium pebbles)
17a	DM MR-C/MSH-P	61.5N/36E	2 (medium sand)
17b	DM MR-C/MSH-P	61.5N/36E	-1.7 (very fine to fine pebbles)
18	DM MSH-P/MSH-Yn	61.5N/36E	2 (medium sand)
19	MSH-Yn	61.5N/36E	2 (medium sand)
20	DM MSH-Yn/MR-F	61.5N/36E	2 (medium sand)
21a	MR-F	61.5N/36E	2 (medium sand)
21b	MR-F	61.5N/36E	-1 (fine pebbles)
22a	MR-R	61.5N/36E	3 (fine sand)
22b	MR-R	61.5N/36E	-1(fine pebbles)

[1] Sample number refers to the stratum sampled and either the associated fine-grained or coarse-grained sub sample. [2]Depositional unit refers to the tephra or tephra-associated dark mat the sample was recorded as in the field, during collection.

Table 2 (Continued). Chemical Analysis Data.

[1]Sample Number	[2]Depositional Layer	Location	Grain size in phi & Wentworth units
23a	DM MSH-W/MR-C	64N/115E	2 (medium sand)
23b	DM MSH-W/MR-C	64N/115E	-1.7 (very fine to fine pebbles)
24a	MR-C	64N/115E	1(coarse sand)
24b	MR-C	64N/115E	-2.7 (fine to medium pebbles)
25	DM MR-C/MSH-P & MSH-P	64N/115E	2 (medium sand)
26	DM MSH-P/MSH-Yn	64N/115E	2 (medium sand)
27	MSH-Yn	64N/115E	2 (medium sand)
28	DM MSH-Yn/F	64N/115E	2 (medium sand)
29	DM Duff/MSH-W	71.5N/66.5E	2 (medium sand)
30	MSH-W & DM MSH-W/MR-C	71.5N/66.5E	2 (medium sand)
31	DM MSH-W/MR-C & MR-C	71.5N/66.5E	2(medium sand)
32	MSH-P	71.5N/66.5E	2 (medium sand)
33	MSH-Yn	71.5N/66.5E	2 (medium sand)
34	DM MSH-Yn/MR-F	71.5N/66.5E	2 (medium sand)
35	MR-F	71.5N/66.5E	2 (medium sand)
37	MSH-W	Off-site	2 (medium sand)
38a	MR-C	Off-site	1(coarse sand)
38b	MR-C	Off-site	-1.7 (very fine to fine pebbles)
39	MSH-Yn	Off-site	2 (medium sand)
40	DM MSH-Yn/MR-F	Off-site	2 (medium sand)
41	MR-F	Off-site	3 (fine sand)
42	MAZ-O	Off-site	3 (fine sand)
43	DM MAZ-O/MR-R	Off-site	3 (fine sand)
44	MR-R	Off-site	1 (coarse sand)
45a	Feature R (DM MSH-W/MR-C)	61.5N/36E	1 (coarse sand)
45b	Feature R (DM MSH-W/MR-C)	61.5N/36E	-1.7 (very fine to fine pebbles)
46a	Feature AA (DM MR-C/MSH-P)	71.5N/66.5E	1 (coarse sand)
46b	Feature AA DM MR-C/MSH-P)	71.5N/66.5E	-1.7 (very fine to fine pebbles)
47a	Feature E (DM MSH-P/MSH-Yn)	28N 25E	2 (medium sand)
47b	Feature E (DM MSH-P/MSH-Yn)	28N 25E	-1.7 (very fine to fine pebbles)

Chemistry of selected modes was measured using the X-ray fluorescence (XRF) technique at Washington State University's (WSU) Geoanalytical Lab, using a

ThermoARL Advant'XP+ sequential X-ray fluorescence spectrometer. This XRF spectrometer measures the amount of 29 major, minor, and trace elements. Major and minor elements measured that are discussed in this study: silica (S), potassium (K), sodium (Na), nickel (Ni), chromium (Cr), barium (Ba), and strontium (Sr). Mode samples were brought to WSU and prepared by the author with the assistance of lab technicians using the lab's standard operating procedure (Johnson et al., 1999). Concentrations of 29 elements were measured by a ThermoARL Advant'XP+ automated sequential wavelength spectrometer. Elemental concentrations are converted into an Excel spreadsheet containing major and minor elements expressed in weight percentage oxides and trace elements expressed in ppm. These were the concentrations used to analyze TAS relationships and create TAS diagrams.

RESULTS

The GSA resulted in the measurement of the entire grain-size distribution for all 47 samples. Only 30N/24E results will be discussed here due to it being the most representative site profile. Figure 5 shows percentages of gravel, sand, silt, and clay for 30N/24E. Percentages are displayed beside the sample's stratigraphic position, showing trends. Stratum numbers correspond to samples described in Table 2 in the preceding section. Shaded squares in the following profile are those recorded as dark mats. No-fill indicates strata recorded as poorly weathered tephra.

Tables 4 summarize grain-size results that consist of texture, mode and modes (if polymodal), and grain-size distribution statistics: mean, standard deviation (sorting), skewness, and kurtosis. Mode(s) and statistics are expressed in phi units. Figure 6 shows grain-size probability curves for 30N/24E. Probability curves are grouped by proximity of stratigraphic position. Groupings are intended to show similarities and differences in the distributions of adjacent strata. See supplemental materials for grain-size data from other units and features.

The geochemical analysis resulted in the measurement of 29 major and trace elements of 67 samples. See supplemental materials for all raw data. Figures 7 shows the amount of four selected trace elements from 30N/24E: strontium (Sr), barium (Ba), chromium (Cr), and nickel, which are placed beside each associated sample in stratigraphic position, showing trends. When grain-size distributions had multiple modes and were measured twice, the coarser of the two modes is represented with circles and is the lower of the two in stratigraphic position.

Excavation Unit 30N/24E Results

Excavation unit 30N/24E contains thirteen strata, seven of which were recorded as dark mats, and six recorded as tephra (Table 3). Gravel ranges from 3% (S7) to 28.9% (S4), sand ranges from 48.3% (S13) to 84.1% (S7), silt ranges from 4% (S3) to 31% (S11), and clay ranges from 0.3% (S3) to 1.7% (S8) (Figure 5). There are higher percentages of coarser, gravel-sized grains in S1 through S5, decreasing sharply to mostly sand-sized grains by S7 (Figure 5). Below S7, grain sizes becomes gradually coarse again, with notable spikes in silt content in S8 and S11.

Table 3. Excavation Unit 30N/24E Samples.

[1]Sample Number	[2]Depositional Unit	Location	Grain size in phi & Wentworth units
1	MSH-W	30N/24E	2 (medium sand)
2	[3]DM MSH-W/MR-C	30N/24E	1 (coarse sand)
3	MR-C	30N/24E	1 (coarse sand)
4a	DM MR-C/MSH-P	30N/24E	1 (coarse sand)
4b	DM MR-C/MSH-P	30N/24E	-2.7 (fine to medium pebbles)
5a	MSH-P	30N/24E	2 (medium sand)
5b	MSH-P	30N/24E	-1.7 (very fine to fine pebbles)
6a	DM MSH-P/MSH-Yn	30N/24E	3 (fine sand)
6b	DM MSH-P/MSH-Yn	30N/24E	-1.7 (very fine to fine pebbles)
7	MSH-Yn	30N/24E	2 (medium sand)
8a	DM MSH-Yn/MR-F	30N/24E	-1 (very fine pebbles)
8b	DM MSH-Yn/MR-F	30N/24E	4 (very fine sand)
9a	MR-F	30N/24E	2 (medium sand)
9b	MR-F	30N/24E	-1 (very fine pebbles)
10a	DM MR-F/MAZ-O	30N/24E	3 (fine sand)
10b	DM MR-F/MAZ-O	30N/24E	-1 (very fine pebbles)
11a	MAZ-O	30N/24E	3 (fine sand)
11b	MAZ-O	30N/24E	-1 (very fine pebbles)
12a	DM MAZ-O/MR-R	30N/24E	3 (fine sand)
12b	DM MAZ-O/MR-R	30N/24E	-1 (very fine pebbles)
13a	MR-R	30N/24E	4 (very fine sand)
13b	MR-R	30N/24E	-1 (very fine pebbles)

[1] Sample number refers to the stratum sampled and either the associated fine-grained or coarse-grained sub sample. [2]Depositional unit refers to the tephra or tephra-associated dark mat the sample was recorded as in the field, during field collection in 2011-2013. [3] Dark Mats are abbreviated as "DM".

Mean grain size ranges from 2.85 phi (S8) to -0.01 phi (S3), standard deviation ranges from 1.71 phi (S7) to 2.93 phi (S5), skewness ranges from -0.17 phi (S5) to 0.32 phi (S7), and kurtosis ranges from 0.81 phi (S13) to 1.71 phi (S3) (Table 4). Probability curves exhibit pronounced deviations from normal distributions in S3, S6, and S7 (Figure 6). Deviations take the form of multiple line segments as opposed to one smooth line.

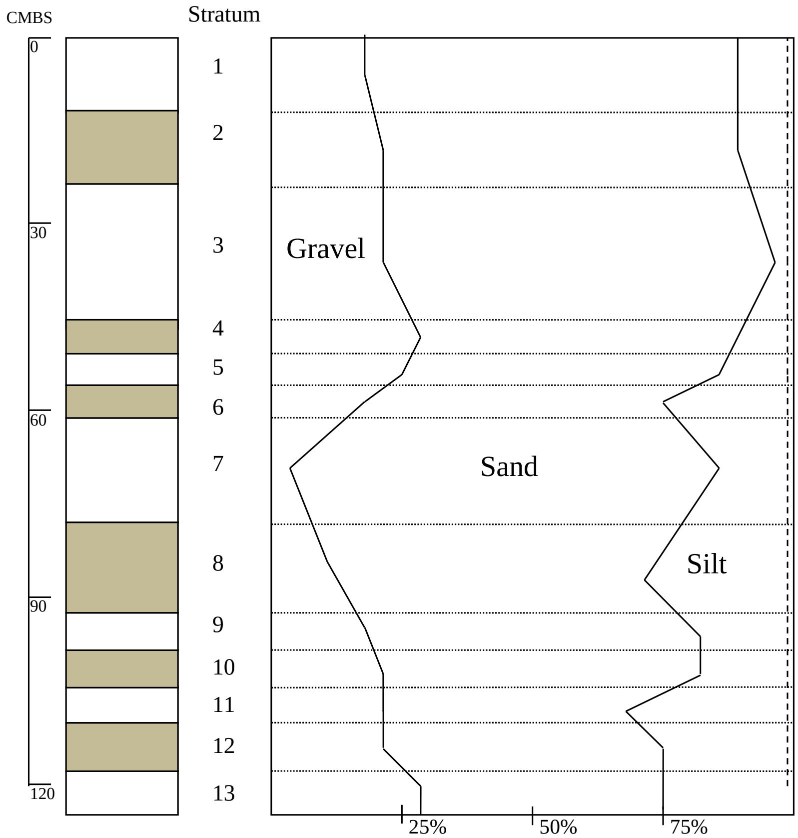

Figure 5. Profile of unit 30N/24E (left) and associated texture by strata (right), organized by cumulative percent. Clay content (dashed line) is 0.3% to 1.7%, peaking in stratum 8. Dark mats (strata 2, 4, 6, 8, 10, & 12) are shaded dark.

Table 4. Excavation Unit 30N/24E Grain-Size Data.

#	[1]Texture	Mode 1	Mode 2	$\bar{x}$	σ	*Sk*	*K*
1	Gravelly Sand	1.5	-	0.945	2.495	-0.082	1.575
2	Gravelly Loamy Sand	0.5	-4.167	0.865	2.678	0.065	1.369
3	Gravelly Sand	0.5	-	-0.006	1.790	-0.112	1.705
4	Gravelly Sand	0.5	-3.167	0.550	2.797	-0.070	0.893
5	Gravelly Sand	1.5	-2.167	1.171	2.934	-0.167	0.947
6	Gravelly Loamy Sand	2.5	-1.334	2.171	2.856	-0.147	1.092
7	Sand	1.5	-	1.881	1.706	0.319	1.171
8	Sandy Loam	3.5	-1.334	2.853	2.553	0.020	1.114
9	Gravelly Loamy Sand	1.5	-1.334	1.785	2.643	-0.121	1.126
10	Gravelly Loamy Sand	2.5	-1.334	1.618	2.714	-0.088	1.062
11	Gravelly Sandy Loam	-1.34	2.5	2.293	3.079	-0.137	0.869
12	Gravelly Sandy Loam	2.5	-1.334	2.050	2.945	-0.066	0.955
13	Gravelly Sandy Loam	-1.34	3.5	1.702	3.227	0.065	0.809

[1]Texture based on USDA classification.

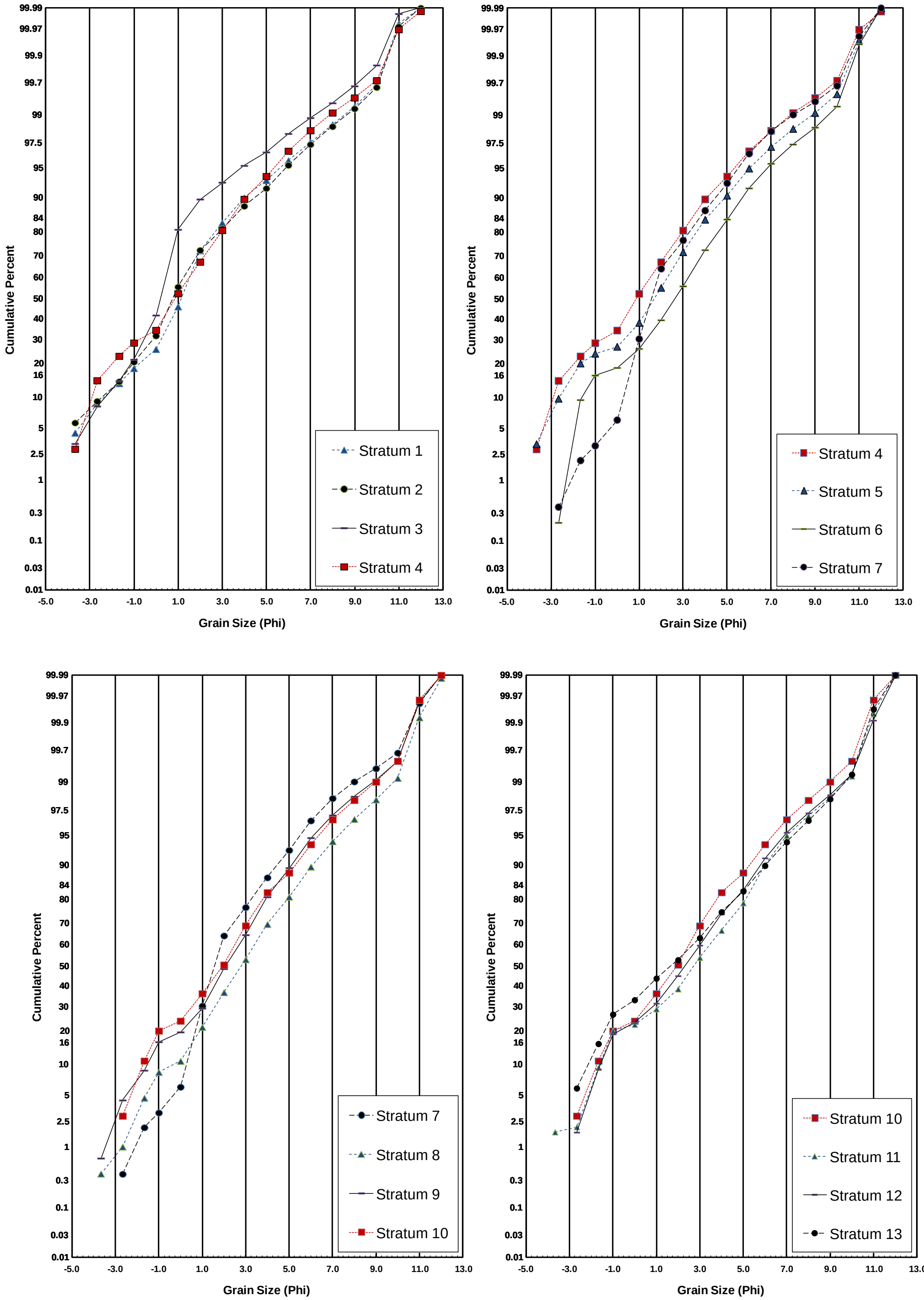

Figure 6. Probability curves of grain size within each stratum from unit 30N/24E.

Silica content ranges from 58.1% (S3) to 61.4% (S11), and total alkali content ranges from 4.52% (S13b) to 5.8% (S1). Silica content is lowest among samples adjacent to S3, S8, and S13 in stratigraphic position. Silica content is highest in S1, S7, and S11. Trace element trends are summarized here (Figure 7) and show abrupt decreases in Cr and Ni from S4 to S5 to below 75 ppm and 50 ppm, respectively, and abrupt changes in Sr and Ba proportions from S6 to S7.

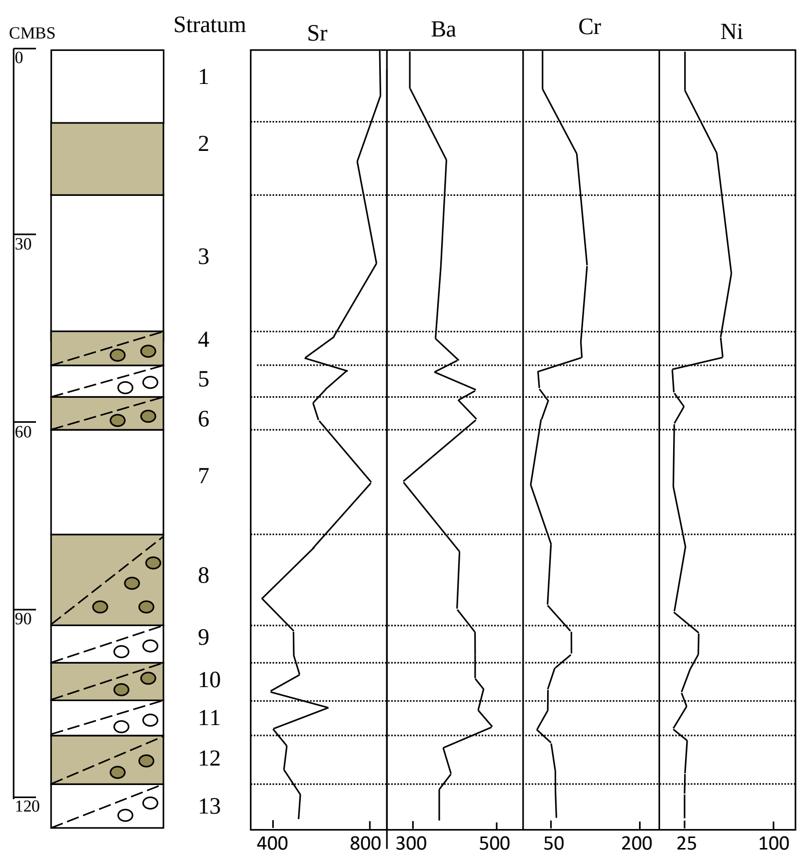

Figure 7. Profile of unit 30N/24E (left) with strata associated trace element proportions (right) expressed in parts per million (ppm). Dark mats (strata 2, 4, 6, 8, 10, & 12) are shaded dark. Circles denote the coarser grain-size class sampled within that stratum, which is expressed as the lower measurement.

Organic matter content ranges from 1.93% (S3) to 8.87% (S4), $CaCO_3$ content ranges from 0.05% (S1) to 1.68% (S11), and pH ranges from 4.91 (S1) to 5.84 (S9) (Table 5). This pH range places all strata on the acidic side of neutral. Organic matter content is higher in four of six dark mats compared to underlying, adjacent tephra strata (see Table 5). Color ranges from 10YR 3/2-very dark grayish brown (S1 and S2) to 10YR 6/8-brownish yellow. These color ranges have a low hue and chroma (dark) to a moderate hue and chroma (less dark), respectively, with dark mats typically darker than adjacent/underlying tephras.

Table 5. Excavation Unit 30N/24E OM, $CaCO_3$, and pH Data.

Sample Number	[1]Depositional Unit	Excavation Unit	OM (%)	$CaCO_3$ (%)	pH
1	MSH-W	30N/24E	3.83	0.05	4.91
2	DM MSH-W/MR-C	30N/24E	3.02	0.12	5.12
3	MR-C	30N/24E	1.93	0.10	5.51
4	DM MR-C/MSH-P	30N/24E	8.87	0.27	5.23
5	MSH-P	30N/24E	3.91	0.17	5.29
6	DM MSH-P/MSH-Yn	30N/24E	3.24	0.24	5.52
7	MSH-Yn	30N/24E	5.16	0.57	5.47
8	DM MSH-Yn/MR-F	30N/24E	6.44	0.17	5.19
9	MR-F	30N/24E	4.28	0.77	5.84
10	DM MR-F/MAZ-O	30N/24E	7.23	1.29	5.75
11	MAZ-O	30N/24E	7.52	1.68	5.82
12	DM MAZ-O/MR-R	30N/24E	7.62	1.46	5.66
13	MR-R	30N/24E	6.73	1.49	5.58

[1] Denotes depositional unit as recorded in the field by field school students.

Excavation Unit 30N/24E Interpretation

Coarse, lapilli-sized (gravel-sized) grains that occur in significant proportions (≥ 8.7% gravel) in all 13 samples except S7 are consistent with grain sizes from Mount Rainier eruptions (Mullineaux 1974; Sisson & Vallance, 2009). Sample 7 grain sizes are consistent with MSH-Yn ash that should be primarily sand sized (ash sized) (Mullineaux, 1974; Sisson and Vallance, 2009). Depositional environments unrelated to volcanism require well-sorted grain sizes, and grain-size distributions with standard deviations of approximately 1.5 phi or lower (Pettijohn, 1974; Lewis & McConchie, 1994). Standard deviation (1.71 phi to 2.93 phi) and skewness (-0.17 phi to 0.32 phi) of 30N/24E grain-size distributions are consistent with tephra and ash air fall in volcanic-related depositional environments (Lirer et al., 1996). Figure 8 shows the relationship between the standard deviation (sorting) and skewness of all 47-sample grain-size distributions, which are overlain atop established sorting and skewness relationships for specific depositional environments and volcanic deposits. Mount St. Helens-Yn ash consistently had the most well sorted grain sizes (lowest standard deviation) and was always positively skewed, which is reflected by the upper left four samples' placement in Figure 8.

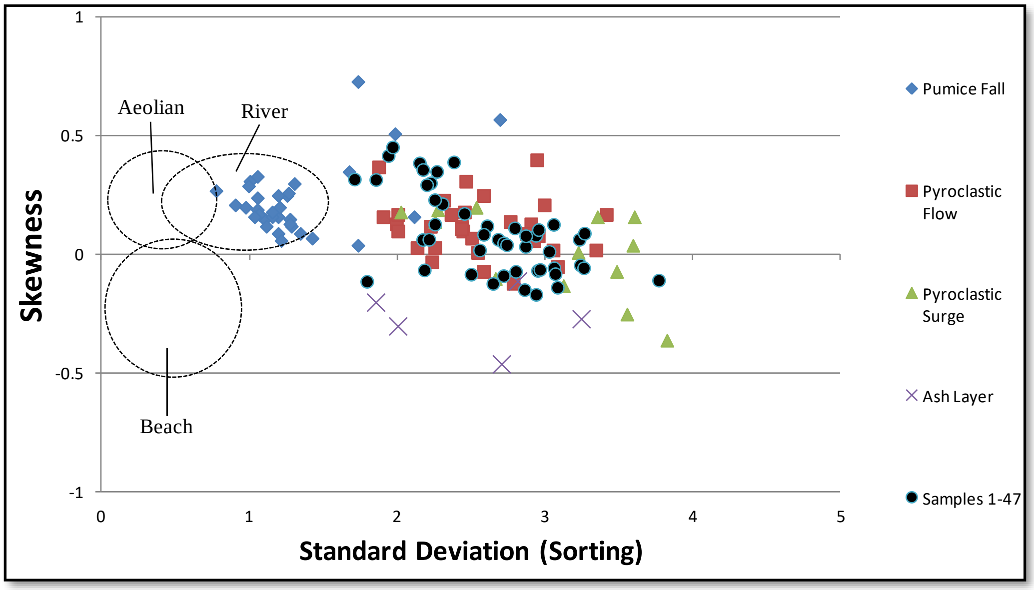

Figure 8. Relationship between standard deviation and skewness of grain-size distributions from different depositional environments, tephra deposits, and samples of this study. Pumice fall, pyroclastic flow, pyroclastic surge, and ash data from Lirer et al. (1996). Aeolian, river, and beach data from Lewis and McConchie (1994) and Pettijohn (1975). Created in Microsoft Excel by Sean Stcherbinine.

Figure 9 shows the relationship between total alkali (combined weight percentage of aluminum and potassium) and silica for all 67 chemistry samples, which are overlain atop a grid of established volcanic rock-type parent materials. Chemistry measurements from S1 through S13 resulted in silica content (58.1% to 61.4%) and total alkali content (4.52% to 5.8%) consistent with andesitic parent materials (Figure 9). An andesitic parent material determination requires silica content be approximately 57% to 63%, and total alkali content be approximately 4% to 6% (La Bas et al., 1986). Low silica content in S3, S8, and S13, which were either recorded as Mount Rainier tephras (S3 and S13) or a Mount Rainier tephra-associated dark mat (S8), is consistent with low silica content for tephra from Mount Rainier eruptions (Mullineaux 1974; Sisson & Vallance, 2009).

Tephra from Mount Rainer eruptions should have a silica content not exceeding approximately 60% (Mullineaux, 1974). Low silica content in S4 (58.1%) is a good example of a sample that was recorded as Mount St. Helens tephra, in this case DM C/P, but contains silica content typical of Mount Rainier tephra. Additionally, lapilli-sized grains in S4 through S6 are larger than the typical sand-sized grains deposited by Mount St. Helens eruptions (Mullineaux, 1974). The occurrence of MR-C slightly below the main deposit is understandable because of the nature of how a thick deposit of lapilli-sized grains would blanket a thin layer of Mount St. Helens-derived sand-sized grains. It is also consistent with field observations of bioturbation and mild sediment mixing (Dampf, 2002; Evans, 2011). Trace element trends of abrupt decreases in Cr and Ni from S4 to S5 mirror the previously stated contribution of Mount Rainier lapilli in S4 as they both drop below normal parts per million proportions for MR-C tephra, which are approximately 75 ppm (Cr) and 50 ppm (Ni) (Sisson & Vallance, 2009). Abrupt changes in Sr and Ba proportions from S6 to S7 underline a stratigraphic change to a poorly weathered MSH-Yn ash (see Figure 7).

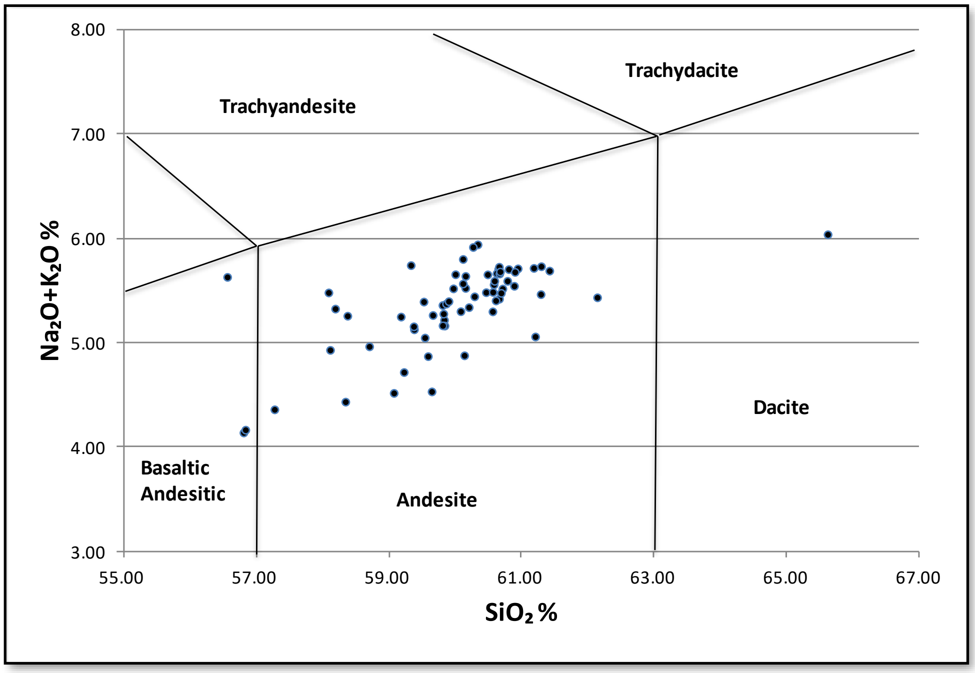

Figure 9. Total alkali silica (TAS) diagram for all 67 geochemistry samples superimposed on interpretative grid with rock type definitions from La Bas et al. (1986). Created in Microsoft Excel by Sean Stcherbinine.

All samples have less than 20% OM and meet the definition of a mineral soil (Soil Survey Staff, 2014). The definition of an A horizon is a mineral soil horizon that is typically a darker Munsell color than underlying horizons, and has a higher OM content due to the humification of organic materials. Four dark mats (S2, S4, S8, and S12) have higher OM content compared to adjacent, underlying tephra strata. Two dark mats (S6 and S10) have less OM content, with S10 containing 7.23% OM content compared to the underlying S11 with 7.62% OM content, a negligible difference. All six dark mats are as dark, or darker than underlying tephra strata. Based on organic content being typically higher than underlying strata, and color darker than underlying strata, dark mats in 30N/24E are interpreted as buried A horizons–the result of soil formation. In other words, dark mats formed due to tephra weathering in place on the ground surface with additions of humified organic materials, before being covered by subsequent volcanic ejecta that removed the A horizon from major soil forming processes, thereby arresting soil formation.

Calcium carbonate ($CaCO_3$) content (0.05% to 1.68%) is far lower than the necessary 50% needed for the soil taxonomy suffix symbol “k” to be used (Soil Survey Staff, 2014). Tipsoo, Owyhigh, Mysticlake, and Mountwow soil series’ that are mapped at or near the SRBP site all lack $CaCO_3$ content necessary to include soil horizons with “k” suffixes (Soil Survey Staff, 2018). Acidity (pH of 4.91 to 5.84) is similar to pH content described in Tipsoo, Owyhigh, Mysticlake, and Mountwow soil series’, which have mineral soil horizon pH ranges of 5.2 to 5.4 (Soil Survey Staff, 2018). Collectively, soil properties of volcanic parent material, presence of diagnostic tephra layers, the occurrence of buried A horizons, low acidity and $CaCO_3$ content are all consistent with soil series’ discussed previously, but compare best to the Mountwow series, which is an Andisol.

Results of grain-size measurements exhibit one clear discrepancy compared to the expected results of grain sizes for each regional tephra recorded at the SRBP site. Sample 8 and 9 were recorded as a MR-F-related dark mat and tephra, respectively (see Figure 5). Data generated from this study suggest these strata may be the result of additional Mount Rainier eruptions occurring before MSH-Yn and after MAZ-O. MR-F deposits have one uniquely distinguishable characteristic– they contain between 5% to 25% clay (Mullineaux, 1974). Sample 8 and 9 contain 1.7% and 0.9% clay, respectively, and the highest clay content of any sample of this study is 2.1%. The plume of MR-F is well documented in this part of MORA, but so are plumes of MR-S, MR-N, MR-D, and MR-A, which contain similar grain sizes as MR-F (Mullineaux, 1974; Soil Survey Staff, 2018).

Excavation unit 30N/24E contains an Andisol soil profile of tephra and intercalated A horizons whose primary constituents (parent material) are andesitic–the result of regional volcanism (see Figure 9). The profile appears to have been recorded accurately, the only exception being a zone below S7 (MSH-Yn) and above S10 (DM F/O), which cannot be directly attributable to MR-F, but may contain tephra from temporally close Mount Rainier eruptions. Differentiating between Mount Rainier eruptions is difficult because they have similar grain sizes and chemistry profiles. Depositional environment is direct ash and tephra fall based on grain-size statistics (see Figure 8). After deposition, soil forming processes weathered tephra surfaces into A horizons, creating the dark mat-over-weakly weathered tephra sequence observed during excavations. Whether as a surface horizon or horizon buried by subsequent eruptions, post-depositional alterations took place as evidenced by probability curve deviations and the displaced occurrence of Mount Rainier lapilli-sized grains. Post-depositional alterations, interpreted as reworked surfaces, occurred in S1, S4, S5, S6, S10, S11, all samples recorded as non-Mount Rainier ash. See Table 6 for a complete list of S1 through S13 interpretations.

Table 6. All Samples Interpretations.

Sample	Originally Recorded As	Interpretation
1	MSH-W	Reworked MSH-W ash with MR-C lapilli
2	DM MSH-W/MR-C	Buried A horizon: MR-C tephra
3	MR-C	Poorly weathered parent material: MR-C tephra
4	DM MR-C/MSH-P	Reworked MSH-P or Yn buried A horizon with MR-C lapilli
5	MSH-P	Reworked MSH-P or Yn buried A horizon with MR-C lapilli
6	DM MSH-P/MSH-Yn	Reworked MSH-Yn buried A horizon with MR-C lapilli
7	MSH-Yn	Poorly weathered parent material: MSH-Yn ash
8	DM MSH-Yn/MR-F	MR-FSNDA buried A horizon
9	MR-F	MR-FSNDA parent material
10	DM F/MAZ-O	Reworked MAZ-O buried A horizon and FSNDAR ash and lapilli
11	MAZ-O	Reworked MAZ-O ash and MR-FSNDAR ash and lapilli
12	DM MAZ-O/MR-R	Buried A horizon: MR-R tephra
13	MR-R	Poorly weathered parent material: MR-R
14	MSH-W	Reworked MSH-W ash and MR-C lapilli
15	DM MSH-W/MR-C	Buried A horizon: MR-C tephra
16	MR-C	Poorly weathered parent material: MR-C tephra
17	DM MR-C/MSH-P	Reworked MSH-P or Yn buried A horizon with MR-C lapilli
18	DM MSH-P/MSH-Yn	Buried A horizon: MSH-Yn ash
19	MSH-Yn	Poorly weathered parent material: MSH-Yn ash
20	DM Yn/F	Reworked Buried A horizon: pre MSH-Yn (MR-FSNDAR)
21	MR-F	Reworked parent material: pre MSH-Yn (MR-FSNDAR)
22	MR-R	Poorly weathered parent material: pre MSH-Yn (MR-FSNDAR)
23	DM MSH-W/MR-C	Buried A horizon: MR-C tephra
24	MR-C	Poorly weathered parent material: MR-C
25	DM MR-C/MSH-P & MSH-P	Reworked MSH-P or Yn buried A horizon with MR-C lapilli
26	DM MSH-P/MSH-Yn	Buried A horizon: MSH-Yn ash
27	MSH-Yn	Poorly weathered parent material: MSH-Yn ash
28	DM MSH-Yn/MR-F	Buried A horizon: pre MSH-Yn (MR-FSNDAR)
29	DM Duff/MSH-W	A horizon: MSH-W ash
30	MSH-W & DM MSH-W/MR-C	Reworked MSH-W ash and buried A horizon of MR-C ash and lapilli

Table 6 (Continued). All Samples Interpretations.

Sample	Originally Recorded As	Interpretation
31	DM MSH-W/MR-C & MR-C	Reworked buried A horizon and parent tephra: MR-C tephra
32	MSH-P	Reworked MSH-Yn with possibly MSH-P
33	MSH-Yn	Poorly weathered parent material: MSH-Yn ash
34	DM MSH-Yn/MR-F	Buried A horizon: pre MSH-Yn (MR-FSNDAR)
35	MR-F	Poorly weathered parent material: (MR-FSNDAR)
36	DM Duff/MSH-W	Highly-weathered organic horizon (Oa Horizon)
37	MSH-W	Reworked MSH-W ash and MR-C lapilli
38	MR-C	Poorly weathered parent material: MR-C
39	MSH-Yn	Reworked MSH-Yn ash with MR-C lapilli
40	DM Yn/F	Buried A horizon: pre MSH-Yn (MR-FSNDA)
41	MR-F	Poorly weathered parent material: (MR-FSNDA)
42	MAZ-O	Reworked MAZ-O ash and MR-FSNDAR ash and lapilli
43	DM MAZ-O/MR-R	Buried A horizon: MR-R tephra
44	MR-R	Poorly weathered parent material: MR-R tephra
45	Feature R (DM MSH-W/MR-C)	Reworked buried A horizon: MR-C tephra
46	Feature AA (DM MR-C/MSH-P)	Reworked buried A horizon: MSH-Yn ash with MR-C lapilli
47	Feature E (DM MSH-P/MSH-Yn)	Reworked buried A horizon: MSH-Yn ash

New Site Depositional History Model

The new site depositional history model builds on previous site stratigraphic data, sediment data, and depositional histories (Dampf, 2002; Nickels, 2002; Evans, 2011). The depositional history model is organized similar to models discussed previously (Fedje et al., 1995; Neall et al., 2008; Fitzsimmons et al., 2014), and summarizes this study's results and interpretations into one comprehensive model that will aid in interpreting artifact frequencies (Figure 10). The model consists of a representative stratigraphic profile with accompanying parent material, depositional environment, soil horizon and strata-associated site data. Site data consists of feature locations, radiocarbon dates, chipped stone artifact totals, bone totals, and estimated surface exposure ranges.

Site data comes from excavations conducted during the 1997 to 2001 and 2011 to 2013 summer field schools. Only data recorded with associations to a specific tephra unit or dark-mat related tephra unit are used. Only features incorporated into this study are placed in the model. For information on additional features see McCutcheon et al. (2017). Only chipped stone and bone totals recovered from depositional units incorporated into the model are listed. For example, three chipped stone artifacts were recovered from a stratum recorded as being a combination of multiple depositional units: MR-C tephra and the dark mat overlying MR-C tephra. Because no such horizon was incorporated into the model, said counts are disregarded. Counts like this example represent an insignificant proportion of the site assemblage.

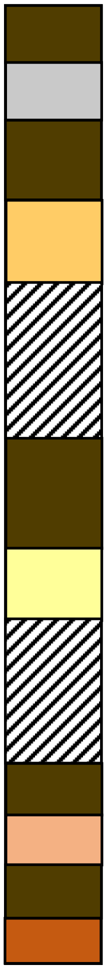

110 CMBS

PM[1]	DE[2]	SH[3]	O[4]	Feature	Dates in cal BP[10]	Chipped Stone[11]	Bone	Exposure [12]
MSH-W	[5]DA	A	[7]MS			86 (694/m^3)	0	0-471
MSH-W	DA	C	[8]SW			742 (586/m^3)	1	0-471
MR-C	DA	Ab2	SW	45(R) 46(AA)	1350-1521; 1417-1688 1445-1707; 1636-1821	6201 (2338/m^3)	249 (94/m^3)	471-2200
MR-C	DA	C2	SW	45(R) 46(AA)		883 (338/m^3)	9 (3/m^3)	471-2200
MR-C, MSH-P, MSH-Yn	[6]RDA	Ab/C3	SW	46(AA) 47(E)	2158-2338 2350-2677 2351-2682 2354-2684	2099 (1127/m^3)	334 (179/m^3)	2200-3700
MSH-Yn	DA	Ab4	SW	47(E)	2520-2758 2991-3176	841 (455/m^3)	101 (55/m^3)	2200-3700
MSH-Yn	DA	C4	SW		2543-2758 3899-4086	869 (360/m^3)	144 (60/m^3)	2200-3700
MR-F,S,N,D, A	RDA	Ab/C5	MS	46(AA)		970 210/m^3	23 (5/m^3)	3700-7700
MAZ-O	RDA	Ab6	[9]FL			41 (43/m^3)	35 (37/m^3)	3700-7700
MAZ-O	DA	C6	FL			27 (34/m^3)	60 (74/m^3)	5600-7700
MR-R	DA	Ab7	FL			16 (59/m^3)	59 (219/m^3)	7700-10000
MR-R	DA	C7	FL			0	0	7700-10000

Figure 10. New Site Depositional History Model. Dark-shaded boxes represent A horizons. Colored strata represent poorly weathered tephra C horizons. Hatched strata represent reworked deposits of multiple parent materials. “b” denotes a buried horizon. Ab/C represents a buried horizon with characteristics of an A and C horizon. Abbreviations: [1]PM (parent material), [2]DE (depositional environment), [3]SH (soil horizon), [4]O (Occurrence), [5]DA (direct ash fall), [6]RDA (reworked direct ash fall), [7]MS (most of site), [8]SW (site wide), [9]FL (few locations). [10]Dates are in c14 years before present calibrated at 2σ from McCutcheon et al. (2017). [11] Chipped stone artifacts expressed in counts and (counts per m^3). [12] Exposure is in calibrated years BP with ranges of the maximum amount of time exposed as potential ground surface inferred from Mullineaux (1974) and Sisson and Vallance (2009). Feature locations, chipped stone and bone counts, and carbon dating information is from McCutcheon et al. (2017).

DISCUSSION

The new site depositional history model organizes site stratigraphy into three types of strata: (1) A horizons that formed in tephra parent material from a single eruption; (2) C horizons of poorly weathered tephra parent material from the same eruption as the overlying A horizon; and (3) deposits of reworked sediment containing parent materials from multiple eruptions or undetermined eruptions (e.g. combination of A horizons and C horizons of MSH-Yn, MSH-P, and MR-C parent materials). The following discusses how site data can be incorporated into the depositional history model, specifically, how data associated with each tephra relates to buried stable surfaces and site occupation at the SRBP site. Discussion is organized in stratigraphic order from youngest to oldest deposits. All subsequent archaeological data is from McCutcheon et al. (2017).

Mount St. Helens-W tephra is the first tephra in the stratigraphic sequence, mantled only by an organic horizon of forest duff (O horizon), and at times Mount St. Helens 1980 ash in the forest duff. This tephra consists of an altered A horizon overlying a poorly weathered C horizon. (A and C in Figure 10). High artifact counts in the C horizon are likely due to post-depositional processes, with bioturbation or cryoturbation the likely mixing agent. Taking into account volume excavated, similar artifact densities occur throughout MSH-W poorly weathered tephra and overlying A horizon (694 vs. 586/m^3). Upper elevations of the A horizon that formed in MSH-W tephra, when present, represents a stable surface since deposition 471 years BP, the date of which is a dendrochronology date (Sisson & Vallance, 2009).

Mount Rainier-C tephra is the next tephra in the stratigraphic sequence, consisting of a buried A horizon overlying a poorly weathered C horizon (Ab2 and C2 in Figure 10). Chipped stone artifact density is high in the buried A horizon that formed in MR-C tephra. In fact, 48% of all chipped stone recovered between 2011 and 2013 was from this stratum. The existence of so much of the site artifact assemblage occurring within a discrete, buried A horizon suggests this stratum is an intact buried surface. This abrupt change in parent material between poorly weathered MSH-W tephra and the A horizon that formed in MR-C tephra represents the ground surface exposed for approximately 1,730 years between initial deposition of MR-C 2,200 cal BP and the deposition of MSH-W 471 years BP.

There are four radiocarbon dates from charcoal and calcined bone recovered from the buried A horizon that formed in MR-C tephra (see Figure 10). All four dates fall within the surface-age exposure range of 471 years BP to 2,200 cal years BP noted above. Two of the three features incorporated into this study were observed in association with MR-C tephra. Feature R (sample 45) was observed most often in association with the A horizon that formed in MR-C tephra. Feature R was also observed in poorly weathered MR-C tephra. The three youngest radiocarbon dates from MR-C tephra were from charcoal and calcine bone collected within Feature R. Grain size and chemical properties of Feature R are consistent with a reworked A horizon of MR-C tephra. Collectively, this suggests the following depositional history for Feature R: excavation into the A horizon that formed in MR-C tephra, down into but not exceeding the lower limits of poorly weathered MR-C tephra.

Underlying poorly weathered MR-C tephra is a zone that cannot be attributed to a single volcanic eruption based on the data resulting from this analysis. Instead, samples recovered from this zone were recorded during 2011-2013 as three discrete tephra strata resulting from single volcanic eruptions. Grain size and chemical properties of samples recovered from this zone show characteristics of tephra other than what was recorded during 2011 to 2013, primarily due to the occurrence MR-C lapilli in tephra recorded as non-Mount Rainier tephra. Though no stable surface can be inferred from within this zone, artifacts recovered can be granted relative ages. The existence of intact stratigraphy directly overlying and underlying this zone, within MR-C and MSH-Yn tephra strata, respectively, allows for the reasonable assumption that cultural materials recovered are likely the result of occupation before the deposition of MR-C tephra (2,200 years BP) and after the deposition of MSH-Yn tephra (3,700 cal years BP).

There are four radiocarbon dates from charcoal and calcined bone recovered from the zone between MR-C and MSH-Yn tephra (see Figure 10). All four dates are consistent with the age range of 2,200 to 3,700 cal years BP, further suggesting cultural materials recovered from this zone can be attributed to said age range. Two of the three features incorporated into this study were observed in association with this zone, Feature E and Feature AA. Feature AA (sample 46) was observed most often in association with the dark mat directly underlying poorly weathered MR-C tephra. It was also observed in poorly weathered MR-C tephra and directly underlying MSH-Yn tephra. The oldest radiocarbon date from material collected in MR-C tephra is from charcoal recovered from Feature AA (1,636-1,821 cal years BP). Radiocarbon dates from Feature AA occurring in the zone between MR-C and MSH-Yn tephra are from 2,158 to 2,338 cal years BP and 2,351 to 2,682 cal years BP These ranges, in conjunction with grain size and chemical properties characteristic of MR-C and MSH-Yn, suggest a depositional history for Feature AA that may be unknowable based on the samples available and techniques used. One explanation is tied to precontact land use at the site and increased feature occurrence that would cause disturbances of thinner MSH-P-sized tephra strata compared to the thicker deposits of MR-C and MSH-Yn tephras.

Mount St. Helens Yn tephra is the next tephra in the stratigraphic sequence. This tephra consists of a buried A horizon overlying a poorly weathered C horizon (Ab4 and C4 in Figure 10). Chipped stone artifact density is slightly higher in the buried A horizon that formed in MSH-Yn tephra compared to the C horizon. Similar to artifacts located in poorly weathered MR-C tephra (C horizon), such a density is likely due to bioturbation and/ or cryoturbation. The existence of a buried A horizon with a measurable boundary to the overlying zone, and a higher artifact density than the underlying C horizon suggests this stratum is an intact buried surface. The buried A horizon represents the past ground surface exposed for a minimum of 700 years between the eruption depositing MSH-Yn (3,700 cal years BP) and the eruption depositing MSH-P tephra (2,600 to 3,000 cal years BP). At maximum, and disregarding relatively thin deposits of MSH-P tephra sets, the A horizon that formed in MSH-Yn tephra could have been a stable surface for a maximum of 1,500 years from the deposition of MSH-Yn (3,700 cal years BP) until the eruption depositing MR-C (2,200 cal years BP).

There are four radio carbon dates from charcoal and calcined bone recovered from MSH-Yn tephra (see Figure 10). Three of the four dates are consistent with the potential exposure range noted above, one is not. The outlier is a date of 3,899 to 4,086 cal years BP generated from charcoal recovered from the lower limits of the poorly weathered C horizon of MSH-Yn tephra. The location of this charcoal near the contact with underlying deposits markedly older than 3,700 years BP is not overly problematic and does not change the interpretations and depositional history of MSH-Yn tephra at the site. An explanation for this is that the charcoal was on the pre MSH-Yn surface and was covered by MSH-Yn tephra.

Feature E (stratum 47) is one of the three features incorporated into this study and was observed in association with the buried A horizon that formed in MSH-Yn tephra. Feature E was also observed in the mixed zone overlying MSH-Yn tephra. There are no radiocarbon dates associated with Feature E, but grain size and chemical properties are characteristic of a reworked A horizon of MSH-Yn tephra. This suggests the following depositional history for Feature E: sometime after 3,700 years BP excavation into the A horizon that formed in MSH-Yn tephra down into but not reaching poorly weathered MSH-Yn tephra.

Underlying poorly weathered MSH-Yn tephra is again referred to as a zone because it cannot be attributable to a single volcanic eruption. Grain size and chemical properties of samples recovered from this zone do not point to any single volcanic event, though MR-F is a likely a candidate. Feature AA (stratum 46) was observed in association with this zone, but it appears sediments in this zone were excavated into long after original deposition, once a mantle representing at least 2,400 years had been deposited.

Mount Mazama (MAZ-O) tephra is next in the stratigraphic sequence. This tephra consists of a buried A horizon overlying a poorly weathered C horizon. MAZ-O was only observed in a few locations at the site, and chipped stone was only recovered from MAZ-O in the 30N and 61.5N areas. Chipped stone artifact density is slightly higher in the buried A horizon that formed in MAZ-O tephra compared to the C horizon. No radio carbon dates are associated with MAZ-O tephra. The fact that the buried A horizon has a measurable boundary with the overlying zone and a higher artifact density than the underlying C horizon suggests this stratum is an intact buried surface. However, the existence of a low artifact density coupled with a lack of datable materials at a site that exhibits reworked sediments, presents the potential that artifacts in MAZ-O tephra were recovered from a secondary context. More data is needed to conclusively determine the depositional context of artifacts recovered from MAZ-O.

Mount Rainier-R tephra is the final tephra in the stratigraphic sequence. Similar to MAZ-O, it was observed in few locations at the site. This tephra consists of a buried A horizon overlying a poorly weathered C horizon. The A horizon contained 16 chipped stone artifacts and 59 pieces of bone recovered from 0.27 m^3 of sediment, equating to 59 chipped stone artifacts/m^3 and 219 pieces of bone/m^3. No chipped stone artifacts or bone was recovered from the C horizon. Existence of a buried A horizon with measurable boundary with the overlying poorly weathered MAZ-O tephra suggests this stratum is an intact buried surface. However, the existence of a low artifact density combined with a lack of datable materials at a site that exhibits reworked sediments presents the potential that artifacts in MR-R tephra were recovered from a secondary context. Chipped stone artifacts recovered from MAZ-O and MR-R tephra deposits represent less than 1% (n = 91 of 13,036) of the total chipped stone artifact assemblage recovered between 2011 and 2013. Similar to artifacts recovered in MAZ-O tephra, more data is needed to conclusively determine whether artifacts recovered from MR-R tephra are from a secondary context.

New Site Depositional History Model

The new site depositional history model provides a framework for interpreting site data recovered from complex stratigraphy. The model proposes buried surfaces at the upper contact of MSH-W tephra (471 years BP), MR-C tephra (2,200 cal years BP), MSH-Yn (3,700 cal years BP), as well as MAZ-O tephra (7,700 cal years BP), and MR-R tephra (10,000 cal years BP) when present. However, site occupation can only be conclusively associated with the surfaces of MSH-W tephra, MR-C tephra, and MSH-Yn tephra. This determination is reinforced by the level of disturbance documented in Evans' (2011), total artifact counts in deeper tephras, and descriptions of krotovinas in field notes (McCutcheon et al., 2017).

Previous investigations organized the site assemblage into two archaeological components for analysis: (1) cultural materials observed within and above MR-C tephra; and (2) cultural materials observed below MR-C tephra. This organization is reaffirmed based on the results of this study. Cultural materials recovered from MR-C tephra and above are the result of site use dating back no older than 2,200 years BP. Cultural materials from the zone between MR-C and MSH-Yn should be viewed with some caution, as characteristics of MR-C were observed in samples collected from tephra strata and dark mats in the upper elevations of this zone, meaning that some post-depositional mixing occurred, which could potentially be from site use. Otherwise, lower elevations of poorly weathered MR-C act as a barrier between components, with cultural materials recorded below MR-C, especially those associated with MSH-Yn and below, the result of site use before 2,200 years BP.

Conclusions and Recommendations for Future Research

The SRBP site contains tephra-derived strata that form a mostly intact stratigraphic profile. Non-intact zones of the profile are discrete and occur between buried surfaces with known ages. Evidence of occupation is most closely associated with these buried surfaces, determined to be A horizons (Table 4 and Figure 10) that formed in tephra deposited by Mount Rainier, Mount St. Helens, and Mount Mazama eruptions. Knowledge of the timing of these eruptions and subsequent ranges of post-depositional stable surfaces allows site use intensity and periodicity to be inferred when radiometric dating and diagnostic artifacts are lacking at a specific location.

Site use is most closely associated with the dark mat that directly overlies poorly weathered MR-C tephra. This dark mat is an A horizon that formed in MR-C tephra and mostly remained a stable surface from initial deposition of around 2,200 years B.P to deposition of MSH-W tephra around 471 years BP. Clear evidence of occupation also occurs in MSH-W and MSH-Yn tephra, both of which contain developed A horizons, underlining their stable nature. Occupation associated with MSH-W, MR-C, and MSH-Yn tephra is backed up by radiocarbon dates and diagnostic projectile points that further substantiate assigning a primary context to artifacts recovered from those tephra strata (McCutcheon et al., 2017).

Such certainty cannot be held about other locations of the profile. The zone underlying MR-C and overlying MR-Yn tephra appears to be the combination of poorly weathered MR-C, the A horizon that formed in MSH-Yn, and probably a small component of the MSH-P set and associated A horizons, which were observed *in situ* during the 1999 field school. The zone underlying MSH-Yn tephra has an unclear depositional history but is likely MR-F (5,000 years cal BP). Parent material could also be MR-S, MR-N, MR-D, or MR-A tephra, all of which had eruption plumes extending to the SRBP site (Mullineaux, 1974). Although these tephras were not observed on the landform, Mullineaux's (1974) interpolated plume models overlap Sunrise Ridge near the SRBP site. However, Mullineaux (1974) did not look for stratigraphic exposures in forested areas because of roots, bioturbation, etc.

The unclear depositional history and low artifact density below MSH-Yn is problematic for discussing if the SRBP site assemblage shows evidence of a shift from forager to collector strategies around 4,500 to 3,500 cal years BP (Burtchard, 2007). That is not to say that technological change through time cannot be measured, as evidenced by Lewis (2015). Currently, the SRBP site assemblage is split into two components using the MR-C tephra deposit. The results of this study support that organization. The only additional component that could be created would be based on cultural materials recovered from MSH-Yn tephra. This is unnecessary for two reasons. Mount St. Helens Yn tephra is overlain by a zone with multiple parent materials and underlain by a zone with several possible parent materials. Secondly, the creation of a third component associated with MSH-Yn would still not inform the forager to collector transition in the Cascade Range as it is too recent. This last point is underlined by the already extreme selective conditions of Mount Rainier that would limit technological functional variability, and its ability to be measured (Burtchard, 2003; McCutcheon et al., 2017).

There are several types of data that would have assisted in this study. More accurate eruption plume maps based less on interpolation (Mullineaux, 1974) and more on ground-truthing would assist in identifying candidates for potential eruptions for the zone underlying MSH-Yn tephra. Chemistry data from bulk samples collected in a similar fashion as those used for this study would assist in comparing these results to other studies. Chemistry data exists for tephra discussed in this study but the data is typically based on glass samples, not bulk samples (e.g. Sisson &Vallance, 2009)

This study was the first to focus on dark mats intercalated between tephra deposits in the Cascade Range. Results should assist in interpreting artifacts assemblages located in complex stratigraphy in similar locations of the upland forest zone of MORA and the Cascade Range. Forest soils that form in tephra parent material are influenced by post-depositional process that can obscure buried surfaces, much more than that of higher elevation subalpine parkland settings. The techniques are available to test buried surface stability and give greater context to cultural materials recovered from archaeological sites in the Cascade Range.

This study demonstrates that grain-size and chemical analyses can be a useful tool when attempting to understand complex tephra-derived stratigraphy in a forest setting. Dark mats were determined to be A horizons that formed in parent tephra. Well developed, buried A horizons indicate the existence of intact surfaces at an archaeological site, which is necessary when interpreting a stratified archaeological record, such as the SRBP site. Techniques used in this study are relatively inexpensive and can be used in similar studies when understanding parent material and depositional environment is critical to determining relationships between artifact bearing strata.

REFERENCES

Balsillie, J.H., Donogue, J.F., Butler, K.M. & Butler, K.M. (2002). Plotting Equation for Gaussian Percentiles and a Spreadsheet Program for Generating Probability Plots. *Journal of Sedimentary Research*, 22(6), 929-933.

Blott, S. J. & Pye K. (2001). GRADISTAT: A Grain size Distribution and Statistics Package for the Analysis of Unconsolidated Sediments. *Earth Surface Processes and Landforms*, 26, 1237-1248.

Burtchard, G. C. (2003). *Environmental Prehistory & Archaeology of Mount Rainier National Park, Washington*. Seattle: National Park Service.

Burtchard, G. C. (2007). Holocene Subsistence and Settlement Patterns: Mount Rainier and the Montane Pacific Northwest. *Archaeology in Washington*, 13, 3-34.

Burtchard, G. C. & Hamilton, S. C. (1998). Archaeological Resources of Mount Rainier National Park, Washington, 1995 Reconnaissance Data. Report prepared for USDI National Park Service, Columbia Cascades System Support Office, Seattle. Honolulu: International Archaeological Research Institute, Inc.

Crandell, D. R. & Miller R. D. (1974). *Quaternary Stratigraphy and the Extent of Glaciation in the Mount Rainier Region, Washington*. United States Geologic Survey Professional Paper 847. Washington: U.S. Government Printing Office.

Dampf, S. K. (2002) The Sunrise Ridge Borrow Pit Site (45PI408): Subsurface Reconnaissance for a Significance Evaluation. (Unpublished master's thesis). Resource Management Department. Central Washington University, Ellensburg.

Evans, H. R. (2011). The Sunrise Ridge Borrow Pit Site: Sediment Stratigraphy, Particle Size Analysis and Microarchaeology. (Unpublished master's thesis). Resource Management Department. Central Washington University, Ellensburg.

Fedje, D. W., White, J. M., Wilson, M. C., Nelson, D. E., Vogel, J. S. & Southon, J. R. (1995). Vermilion Lakes Site: Adaptations and Environments in the Canadian Rockies during the Latest Pleistocene and Early Holocene. *American Antiquity*, 60(1), 81-108.

Franklin, J.F. (1966). Vegetation and Soils in the Subalpine Forests of the Southern Washington Cascade Range. (Unpublished doctoral dissertation). School of the Environment. Washington State University, Pullman.

Franklin, J. F., Moir, W. H., Hemstrom, M. A., Greene, S. E., & Smith, B. G. (1988). *The Forest Communities of Mount Rainier National Park*, National Park Service Scientific Monograph Series, No. 19. Washington D.C.: U.S. Government Printing Office.

Friedman, G. M., Sanders, J. E. & Kopaska-Merkel, D. C. (1992). *Principles of Sedimentary Deposits*. New York: Macmillan Publishing Company.

Gatti, E., Saidin, M., Talib, Kl, Rashidi, N., Gibbard, P. & Oppenheimer, C. (2013). Depositional Processes of Reworked Tephra from the Late Pleistocene Youngest Toba Tuff Deposits in the Lenggong Valley, Malaysia. *Quaternary Research*, 79, 228-241.

Goldberg, P. & Macphail, R. I. (2006). *Practical and Theoretical Geoarchaeology*. Malden: Blackwell Publishing.

Jensen, J.L., Schjonning, P., Watts, C.W., Christensen, B.T. & Munkholm, L.J. (2017) Soil Texture Analysis Revisited: Removal of Organic Matter Matters More Than Ever. *PLoS ONE*, 12(5): 1-10.

Lewis, D. W. & McConchie D. (1994). *Analytical Sedimentology*. New York: Chapman & Hill.

Lewis, P. C. (2015). Measuring the Cost and Performance of Lithic Industries at the Sunrise Ridge Borrow Pit Site (45PI408). (Unpublished master's thesis), Resource Management Department, Central Washington University, Ellensburg.

Lirer, L., Sheridan, M., & Vinci A. (1996). Deconvolution of Pyroclastic Grain-size spectra for Interpretation of Transport Mechanisms: an Application to the AD 79 Vesuvio Deposits. *Sedimentology* 43, 913-926.

Lirer, L. & Vinci A. (1991). Grain-size Distributions of Pyroclastic Deposits. *Sedimentology* 38, 1075-1083.

Malvern Instruments Ltd (1997). Malvern Mastersizer User Manual. Electronic document, http://www.ceic.unsw.edu.au/centers/partcat/facilities/Mastersizer.pdf, accessed 2/20/2014.

McCutcheon, P. T., Parfitt, A. B., Brown J., Davis D. R., Limberg, C. & Middleton, S. (2017). Investigating Intra-Site Variation for Holocene Epoch Human Land Use at the Sunrise Ridge Borrow Pit Site (45PI408). Department of Anthropology and Museum Studies. Central Washington University, Ellensburg. Report in preparation.

Mullineaux, D. R. (1974). *Pumice and other pyroclastic deposits in Mount Rainier National Park, Washington.* Washington D. C.: U.S. Govt. Printing Office.

Neall, V.E., Wallace, R.C., & Torrence R. (2008). The Volcanic Environment for 40,000 Years of Human Occupation on the Willauhez Isthmus, West New Britain, Papua New Guinea. *Journal of Volcanology and Geothermal Research*, 176(3), 330-343.

Nickels, A. M. (2001). Mount Rainier National Park Field Site Inspection Record, 45PI408, Seattle: National Park Service.

Nickels, A. M. (2002). History Under Fire: Understanding Human Fire Modification of the Landscapes at Mount Rainier National Park. (Unpublished master's thesis), Resource Management Department, Central Washington University, Ellensburg.

Pettijohn, J. F. (1975). *Sedimentary Rocks*. 3rd ed. New York: Harper & Row Publishers, Inc.

Sisson T.W., & Vallance J. W. (2009). Frequent Eruptions of Mount Rainier over the last ~2,600 years. *Bulletin of Volcanology,* 71(6), 595-618.

Soil Survey Staff (2018). Web Soil Survey. United States Department of Agriculture: Natural Resources Conservation Service.

https://websoilsurvey.sc.egov.usda.gov/App/HomePage.htm Web accessed January, 2018.

Soil Survey Staff (2014). Keys to Soil Taxonomy. 12th Edition. United States Department of Agriculture: Natural Resources Conservation Service.

Sperazza, M., Moore. J. N., & Hendrix M. S. (2002). Methodology for Sediment Grain Size Analysis by Laser Diffraction: A High Resolution Application. *Journal of Sedimentary Research*, 74(5):736-743.

Washington State University (WSU) (2015). Peter Hooper Geoanalytical Lab Webpage. Electronic document, http://environment.wsu.edu/facilities/geolab/, accessed 2/14/2015.

COMPREHENSIVE REFERENCES

Balsillie, J.H., Donogue, J.F., Butler, K.M. & Butler, K.M. (2002). Plotting Equation for Gaussian Percentiles and a Spreadsheet Program for Generating Probability Plots. *Journal of Sedimentary Research*, 22(6), 929-933.

Bertrand, S., Castiaux, J., & Juvigne, E. (2008). Tephrostratigraphy of the Late Glacial and Holocene Sediments of Puyehue Lake (Southern Volcanic Zone, Chile, 40°S). *Quaternary Research*, 70, 343-357.

Bertrand, S., & Fagel N. (2007). Nature, Origin, Transport and Deposition of Andosol Parent Material in South-Central Chile (36-42°S). *Catena*, 73, 10-22.

Binford, L. R. (1980). Willow Smoke and Dogs' Tails: Hunter-Gatherer Settlement Systems and Archaeological Site Formation. *American Antiquity*, 45(1), 4-20.

Blott, S. J. & Pye K. (2001). GRADISTAT: A Grain size Distribution and Statistics Package for the Analysis of Unconsolidated Sediments. *Earth Surface Processes and Landforms*, 26, 1237-1248.

Brady, N. C., & Weil, R. R. (2010). *Elements of the Nature and Properties of Soil*. Boston: Prentice Hall Press.

Brown, J. W., Feathers J. K., Chatters, J. C., McCutcheon, P. T., & Hackenberger S. (2017). Chronometric Precision and Accuracy: Radiocarbon and Luminescence Age Estimates for Pacific Northwest Cooking Features. (Unpublished manuscript).

Buol, S.W., Southard, R.J., Graham, R.C., & McDaniel, P.A. (2011). *Soil Genesis and Classification, 6th Edition*. Ames: John Wiley and Sons, Inc.

Burtchard, G. C. (2003). *Environmental Prehistory & Archaeology of Mount Rainier National Park, Washington*. Seattle: National Park Service.

Burtchard, G. C. (2007). Holocene Subsistence and Settlement Patterns: Mount Rainier and the Montane Pacific Northwest. *Archaeology in Washington*, 13, 3-34.

Burtchard, G. C. & Hamilton, S. C. (1998). Archaeological Resources of Mount Rainier National Park, Washington, (1995). Reconnaissance Data. Report prepared for USDI National Park Service, Columbia Cascades System Support Office, Seattle. Honolulu: International Archaeological Research Institute, Inc.

Chatters, J.C., Brown, J.W., Hackenberger, S., McCutcheon, P., & Adler, J. (2017). Calcined Bone as a Reliable Medium for Radiocarbon Dating: A Test Using Paired North American Samples. *American Antiquity*, 82(3), 593-608.

Crandell, D. R. & Miller R. D. (1974). *Quaternary Stratigraphy and the Extent of Glaciation in the Mount Rainier Region, Washington*. United States Geologic Survey Professional Paper 847. Washington: U.S. Government Printing Office.

Dampf, S. K. (2002). The Sunrise Ridge Borrow Pit Site (45PI408): Subsurface Reconnaissance for a Significance Evaluation. (Unpublished master's thesis). Resource Management Department. Central Washington University, Ellensburg.

Department of Natural Resources (DNR) (2018). Washington Interactive Geology Map. https://fortress.wa.gov/dnr/geology/?Theme=wigm Web accessed February, 2018.

Donoghue, S. L., Vallance, J., Smith, I. E.M., & Stewart, R. B. (2007). Using Geochemistry as a Tool for Correlating Proximal Andesitic Tephra: Case Studies form Mt Rainier (USA) and Mt Ruapehu (New Zealand). *Journal of Quaternary Science*, 22(4), 395-410.

Dunwiddie, P. W. (1986). A 6000-Year Record of Forest History on Mount Rainier, Washington. *Ecological Society of America*, 67(1), 58-68.

Evans, H. R. (2011). The Sunrise Ridge Borrow Pit Site: Sediment Stratigraphy, Particle Size Analysis and Microarchaeology. (Unpublished master's thesis). Resource Management Department. Central Washington University, Ellensburg.

Fedje, D. W., White, J. M., Wilson, M. C., Nelson, D. E., Vogel, J. S. & Southon, J. R. (1995). Vermilion Lakes Site: Adaptations and Environments in the Canadian Rockies during the Latest Pleistocene and Early Holocene. *American Antiquity*, 60(1), 81-108.

Ferring, C.R., & Peter, D.E. (1987). Geoarchaeology of the Dyer Site, A Prehistoric Occupation in the Western Ouachitas, Oklahoma. *Plains Anthropologist*, 32(118), 351-366.

Ferry, J. (2015). Significance Evaluation of the Forgotten Creek Site (45PI429). (Unpublished master's thesis). Resource Management Department. Central Washington University, Ellensburg.

Fisher, R.V. & Schminske H.U. (1984). *Pyroclastic Rocks.* New York: Springer-Verlag.

Fitzsimmons, K.E., Stern, N. & Murray-Wallace, C.V. (2014). Depositional History and Archaeology of the Central Lake Mungo Iunette, Willandra Lakes, Southeast Australia. *Journal of Archaeological Science*, 41, 349-364.

Franklin, J.F. (1966). Vegetation and Soils in the Subalpine Forests of the Southern Washington Cascade Range. (Unpublished doctoral dissertation). School of the Environment. Washington State University, Pullman.

Franklin, J. F., Moir, W. H., Hemstrom, M. A., Greene, S. E., & Smith, B. G. (1988). *The Forest Communities of Mount Rainier National Park*, National Park Service Scientific Monograph Series, No. 19. Washington D.C.: U.S. Government Printing Office.

Friedman, G. M., Sanders, J. E. & Kopaska-Merkel, D. C. (1992). *Principles of Sedimentary Deposits*. New York: Macmillan Publishing Company.

Gatti, E., Saidin, M., Talib, Kl, Rashidi, N., Gibbard, P. & Oppenheimer, C. (2013). Depositional Processes of Reworked Tephra from the Late Pleistocene Youngest Toba Tuff Deposits in the Lenggong Valley, Malaysia. *Quaternary Research*, 79, 228-241.

Goldberg, P. & Macphail, R. I. (2006). *Practical and Theoretical Geoarchaeology.* Malden: Blackwell Publishing.

Haynes, V.C., (2008). Younger Dryas "Black Mats" and the Rancholabrean termination in North American. *Proceedings of the National Academy of Sciences of the United States of America*, 105(18), 6520-6525.

Holdaway, S. & Wandsnider, L. (2009). *Time in Archaeology: Time Perspectism Revisited.* Salt Lake City: University of Utah Press.

Jensen, J.L., Schjonning, P., Watts, C.W., Christensen, B.T. & Munkholm, L.J. (2017) Soil Texture Analysis Revisited: Removal of Organic Matter Matters More Than Ever. *PLoS ONE*, 12(5): 1-10.

Jones, S. C. (2010). Paleoenvironmental response to the ~74 ka Toba Ash-fall in the Jurreru and Middle Son Valleys in Southern and North-central India. *Quaternary Research*, 73, 336-350.

Kimsey, M., Gardner, B. & Busacca A. (2007). *Ecological and Topographic Features of Volcanic-Ash-Influenced Forest Soils*, in *Volcanic-Ash-Derived Forest Soils of the Inland Northwest: Properties and Implications for Management and Restoration*. Coeur d'Alene: United States Department of Agriculture.

Kowalewski, M. (1996). Time Averaging, Overcompleteness, and the Geological Record. *The Journal of Geology*, 104, 317-326.

Le Bas, M.J., Le Maitre, R.W., Streckeisen A., Zanettin B., & IUGS (1986). A Chemical Classification of Volcanic Rocks Based on the Total Alkali-Silica Diagram. *Journal of Petrology* 27(3), 745-750.

Lewis, D. W. & McConchie D. (1994). *Analytical Sedimentology*. New York: Chapman & Hill.

Lewis, P. C. (2015). Measuring the Cost and Performance of Lithic Industries at the Sunrise Ridge Borrow Pit Site (45PI408). (Unpublished master's thesis), Resource Management Department, Central Washington University, Ellensburg.

Lewis, P. C., McCutcheon P. T., & Vaughn, K. A. (2011) Intra-Site Analysis at the Sunrise Ridge Borrow Pit Site (45PI408). (Unpublished), paper presented at the 64th annual Northwest Anthropology Conference, April 21-23rd, Moscow, Idaho.

Lirer, L., Sheridan, M., & Vinci A. (1996). Deconvolution of Pyroclastic Grain-size spectra for Interpretation of Transport Mechanisms: an Application to the AD 79 Vesuvio Deposits. *Sedimentology* 43, 913-926.

Lirer, L. & Vinci A. (1991). Grain-size Distributions of Pyroclastic Deposits. *Sedimentology* 38, 1075-1083.

Lowe, D.J. (2010). Quaternary Volcanism, Tephras, and Tephra-derived Soils in New Zealand: An introductory Review. *In*: Lowe, D.J.; Neall, V.E., Hedley, M; Clothier, B.; Mackay, A. 2010. Guidebook for Pre-conference North Island, New Zealand „Volcanoes to Oceans" field tour (27-30 July). 19th World Soils Congress, International Union of Soil Sciences, Brisbane. *Soil and Earth Sciences Occasional Publication No. 3*, Palmerston North, Massey University.

Malvern Instruments Ltd (2007). Malvern Mastersizer User Manual. Electronic document, http://www.ceic.unsw.edu.au/centers/partcat/facilities/Mastersizer.pdf, Web accessed February, 2014.

McClure, R. H. Jr. (1990). Previous Archaeology of Mount Rainier National park. Draft report manuscript and associated miscellaneous field notes, inter-office memoranda, photographs and topographic maps. Material associated with an incomplete cultural resource overview for Mount Rainier National Park. Manuscript on file USDI national Park service, Columbia Cascades System Support Office. Manuscript and supporting materials in possession of Greg C. Burtchard, Seattle.

McCutcheon, P. T., Parfitt, A. B., Brown J., Davis D. R., Limberg, C., & Middleton, S. (2017). Investigating Intra-Site Variation for Holocene Epoch Human Land Use at the Sunrise Ridge Borrow Pit Site (45PI408). Department of Anthropology and Museum Studies. Central Washington University, Ellensburg. Report in preparation.

McDaniel, P.A., & Wilson, M.A (2007). Physical and Chemical Properties of Ash-Influenced Soils of Inland Northwest Forests, *in* Volcanic-Ash-Derived Forest Soils of the Inland Northwest: Properties and Implications for Management and Restoration. United States Department of Agriculture, Coeur d'Alene.

Mullineaux, D. R. (1974). *Pumice and other pyroclastic deposits in Mount Rainier National Park, Washington.* Washington D. C.: U.S. Govt. Printing Office.

Mycielsk-Dowgiallo, E. & Ludwikowska-Kedzia M. (2011). Alternative Interpretations of Grain-size Data from Quaternary Deposits. *Geologos* 17(4), 189-203.

Neall, V.E., Wallace, R.C., & Torrence R. (2008). The Volcanic Environment for 40,000 Years of Human Occupation on the Willauhez Isthmus, West New Britain, Papua New Guinea. *Journal of Volcanology and Geothermal Research*, 176(3), 330-343.

Nickels, A. M. (2001). Mount Rainier National Park Field Site Inspection Record, 45PI408, Seattle: National Park Service.

Nickels, A. M. (2002). History Under Fire: Understanding Human Fire Modification of the Landscapes at Mount Rainier National Park. (Unpublished master's thesis), Resource Management Department, Central Washington University, Ellensburg.

Pansu, M. & Gautheyrou, G. (2006). *Handbook of Soil Analysis: Mineralogical, Organic and Inorganic Methods.* New York: Springer.

Parfitt, A.B, & McCutcheon, P.T. (2017). Chemical Sourcing of Obsidian Artifacts from the Grissom Site (45-KT-301) to Study Source Variability. *Journal of Northwest Anthropology*, 51(1), 37-72.

Pettijohn, J. F. (1975). *Sedimentary Rocks*. 3rd ed. New York: Harper & Row Publishers, Inc.

Prognon, F., Cojan, I., Kindler, P., Thiry, M. & Demange, M. (2011). Mineralogical Evidence for a Local Volcanic Origin of the Parent Material of Bermuda Quaternary Paleosols. *Quaternary Research* 75(1), 256-266.

Scarciglia, F., Zumpano, V., Sulpizio, R., Terribile, F., Pulice, I. & La Russa, M.F. (2014). Major Factors Controlling Late Pleistocene to Holocene Soil Development in the Vesuvius Area (Southern Italy). *European Journal of Soil Science*, 65, 406-419.

Schoeneberger, P.J., Wysocki, D.A., Benham, E.C. & Soil Survey Staff (2012). *Field Book for Describing and Sampling Soils, Version 3.0.* Natural Resources Conservation Service. Lincoln: National Soil Survey Center,

Sheldon, D., McCutcheon, P. T., Davis, D. R., Kassa, S., Lewis, P.C., Limberg, C., & Parfitt, A. B. (2014). Archaeological Investigations at the Sunrise Ridge Borrow Pit Site (45PI408) in Mount Rainier National Park. (Unpublished), poster presented at the annual Northwest Anthropological Conference, Bellingham.

Sisson T.W., & Vallance J. W. (2009). Frequent Eruptions of Mount Rainier over the last ~2,600 years. *Bulletin of Volcanology*, 71(6), 595-618.

Soil Survey Staff (2018). Web Soil Survey. United States Department of Agriculture: Natural Resources Conservation Service. https://websoilsurvey.sc.egov.usda.gov/App/HomePage.htm Web accessed January, 2018.

Soil Survey Staff (2014). Keys to Soil Taxonomy. 12th Edition. United States Department of Agriculture: Natural Resources Conservation Service.

Sperazza, M., Moore. J. N., & Hendrix M. S. (2002). Methodology for Sediment Grain Size Analysis by Laser Diffraction: A High Resolution Application. *Journal of Sedimentary Research*, 74(5):736-743.

Stcherbinine, S. (2014). Geoarchaeological Lab Analysis of Stratigraphy at the Sunrise Ridge Borrow Pit Site (45PI408). (Unpublished), graduate research project, Central Washington University, Ellensburg.

Stein, J. K., & Deo J. N. (2003). Big Sites----Short Time: Accumulation Rates in Archaeological Sites. *Journal of Archaeological Science*, 30, 297-316.

Suttles, W. (1990). *Handbook of the North American Indian, Volume 7:Northwest Coast*. Washington D.C.: Smithsonian Institute.

Vallance, J. W., & Pringle, P. T. (2008). Lahars, Tephra, and Buried Forests---The Post-Glacial History of Mount Rainier, in *Roadside Geology of Mount Rainier National Park and Vicinity*. Washington Department of Natural Resources, Olympia.

Vaughn, K. A. (2010). A Comparison of Lithic Technology and Function Across Environmental Zones in the Southern Cascades. (Unpublished master's thesis), Resource Management Department. Central Washington University, Ellensburg.

Walker, D. E. Jr. (1998). *Handbook of the North American Indian, Volume 12:Plateau*. Smithsonian Institute, Washington D.C.

Walsh, M.K., Lukins, M.L., McCutcheon, P.T., & Burtchard, G.C. (2017). Fire-climate-human Interactions during the Postglacial Period at Sunrise Ridge, Mount Rainier National Park, Washington (USA). *Quaternary Science Reviews*, 177: 246-264.

Washington State University (WSU) (2015). Peter Hooper Geoanalytical Lab Webpage. Electronic document, http://environment.wsu.edu/facilities/geolab/, Web accessed February, 2015.

Waters, M. R. (1992). *Principles of Geoarchaeology: A North American Perspective.* Tucson: The University of Arizona Press.

Western Regional Climate Center (2018). White River Ranger Station Precipitation and Temperature Averages for 1971 to 2000 Climate Normal. Electronic document https://wrcc.dri.edu/cgi-bin/cliMAIN.pl?wa9171 Web accessed March, 2018.

Appendix A: Soil Survey Data

Only one mapped soil unit at SRBP site: Tipsoo-Owyhigh-Mysticlake complex, 20-65 percent slopes, which has characteristics of three soil series'. See below for data on each series of the complex. The SRBP site is relatively flat compared to the mapped soil unit, which is a 20-65 percent slope. However, the only mapped soil units within a kilometer of the site with moderate to low slopes occur on ridges or valley floors; landforms contrasting to the south-facing valley sidewall the site is situated on.

Tipsoo: Taxonomic class: medial, glassy Andic Haplocryods, found on mountain slopes, cirques, glacial valley walls, and ridges. Parent material is volcanic ash over colluvium derived from andesite, 15-100 percent slopes; depth to lithologic discontinuity: 73cm; Andic soil properties: 5-150cm. **Typical Pedon**: Tipsoo paragravelly medial sandy loam on a forested, north-facing ridge with slope of 40 percent and elevation of 1745m.

Table 1. Properties of the Tipsoo Series

Horizon	**Depth (cm)**	**Texture**	**Clay %**	**Color (Munsell #)**	**Color**	**pH**	**Boundary**	**[1]PM**
Oi	0-2	No data	No data	No data	No data	4.5	abrupt, smooth	Plant matter
Oe	2-5	No data	No data	No data	No data	4.5	abrupt, wavy	Plant matter
E	5-9	sandy loam, loamy sand	1-5	7.5YR 6/1 to 7.5YR 3/1	gray to very dark gray	4.7	abrupt, wavy	MSH-W
Bhs	9-42	sandy loam, loamy sand	1-5	7.5YR 3/2 to 7.5YR 2.5/2	Dark brown to very dark brown	5.2	abrupt, irregular	MR-C
Bs1	42-57	sandy loam	1-10	7.5YR 4/3 to 7.5YR 3/3	Brown to dark brown	5.2	clear, wavy	MSH-P
Bs2	57-73	Loamy sand, sandy loam	1-10	7.5YR 5/3 to 7.5YR 4/3	Brown	5.2	clear, irregular	MSH-Yn
2Bw1	73-110	Sandy loam	1-10	10YR 6/6 to 10YR 5/6	Brownish yellow to yellowish brown	5.4	gradual, wavy	colluvium
2Bw2	110-150	Sandy loam	1-10	10YR 5/6 to 10YR 3/6	Yellowish brown to dark yellowish brown	5.4	No data	colluvium

[1] Denotes specific parent material if defined in the soil survey

Owyhigh: Taxonomic class: medial, glassy Andic Haplocryods, found on bedrock benches, ridges, glacial valley walls, cirques. Parent material: volcanic ash over colluvium over andesite, 15-100 percent slopes; depth to lithic contact: 80cm; Andic soil properties: 6-80cm.

Typical Pedon: Owyhigh medial sandy loam on a forested, north-facing glacial valley wall with a slope of 35 percent and at an elevation of 1597m.

Table 2. Characteristics of the Owyhigh Series

Horizon	Depth (cm)	Texture	Clay %	Color (Munsell #)	Color	pH	Boundary	[1]PM
Oi	0-1	No data	No data	No data	No data	4.5	abrupt, smooth	Plant matter
Oe	1-6	No data	No data	No data	No data	4.5	abrupt, wavy	Plant matter
E	6-18	sandy loam, loamy sand	1-5	7.5YR 6/2 to 7.5YR 3/2	Pinkish gray to dark brown	4.7	abrupt, wavy	MSH-W
Bs1	18-34	sandy loam, loamy sand	1-10	7.5YR 5/4 to 7.5YR 3/4	brown to dark brown	5.2	clear, irregular	MR-C
Bs2	34-52	sandy loam, loamy sand	1-10	7.5YR 5/4 to 7.5YR 3/4	Brown to dark brown	5.2	clear, wavy	MSH-Yn
Bs3	52-80	sandy loam	1-10	7.5YR 5/4 to 7.5YR 4/4	Brown	5.4	clear, irregular	No data
2R	80	Fractured andesite	No data	No data	No data	No data	No data	bedrock

[1] Denotes specific parent material if defined in the soil survey

Mysticlake: Taxonomic class: medial, glassy Typic Cryaquands, found on debris aprons, glacial valley walls, cirques. Parent material: volcanic ash over colluvium, 0-35 percent slopes; depth to lithologic discontinuity: 120cm; Andic soil properties: 3-150cm.

Typical Pedon: Mysticlake medial sandy loam on a west-facing forested debris apron with a slope of 20 percent and at an elevation of 1625m.

Table 3. Characteristics of the Mysticlake Series

Horizon	Depth (cm)	Texture	Clay %	Color (Munsell #)	Color	pH	Boundary	[1]PM
Oi	0-1	No data	No data	No data	No data	4.5	abrupt, smooth	Plant matter
Oe	1-3	No data	No data	No data	No data	4.5	abrupt, smooth	plant
A1	3-6	sandy loam, loamy sand	No data	10YR 4/1 to 10YR 2/1	Dark gray to black	5.2	abrupt, smooth	No data
A2	6-20	sandy loam, loamy sand	No data	10YR 5/3 to 10YR 3/3	brown to dark brown	5.2	abrupt, irregular	MSH-W
Bw	20-32	sandy loam, loamy sand	No data	7.5YR 5/4 To 7.5YR 3/4	Brown to dark brown	5.2	abrupt, irregular	MR-C
Bg1	32-48	sandy loam, loamy sand	No data	10YR 5/2 to 10YR 3/2	Grayish brown to very dark grayish brown	5.2	clear, wavy	MSH-P
Bg2	48-70	sandy loam, loamy sand	No data	10YR 5/4 to 10YR 3/4	Yellowish brown to dark yellowish brown	5.4	clear, wavy	MSH-Yn
Bg3	70-120	sandy loam, loamy sand	No data	10YR 5/3 To 10YR 3/3	brown to dark brown	5.4	gradual, wavy	MR-F
2Bg4	120-150	sandy loam, loam	No data	10YR 5/3 To 10YR 3/3	brown to dark brown	5.4	N/A	colluvium

[1] Denotes specific parent material if defined in the soil survey

Mountwow: Taxonomic class: medial, glassy, acid Thaptic Cryaquands, found on swales cirques, and parklands. Parent material: volcanic ash over colluvium, 0-65 percent slopes; depth to lithologic discontinuity: 66cm; Andic soil properties: 2-150cm.

Typical Pedon: Mountwow medial sandy loam on a meadow on a north-facing cirque with a slope of 2 percent and at an elevation of 1805m.

Table 3. Characteristics of the Mountwow Series

Horizon	Depth (cm)	Texture	Clay %	Color (Munsell #)	Color	pH	Boundary	[1]PM
Oi	0-2	No data	No data	No data	No data	4.5	abrupt, wavy	plant
A	2-10	sandy loam, loamy sand	No data	10YR 5/2	Grayish brown	5.2	abrupt, wavy	MSH-W
Bw1	10-14	sandy loam, loamy sand	No data	7.5YR 7/3 & 7.5YR 3/3	Brown to dark brown	5.2	abrupt, smooth	MR-C
Bw2	14-26	sandy loam, loamy sand	No data	10YR 6/2 to 10YR 4/2	Light brownish gray to dark grayish brown	5.2	clear, wavy	MSH-P
Bw3	26-37	sandy loam, loamy sand	No data	10YR 7/4 To 10YR 5/4	Very pale brown to yellowish brown	5.2	abrupt, irregular	MSH-Yn
Agb	37-44	sandy loam, loamy sand	No data	10YR 4/2 to 10YR 2/2	Dark grayish brown to very dark brown	5.2	clear, wavy	No Data
Bgb1	44-51	sandy loam, loamy sand	No data	7.5YR 5/4 to 7.5YR 3/4	Brown to dark brown	5.2	clear, wavy	MR-F
Bgb2	51-60	sandy loam, loamy sand	No data	10YR 5/3 To 10YR 3/3	brown to dark brown	5.2	abrupt, wavy	MR-D
Bgb3	60-66	sandy loam, loamy sand	No data	7.5YR 7/6 To 7.5YR 5/6	Reddish yellow to strong brown	5.2	abrupt, smooth	MAZ-O
2Agb2		sandy loam,	No data	10YR 4/2 To	Dark grayish	5.4	abrupt, wavy	colluvium

Horizon	Depth (cm)	Texture	Clay %	Color (Munsell #)	Color	pH	Boundary	[1]PM
		loamy sand		10YR 2/2	brown to very dark brown			
2Bgb4		sandy loam, loamy sand	No data	10YR 5/4 To 10YR 3/4	Yellowish brown to dark yellowish brown	5.4	Clear, wavy	colluvium
2Bgb5		sandy loam, loamy sand	No data	10YR 5/4 To 10YR 3/4	Yellowish brown to dark yellowish brown	5.4	N/A	colluvium

[1] Denotes specific parent material if defined in the soil survey

All above data from https://websoilsurvey.sc.egov.usda.gov/App/WebSoilSurvey.aspx

Appendix B: Study Sample Data

Table 1. Sediment samples used for this study.

Sample Number	[1]Depositional Layer	Location	Elevation (cmbs)
1	MSH-W	30N/24E	0-13
2	DM MSH-W/MR-C	30N/24E	13-26
3	MR-C	30N/24E	26-45
4	DM MR-C/MSH-P	30N/24E	45-51
5	MSH-P	30N/24E	51-57
6	DM MSH-P/MSH-Yn	30N/24E	57-63
7	MSH-Yn	30N/24E	63-76
8	DM MSH-Yn/MR-F	30N/24E	76-93
9	MR-F	30N/24E	93-98
10	DM MR-F/MAZ-O	30N/24E	98-104
11	MAZ-O	30N/24E	104-108
12	DM MAZ-O/MR-R	30N/24E	108-115
13	MR-R	30N/24E	115-123
14	MSH-W	61.5N/36E	0-13
15	DM MSH-W/MR-C	61.5N/36E	13-26
16	MR-C	61.5N/36E	26-40
17	DM MR-C/MSH-P	61.5N/36E	40-51
18	DM MSH-P/MSH-Yn	61.5N/36E	51-59
19	MSH-Yn	61.5N/36E	59-69
20	DM MSH-Yn/MR-F	61.5N/36E	69-88
21	MR-F	61.5N/36E	88-100
22	MR-R	61.5N/36E	100-112
23	DM MSH-W/MR-C	64N/115E	0-14
24	MR-C	64N/115E	14-32
25	[2]DM MR-C/MSH-P & MSH-P	64N/115E	32-51
26	DM MSH-P/MSH-Yn	64N/115E	51-61
27	MSH-Yn	64N/115E	61-83
28	DM MSH-Yn/F	64N/115E	83-105
29	DM Duff/MSH-W	71.5N/66.5E	0-13
30	MSH-W & DM MSH-W/MR-C	71.5N/66.5E	13-27
31	[2]DM MSH-W/MR-C & MR-C	71.5N/66.5E	27-51
32	MSH-P	71.5N/66.5E	51-59
33	MSH-Yn	71.5N/66.5E	59-80
34	DM MSH-Yn/MR-F	71.5N/66.5E	80-94
35	MR-F	71.5N/66.5E	94-103
36	Duff/MSH-W	Off site	0-9
37	MSH-W	Off site	9-18
38	MR-C	Off site	18-40

Sample Number	[1]Depositional Layer	Location	Elevation (cmbs)
39	MSH-Yn	Off site	40-73
40	DM MSH-Yn/MR-F	Off site	73-87
41	MR-F	Off site	87-106
42	MAZ-O	Off site	106-113
43	DM MAZ-O/MR-R	Off site	113-130
44	MR-R	Off site	130-147
45	Feature R (DM MSH-W/MR-C)	61.5N/36E	19-35
46	Feature AA (DM MR-C/MSH-P)	71.5N/66.5E	20-35
47	Feature E (DM MSH-P/MSH-Yn)	28N 25E	45-55

[1]Depositional layers listed as recorded in the field during collection.
[2]Depositional layer containing multiple depositional units.

APPENDIX C: Hand Drawn Distribution Curves

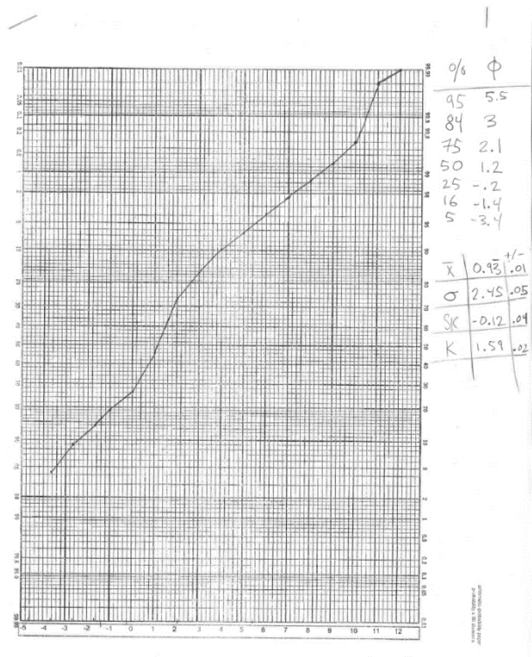

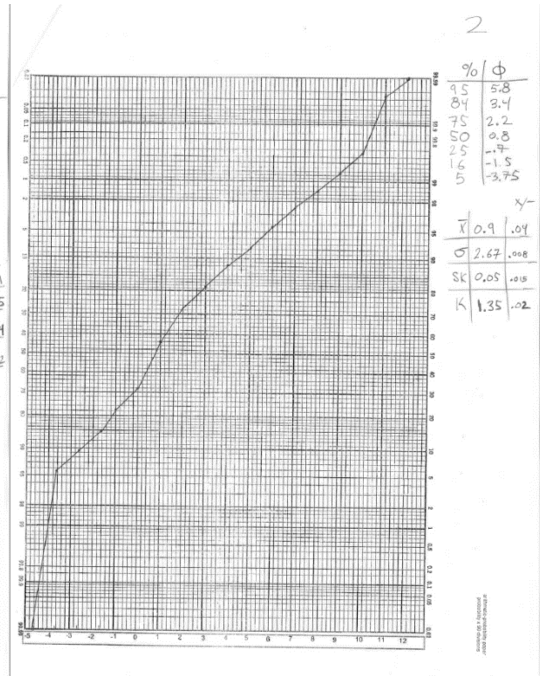

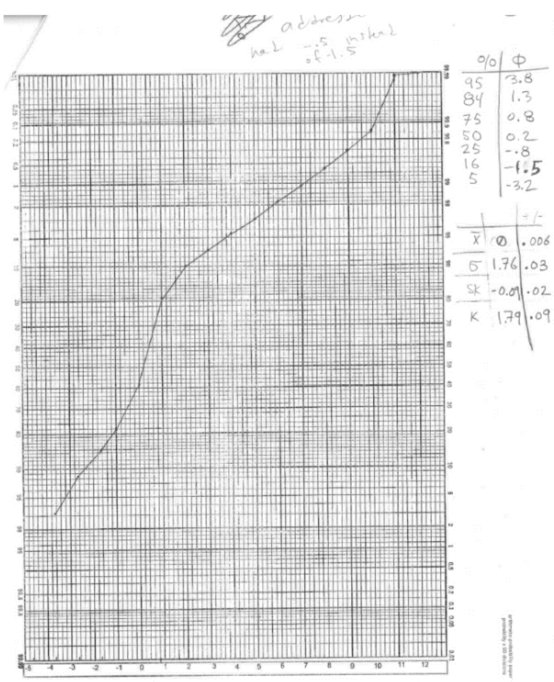

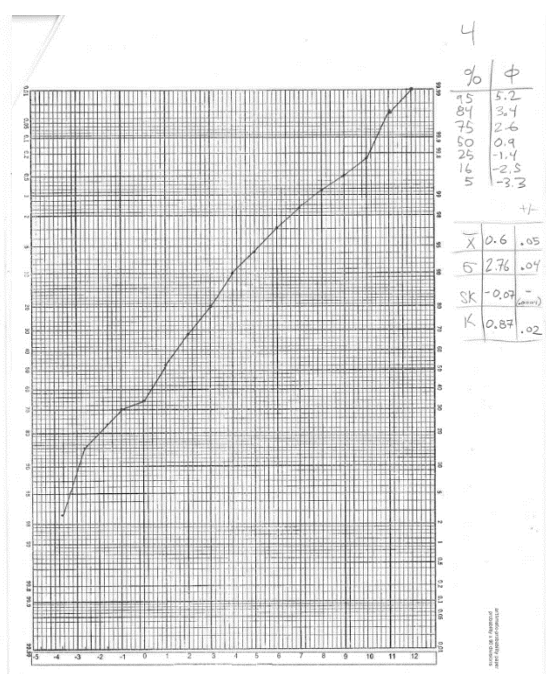

5

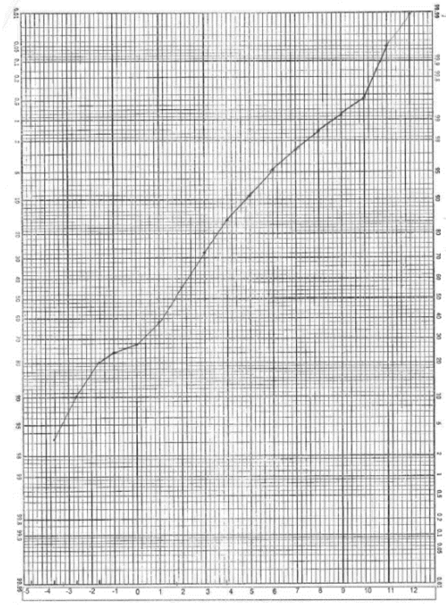

%	φ
95	5.9
84	3.9
75	3.2
50	1.7
25	-.7
16	-2
5	-3.3

		+/-
$\bar{X}$	1.2	0.03
σ	2.87	.06
SK	-0.17	.003
K	0.97	.02

6

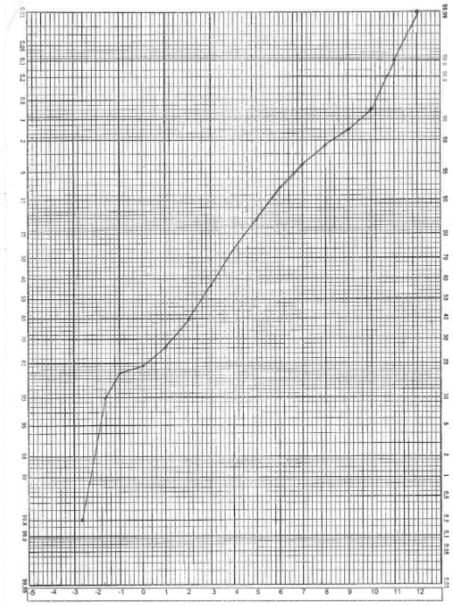

%	φ
95	6.7
84	4.9
75	4.1
50	2.6
25	0.8
16	-1.1
5	-1.9

		+/-
$\bar{X}$	$2.1\bar{3}$	.04
σ	2.8	.06
SK	-0.14	.007
K	1.07	.02

7

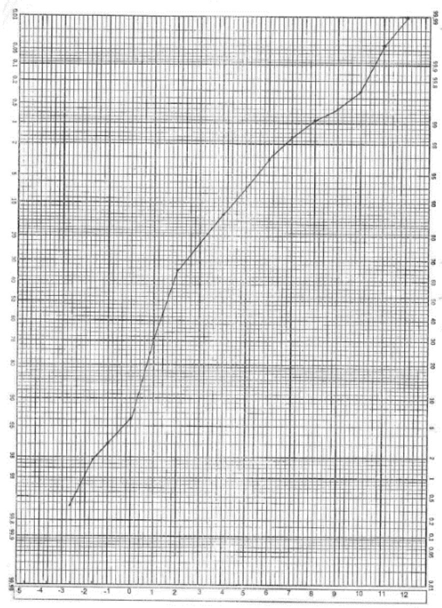

%	φ
95	5.4
84	3.6
75	2.8
50	1.6
25	0.8
16	0.5
5	-.3

		+/-
$\bar{X}$	1.9	.02
σ	1.64	.07
SK	0.31	.001
K	1.17	.001

8

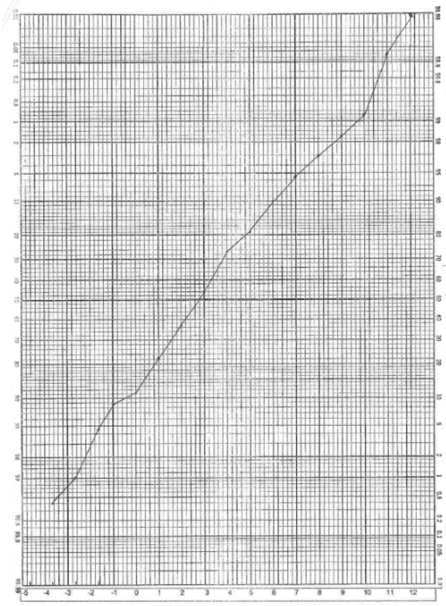

%	φ
95	7.2
84	5.2
75	4.2
50	2.8
25	1.2
16	0.5
5	-1.6

		+/-
$\bar{X}$	$2.8\bar{3}$	.02
σ	2.51	.04
SK	0.01	.01
K	1.2	.09

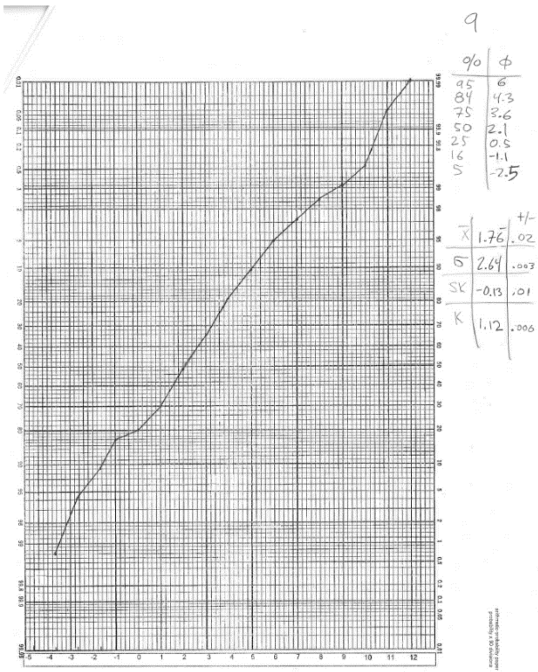
9
% φ
95 6
84 4.3
75 3.6
50 2.1
25 0.5
16 -1.1
5 -2.5
+/-
X̄ 1.76 .02
σ 2.64 .003
SK -0.13 .01
K 1.12 .006

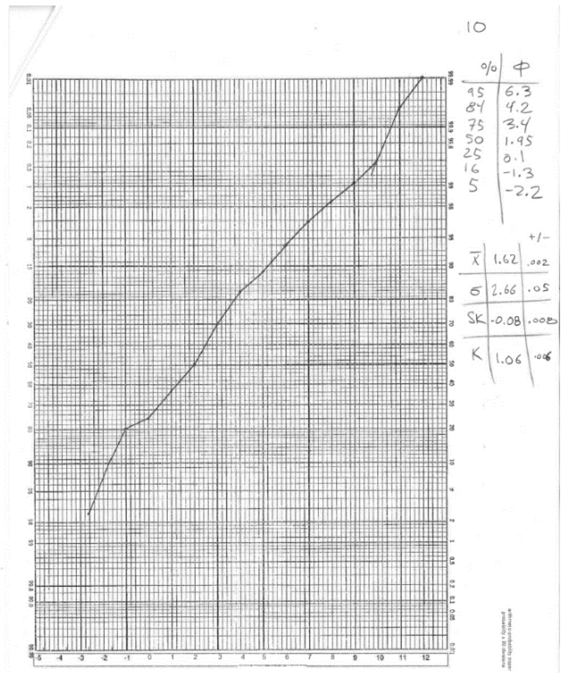
10
% φ
95 6.3
84 4.2
75 3.4
50 1.95
25 0.1
16 -1.3
5 -2.2
+/-
X̄ 1.62 .002
σ 2.66 .05
SK -0.08 .008
K 1.06 .006

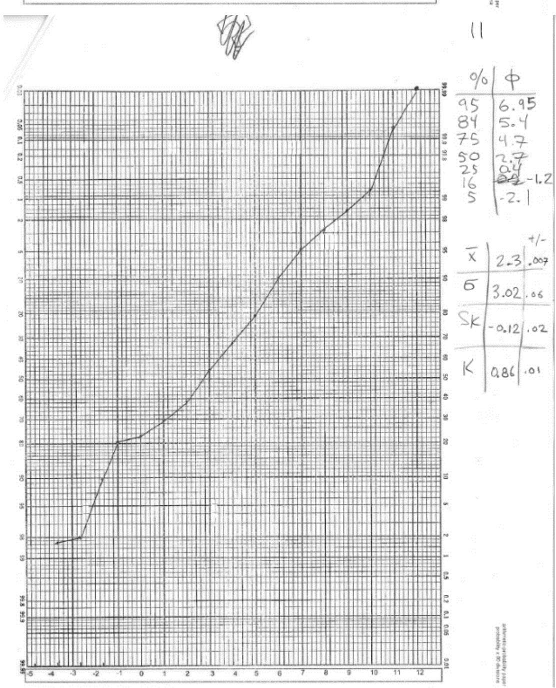
11
% φ
95 6.95
84 5.4
75 4.7
50 2.7
25 0.4
16 -1.2
5 -2.1
+/-
X̄ 2.3 .007
σ 3.02 .06
SK -0.12 .02
K 0.86 .01

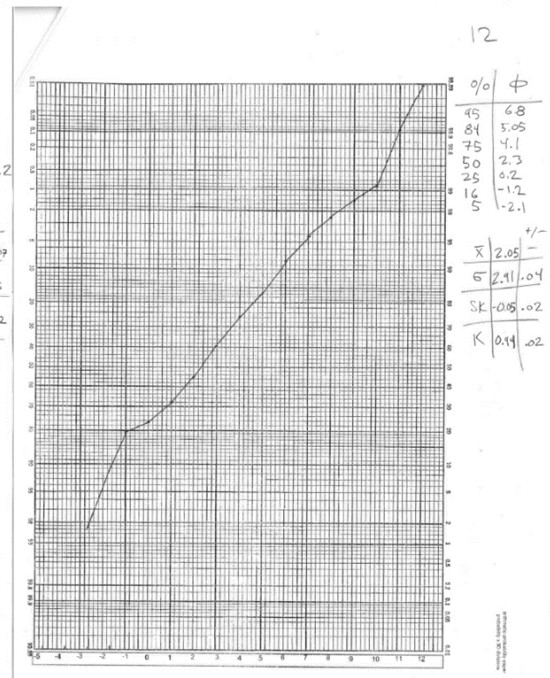
12
% φ
95 6.8
84 5.05
75 4.1
50 2.3
25 0.2
16 -1.2
5 -2.1
+/-
X̄ 2.05 –
σ 2.91 .04
SK -0.05 .02
K 0.94 .02

13

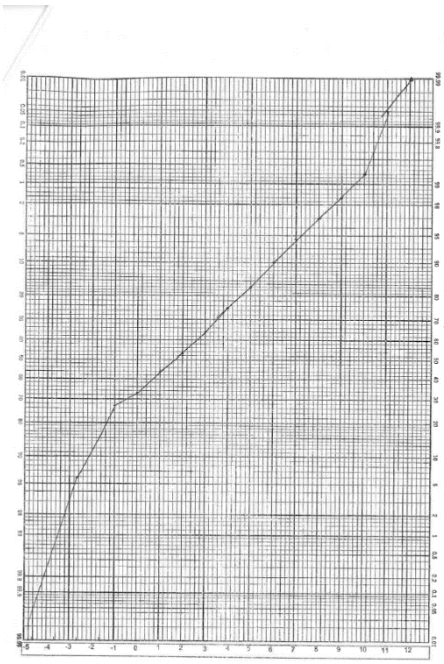

%	ϕ
95	7.2
84	5.1
75	4
50	1.7
25	-1.1
16	-1.6
5	-2.8

		+-
$\bar{x}$	1.73	.03
σ	3.19	.04
Sk	0.06	.005
K	0.8	.01

~~14~~ 14

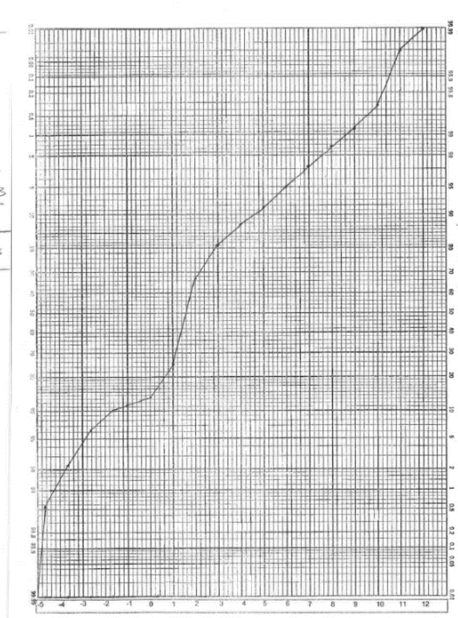

%	ϕ
95	6
84	3.4
75	2.5
50	1.6
25	1
16	0.3
5	-2.9

		+/-
$\bar{x}$	1.77	.02
σ	2.12	.05
Sk	0.08	.07
K	2.43	.1

15

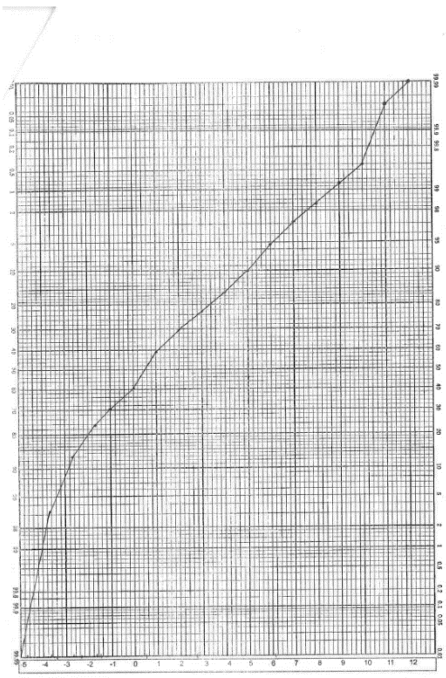

%	ϕ
95	6.1
84	4
75	2.7
50	0.5
25	
16	-1.5 -2.4
5	-3.3

All / but SD look good as expected

		+/-
$\bar{x}$	0.7	.08
SD	3.02	.03
SK	0.14	.01
K	0.92	.002

16

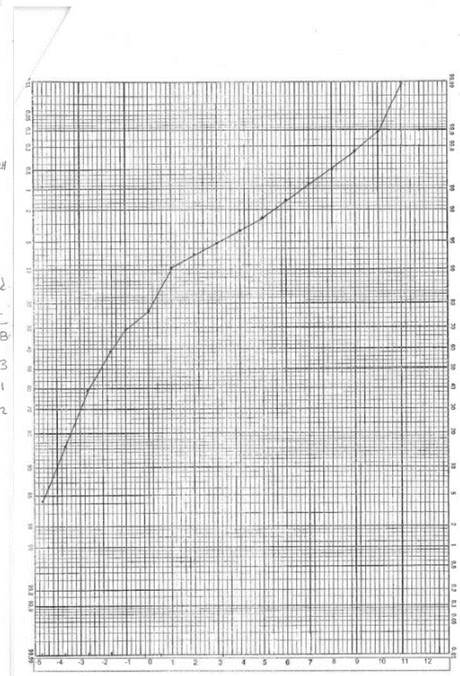

%	ϕ
95	3.2
84	0.5
75	-0.2
50	-2.2
25	-3.2
16	-3.6
5	-4.5

		+/-
$\bar{x}$	-1.77	.02
σ	2.19	.03
Sk	0.36	.06
K	1.05	.03

17

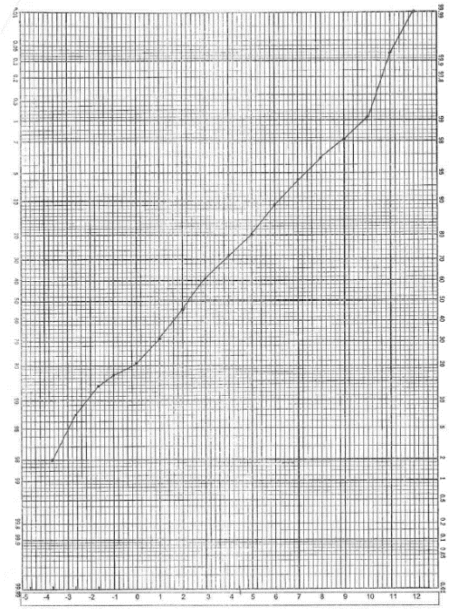

%	ϕ
95	7.4
84	5.4
75	4.4
50	2.2
25	0.4
16	-1.2
5	-3

		+/-
$\bar{X}$	2.13	.02
σ	3.23	.004
SK	-0.02	.02
K	1.07	.02

18

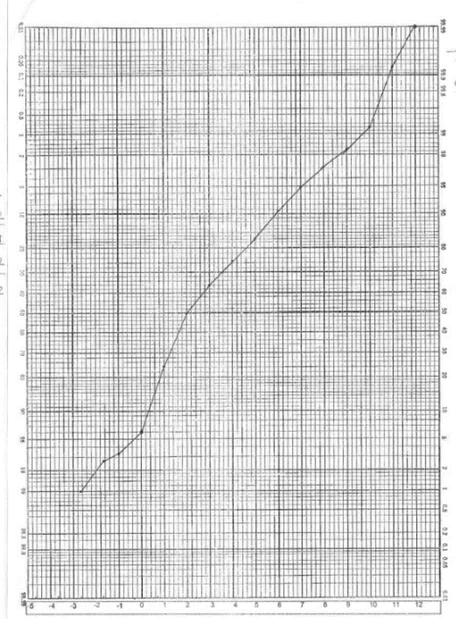

%	ϕ
95	7.05
84	5.1
75	4.1
50	2.05
25	1.05
16	0.7
5	-0.3

		x/-
$\bar{X}$	2.62	.07
σ	2.21	.05
SK	0.37	.02
K	0.99	.02

19

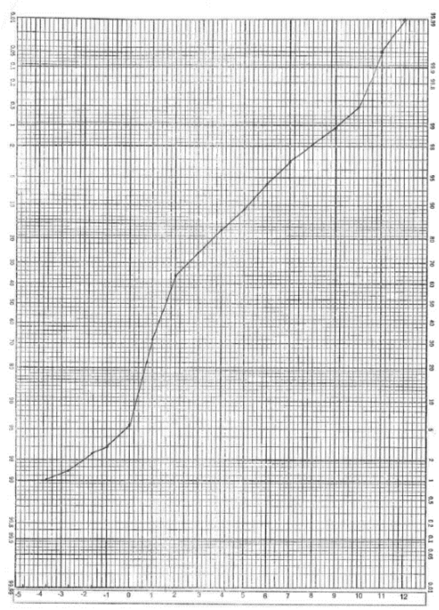

%	ϕ
95	6.3
84	4.2
75	3.1
50	1.6
25	0.8
16	0.5
5	-.2

		+/-
$\bar{X}$	2.1	.06
σ	1.91	.03
SK	0.43	.01
K	1.16	.003

20

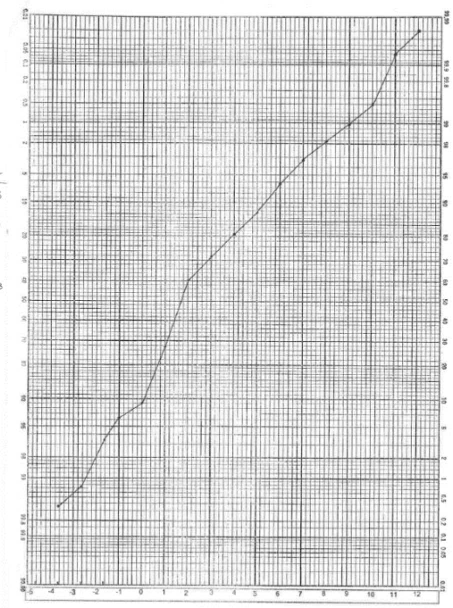

%	ϕ
95	6.4
84	4.5
75	3.4
50	1.7
25	0.9
16	0.5
5	-1.2

		+/-
$\bar{X}$	2.23	.04
σ	2.15	.05
SK	0.32	.03
K	1.25	.003

1/10th of 1 Φ is the width of a dot/thickness of pencil lead

21

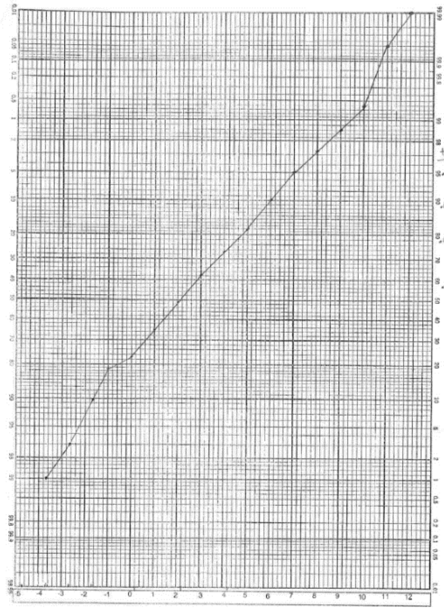

%	Φ
95	6.9
84	5.2
75	4.2
50	2.2
25	0.2
16	-1.1
5	-2.2

+/-	
.06	$\bar{X}$ = 2.1
.07	σ = 2.95
.08	SK = -0.007
.02	K = 0.93

22

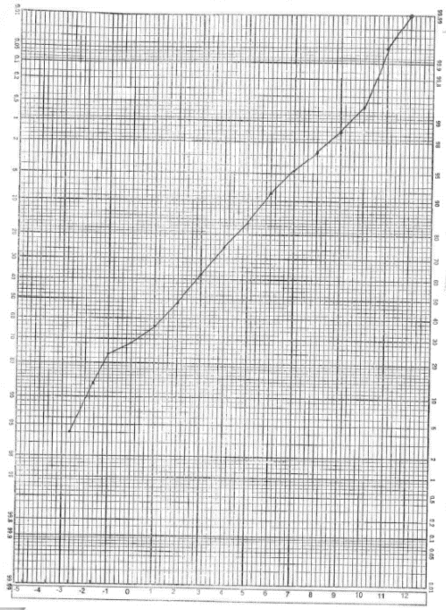

%	Φ
95	6.8
84	5
75	4
50	2.1
25	-0.7
16	-1.5
5	-2.5

		+/-
$\bar{X}$	1.87	.006
σ	3.03	.03
SK	-0.05	.005
K	0.81	.02

23

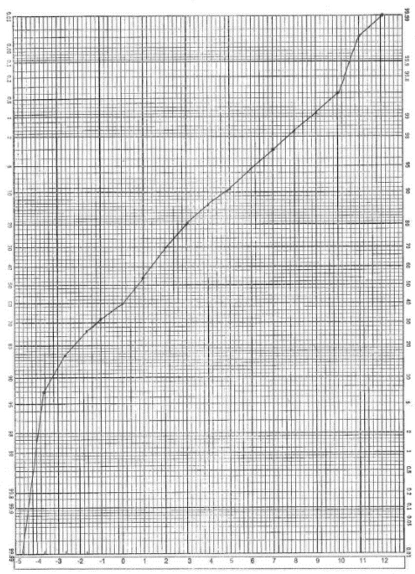

%	Φ
95	6.1
84	3.5
75	2.5
50	0.7
25	-1.8
16	-2.7
5	-3.7

		+/-
$\bar{X}$	0.5	.05
σ	3.03	.1
SK	0.063	.08
K	0.93	.1

24

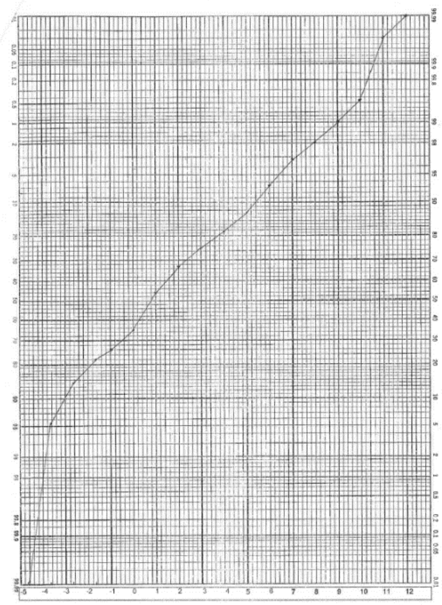

%	Φ
95	6.4
84	4.4
75	3
50	0.8
25	-1.1
16	-2.4
5	-3.7

		+/-
$\bar{X}$	0.93	.005
σ	3.23	.03
SK	0.08	.01
K	1.01	.01

20 pencil lines per Φ @ 0.5 lead → so 1/10th Φ error = twice the thickness of pencil lead

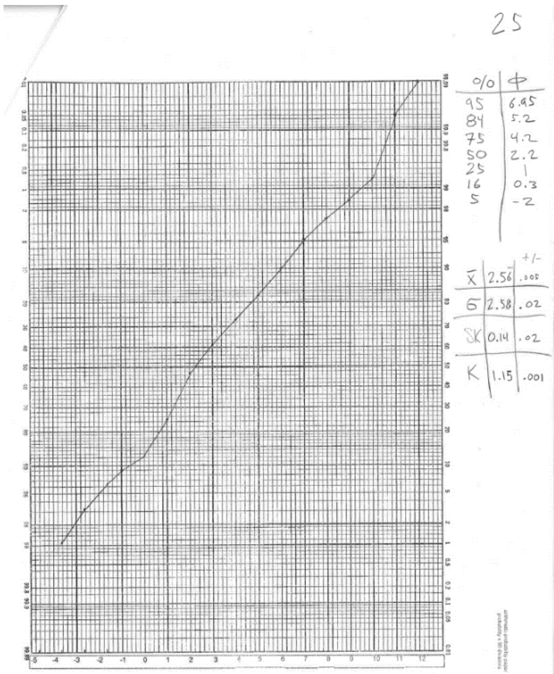
25
% φ
95 6.95
84 5.2
75 4.2
50 2.2
25 1
16 0.3
5 -2
+/-
X̄ 2.56 .005
σ 2.38 .02
SK 0.14 .02
K 1.15 .001

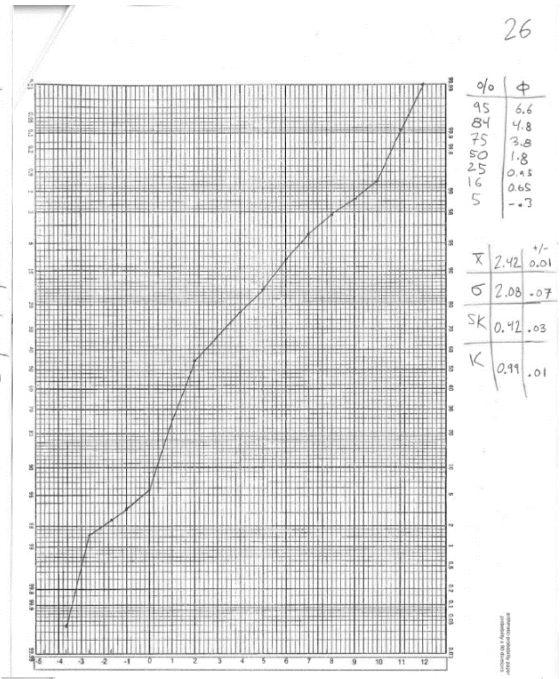
26
% φ
95 6.6
84 4.8
75 3.8
50 1.8
25 0.95
16 0.65
5 -.3
+/-
X̄ 2.42 0.01
σ 2.08 .07
SK 0.42 .03
K 0.99 .01

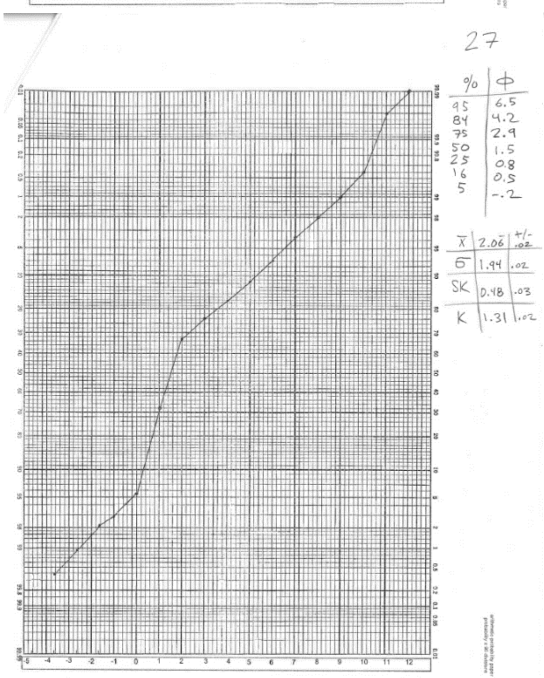
27
% φ
95 6.5
84 4.2
75 2.9
50 1.5
25 0.8
16 0.5
5 -.2
+/-
X̄ 2.06 .02
σ 1.94 .02
SK 0.48 .03
K 1.31 .02

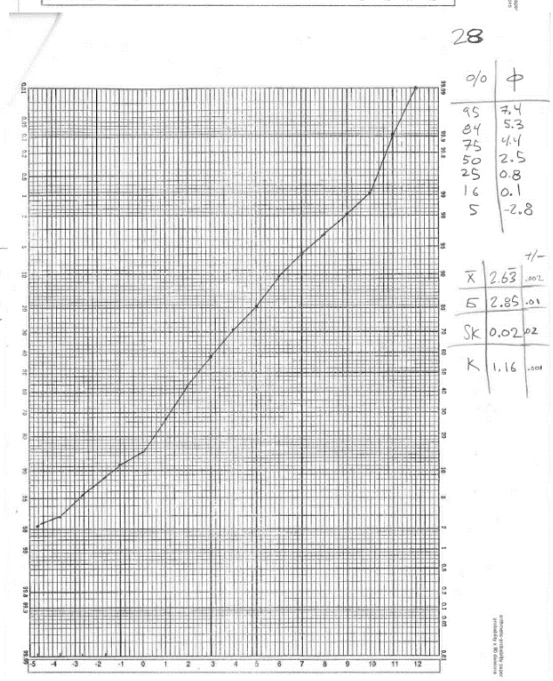
28
% φ
95 7.4
84 5.3
75 4.4
50 2.5
25 0.8
16 0.1
5 -2.8
+/-
X̄ 2.63 .002
σ 2.85 .01
SK 0.02 .02
K 1.16 .004

29

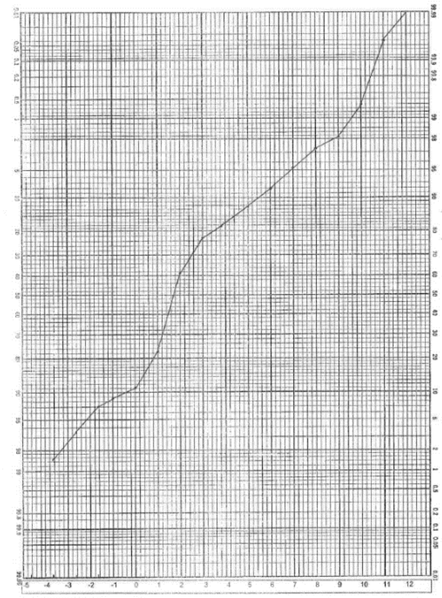

%	Φ
95	6.9
84	4.2
75	2.9
50	1.7
25	1.1
16	0.5
5	-2.2

		+/-
$\bar{X}$	2.13	.08
σ	2.3	—
SK	0.25	-.04
K	2.07	.06

Neel to fix

30

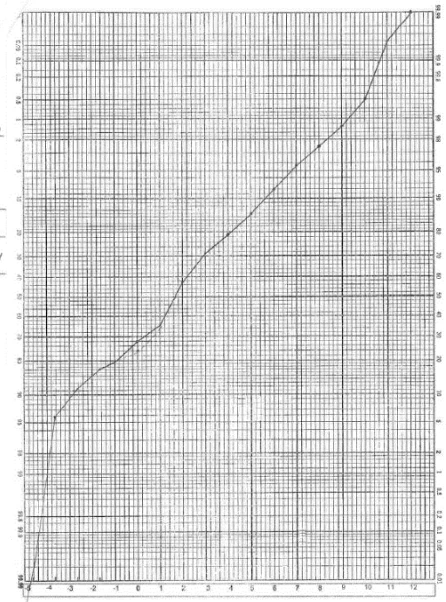

%	Φ
95	6.8
84	4.7
75	3.5
50	1.7
25	-.3 (?)
16	-1.8
5	-3.7

$\bar{X}$	1.53	.04
σ	3.22	.04
SK	-0.05	.005
K	1.13	.16

31

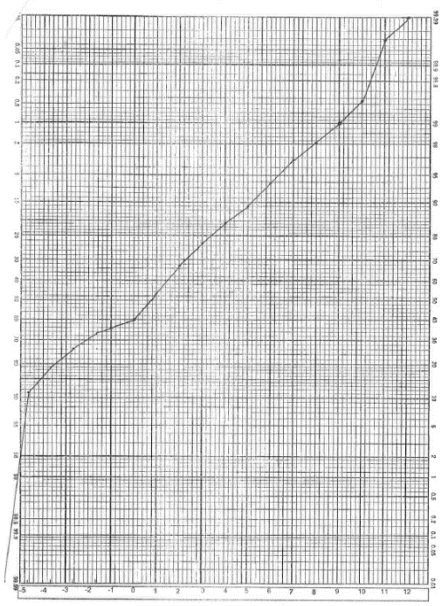

%	Φ
95	6.4
84	3.5
75	2.8
50	0.8
25	-2.8
16	-4
5	-4.8

		+/-
$\bar{X}$	0.25	.03
σ	3.68	.08
SK	-0.1	.003
K	0.82	.03

32

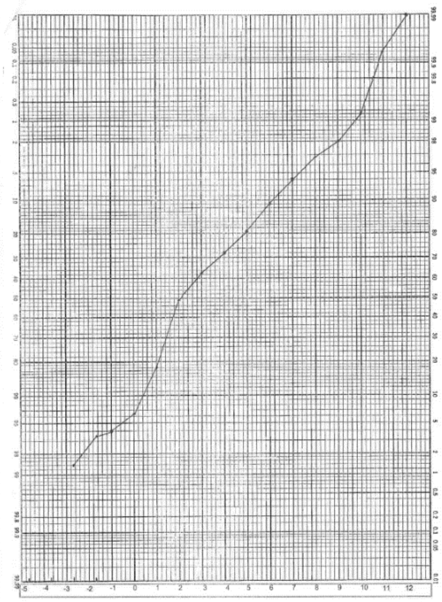

%	Φ
95	7.3
84	5.4
75	4.3
50	2.1
25	1.3
16	0.8
5	-0.6

		+/-
$\bar{X}$	2.76	.04
σ	2.35	.03
SK	0.38	.01
K	1.08	.05

33

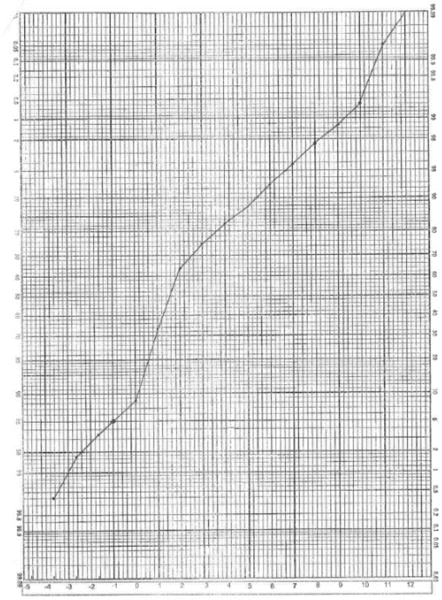

%	ϕ
95	6.7
84	4.2
75	3
50	1.6
25	0.8
16	0.4
5	-1

$\bar{x}$	2.06	.001
σ	2.12	.05
SK	0.35	.001
K	1.43	.06

Kurtosis is off by ~~0.4 ϕ~~
Found mistake

34

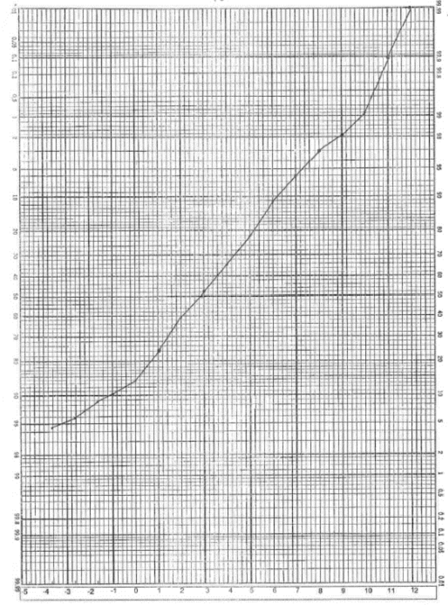

%	ϕ
95	7.3
84	5.5
75	4.8 Fixed
50	2.9
25	1.1
16	0.3
5	-3.2

		+/-
$\bar{x}$	2.9	.03
σ	2.89	.07
SK	-0.08	.02
K	1.16	.03

Fixed!

35

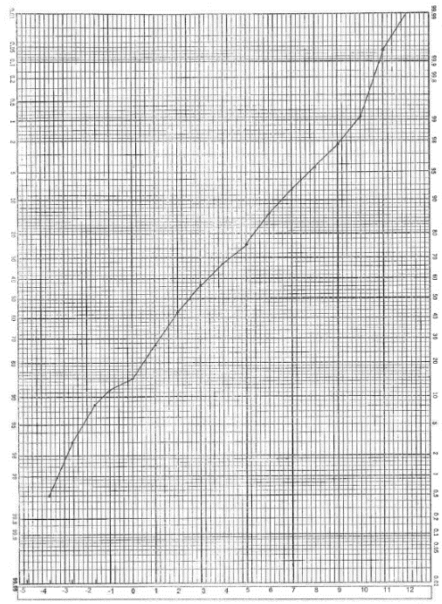

%	ϕ
95	7.8
84	5.8
75	4.95
50	2.5
25	0.8
16	0.1
5	-2.2

		+/-
$\bar{x}$	2.8	.005
σ	2.94	.01
SK	0.11	.004
K	0.99	.025

36

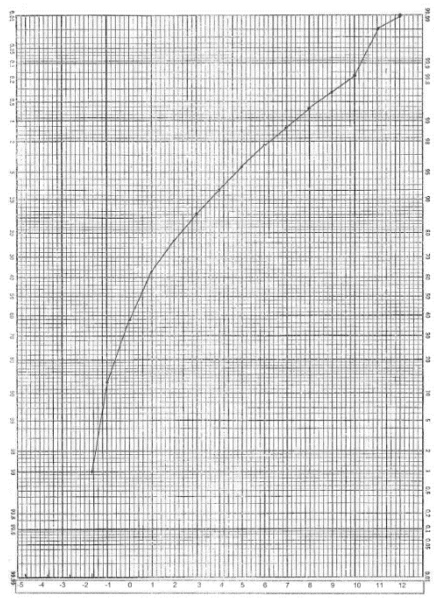

%	ϕ
95	4.8
84	2.75
75	1.85
50	0.5
25	-0.4
16	-.8
5	-1.3

		+/-
$\bar{x}$	0.816	.03
σ	1.81	.04
SK	0.34	.02
K	1.1	.002

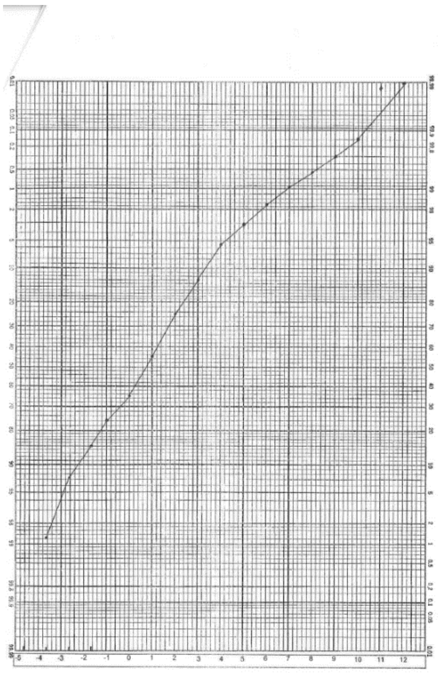

37

%	Φ
95	4.2
84	2.7
75	1.95
50	0.7
25	-0.9
16	-1.6
5	-2.9

$\bar{X}$	0.6	.03
σ	2.15	.03
SK	-0.04	.03
K	1.02	.005

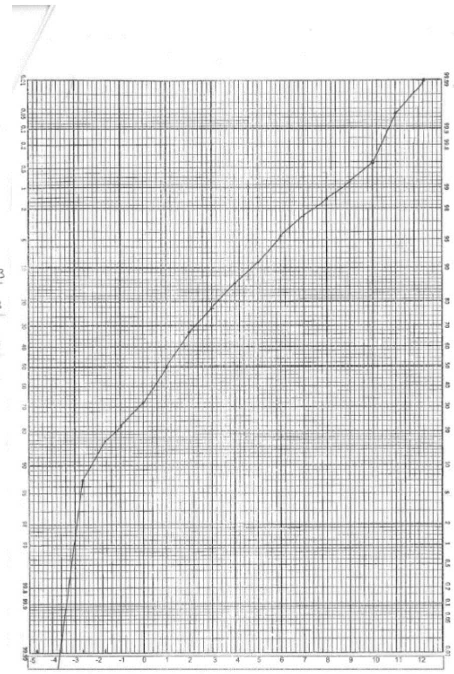

38

%	Φ
95	5.9
84	3.7
75	2.7
50	1
25	-0.7
16	-1.7
5	-2.7

		+/-
$\bar{X}$	1	.02
σ	2.65	.07
SK	0.07	.02
K	1.04	.0006

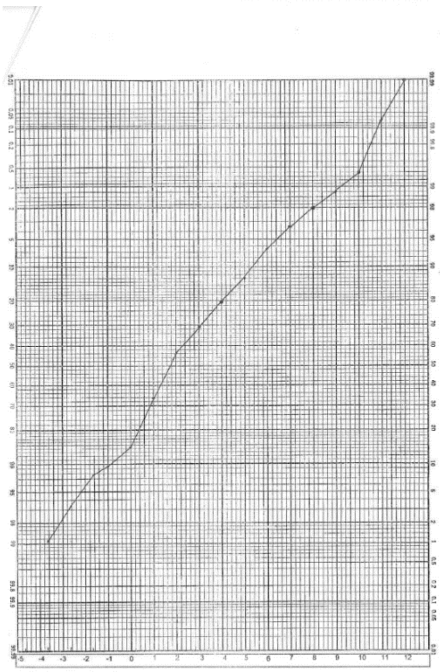

39

%	Φ
95	6.4
84	4.5
75	3.6
50	1.8
25	0.6
16	.1
5	-2.2

$\bar{X}$	$2.1\bar{3}$	.01
σ	2.4	.05
SK	0.15	.02
K	1.17	.03

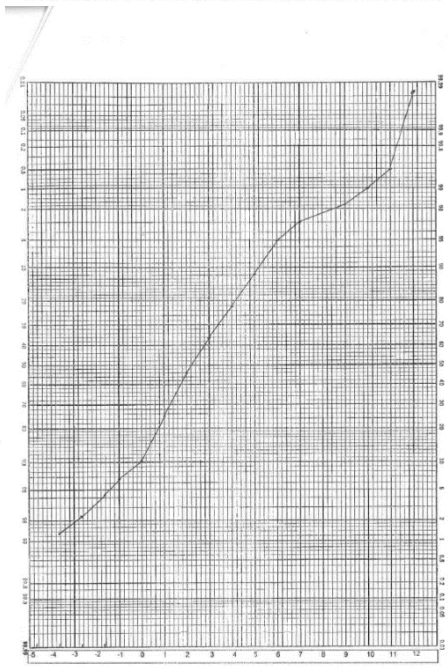

40

%	Φ
95	6
84	4.5
75	3.8
50	2.3
25	1
16	0.5
5	-1.4

		+/-
$\bar{X}$	$2.4\bar{3}$	.05
σ	$2.\overline{12}$	.09
SK	0.05	.02
K	1.08	.002

41

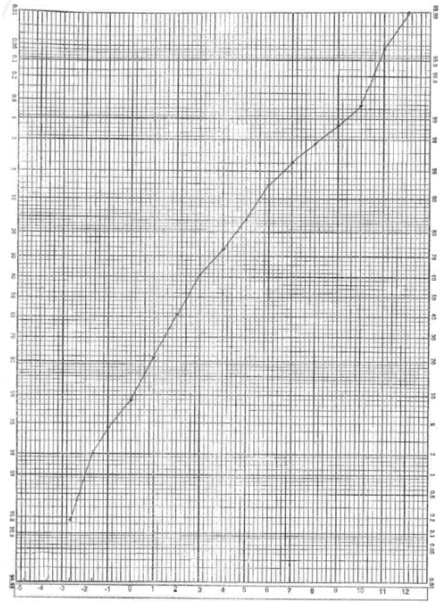

%	Φ
95	6.6
84	4.85
75	4.2
50	2.45
25	1.2
16	0.6
5	-.8

		+/-
x̄	2.67	.01
σ	2.21	.04
SK	0.14	.01
K	1.01	.03

42

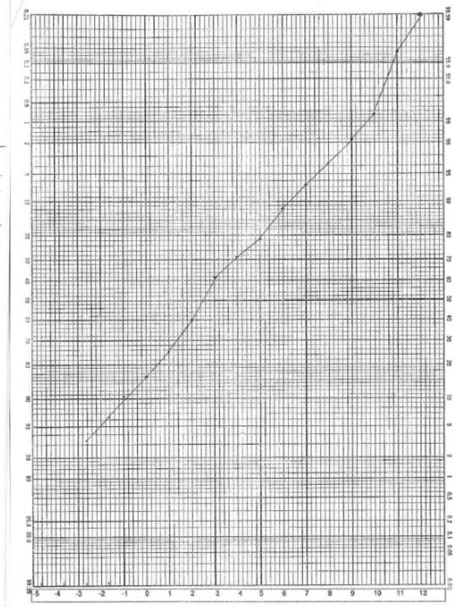

%	Φ
95	7.5
84	5.5
75	4.5
50	2.5
25	0.95
16	0
5	-2

		+/-
x̄	2.6	.01
σ	2.81	.06
SK	0.07	.01
K	1.1	.007

43

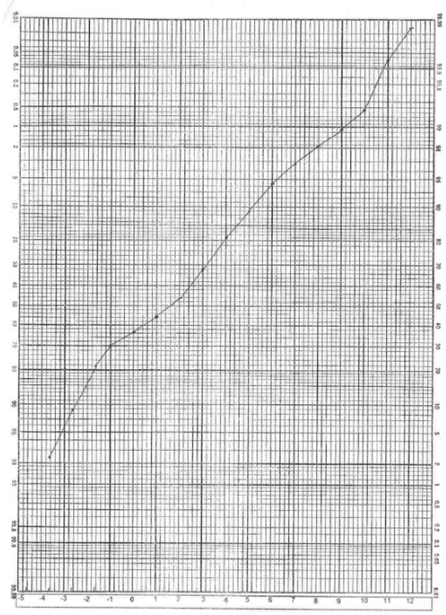

%	Φ
95	6.2
84	4.4
75	3.5
50	1.6
25	-1.7
16	-2
5	-3.1

		+/-
x̄	1.3	.04
σ	3.01	.05
Sk	-0.07	.01
K	0.71	.003

44

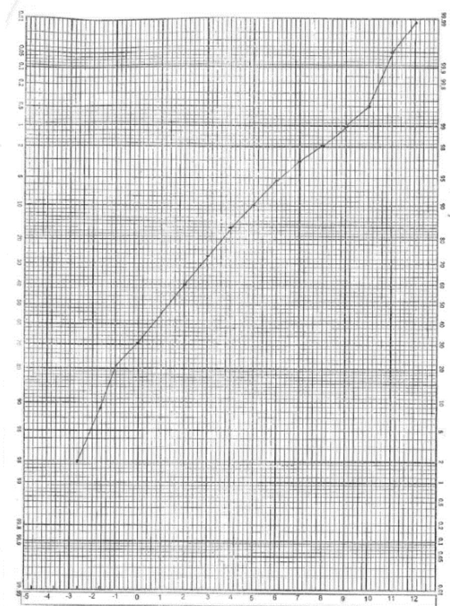

%	Φ
95	6.1
84	4
75	3.2
50	1.3
25	-.6
16	-1.2
5	-2.1

x̄	1.36	.02
σ	2.54	.04
SK	0.1	.01
K	0.88	.03

45

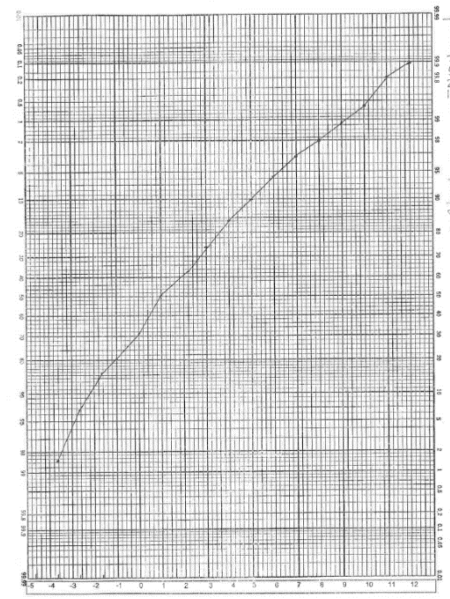

%	φ
95	6.6
84	4
75	3.2
50	0.95
25	-0.05
16	-1.6
5	-2.9

		+/-
$\bar{X}$	$1.1\bar{6}$	.003
σ	2.84	.05
SK	0.14	.03
K	1.2	0.15

46

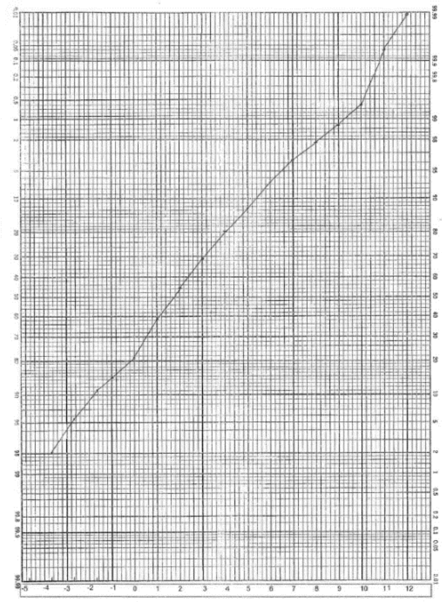

%	φ
95	6.5
84	4.5
75	3.5
50	1.8
25	0.2
16	-.8
5	-2.8

		+/-
$\bar{X}$	$1.8\bar{3}$	.04
σ	2.73	.002
SK	0.01	.03
K	1.15	.01

47

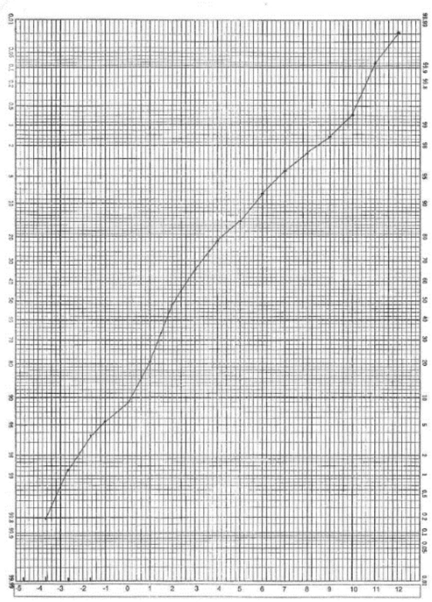

%	φ
95	6.8
84	4.8
75	3.7
50	2.1
25	1.1
16	0.6
5	-1.2

		+/-
$\bar{X}$	2.5	.03
σ	2.26	.01
SK	0.23	.002
K	1.26	.001

Appendix D: Raw Chemistry Data

Samp#	1	2	3	4a	4b	5a	5b
Phi size	2	1	1	1	-2.7	2	-1.7
Unit	MSH-W	DM W/C	MR-C	DM C/P	DM C/P	MSH-P	MSH-P
SiO2	60.11258	59.37594	58.11031	58.70096	58.08645	60.5778	59.96687
TiO2	0.582363	0.76917	0.756731	0.790132	1.136922	0.754355	0.954889
Al2O3	20.20422	18.24317	18.76315	18.66121	18.32486	19.26472	19.06993
FeO*	4.382309	5.482395	5.500666	6.027939	6.2111	5.076552	5.870876
MnO	0.086906	0.102233	0.101811	0.10497	0.103206	0.091537	0.09591
MgO	2.349703	4.056361	4.362377	4.238156	4.077552	2.723932	2.786588
CaO	6.385201	6.684141	7.324907	6.329996	6.296968	5.804556	5.488966
Na2O	4.99668	3.933278	3.854504	3.831204	3.931462	4.413356	3.982781
K2O	0.806482	1.195547	1.077205	1.134104	1.550728	1.146017	1.538441
P2O5	0.093547	0.157749	0.148338	0.181334	0.280757	0.147184	0.244771
Total	99.99999	99.99999	100	100	100	100	100
NiO	20.78671	53.28957	61.73024	53.54153	56.43907	15.21432	15.99947
Cr2O3	33.71413	100.7083	115.3226	103.3128	104.0363	28.50362	29.66264
Sc2O3	13.97035	22.01849	22.47405	22.01849	21.86664	18.63941	18.5259
V2O3	85.34579	140.3982	150.3018	142.2915	167.6331	123.1213	149.428
BaO	262.5169	370.508	357.5756	338.3428	420.8007	340.7243	443.5706
Rb2O	21.54502	31.07246	27.49967	27.93273	38.65111	29.5797	37.89324
SrO	834.0641	763.8173	844.4841	659.1495	530.5978	724.5784	628.475
ZrO2	115.2233	156.0174	138.457	152.5053	209.5091	171.1464	216.5333
Y2O3	11.81816	14.58412	15.08702	17.72725	22.88198	16.17918	20.9961
Nb2O5	6.373068	10.48016	8.497424	9.347166	16.42835	10.65468	13.7375
Ga2O3	28.87818	26.34968	27.81355	27.14815	26.08352	29.37689	28.34586
CuO	14.87122	22.30683	21.68719	34.69951	37.05412	21.46813	35.93878
ZnO	74.8014	86.13868	85.64575	86.87807	81.45589	85.39058	89.34269
PbO	6.185419	6.078774	7.358516	7.571806	7.03858	8.023163	8.531613
La2O3	10.44941	19.62168	19.62168	19.50557	21.01493	17.81443	23.80144
CeO2	22.75716	33.22302	31.39758	41.25496	46.1228	36.86284	50.74725
ThO2	2.621753	3.277191	4.041869	3.82339	5.789704	3.784769	6.008184
Nd2O3	11.89367	14.43407	15.01143	19.74581	23.78734	19.31774	24.36471
U2O3	0.326946	0	1.198801	0.762874	1.634729	1.94186	2.942512
sum tr.	1578.143	1874.324	1955.206	1767.559	1838.826	1702.322	1844.845
in %	0.157814	0.187432	0.195521	0.176756	0.183883	0.170232	0.184484

Samp#	6a	6b	7	8b	8a	9a	9b
Phi size	3	-1.7	2	-1	4	2	-1
Unit	DM P/Yn	DM P/Yn	MSH-Yn	DM Yn/F	DM Yn/F	MR-F	MR-F
SiO2	59.65808	60.15048	60.64693	56.55903	61.20334	60.07834	60.65891
TiO2	0.999066	0.945942	0.587666	1.120334	1.007548	1.102405	1.034373
Al2O3	17.98028	19.0858	20.33598	21.88455	18.19133	18.17494	18.41167
FeO*	6.58071	5.618757	4.314338	7.068187	5.470012	6.551916	6.069742
MnO	0.110322	0.089695	0.079626	0.119507	0.092033	0.101892	0.093644
MgO	3.49191	2.573688	2.161282	2.846143	2.906817	3.584217	3.239948
CaO	5.694695	5.783647	6.095415	5.021232	5.327625	4.882239	4.863332
Na2O	3.844726	4.014205	4.892088	3.534197	4.077992	3.645865	3.732157
K2O	1.421102	1.51134	0.815368	1.525523	1.553611	1.656545	1.689873
P2O5	0.219106	0.226445	0.071308	0.321305	0.169703	0.22165	0.20635
Total	99.99999	100	100	100	100	100	100
NiO	18.64505	14.10977	13.35389	13.1681	19.90485	34.64452	35.04282
Cr2O3	40.22544	34.29291	18.37637	38.8289	49.77536	88.26445	86.79995
Sc2O3	23.53701	20.65183	13.66665	16.78805	20.80368	25.05553	22.24704
V2O3	179.2844	159.6228	90.00631	121.6392	149.7192	174.7695	164.354
BaO	416.4899	451.1974	255.2217	415.8161	422.0166	448.3236	452.5484
Rb2O	38.32631	40.16684	20.46235	29.37957	43.41483	45.79669	47.15604
SrO	565.7212	590.3076	818.9611	346.7716	570.9897	486.4594	485.1384
ZrO2	209.5091	221.9365	131.1627	155.0719	207.4829	230.4465	235.5796
Y2O3	22.12763	20.9961	13.07542	34.36996	18.9845	23.88778	23.77094
Nb2O5	14.72887	13.87913	5.240078	11.10244	14.87049	16.85322	16.5428
Ga2O3	26.88199	27.94663	29.4105	20.06269	26.34968	27.01507	28.05954
CuO	33.7081	37.79768	13.50802	61.03083	31.47741	26.27249	33.49029
ZnO	99.32443	87.12453	76.89633	49.41762	83.79728	88.6033	84.41468
PbO	8.958193	10.02464	6.612	4.287351	8.958193	9.811354	9.606682
La2O3	23.45313	22.40819	11.72656	49.94374	23.45313	26.23964	23.79089
CeO2	50.01707	43.93227	24.82599	54.42825	44.78414	53.91135	48.06625
ThO2	4.806547	6.008184	2.512513	3.8427	6.445142	6.554382	5.839359
Nd2O3	23.20998	21.13148	14.3186	39.3429	20.32317	25.40396	27.31917
U2O3	1.198801	1.525747	1.416765	0.219065	1.743711	0.435928	3.560077
sum tr.	1800.153	1825.06	1560.754	1465.511	1765.294	1838.749	1833.327
in %	0.180015	0.182506	0.156075	0.146551	0.176529	0.183875	0.183333

Samp#	10a	10b	11a	11b	12a	12b	13a
Phi size	3	-1	3	-1	3	-1	4
Unit	DM F/O	DM F/O	Maz-O	Maz-O	DM O/R	DM O/R	MR-R
SiO2	59.82959	59.8056	60.28622	61.41716	60.13382	59.64207	59.58536
TiO2	1.017221	0.922028	0.883955	0.882708	1.012644	1.179405	1.002072
Al2O3	20.5157	22.93407	20.57495	22.2198	19.60482	20.53788	20.55435
FeO*	6.019783	5.59049	5.420098	5.03226	6.307807	6.528481	5.968283
MnO	0.086083	0.068938	0.082512	0.06612	0.094513	0.082202	0.082663
MgO	2.761707	1.812088	2.612763	1.514748	3.32731	2.916906	2.936224
CaO	4.327953	3.229729	4.532623	2.959313	4.4497	4.375783	4.826293
Na2O	3.662123	3.659363	3.97254	3.915529	3.459774	3.227801	3.507806
K2O	1.557063	1.702145	1.472275	1.775831	1.419606	1.305442	1.363657
P2O5	0.222775	0.275555	0.162051	0.21653	0.189998	0.20403	0.173288
Total	100	100	99.99999	100	99.99999	100	100
NiO	25.57395	17.72629	23.55827	13.22791	24.56611	23.43229	22.42445
Cr2O3	65.6919	44.35512	47.60493	28.93916	47.17084	55.4185	51.8011
Sc2O3	20.65183	16.63543	21.41109	15.18517	21.25923	19.28516	21.10738
V2O3	152.6321	113.7348	134.4269	102.5315	148.6997	171.4198	153.3603
BaO	452.0817	479.916	463.9088	515.0857	371.945	388.525	364.3182
Rb2O	40.2751	36.34361	34.10392	36.26925	36.70231	33.12952	34.64525
SrO	516.6655	382.4254	642.2903	411.2952	467.6098	443.7259	522.9877
ZrO2	243.4142	279.8858	230.4465	318.9239	209.7793	219.9103	199.108
Y2O3	24.13923	33.35907	25.89938	38.4719	26.15083	31.93419	22.12763
Nb2O5	14.58724	12.09881	10.90503	11.75477	12.88776	15.72023	12.46289
Ga2O3	30.20897	27.15151	27.54739	29.67666	28.87818	29.01126	28.34586
CuO	35.44307	45.08808	35.81485	43.8701	45.729	55.51922	46.10078
ZnO	78.7448	57.71581	70.4883	56.80963	85.89222	72.46	75.54079
PbO	12.47748	11.03993	10.02464	13.43729	9.811354	9.064838	10.45123
La2O3	23.56923	38.62472	21.94377	39.24335	31.81266	46.67405	25.42691
CeO2	60.23954	58.83143	59.87445	62.67346	52.81608	43.0804	48.43503
ThO2	4.915787	6.038528	4.478828	5.571225	5.025026	4.478828	5.025026
Nd2O3	24.01829	34.3525	27.82888	40.18445	30.60022	34.75724	24.36471
U2O3	2.615566	2.519244	0.871855	2.83353	0.980837	2.397603	2.615566
sum tr.	1827.945	1697.842	1893.428	1785.984	1658.316	1699.944	1670.649
in %	0.182795	0.169784	0.189343	0.178598	0.165832	0.169994	0.167065

Samp#	13b	14a	14b	15a	15b	16a	16b
Phi size	-1	2	1	1	-1.7	1	-2.7
Unit	MR-R	MSH-W	MSH-W	DM W/C	DM W/C	MR-C	MR-C
SiO2	59.07065	60.33554	65.61356	58.37137	59.32754	57.27123	60.11322
TiO2	1.233526	0.530903	0.625685	0.7423	0.902809	0.758388	0.981699
Al2O3	20.58675	20.67131	16.62565	18.84346	18.30702	16.99773	17.49361
FeO*	6.609	4.047083	4.275176	5.233987	5.490829	6.36479	5.576122
MnO	0.082342	0.087833	0.11728	0.134239	0.184849	0.131467	0.099986
MgO	3.050701	1.865435	2.166784	3.948261	3.190993	6.228428	3.883716
CaO	4.647903	6.424522	4.374788	7.113206	5.971896	7.689092	5.963733
Na2O	3.257208	5.168455	4.340056	3.751058	3.771142	3.360157	3.964433
K2O	1.261948	0.774693	1.699923	1.5079	1.973044	1.001264	1.603508
P2O5	0.199951	0.094221	0.161084	0.35421	0.879865	0.197458	0.319988
Total	99.99998	100	99.99999	99.99999	99.99999	100	100
NiO	22.92837	12.22007	23.68425	54.29741	44.47097	107.3732	69.28904
Cr2O3	56.72076	19.24454	42.25118	100.4189	67.57295	204.5385	112.8627
Sc2O3	21.41109	12.14813	13.2111	21.71479	18.5259	31.26611	19.58887
V2O3	191.5183	76.17039	84.90887	139.3787	141.8546	169.1116	168.6526
BaO	367.7447	257.1007	426.4379	380.8982	467.2248	313.0418	452.966
Rb2O	32.69646	18.73009	44.28096	37.89324	50.01908	26.25734	43.5231
SrO	488.8009	859.1188	509.7579	797.4187	593.5858	746.2509	600.1422
ZrO2	219.2349	110.2253	180.1968	148.3179	204.6462	125.7595	216.3982
Y2O3	24.76786	9.680837	16.09282	15.21274	20.36748	15.5569	20.9961
Nb2O5	16.7116	6.514691	8.780671	9.205542	12.60451	8.131205	16.00348
Ga2O3	30.07589	29.94281	25.01888	26.08352	25.28504	25.29311	26.2166
CuO	43.37439	13.75588	27.38783	30.85778	50.93392	22.20418	32.3449
ZnO	73.93878	75.91048	90.20531	108.9365	131.7343	98.19916	85.39929
PbO	10.87781	4.585742	9.064838	7.785096	7.465161	6.861916	9.491419
La2O3	29.49057	11.84267	17.99621	18.22842	23.45313	17.46964	26.12354
CeO2	41.01157	19.83646	35.65694	40.64648	52.3293	37.22424	50.26047
ThO2	4.806547	1.420116	3.167951	4.041869	6.008184	2.59527	5.243506
Nd2O3	27.02058	6.697408	17.6673	17.43635	23.44093	18.40329	24.13376
U2O3	1.634729	0.762874	1.198801	2.397603	1.743711	1.618217	0.435928
sum tr.	1704.766	1545.908	1576.966	1961.17	1943.266	1977.156	1980.072
in %	0.170477	0.154591	0.157697	0.196117	0.194327	0.197716	0.198007

Samp#	17a	17b	18	19	20	21a	21b
Phi size	**2**	**-1.7**	**2**	**2**	**2**	**2**	**-1**
Unit	**DM C/P**	**DM C/P**	**DM P/Yn**	**MSH-Yn**	**DM Yn/F**	**MR-F**	**MR-F**
SiO2	60.88509	60.15162	61.29235	60.65784	60.62133	60.55972	59.83668
TiO2	0.778387	0.954381	0.593123	0.573264	0.634905	0.983453	0.982946
Al2O3	18.32658	18.0083	19.76833	20.27127	19.98006	19.65954	21.50454
FeO*	5.264417	5.570685	4.220539	4.24383	4.484705	5.908415	5.748177
MnO	0.104624	0.125676	0.081743	0.081807	0.084416	0.094938	0.084102
MgO	3.030578	3.197495	2.224515	2.175145	2.352561	3.081423	2.490827
CaO	5.865539	5.881065	6.006141	6.203399	6.093982	4.205237	3.96101
Na2O	4.302873	3.972105	4.822001	4.950169	4.780742	3.616621	3.528927
K2O	1.242984	1.668233	0.911575	0.778396	0.886034	1.684177	1.635944
P2O5	0.19894	0.470444	0.079666	0.064882	0.081254	0.206472	0.226841
Total	100	100	99.99999	100	99.99999	100	99.99999
NiO	33.55488	38.42392	15.87349	13.98379	14.73967	33.63668	26.20385
Cr2O3	37.91031	65.40251	20.8362	18.81046	27.7816	79.43801	69.45399
Sc2O3	19.74072	18.5259	13.97035	14.12221	14.88146	18.5259	15.79257
V2O3	136.9028	157.0013	98.89043	95.2494	106.9007	143.6023	138.3592
BaO	364.9814	470.9829	277.9916	246.7106	273.0175	459.0453	434.7279
Rb2O	30.96419	43.8479	23.60208	19.48795	22.73595	43.09003	39.51724
SrO	704.4587	619.2259	803.3897	847.8793	797.7699	450.6335	414.8076
ZrO2	168.4448	217.749	135.3502	128.7313	139.5377	248.6823	253.8154
Y2O3	15.71564	22.12763	12.44679	12.32107	13.95549	23.25915	23.38488
Nb2O5	10.48016	14.44562	5.948197	5.664949	7.789305	14.58724	13.87913
Ga2O3	27.14815	26.88199	29.54358	28.07971	28.21278	27.14815	27.28123
CuO	31.35349	43.37439	17.1019	13.8798	16.60619	34.2038	41.76334
ZnO	93.90225	98.8315	80.22358	80.22358	81.82558	83.67405	75.29432
PbO	6.185419	8.744903	5.758838	5.332258	5.225613	10.55787	11.62432
La2O3	17.41569	29.72278	10.68162	13.93255	10.2172	28.21342	26.12354
CeO2	35.65694	56.22357	17.88932	21.17511	25.67787	52.57269	53.05947
ThO2	3.71415	4.041869	1.857075	1.092397	1.638596	5.789704	5.352745
Nd2O3	18.59108	25.86585	9.584221	10.96989	13.0484	22.05526	23.44093
U2O3	0	3.051494	0.871855	0.54491	1.525747	1.852693	1.198801
sum tr.	1757.121	1964.471	1581.811	1578.191	1603.087	1780.568	1695.08
in %	0.175712	0.196447	0.158181	0.157819	0.160309	0.178057	0.169508

Samp#	22a	22b	23a	23b	24a	24b	25
Phi size	3	-1	2	-1.7	1	-2.7	2
Unit	MR-R	MR-R	DM W/C	DM W/C	MR-C	MR-C	DM C/P
SiO2	59.22257	58.34103	59.85958	60.4605	59.53829	59.52133	60.71004
TiO2	1.042468	1.213165	0.693415	0.99666	0.712273	1.024578	0.727088
Al2O3	20.48524	21.34857	19.38443	18.12052	18.68675	18.17464	18.90002
FeO*	6.599166	6.724899	5.137169	5.629081	5.263153	5.853745	5.171773
MnO	0.099537	0.094717	0.11122	0.100953	0.099331	0.096522	0.094874
MgO	3.293848	3.144999	3.203464	3.391133	3.862296	3.815494	2.859982
CaO	4.293359	4.419732	6.091143	5.580882	6.658985	5.867852	5.923181
Na2O	3.322636	3.151259	4.406124	3.901429	3.97426	3.877457	4.457231
K2O	1.396335	1.283897	0.969294	1.583108	1.075036	1.517281	1.062184
P2O5	0.244843	0.277732	0.144158	0.235725	0.129641	0.251109	0.093642
Total	100	100	100	99.99999	100	100	100
NiO	26.70778	28.21954	29.98326	50.14007	52.25246	65.25768	20.45204
Cr2O3	53.39276	64.67903	53.68215	80.45088	96.25342	106.2067	36.52473
Sc2O3	22.3222	22.47405	16.55183	18.5259	22.24704	21.86664	17.7375
V2O3	165.5941	180.4495	115.6392	159.0403	133.7899	168.507	123.698
BaO	368.2974	364.9814	296.119	447.5498	334.4875	426.5485	321.4669
Rb2O	36.81058	35.07832	24.25168	41.35777	27.54341	40.81644	27.86493
SrO	457.3069	437.989	713.1225	589.6051	761.8967	565.37	744.3965
ZrO2	218.2893	229.2308	136.5659	220.5857	144.8058	216.6684	159.7997
Y2O3	24.76786	23.63633	13.70404	19.4874	15.05908	21.12183	15.18354
Nb2O5	13.87913	16.42835	7.364434	15.86186	8.691977	14.72887	8.411591
Ga2O3	28.21278	29.27742	28.21278	28.21278	28.45475	26.48276	27.66434
CuO	46.59649	48.45539	21.31541	29.99029	25.14838	32.71668	21.10011
ZnO	93.40932	85.76898	85.0296	82.19528	83.80475	81.08619	89.41613
PbO	10.77116	10.34458	5.758838	8.424967	7.495323	7.891742	6.65078
La2O3	26.00743	26.47185	15.67412	19.62168	11.95291	21.36325	12.87236
CeO2	53.30287	37.72577	28.47687	46.73128	31.5623	50.62555	31.2009
ThO2	5.243506	5.571225	3.058712	5.134266	4.001042	5.352745	3.460361
Nd2O3	26.55869	22.86356	13.16387	20.90053	16.57439	23.32545	16.91731
U2O3	0.980837	1.852693	0	0.435928	2.697028	2.724548	1.078811
sum tr.	1678.451	1671.498	1607.674	1884.252	1808.718	1898.661	1685.897
in %	0.167845	0.16715	0.160767	0.188425	0.180872	0.189866	0.16859

Samp#	26	27	28	29	30	31	32
Phi size	2	2	2	2	2	2	2
tephra	DM P/Yn	MSH-Yn	DM Yn/F	DM Or/W	MSH W& I	DM W/C&	MSH-P
SiO2	60.66299	60.48438	60.60797	60.26464	60.67268	60.68741	61.18022
TiO2	0.585754	0.573845	0.824946	0.513273	0.613506	0.721189	0.609643
Al2O3	20.11334	20.3685	18.59068	20.88062	19.85443	18.86902	19.56245
FeO*	4.438994	4.330204	5.407544	3.909293	4.400487	5.161911	4.436246
MnO	0.087641	0.084696	0.100809	0.083121	0.08939	0.097806	0.084399
MgO	2.269527	2.214576	3.29327	1.847036	2.487664	2.999869	2.326012
CaO	6.125263	6.237537	5.658481	6.488506	6.043564	5.85668	5.998225
Na2O	4.863969	4.901294	4.238407	5.168729	4.717664	4.427131	4.785604
K2O	0.800005	0.754201	1.167107	0.749403	0.965127	1.051163	0.931871
P2O5	0.05251	0.050782	0.110788	0.095376	0.155471	0.127821	0.085328
Total	100	100	100	100	99.99999	100	100
NiO	16.08727	14.10977	31.92513	10.22602	21.82382	26.70778	14.23575
Cr2O3	20.4825	20.54681	63.30954	21.19867	39.67589	45.43449	25.32177
Sc2O3	13.67892	13.36295	20.29291	10.67257	16.8356	18.67776	13.66665
V2O3	93.56643	96.26888	141.8634	72.37342	100.9191	125.2515	101.8033
BaO	252.7531	239.4154	337.9889	253.4096	290.3925	318.7784	277.9916
Rb2O	20.36283	19.05489	31.83032	19.61262	24.97126	28.47407	23.81861
SrO	829.4638	854.6699	666.8625	862.1463	769.8935	717.1031	792.2673
ZrO2	132.6486	129.5417	172.3621	107.6588	137.2413	156.6928	139.6727
Y2O3	12.69443	11.69244	17.05036	9.583051	12.81889	14.45839	13.32687
Nb2O5	6.028307	5.664949	11.21545	6.308693	7.991012	9.630413	7.930929
Ga2O3	28.98169	30.07589	26.34699	28.98169	27.92781	27.41431	27.68047
CuO	14.59833	18.58902	27.11118	13.2489	16.07043	19.95222	14.62337
ZnO	80.02317	80.34681	89.29415	69.16637	77.21748	89.21946	77.75895
PbO	6.228508	5.012322	7.073051	6.017372	6.545212	6.931935	5.652193
La2O3	10.57373	10.56552	20.11307	10.22893	12.29771	15.90633	10.1011
CeO2	21.20216	23.60903	33.0079	25.29803	26.74363	31.03249	25.67787
ThO2	2.59527	2.184794	3.244088	1.622044	2.270862	4.041869	1.638596
Nd2O3	10.63047	11.20084	14.74549	10.05894	12.11645	14.43407	12.81745
U2O3	1.510336	1.743711	1.294573	0.97093	1.186692	1.852693	0
sum tr.	1574.11	1587.656	1716.931	1538.783	1604.939	1671.994	1585.985
in %	0.157411	0.158766	0.171693	0.153878	0.160494	0.167199	0.158599

Samp#	33	34	35	37	38a	38b	39
Phi size	2	2	2	2	1	-1.7	2
Unit	MSH-Yn	DM Yn/F	MR-F	MSH-W	MR-C	MR-C	MSH-Yn
SiO2	60.80309	60.78325	60.56417	60.94011	59.3702	59.89744	60.58843
TiO2	0.559149	0.785776	0.795913	0.691834	0.741811	1.00857	0.654956
Al2O3	20.15485	18.76739	19.09229	19.06146	19.04576	18.65561	19.54149
FeO*	4.235159	5.193046	5.347223	4.749054	5.332821	5.85369	4.804416
MnO	0.082376	0.095303	0.096546	0.087701	0.096137	0.097053	0.088512
MgO	2.211255	2.886926	2.933766	2.600195	3.612478	3.334399	2.612986
CaO	6.163122	5.765427	5.54608	6.025433	6.490147	5.514912	6.040573
Na2O	4.894913	4.42454	4.296289	4.687095	4.009176	3.848549	4.658595
K2O	0.811091	1.169189	1.190971	1.02601	1.148049	1.549741	0.935008
P2O5	0.084979	0.129149	0.136752	0.131078	0.153415	0.240042	0.075044
Total	99.99998	100	99.99999	99.99998	100	100	100
NiO	15.11761	23.43229	25.81446	18.89701	45.98273	44.34499	20.91269
Cr2O3	20.54681	48.4731	56.72076	34.5823	88.11976	76.83348	30.09673
Sc2O3	12.60369	18.67776	18.63941	13.2111	21.41109	20.49998	16.39998
V2O3	93.21042	131.8054	130.6182	91.89965	130.4946	162.39	111.4156
BaO	252.3478	336.6848	342.9126	282.7445	345.1959	427.1011	285.5078
Rb2O	20.67888	32.37166	31.72315	23.81861	29.665	40.38337	24.46821
SrO	842.4938	692.868	662.1107	658.9153	729.6305	572.2776	776.4617
ZrO2	128.8663	166.8238	179.7915	125.0841	153.0457	216.9385	141.5639
Y2O3	12.19534	16.59572	17.05036	10.30946	15.08702	19.9903	14.83557
Nb2O5	6.231444	10.19691	11.63603	6.939563	8.639047	15.15374	7.22281
Ga2O3	28.34586	27.81355	26.87393	23.95425	27.41431	28.21278	28.47894
CuO	13.26017	24.90929	25.02571	18.09332	24.0418	30.11422	18.09332
ZnO	77.88218	84.6599	83.43879	75.66402	82.44174	82.56497	82.93466
PbO	5.972129	8.318322	7.706459	8.851548	7.678451	9.598064	6.718645
La2O3	14.16476	16.95127	22.18184	13.35203	17.41569	22.87261	16.37075
CeO2	20.32324	31.39758	35.41724	21.78359	31.39758	36.8739	25.31278
ThO2	1.201637	3.60491	4.217315	1.966315	3.167951	6.445142	2.512513
Nd2O3	11.20084	15.01143	18.5176	11.08536	15.81974	19.16844	14.3186
U2O3	1.525747	1.743711	1.186692	0.871855	2.070657	1.634729	0.653892
sum tr.	1578.169	1692.339	1701.583	1442.024	1778.719	1833.398	1624.279
in %	0.157817	0.169234	0.170158	0.144202	0.177872	0.18334	0.162428

Samp#	40	41	42	43	44	45a	45b
Phi size	2	3	3	3	1	1	-1.7
Unit	DM Yn/F	MR-F	MAZ-O	DM O/R	MR-R	Feat R	Feat R
SiO2	60.20234	59.80758	59.81958	56.80454	56.83327	59.17716	59.99878
TiO2	0.887022	1.015511	0.96231	1.168406	1.107012	0.783415	0.938091
Al2O3	19.14612	19.8796	20.98975	23.22406	21.00191	18.39356	18.18981
FeO*	5.733524	6.24389	5.971977	7.317684	7.331191	5.577435	5.68585
MnO	0.096983	0.094298	0.086119	0.095411	0.107898	0.105337	0.105976
MgO	3.098347	3.084639	2.611745	3.067595	4.197865	3.893972	3.216783
CaO	5.360808	4.539345	4.126638	3.914466	5.049358	6.566576	5.65909
Na2O	4.043981	3.650556	3.787991	2.911119	3.044426	3.802665	3.837656
K2O	1.297289	1.516102	1.490908	1.228491	1.121723	1.44791	1.819209
P2O5	0.133576	0.168486	0.152982	0.268237	0.205362	0.251972	0.548754
Total	99.99999	100	100	100	100	100	100
NiO	28.09356	31.87296	27.22251	24.43695	38.7446	48.88027	40.4396
Cr2O3	64.53434	71.33504	48.13621	52.49901	83.91115	93.6182	66.41538
Sc2O3	64.53434	20.34812	18.31423	25.79254	28.53968	21.86664	17.9185
V2O3	64.53434	162.5357	146.5232	185.7522	194.0957	142.5828	137.631
BaO	64.53434	443.3496	452.032	337.6076	325.6097	379.7928	452.966
Rb2O	64.53434	39.95031	35.47311	33.07922	29.05313	37.02711	43.1983
SrO	64.53434	537.3883	546.6919	394.0747	457.2632	738.2943	543.9447
ZrO2	64.53434	225.9889	244.765	231.1219	198.4326	161.6908	198.0273
Y2O3	64.53434	20.74465	20.47034	22.11302	17.69042	15.96709	18.73305
Nb2O5	64.53434	13.87913	10.53309	15.37261	12.81051	10.33853	12.17964
Ga2O3	64.53434	28.07971	27.68652	30.09404	29.96029	26.74891	25.01888
CuO	64.53434	34.69951	40.23053	64.89197	42.09882	29.74244	41.88727
ZnO	64.53434	88.72654	80.50489	90.04162	88.55538	99.07796	101.7891
PbO	64.53434	10.13129	13.07642	10.61119	9.539355	8.424967	7.358516
La2O3	64.53434	21.24714	15.98667	26.48885	20.771	16.95127	21.82766
CeO2	64.53434	43.0804	43.29798	63.11231	45.74419	43.68888	41.25496
ThO2	64.53434	6.445142	5.160197	5.928737	4.501448	4.151109	5.243506
Nd2O3	64.53434	21.47789	20.54187	26.69282	19.49736	19.86128	20.2077
U2O3	64.53434	1.961675	3.7241	2.081115	0.766726	2.506585	1.961675
sum tr.	64.53434	1823.242	1800.371	1641.792	1647.585	1901.212	1798.003
SiO3	64.53434	0.182324	0.180037	0.164179	0.164759	0.190121	0.1798

Samp#	46a	46b	47a	47b			
Phi size	1	-1.7	2	-1.7			
Unit	Feat AA	Feat AA	Feat E	Feat E			
SiO2	62.13806	61.2862	60.89619	58.18715			
TiO2	0.727024	0.983632	0.672993	0.928282			
Al2O3	18.04107	18.05145	19.54654	20.51383			
FeO*	4.974146	5.622147	4.690839	5.653869			
MnO	0.099613	0.129352	0.085841	0.094702			
MgO	2.955205	3.001267	2.430047	2.999628			
CaO	5.435718	5.145081	5.836049	5.848176			
Na2O	4.044914	3.824602	4.586504	3.760183			
K2O	1.390751	1.641359	1.093171	1.567003			
P2O5	0.193492	0.314907	0.161833	0.447176			
Total	99.99999	100	100	100			
NiO	31.67572	38.67588	19.90485	32.62884			
Cr2O3	65.02835	64.24495	30.38612	49.63067			
Sc2O3	18.78973	19.58887	14.27406	16.24813			
V2O3	122.6888	151.3213	109.6679	114.6197			
BaO	396.3081	512.4329	313.2517	613.0184			
Rb2O	38.15352	44.60576	27.49967	31.83032			
SrO	624.7924	505.7772	734.5478	475.3369			
ZrO2	184.6544	224.3679	146.832	164.9327			
Y2O3	17.42373	24.39068	16.09282	30.29976			
Nb2O5	10.09391	14.02075	9.630413	10.33853			
Ga2O3	25.82005	24.22041	27.14815	20.62727			
CuO	36.67984	45.35722	25.52893	79.68495			
ZnO	86.9764	82.6882	84.41344	71.72062			
PbO	8.973274	8.424967	8.531613	6.612			
La2O3	16.32032	21.71156	14.39697	40.86882			
CeO2	37.94704	49.40859	27.50331	68.14978			
ThO2	4.433587	6.445142	3.277191	5.789704			
Nd2O3	17.37454	25.40396	12.70198	34.29535			
U2O3	0.97093	2.070657	1.961675	2.397603			
sum tr.	1745.105	1865.157	1627.551	1869.03			
in %	0.17451	0.186516	0.162755	0.186903			

Samp#	2	2*	15a	15a*	31	31	
Phi size	1	1	1	1	2	2	
Unit	DM W/C	DM W/C	DM W/C	DM W/C	DM W/C&	DM W/C&MR-C	
SiO2	59.37594	59.24474	58.37137	58.3436	60.68741	60.62639	
TiO2	0.76917	0.767858	0.7423	0.739782	0.721189	0.725234	
Al2O3	18.24317	18.29182	18.84346	18.83835	18.86902	18.93409	
FeO*	5.482395	5.557011	5.233987	5.298964	5.161911	5.163785	
MnO	0.102233	0.101962	0.134239	0.133661	0.097806	0.098771	
MgO	4.056361	4.070223	3.948261	3.955628	2.999869	3.001694	
CaO	6.684141	6.706977	7.113206	7.087983	5.85668	5.860839	
Na2O	3.933278	3.909825	3.751058	3.744712	4.427131	4.409158	
K2O	1.195547	1.192038	1.5079	1.50303	1.051163	1.05204	
P2O5	0.157749	0.15755	0.35421	0.354297	0.127821	0.12799	
Total	99.99999	100	99.99999	100	100	99.99999	
NiO	53.12809	53.39646	54.13287	55.38886	26.62684	26.25005	
Cr2O3	100.4031	103.079	100.1146	102.567	45.29681	46.88364	
Sc2O3	21.95177	20.8497	21.64899	21.4976	18.62116	17.25863	
V2O3	139.9727	140.2687	138.9563	134.7455	124.8719	123.7103	
BaO	369.3853	370.1764	379.7439	379.3031	317.8124	313.8452	
Rb2O	30.9783	31.99272	37.77842	37.67048	28.38778	28.06397	
SrO	761.5027	761.5904	795.0023	797.8036	714.9301	715.9806	
ZrO2	156.0174	155.0719	148.3179	148.3179	156.6928	155.6122	
Y2O3	14.53992	15.13591	15.16664	14.91596	14.41458	14.66527	
Nb2O5	10.4484	9.299958	9.177647	8.895258	9.60123	8.612868	
Ga2O3	26.26983	27.01104	26.00448	27.46391	27.33124	27.72926	
CuO	22.23923	24.66019	30.76427	30.64072	19.89176	19.39755	
ZnO	85.87765	84.35494	108.6064	107.1321	88.9491	90.66911	
PbO	6.060353	7.109138	7.761505	6.272997	6.910929	7.655183	
La2O3	19.56222	18.71395	18.17318	17.82593	15.85813	16.78415	
CeO2	33.12234	36.80875	40.52331	36.51951	30.93845	31.42376	
ThO2	3.26726	3.043264	4.029621	4.356347	4.029621	3.376169	
Nd2O3	14.39033	14.93562	17.38352	16.8079	14.39033	16.57766	
U2O3	0	2.385493	2.390337	0.977865	1.847079	2.173034	
sum tr.	1869.117	1879.884	1955.676	1949.103	1667.402	1666.669	
in %	0.186912	0.187988	0.195568	0.19491	0.16674	0.166667	

Appendix E: Organic, Carbonate, and Acidity Data

Table 1. Organic Matter (OM) Content, Calcium Carbonate ($CaCO_3$) Content, and pH Content of all Samples Discussed in this Study.

Sample Number	[1]Depositional Unit	Excavation Unit	OM (%)	$CaCO_3$ (%)	pH
1	MSH-W	30N/24E	3.83	0.05	4.91
2	DM MSH-W/MR-C	30N/24E	3.02	0.12	5.12
3	MR-C	30N/24E	1.93	0.10	5.51
4	DM MR-C/MSH-P	30N/24E	8.87	0.27	5.23
5	MSH-P	30N/24E	3.91	0.17	5.29
6	DM MSH-P/MSH-Yn	30N/24E	3.24	0.24	5.52
7	MSH-Yn	30N/24E	5.16	0.57	5.47
8	DM MSH-Yn/MR-F	30N/24E	6.44	0.17	5.19
9	MR-F	30N/24E	4.28	0.77	5.84
10	DM MR-F/MAZ-O	30N/24E	7.23	1.29	5.75
11	MAZ-O	30N/24E	7.52	1.68	5.82
12	DM MAZ-O/MR-R	30N/24E	7.62	1.46	5.66
13	MR-R	30N/24E	6.73	1.49	5.58
14	MSH-W	61.5N/36E	3.83	0.05	4.91
15	DM MSH-W/MR-C	61.5N/36E	5.35	0.34	5.83
16	MR-C	61.5N/36E	2.01	0.18	5.87
17	DM MR-C/MSH-P	61.5N/36E	2.88	0.29	6.20
18	DM MHS-P/MSH-Yn	61.5N/36E	2.35	0.28	5.99
19	MSH-Yn	61.5N/36E	2.61	0.40	6.06
20	DM MSH-Yn/MR-F	61.5N/36E	3.07	0.51	6.00
21	MR-F	61.5N/36E	6.94	1.65	6.17
22	MR-R	61.5N/36E	8.50	1.87	6.08
23	DM MSH-W/MR-C	64N/115E	6.56	0.46	5.33
24	MR-C	64N/115E	3.91	0.56	6.21
25	DM MR-C/MSH-P & MSH-P	64N/115E	3.08	0.12	5.73
26	DM MSH-P/MSH-Yn	64N/115E	3.22	0.15	5.77
27	MSH-Yn	64N/115E	2.88	0.13	6.63
28	DM MHS-Yn/F	64N/115E	5.35	0.27	6.12
29	DM Duff/MSH-W	71.5N/66.5E	5.08	0.04	5.105
30	MSH-W & DM MSH-W/MR-C	71.5N/66.5E	6.22	0.12	5.25
31	DM MSH-W/MR-C & MR-C	71.5N/66.5E	4.41	0.18	5.47
32	MSH-P	71.5N/66.5E	2.90	0.10	5.64
33	MSH-Yn	71.5N/66.5E	3.10	0.14	5.57
34	DM MSH-Yn/MR-F	71.5N/66.5E	5.51	0.26	5.59
35	MR-F	71.5N/66.5E	5.55	0.35	6.21
36	DM O/W	Off-site	67.48	0.14	3.71
37	MSH-W	Off-site	14.77	0.08	3.66
38	MR-C	Off-site	5.49	0.26	5.91
39	MSH-Yn	Off-site	2.67	0.14	6.96
40	DM MSH-Yn/MR-F	Off-site	4.11	0.27	7.36
41	MR-F	Off-site	5.90	0.50	7.42
42	MAZ-O	Off-site	7.67	0.58	7.33
43	DM MAZ-O/MR-R	Off-site	8.34	0.57	7.64

Sample Number	[1]Depositional Unit	Excavation Unit	OM (%)	$CaCO_3$ (%)	pH
44	MR-R	Off-site	7.11	0.59	7.46
45	Feature R (DM MSH-W/MR-C)	61.5N/36E	5.42	0.11	6.91
46	Feature AA (DM MR-C/MSH-P)	71.5N/66.5E	4.34	0.20	6.56
47	Feature E (DM MHS-P/MSH-Yn)	28N 25E	5.18	0.16	5.98

[1] Denotes depositional unit as recorded in the field by field school students.

Appendix F: SRBP Site Stratigraphic Data

Table 1. Color of sediments from excavation levels, their recorded depositional unit, and approximate correlation to column samples from Unit 30N/24E. Note: these are not colors of column samples but associated excavation levels.

Level	Munsell Color #	Munsell Color	Depositional Unit	Sample #
1	No data	No data	Organic layer	N/A
2	10YR 3/2	Very dark grayish brown	MSH-W and into DM W/C	1 & 2
3	10YR 3/4	Dark yellowish brown	DM W/C	2
4	10YR 5/8	Yellowish brown	DM W/C	2
5	10YR 3/4	Dark yellowish brown	MR-C	3
6	10YR 4/6 & 10YR 3/2	Dark yellowish brown and very dark grayish brown	MR-C	3
7	10YR 4/4 & 10YR 5/6	Dark yellowish brown and yellowish brown	MSH-P and DM P/Yn	5 & 6
8	10YR 5/6	Yellowish brown	MSH-P and DM P/Yn	5 & 6
9	No Data	No Data	MSH-Yn	7
10	No Data	No Data	MSH-Yn	7
11	No Data	No Data	MSH-Yn	7
12	10YR 3/3	Dark brown	DM Yn/F	8
13	10YR 4/6	Dark yellowish brown	MR-F	9
14	10YR 3/3	Dark brown	MR-F and DM F/O	10
15	10YR 6/8	Brownish yellow	MAZ-O	11
16	10YR 5/6	Yellowish brown	DM O/R	12
17	No Data	Thick R to 133cm	MR-R	13

Table 2. Color of sediments from excavation levels, their recorded depositional unit, and approximate correlation to column samples from Unit 61.5N/36E. Note: these are not colors of column samples but associated excavation levels.

Level	**Munsell Color #**	**Munsell Color**	**Depositional Unit**	**Sample #**
1	10YR 3/2	Very dark grayish brown	Duff, DM O/W, MSH-W	14
2	10YR 5/1	gray	Duff, DM O/W, MSH-W	14
3	10YR 5/1	gray	Duff, DM O/W, MSH-W	14
4	10YR 5/3	brown	DM W/C	15
5	10YR 4/2	Dark grayish brown	DM W/C	15
6	10YR 4/6	Dark yellowish brown	DM W/C	15
7	10YR 3/6	Dark yellowish brown	MR-C	16
8	10YR 3/6	Dark yellowish brown	MR-C	16
9	10YR 4/3	brown	DM C/P	17
10	10YR 5/4	Yellowish brown	DM P/Yn	18
11	10YR 5/4	Yellowish brown	MSH-Yn	19
12	10YR 4/4	Dark yellowish brown	MSH-Yn	19
13	10YR 4/4	Dark yellowish brown	DM Yn/F	20
14	10YR 4/4	Dark yellowish brown	DM Yn/F	20
15	10YR 4/4	Dark yellowish brown	MR F	21
16	10YR 3/4	Dark yellowish brown	MR-R	22

Table 3. Color of sediments from excavation levels, their recorded depositional unit, and approximate correlation to column samples from Unit 64N/36E. Note: these are not colors of column samples but associated excavation levels.

Level	Munsell Color #	Munsell Color	Depositional Unit	Sample #
1	10YR 4/2 & 10YR 4/1	Dark grayish brown, dark gray	duff	N/A
2	10YR 4/1	Dark gray	MSH-W	N/A
3	10YR 4/2 & 10YR 4/4	Dark grayish brown, dark yellowish brown	DM W/C	23
4	10YR 4/4	Dark yellowish brown	DM W/C	23
5	10YR 4/6	Dark yellowish brown	DM W/C	23
6	10YR 4/6	Dark yellowish brown	MR C	24
7	10YR 4/4, 10YR 4/6 & 10YR 4/3	Dark yellowish brown, brown	DM C/P	25
8	10YR 5/6, 10YR6/6 & 10YR 4/6	Yellowish brown, brownish yellow, dark yellowish brown	DM P/Yn	26
9	10YR 4/4	Dark yellowish brown	DM P/Yn	26
10	10YR 4/4 & 10YR 4/6	Dark yellowish brown	DM Yn/F	28
11	10YR 4/3	brown	DM Yn/F	28
12	10YR 4/3	brown	DM Yn/F	28

Table 4. Color of sediments from excavation levels, their recorded depositional unit, and approximate correlation to column samples from Unit 71.5N/66.5E. Note: these are not colors of column samples but associated excavation levels.

Level	Munsell Color #	Munsell Color	Depositional Unit	Sample #
1	10YR 3/6	Dark yellowish brown	duff	N/A
2	10YR 5/1	gray	DM O/W	29
3	10YR 4/4	Dark yellowish brown	DM W/C	30 & 31
4	10YR 4/4	Dark yellowish brown	DM W/C	30 & 31
5	10YR 4/4	Dark yellowish brown	DM W/C	30 & 31
6	10YR 4/4 & 10YR 3/3	Dark yellowish brown, brown	DM C/P	N/A
7	10YR 4/6	Dark yellowish brown	MSH Yn, MR-F	33
8	10YR 4/4	Dark yellowish brown	MSH-Yn, MR-F	33
9	10YR 4/4, 10YR 4/6, 10YR 3/4 & 10YR 3/6	Dark yellowish brown	DM Yn/F	34
10	10YR 4/6, 5/6	Dark yellowish brown, yellowish brown	MR-F	35